

UNIVERSITY OF SOUTHAMPTON

FACULTY OF ENGINEERING AND THE
ENVIRONMENT

**Impacts of climate and vegetation on
railway embankment hydrology**

by

Kevin M. Briggs

Thesis for the degree of Doctor of Engineering

October 2011



UNIVERSITY OF SOUTHAMPTON

ABSTRACT

FACULTY OF ENGINEERING AND THE ENVIRONMENT

Doctor of Engineering

**IMPACTS OF CLIMATE AND VEGETATION
ON RAILWAY EMBANKMENT HYDROLOGY**

By Kevin M. Briggs

Field observations and numerical analysis have shown that seasonal changes in pore water pressure affect the stability and shrink-swell behaviour of clay fill railway embankments. However, the soil-atmosphere processes affecting railway embankment hydrology and the worst case conditions for pore water pressure variation are not well understood.

This thesis explores the impact of climate and vegetation on pore water pressures within railway earthworks. Monitoring data from two instrumented embankments and piezometer data collected across the London Underground Ltd network were examined and compared with a hydrological finite element model incorporating a climate boundary condition.

Monitoring and finite element modelling of an instrumented embankment in Kent showed that seasonal pore water variation is dependent on seasonal weather extremes, slope vegetation cover and the saturated permeability of the clay fill.

Examination of London Underground Ltd monitoring data showed that foundation geology influenced maximum pore water pressure measured during an extremely wet winter, with a clear distinction between London clay founded and chalk or terrace gravel founded embankments. A numerical model confirmed that during extreme winter weather maximum pore water pressures are higher in clay fill embankments founded on clay than embankments underdrained by a more permeable foundation.

Monitoring and finite element modelling of tree removal at an instrumented embankment in Essex showed that trees significantly influence pore water pressures, creating soil suctions at depth within their root zone. A finite element model of tree removal showed rewetting and a loss of soil suction within the embankment, in agreement with the monitoring data.

The findings show that climate, vegetation cover and the saturated permeability of both the embankment fill and the foundation influence the extent of seasonal and maximum pore water pressures within railway embankments. This can be used by infrastructure owners during risk assessment of slope failure or poor performance of railway embankments.

Contents

| | |
|--|-----------|
| List of figures | v |
| List of tables | xi |
| List of notation | xvii |
| 1 Introduction | 1 |
| 1.1 Objectives | 3 |
| 1.2 Layout of the thesis | 3 |
| 2 Victorian railway embankments | 7 |
| 2.1 Construction techniques | 7 |
| 2.2 Construction material | 9 |
| 2.3 Observed instability and deformation | 10 |
| 2.4 Modelling embankment failure | 12 |
| 3 Water flow in soils | 15 |
| 3.1 The hydrological cycle | 15 |
| 3.2 Steady state and transient water flow | 17 |
| 3.3 Liquid water flow within soils | 17 |
| 3.4 Liquid-vapour flow within soils | 20 |
| 3.5 Comment | 25 |
| 4 Soil-atmosphere boundary equations | 27 |
| 4.1 Water input - infiltration and runoff | 28 |
| 4.2 Water output - evaporation and transpiration | 34 |
| 4.2.1 Potential evaporation | 34 |
| 4.2.2 Actual evaporation | 35 |
| 4.2.3 Potential evapotranspiration | 37 |

| | | |
|----------|--|-----------|
| 4.2.4 | Actual evapotranspiration | 39 |
| 4.2.5 | Potential transpiration | 40 |
| 4.2.6 | Actual transpiration and root water uptake | 42 |
| 4.3 | Comment | 48 |
| 5 | Soil water retention and hydraulic conductivity | 49 |
| 5.1 | The Soil Water Retention Curve | 49 |
| 5.2 | Hysteresis | 52 |
| 5.3 | Soil Water Retention Curve measurement | 55 |
| 5.4 | Theoretical methods for estimating the Soil Water Retention Curve | 56 |
| 5.4.1 | The Aubertin grain size distribution | 56 |
| 5.4.2 | The van Genuchten equation | 57 |
| 5.4.3 | The Fredlund and Xing equations | 59 |
| 5.4.4 | Soil Water Retention Curve summary | 60 |
| 5.5 | Soil water retention and hydraulic conductivity of a clay fill | 62 |
| 5.5.1 | Structure and composition of clay fill | 62 |
| 5.5.2 | Influence of wetting and drying Soil Water Retention Curve on hydraulic conductivity | 62 |
| 5.5.3 | Influence of van Genuchten (1980) curve fitting parameters on hydraulic conductivity | 65 |
| 5.5.4 | Estimated soil water retention of a clay fill | 65 |
| 5.6 | Comment | 68 |
| 6 | Climate influence on embankment hydrology: Charing embankment case study | 71 |
| 6.1 | Charing embankment | 72 |
| 6.2 | Monitoring results | 73 |
| 6.3 | Finite element modelling | 76 |
| 6.3.1 | Mesh geometry | 76 |
| 6.3.2 | Material properties | 77 |
| 6.3.3 | Boundary and initial pore water pressure conditions | 80 |
| 6.4 | Modelling results | 83 |
| 6.4.1 | Clay fill permeability | 87 |
| 6.4.2 | Extreme climate | 90 |
| 6.5 | Comment and conclusions | 93 |

| | | |
|----------|---|------------|
| 7 | Permeability influence on embankment hydrology: London Underground Ltd study | 95 |
| 7.1 | Analysis of the LUL pore pressure data | 99 |
| 7.1.1 | Method | 99 |
| 7.1.2 | Foundation material | 100 |
| 7.1.3 | Embankment vegetation cover | 100 |
| 7.1.4 | Slope angle, construction history and borehole position | 102 |
| 7.2 | Finite element modelling | 104 |
| 7.2.1 | Mesh geometry | 104 |
| 7.2.2 | Material properties | 105 |
| 7.2.3 | Boundary and initial pore water pressure conditions . | 109 |
| 7.3 | Modelling results | 111 |
| 7.3.1 | Foundation permeability | 112 |
| 7.3.2 | Clay fill permeability | 114 |
| 7.3.3 | Comparison of monitoring data and numerical model . | 115 |
| 7.3.4 | Comparison of climate scenarios | 116 |
| 7.4 | Implications for earthworks assessment | 116 |
| 7.5 | Conclusions | 119 |
| 8 | Tree influence on embankment hydrology: Hawkwell embankment | 121 |
| 8.1 | Hawkwell embankment | 122 |
| 8.1.1 | Instrumentation | 126 |
| 8.1.2 | Climate | 129 |
| 8.2 | Neutron probe monitoring results | 129 |
| 8.2.1 | Seasonal wetting and drying | 135 |
| 8.3 | Piezometer monitoring results | 140 |
| 8.3.1 | Comparison of measured data with Soil Water Retention Curves | 143 |
| 8.4 | Finite element modelling | 144 |
| 8.4.1 | Mesh geometry | 144 |
| 8.4.2 | Material properties | 144 |
| 8.4.3 | Boundary and initial pore water pressure conditions . | 148 |
| 8.5 | Modelling results | 150 |
| 8.5.1 | Tree removal | 153 |
| 8.6 | Comment and conclusions | 153 |

| | |
|---|------------|
| 9 Summary and conclusions | 159 |
| 9.1 Conclusions | 160 |
| 9.2 Implications for earthworks assessment | 161 |
| 9.3 Further work | 162 |
| A London Underground tree study | 165 |
| B Infiltration and flow in an embankment slope | 175 |
| B.1 Finite element modelling | 175 |
| B.1.1 Mesh geometry | 176 |
| B.1.2 Material properties | 176 |
| B.1.3 Boundary and initial pore water pressure conditions . | 177 |
| B.2 Results | 179 |
| B.3 Comment and conclusions | 181 |
| C Charing embankment: Ground investigation | 185 |
| C.1 <i>In situ</i> and laboratory testing | 186 |
| C.2 Results | 186 |
| D Publications | 191 |

List of figures

- 2.1 A conceptual model for dumped clay fill (O'Brien et al., 2004) 10
- 3.1 The hydrological cycle of a railway embankment 16
- 4.1 Infiltration rate versus time (Horton, 1933) (Redrawn from
Gitirana Jr. (2005)) 28
- 4.2 Surface flux with time for varying rainfall infiltration into
Rehevot sand (Redrawn from Rubin (1966b)) 32
- 4.3 Water uptake - soil suction relationship (From Feddes et al.
(1978) showing the anaerobiosis (ψ_{an}), maximum uptake (ψ_d)
and wilting point (ψ_w) 44
- 4.4 Shape of the root water uptake function using a linearly de-
creasing water extraction rate with depth (Prasad, 1988).
(From Nyambayo & Potts (2010)) 45
- 4.5 Comparison of experimental and theoretical soil water re-
moval with depth for five crop types (From Prasad (1988)) . 46
- 5.1 The soil water retention curve (Adapted from Fredlund &
Xing (1994)) 51
- 5.2 Typical Soil Water Retention Curves (After Fredlund & Xing
(1994)) 52
- 5.3 Typical soil water retention and hydraulic conductivity func-
tions for a sand and a clayey silt (From Fredlund (2000)) . . 53
- 5.4 Wetting and drying Soil Water Retention Curves and scan-
ning curves (From Fredlund (2000)) 54
- 5.5 Comparison of calculated pore water pressure variation at 2
m depth using Croney (1977) wetting and drying SWRCs for
London clay 63

| | | |
|------|---|----|
| 5.6 | Soil water retention and hydraulic conductivity curves for wetting and drying of London clay | 64 |
| 5.7 | Soil water retention and hydraulic conductivity curves for varying AEV (based on Croney (1977) London clay) | 66 |
| 5.8 | Soil water retention and hydraulic conductivity curves for varying n and m (based on Croney (1977) London clay) | 67 |
| 5.9 | Soil water retention and hydraulic conductivity curves for London clay (Croney, 1977) and clay fill | 69 |
| 6.1 | Charing embankment cross section at the instrumentation site | 73 |
| 6.2 | Location of MORECS square 174 | 74 |
| 6.3 | Soil moisture deficit data for MORECS square 174 in South East England. (Mott MacDonald, 2009) | 75 |
| 6.4 | Typical value and range of measured pore water pressure variation with depth at Charing Embankment (Glendinning et al., 2009) | 75 |
| 6.5 | Charing Embankment model geometry | 77 |
| 6.6 | Soil water retention curves (SWRCs) describing variation of volumetric water content with pore water pressure | 79 |
| 6.7 | Hydraulic conductivity curves | 79 |
| 6.8 | Surface water balance comparison | 81 |
| 6.9 | Water uptake - soil suction relationship (Feddes et al., 1978) showing the anareobiosis (ψ_{an}), maximum uptake (ψ_d) and wilting point (ψ_w). (From Section 4.2.6) | 82 |
| 6.10 | Calculated seasonal pore water pressure profiles: (a) tree covered mid slope, and (b) grass covered lower slope | 85 |
| 6.11 | Calculated spatial pore water pressure (PWP) distribution: (a) End of summer (September 2007), and (b) End of winter (March 2008) | 86 |
| 6.12 | Comparison of clay fill permeability influence on calculated pore water pressure variation at 1.9 m depth (March 2005 to March 2006) | 88 |
| 6.13 | Calculated spatial pore water pressure (PWP) distribution during extreme weather: (a) End of dry summer, and (b) End of wet winter | 91 |

| | | |
|------|---|-----|
| 6.14 | Wet winter pore water pressure profiles: (a) tree covered mid slope, and (b) grass covered lower slope | 92 |
| 7.1 | Variation of Soil Moisture Deficit (1988-2001) from the Meteorological Office Rainfall and Evaporation Calculation System, MORECS (Hough et al., 1997) with the timing of major earthworks failures indicated. (Reproduced from Ridley et al. (2004)) | 97 |
| 7.2 | Pressure heads measured across the London Underground Ltd network during spring 2001, plotted as depth below the clay surface | 98 |
| 7.3 | Comparison of March / April 2001 measured pressure head by embankment foundation material: (a) London clay foundation; (b) Chalk / terrace gravel foundation | 101 |
| 7.4 | Open standpipe (N2, N3 and N5-N8) and flushable Geo-Piezometer measurements at tree covered, London clay founded embankments in March / April 2001 (tree species and water demand not known) | 103 |
| 7.5 | Comparison of March / April 2001 pressure head by borehole slope position | 103 |
| 7.6 | Model geometry - Soil columns A to D. (Material properties for surface clay fill (SCF), clay fill (CF) and foundation (F) are shown in Table 7.2) | 107 |
| 7.7 | Soil Water Retention Curves for London clay (Croney, 1977), clay fill and chalk/gravel | 108 |
| 7.8 | Hydraulic conductivity curves for London clay, clay fill and chalk/gravel | 108 |
| 7.9 | Comparison of winter rainfall (1 October to 31 March) at Newbury, Heathrow Airport and Shoeburyness | 110 |
| 7.10 | The cumulative surface water balance (Σ rainfall – run off – evapotranspiration) calculated for soil columns A to D using Shoeburyness weather data, between October 2000 and October 2001 | 112 |
| 7.11 | Pressure head profiles in March 2001 plotted with the maximum pressure head envelope (March to May 2001) for finite element model A | 113 |

| | | |
|------|--|-----|
| 7.12 | Maximum March - May 2001 pressure head envelopes calculated using finite element models A to C (foundation permeabilities shown), representative of a grass or Low Water Demand tree covered slope | 114 |
| 7.13 | Change in pressure head at 2 m depth within a soil column of clay fill of typical permeability (model C) and lower permeability (model D) between 1 October and 31 May in 2000/2001, 2002/2003 and 2004/2005 | 115 |
| 7.14 | Comparison of maximum March - May 2001 pressure head envelopes from the finite element model with monitoring data: (a) London clay foundation; (b) Chalk / terrace gravel foundation | 117 |
| 7.15 | Maximum March - May pressure head envelopes calculated for 2001, 2003 and 2005: (a) London clay foundation (model C); (b) Chalk / terrace gravel foundation (model A) | 118 |
| 8.1 | Hawkwell embankment cross section. (Redrawn from Arup (2007)) | 124 |
| 8.2 | Hawkwell embankment tree plan. (Redrawn from Arup (2007)) | 125 |
| 8.3 | Monthly rainfall totals at Hawkwell embankment plotted with the 1971-2000 average rainfall for Greenwich | 129 |
| 8.4 | End of winter (March-April) volumetric water content, south embankment slope | 131 |
| 8.5 | End of winter (March-April) volumetric water content, north embankment slope | 132 |
| 8.6 | End of summer (August-September) volumetric water content, south embankment slope | 133 |
| 8.7 | End of summer (August-September) volumetric water content, north embankment slope | 134 |
| 8.8 | Comparison of summer volumetric water content variation, north midslope | 137 |
| 8.9 | Comparison of winter volumetric water content variation, north crest | 138 |
| 8.10 | Vertical displacements plotted relative to initial magnet positions in April 2006 | 139 |

| | | |
|------|--|-----|
| 8.11 | North crest piezometer measurements at 2.8 m, 3.7 m and 5.8 m depth | 141 |
| 8.12 | North midslope piezometer measurements at 1.3 m and 2.4 m depth | 142 |
| 8.13 | Comparison of SWRCs with field measured pore water pressure and volumetric water content at adjacent boreholes . . . | 143 |
| 8.14 | Model geometry - Soil columns representing the South midslope (SM), South crest (SC), North crest (NC) and North midslope (NM). (Material properties for Near surface clay fill (NSCF), Ash and ballast (A&B), Clay fill (CF) and London clay (LC) are shown in Table 8.2) | 145 |
| 8.15 | Soil water retention curves (SWRCs) describing variation of volumetric water content with pore water pressure | 147 |
| 8.16 | Hydraulic conductivity curves for London clay, clay fill, surface clay fill and ash and ballast | 147 |
| 8.17 | Water uptake - soil suction relationship (From Feddes et al. (1978) showing the anaerobiosis (ψ_{an}), maximum uptake (ψ_d) and wilting point (ψ_w). (See Section 4.2.6) | 149 |
| 8.18 | Comparison of calculated volumetric water content profiles calculated for 9 March 2003 | 151 |
| 8.19 | Calculated pore water pressure variation at 2 m depth from 1 January 2001 to 30 August 2009 | 151 |
| 8.20 | Calculated wetting and drying patterns at the north midslope | 152 |
| 8.21 | Calculated pore water pressure variation at 2 m depth from 1 January 2006 to 30 August 2009 | 154 |
| 8.22 | Comparison of calculated volumetric water content (before and after tree removal) with field measurements at the south embankment slope | 155 |
| 8.23 | Comparison of calculated volumetric water content (before and after tree removal) with field measurements at the north embankment slope | 156 |
| A.1 | Minimum tree planting distance at Site A (seasonal rail movement) | 171 |
| A.2 | Minimum tree planting distance at Site B (no seasonal rail movement) | 172 |

| | | |
|-----|--|-----|
| A.3 | Minimum tree planting distance at Site C (following tree felling) | 173 |
| A.4 | Measured seasonal movement by tree species | 174 |
| B.1 | Embankment model geometry | 178 |
| B.2 | Comparison of calculated pore water pressure at 2 m depth for slope positions at 2 m intervals (model A) | 179 |
| B.3 | Comparison of calculated pore water pressure at 2 m depth between model A and model B at the slope crest, midslope and toe | 180 |
| B.4 | Comparison of calculated pore water pressure at 2 m depth between soil column C and embankment model A | 181 |
| B.5 | Comparison of calculated pore water pressure profiles for March, April and May between soil column C and embankment model A | 182 |
| B.6 | Calculated components of total head (model A, 30 September 2001) | 183 |
| C.1 | Comparison of mean effective stress with local vegetation . . | 189 |

List of tables


| | | |
|-----|--|-----|
| 2.1 | Permeability of London clay fill and natural London clay (From O'Brien 2004) | 9 |
| 4.1 | Probable rooting depth ranges for selected tree species. (Adapted from Crow (2005)) | 47 |
| 5.1 | Summary of soil properties | 68 |
| 6.1 | Summary of soil properties | 78 |
| 6.2 | Charing climate scenarios | 81 |
| 6.3 | Maximum potential daily rainfall infiltration | 88 |
| 6.4 | Permeability measured at infrastructure sites (From Loveridge <i>et al.</i> (2010)) | 89 |
| 6.5 | Charing Model Summary | 94 |
| 7.1 | Summary of London Underground Ltd data | 100 |
| 7.2 | Summary of soil properties | 106 |
| 7.3 | Summary of climate data | 111 |
| 7.4 | Summary of climate boundary conditions | 111 |
| 8.1 | Summary of instrumentation | 128 |
| 8.2 | Summary of soil properties | 146 |
| 8.3 | Summary of climate boundary condition using Shoeburyness weather data | 149 |
| A.1 | Classification of water demand for various tree species (adapted from NHBC (2007)) | 167 |
| B.1 | Summary of soil properties | 176 |

| | | |
|-----|---|-----|
| C.1 | Results of <i>in situ</i> permeability testing at Charing | 187 |
| C.2 | Results of Guelph permeameter testing at Charing | 188 |
| C.3 | Moisture content of clay fill at Charing | 188 |

Declaration Of Authorship

I, Kevin Briggs, declare that the thesis entitled 'Impacts of climate and vegetation on railway embankment hydrology' and the work presented in it are my own. I confirm that:

- this work was done wholly or mainly while in candidature for a research degree at this University;
- where any part of this thesis has previously been submitted for a degree or any other qualification at this University or any other institution, this has been clearly stated;
- where I have consulted the published work of others, this is always clearly attributed;
- where I have quoted from the work of others, the source is always given. With the exception of such quotations, this thesis is entirely my own work;
- I have acknowledged all main sources of help
- where the thesis is based on work done by myself jointly with others, I have made clear exactly what was done by others and what I have contributed myself;
- parts of this work have been published as: journal papers, posters and technical documentation listed in appendix D.

Signed:  Date: 17/11/11

Acknowledgements

I wish to thank all the colleagues and friends who have supported and encouraged me, both directly and indirectly, throughout this research and my time in Southampton.

I would like to thank my sponsors Mott MacDonald, the University of Southampton and EPSRC for funding this research. Also London Underground and Network Rail must be acknowledged for their support in kind.

I am extremely grateful to my supervisors William Powrie, Joel Smethurst and Tony O'Brien for the exciting projects, for their enthusiasm, technical guidance and inspiring attitudes. I would like to thank the staff and research students of the Geomechanics Research Group at Southampton for their help and advice, in particular Fleur Loveridge, who showed me the ropes of applied research.

I wish to thank all the friends I have made in Southampton for an active and entertaining 4 years. In particular I would like to thank Jon, Jack, Nicholas, Cath, Tina and Gabi for the 'epic' adventures and too many good times to remember. Also Jon, Diana, Pete, Mark, Nicolas, Hatice, Ying and Nicola who joined Southampton with me in 2007 and shared the ups and downs of the postgraduate experience.

I thank my parents Mark and Andrea for their constant support throughout my life and my brother David for taking an interest in the technical detail. And finally, I thank Asa for adding that special something.

List of notation

| | |
|------------------|---|
| A | Inverse of relative humidity of the soil surface |
| AEV | Air Entry Value |
| B | Inverse of relative humidity of the air |
| C | Coefficient of consolidation |
| C_w^1 | Coefficient of consolidation with respect to liquid phase |
| C_w^2 | Coefficient of consolidation with respect to vapour phase |
| C_ψ | Fredlund correction function |
| C_ψ | Specific moisture capacity (Section 3.2) |
| D | Coefficient of diffusion (Section 3.4) |
| D | Cumulative infiltration (Section 4.1) |
| D_r | Root zone water depletion |
| E | Evaporative flux (Section 4.2.2) |
| E | Stiffness modulus |
| E_a | Vapour removal parameter |
| ET | Evapotranspiration rate |
| G | Soil heat flux density |
| I | Interception |
| K | Hydraulic conductivity |
| K_c | Crop factor (Section 4.2.3) |
| K_s | Saturated hydraulic conductivity |
| K_{st} | Water stress coefficient |
| L | Latent heat |
| LAI | Leaf Area Index |
| P | Pressure |
| P_v^{air} | Near surface air vapour pressure |
| P_{vsat}^{air} | Surface saturation vapour pressure |
| PE | Potential Evaporation rate |

| | |
|-----------------|---|
| PET | Potential Evapotranspiration rate |
| PT | Potential Transpiration rate |
| Q_n | Net radiant energy |
| R | Rainfall |
| RAW | Readily Available Water |
| RE | Soil water recharge |
| RO | Runoff |
| S | Degree of saturation |
| S | Soil water storage (Chapter 4) |
| S | Sorptivity (Section 4.1) |
| S_a | Degree of saturation due to adhesion |
| S_c | Degree of saturation due to capillary forces |
| S_{max} | Maximum plant extraction rate |
| S_s | Specific storage |
| $SWRC$ | Soil Water Retention Curve |
| TAW | Total Available Water |
| W | Wind speed |
| a | Intercept of water uptake depth relationship |
| a_f, m_f, n_f | Fredlund curve fitting parameters |
| a_v, m_v, n_v | van Genuchten curve fitting parameters |
| b | Gradient of water uptake depth relationship |
| c | Volumetric heat capacity |
| e | The natural number |
| e_a | Actual vapour pressure |
| e_s | Saturation vapour pressure |
| g | Gravitational constant |
| h | Total hydraulic head |
| h_ψ | Pressure head |
| i | Infiltration rate |
| i_0 | Initial infiltration rate |
| i_L | Limiting infiltration rate |
| k | Coefficient of permeability |
| k | Infiltration rate parameter (Section 4.1) |
| n | Porosity |
| p | Fraction of TAW a crop can extract without causing plant stress |
| p_a | Mean air density at constant pressure |

| | |
|-------------|--|
| q | Fredlund tortuosity curve fitting parameter |
| r_a | Aerodynamic resistance of plant leaves |
| r_s | Surface resistance of plant leaves |
| s | Fredlund slope function |
| t | Time |
| u | Pore water pressure |
| v_w | Flow rate of water |
| z_f | Depth of wetting front |
| z_r | Total root zone depth |
| α_h | Plant root water uptake limiting function |
| β | Compressibility of fluid |
| η | Psychrometric constant |
| Γ | Slope of saturation vapour pressure versus temperature curve |
| γ | Unit weight |
| λ | Thermal conductivity |
| ψ_0 | Initial matric suction |
| ψ_{an} | Soil suction at plant anareobiosis point |
| ψ_d | Soil suction at maximum root water uptake |
| ψ_i | Fredlund negative pore water pressure at curve inflection |
| ψ_r | Negative pore water pressure at residual water content |
| ψ_w | Soil suction at plant wilting point |
| ρ | Fluid density |
| θ | Volumetric water content |
| θ_r | Residual volumetric water content |
| θ_s | Saturated volumetric water content |

Chapter 1

Introduction

Seasonal changes in soil water content cause cyclic shrinking and swelling of clay fill embankments. The worst affected of these are old clay railway embankments, most of which were constructed more than 100 years ago. In highly plastic clay this volume change is known to affect track quality, causing disruption to rail services, particularly in London and the South East.

Field monitoring has shown that during dry summers, shrinkage of embankments occurs, causing track deformation and requiring line speed restrictions. During wet winters, embankment swelling and increases in pore water pressure due to water infiltration can cause slope failure. This was experienced during the wet winter of 2000/2001 when more than 100 slopes failed across the UK rail network (Turner, 2001). The need to improve understanding of climate influence on the behaviour of embankments was highlighted in a recent Rail Accident Investigation Report titled ‘Network Rail’s Management of Existing Earthworks’ (RAIB, 2008).

To prioritise and efficiently maintain ageing geotechnical assets, such as embankments, it is vital to provide an accurate evaluation of their current and future performance. Conventional stability analysis using limit equilibrium methods have proven unsuitable for assessing progressive embankment failure (Vaughan et al., 2004) and the transient nature of mechanical and hydrological behaviour. They make ‘steady state assumptions’ (O’Brien, 2007) which do not account for cyclic pore water pressure variation within an embankment in response to seasonal weather patterns. Transient analysis is required to identify the likely limits of pore water pressure during extreme

weather events and the critical parameters governing seasonal variation.

Numerical modelling has shown that changes in the soil water balance at the slope surface drives cyclic pore water pressure variation and the development of progressive failure. Until now, this has been modelled as a simplified, steady state hydraulic pressure at the slope surface, varying between a summer ‘suction’ and winter ‘zero pressure’ condition (Nyambayo et al., 2004; Scott, 2006).

In reality the soil-water balance is a more complex process driven by interdependent weather conditions, slope vegetation cover and unsaturated soil hydraulic conductivity, all of which vary constantly.

While extensive knowledge regarding soil-atmosphere processes is available in the hydrology and soil physics literature, there has been little exploration of how these processes influence pore water conditions within the UK’s infrastructure. Seasonal climate variation, low intensity persistent rainfall and the highly variable properties of clay fill make analysis of climate impacts on the UK’s railway infrastructure particularly unique.

Vegetation, a key component in the soil-water balance, is well documented as affecting pore water pressures and deformation of railway embankments, particularly in the presence of trees (McGinnity et al., 1998; Andrei, 2000; O’Brien et al., 2004). However, while vegetation has been considered as a surface boundary condition in climate-coupled numerical models (Davies et al., 2008; Nyambayo et al., 2004; Scott et al., 2007), the influence of water removal at depth by trees on the pore water pressure regime has not been demonstrated.

Periods of extreme wet weather have been correlated with increases in pore water pressure and embankment failures (Zawadski, 1995; Birch & Dewar, 2002; Ridley et al., 2004; Mott MacDonald, 2005). However, the controlling parameters and worst case conditions for increases in pore water pressure during extremely wet periods are not well understood.

This thesis explores the influence of climate-atmosphere processes and the impact of climate and vegetation on pore water pressures within railway earthworks. Field measurements from three instrumented embankments are presented as case studies. Observed patterns of soil wetting and drying, in response to climate, are compared with a hydrological finite element model incorporating daily weather data and vegetation root water uptake.

1.1 Objectives

- To review methods used to calculate water flow at the soil-atmosphere boundary and within saturated and unsaturated soil
- To critically review methods for estimating unsaturated soil water storage and hydraulic conductivity and derive suitable relationships for a clay fill material
- To examine the influence of weather on pore water pressures measured within an instrumented embankment and use a numerical model to determine the sensitivity of pore water pressure variation to weather extremes, soil permeability and vegetation cover
- To use field data and a numerical model to demonstrate the influence of permeability with depth on the rate and magnitude of pore water pressure increase within railway embankments during an extremely wet winter
- To demonstrate the influence of high water demand tree cover and tree removal on soil water content and pore water pressures within a heavily vegetated, instrumented embankment using field data and a numerical model
- To consider implications of the findings on earthworks assessment

1.2 Layout of the thesis

The first part of the thesis (chapters 2 to 5) presents the literature describing water flow in soils and at the soil-atmosphere boundary. Their applicability to railway embankments and UK climate is considered and unsaturated properties for a clay fill are derived.

Three case studies are presented in the second part of the thesis (chapters 6 to 8). Each examines a theme of climate influence on railway embankments. The chapters are as follows:

Chapter 2- Victorian railway embankments. The construction and composition of the UK's railway embankments is described. Observed ul-

imate limit and serviceability failure of embankments is presented, with a review of existing models of behaviour.

Chapter 3- Water flow in soils. A review of models used to calculate liquid and water vapour flow in saturated and unsaturated soils.

Chapter 4- Soil atmosphere boundary equations. A review of models used to calculate water input and removal from the soil at the soil-atmosphere boundary in response to climate.

Chapter 5- Soil water retention and hydraulic conductivity. A review of literature describing models of soil water retention and hydraulic conductivity in unsaturated soils. The unsaturated soil water retention and hydraulic conductivity of an embankment clay fill is estimated using curve fitting parameters.

Chapter 6- Climate influence on embankment hydrology: Charing embankment. Presentation of results from field monitoring and numerical modelling, examining climate influence on embankment hydrology. Comparison is made between field data and numerical modelling and further analyses consider extreme weather events and the sensitivity of results to clay fill permeability. Results and conclusions from this chapter have been presented in Loveridge et al. (2010) and Briggs (2010).

Chapter 7- Permeability influence on embankment hydrology: London Underground Ltd study. Analysis of field data collected across the London Underground Ltd network during the extremely wet winter of 2001. Comparison of field data with a numerical model investigating the influence of clay fill and foundation permeability on maximum pore water pressures during an extreme wet winter.

Chapter 8- Tree influence on embankment hydrology: Hawkwell embankment. Presentation of monitoring results from a heavily vegetated, instrumented embankment before and after vegetation clearance. Use of a numerical model to investigate the influence of tree removal on embankment pore water pressures and compare with monitoring data. Comparison of monitoring data with the estimated clay fill Soil Water Retention Curve

(SWRC) and prediction of maximum soil suctions.

Chapter 9- Conclusions. The main conclusions drawn from the case studies presented in this thesis are presented and implications for earthworks assessment are considered. Recommendations for further work are made.

Chapter 2

Victorian railway embankments

The United Kingdom has one of the world's oldest railway networks, of which a total of 660 miles was built between 1834 and 1841 and is still in use today (Skempton, 1996). The national rail network is owned and maintained by Network Rail, while the London Underground network is owned by London Underground Limited (LUL), a subsidiary of Transport for London (TfL). London Underground Ltd is responsible for more than 170 miles of surface railway, of which approximately 130 miles is supported by earth structures (embankment or cutting) (Phipps & McGinnity, 2001). In 2007 over 1 billion passenger journeys were recorded on London Underground (TfL, 2007), while the national rail network carried over 3 million passengers a day and 20 billion tonne kilometres of freight a year (Network Rail, 2007). Infrastructure owners are committed to reducing passenger 'delay minutes' by providing serviceable railway infrastructure, of which hundreds of miles of ageing embankment form a substantial part.

2.1 Construction techniques

The construction of the nine main railways built in England between 1834 and 1841 had no precedent and involved the excavation of 54 million m³ of material, most of which was used to form embankments (Skempton, 1996). Embankments were often constructed from locally excavated material, balancing 'cut' and 'fill' over short distances; thus embankment fill material

often reflects the local geology. Where there was insufficient cutting material, borrow pits were excavated either side of the embankment base in a process known as ‘side cutting’.

Embankment construction in shallow, 4 ft layers was specified as early as 1836 by John Macneill on the Slamannan Railway in Scotland. This would have allowed time for consolidation of the embankment and foundation but was considered to be too slow a process for large scale cut and fill. Therefore, the most commonly used construction method of the 1830s was to end-tip fill material from the advancing head of an embankment, constructing a full height embankment with little or no compaction. This construction method was disapproved of by Telford due to the effects of delayed consolidation and an increased likelihood of slippage (Telford, 1829).

Slips within embankments were a common occurrence during construction and were ‘nearly always restricted to clay fills’ (Skempton, 1996). Slips often occurred during wet winter weather but even in dry weather it was difficult to build embankments more than 10 m high by end-tipping or uncompacted work. Sometimes a very shallow slope gradient was required in order to stabilise an embankment, using up large quantities of material. Slips also occurred in clay cuttings and the process of deep-seated progressive softening of the clay was postulated by Charles Gregory in 1844, prior to Terzaghi’s investigations which led to research on the relationship between changes in pore pressure and failure (Terzaghi, 1936). The use of counterfort drains as a remedial measure shows an early appreciation for the importance of effective drainage.

Settlement of clay embankments often took place following construction due to the uncompacted nature of the material. During construction, additional clay would be used to repair the embankment, however an alternative material was used to make up for continuing post construction settlement. Ash was commonly used for this purpose and was also used as ballast up to 1945 (Vaughan et al., 2004). Successive widening of embankments, such as at Northwick Park on the London Underground network, has resulted in successive layers of clay fill, ash and ballast forming the embankment profile (Trans4m, 2005), contributing to a complex, heterogeneous embankment geology.

2.2 Construction material

UK railway infrastructure on both the National and London Underground rail network are often heterogeneous, being highly variable in geology and geometry. Detailed analysis of such infrastructure requires a site specific ground investigation. The embankments under consideration in Chapters 6, 7 and 8 are predominantly constructed of clay fill. Therefore the hydraulic properties of clay fill are described, demonstrating its difference from natural *in situ* clay. The general framework can also be applied to clay fills composed of different parent clays.

The structure and macro fabric of dumped clay fill is quite different from the *in situ*, natural clay. Figure 2.1 illustrates a conceptual model showing relatively stiff clods of original intact clay surrounded by a softer matrix of remoulded clay, silt and sand sized particles. These are likely to have been introduced, along with larger granular material, during embankment construction. This permeable matrix increases the permeability of dumped clay fill, relative to natural clay, and facilitates the growth of plant and tree roots. O'Brien et al. (2004) showed that the *in situ* permeability of dumped clay fill is more than an order of magnitude higher than both 34 laboratory measured and 24 *in situ* measured values for the parent clay, from which the fill is derived. This is shown in Table 2.1. The compressibility and shear modulus of the clay fill is determined by the clods, while the shear strength and permeability is a function of the matrix material (O'Brien et al., 2004).

Table 2.1: Permeability of London clay fill and natural London clay (From O'Brien 2004)

| Permeability (m/s) | | | |
|---------------------|----------------------|---|---------------------|
| Material type | Test type | Range | Median |
| London clay fill | <i>In situ</i> tests | 6×10^{-7} to 2×10^{-9} | 3×10^{-8} |
| London clay fill | Laboratory tests | 3×10^{-9} to 2×10^{-11} | 8×10^{-10} |
| Natural London clay | <i>In situ</i> tests | 1×10^{-9} to 1×10^{-10} | 3×10^{-10} |

When selecting embankment fill properties for analysis a simplified approach is required. Suggested mechanical properties are given in O'Brien et al. (2004), which include a simplified model of post peak degradation of strength. Similar values are used by Nyambayo et al. (2004) and Kovacevic et al. (2001). Standardised mechanical soil properties are used by London Underground (London Underground Ltd, 2000) when assessing slope stabil-

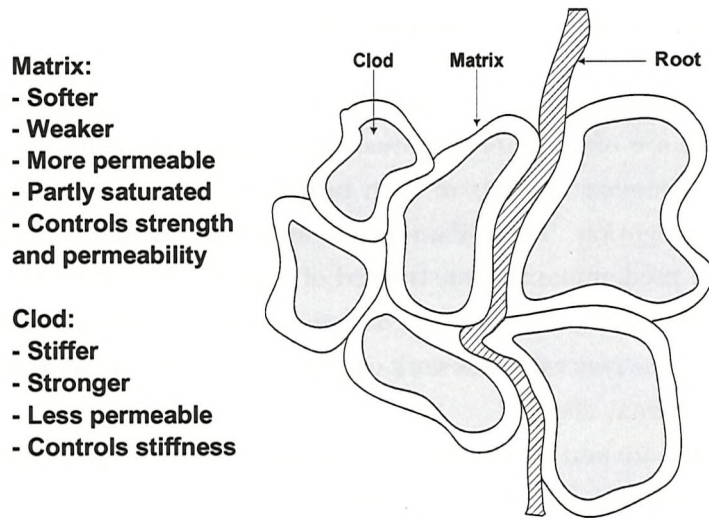


Figure 2.1: A conceptual model for dumped clay fill (O'Brien et al., 2004)

ity, with some modifications for advanced analysis (Mott MacDonald, 2004). However, there is little published information describing the permeability and unsaturated properties of clay fill for use in unsaturated flow analysis. This is addressed in Chapter 5.

2.3 Observed instability and deformation

Seasonal deformation of embankments can affect rail alignment, requiring constant maintenance, while ultimate failure of embankments and cuttings can cause serious damage to rail infrastructure and adjacent property. More than 100 slope failures occurred during the wet winter of 2000/2001 (Turner, 2001) and between August 2003 and December 2009 a total of 429 earthworks failures (embankments and cuttings) were recorded across the national railway network.

Shallow slope failures tend to be translational slips of a layer, not exceeding 2 m depth, which experience major changes in pore pressure due to rapid rainfall infiltration (Perry, 1989). The nature and frequency of shallow slope failures has been empirically related to rainfall characteristics in areas of abundant rainfall and high permeability soils, particularly in tropical areas (Leroueil, 2001). However, this is less common in the UK where rainfall

events are of lower intensity.

Deep seated slope failures occur in both embankments and cuttings due to soil volume change and reduction in soil strength. In cuttings a mechanism of deep seated, progressive failure is promoted by swelling of the soil due to long term recovery of pore water pressures following excavation (Potts et al., 1997). The low permeability of *in situ* London clay (Table 2.1) limits the rate of pore water pressure recovery, resulting in ‘delayed’ cutting slope failures occurring long after initial construction. The mechanism of deep seated failure in railway embankments, constructed of dumped clay fill, differs from that of cuttings due to differences in soil type and pore water pressure regime. During and shortly after construction failure of some embankments occurred during wet weather (Skempton, 1996), which was attributed to loss of suction within the clay fill. While most embankments remained stable following construction, cyclic shrinking and swelling of the clay fill in response to changes in pore water pressure can lead to strain softening of the soil and delayed, progressive failure.

Shrinkage and swelling of clay fill embankments in response to changes in soil water content is particularly problematic in high plasticity clays, where seasonal movements of up to 50 mm are recorded (Ground Engineering, 1996; Andrei, 2000; Scott, 2006). Embankment monitoring (Ridley et al., 2004) showed spring track heave and autumn track settlement due to increase and decrease in pore pressure respectively, in response to seasonal weather patterns. Vegetation has been recognised as beneficial in preventing shallow slips (Gray, 1994; Greenwood et al., 2004) and maintaining negative pore pressures (O’Brien et al., 2004) but trees have proven detrimental to embankment serviceability. Comparison of movements on a grass slope and a tree covered, high plasticity clay fill embankment showed that deformation was more than ten times greater adjacent to trees than grass (Scott et al., 2007). Scott et al. (2007) shows that this is due to their differing ability to remove water from the soil and influence pore pressures. A study of tree influence on seasonal rail deformation is presented in Appendix A.

O’Brien (2007) identified vegetation water demand, climate and clay fill permeability as key parameters governing pore water pressure variation within embankments which must be considered during assessment of serviceability and deep seated instability. Numerical modelling has been used to understand the mechanical behaviour of embankments, with some attempts

to model the influence of vegetation and climate.

2.4 Modelling embankment failure

Numerical modelling at Mott MacDonald investigated delayed failure and serviceability of embankments using the finite difference code FLAC (ITASCA, 1999). O'Brien et al. (2004) and O'Brien (2007) assumed post-peak shear strength degradation and soil stiffness properties based on laboratory testing of block samples obtained from London Underground Ltd embankments. As a development of cutting modelling (Potts et al., 1997; Ellis & O'Brien, 2007), a FLAC model was created with a surface boundary replicating a summer and winter condition for a 'grass covered' and 'high water demand tree covered' slope. This model was used to investigate progressive failure and excessive deformation of an instrumented London Underground embankment (Scott et al., 2007). Applied pore water pressure conditions, modelling grass and tree vegetation cover for a summer and winter condition, were based on an average between *in situ* pressures measured in the laboratory and field measurements (ICON, 1997). Analysis of the grass covered slope subjected to successive shrink-swell cycles showed that it was 'relatively stable' (Scott, 2006), although progressive failure did occur after 35 seasonal pore water pressure cycles. The tree covered slope, with greater surface boundary suctions, did not fail but did show greater strain softening than the grass covered slope. Scott et al. (2007) showed that high suctions applied during the summer cycle were not dissipated during the winter cycle, maintaining stability of the tree covered slope. Removal of the 'high water demand tree covered' boundary condition led to rapid slope failure within the model due to the strain softening previously induced.

O'Brien et al. (2004) found that failures developed in slopes that would otherwise be relatively stable when applying cyclic pore water pressure changes using FLAC. This was attributed to the simplified summer and winter boundary conditions applied to the model. Full pore water pressure equilibrium was assumed during each summer and winter cycle (i.e. cycling instantaneously between a 'summer' and 'winter' condition). This condition is representative of extreme pore water pressure variation occurring every year, when in reality this extreme condition would occur at less regular intervals. While this demonstrates the mechanism of slope failure in response to

cyclic pore water pressure variation, consideration of the natural variability of surface boundary suctions is required to provide a predictive capacity.

Rouainia et al. (2009) coupled a hydrological and mechanical model to predict slope movement in response to pore water pressure variation, induced by climate. Pore water pressure variation was calculated in a hydrological model using SHETRAN (Ewen et al., 2000), with a climate boundary condition. This considered daily weather data, providing seasonal climate boundary variation. The applied surface pore water pressures cycle from low winter to high summer suctions in response to weather conditions, rather than instantaneously switching between a winter and summer suction. The hydrological model was coupled with a geotechnical model, FLAC to flow (ITASCA, 1999), to assess daily slope movements in response to hydrological changes. This allows prediction of the slope response to future climate.

To achieve agreement between the Rouainia et al. (2009) model and pore water pressure profiles measured at a cutting in Newbury (Smethurst et al., 2006) it was necessary to increase the soil mass permeability of the SHETRAN model by two orders of magnitude above that measured in the field (from 1×10^{-9} to $1 \times 10^{-7} \text{ ms}^{-1}$). Rouainia et al. (2009) explains that this may have been necessary to increase the soil mass permeability because a higher surface permeability, which occurs in the field due to cracking and a broken soil surface, was not included in the numerical model. The need to reduce the saturated soil permeability could also be related to definition of the Soil Water Retention Curve (SWRC), which influences unsaturated hydraulic conductivity.

A coupled hydrological and mechanical model has been used to demonstrate climate influence on embankment stability (Rouainia et al., 2009). However, calibration of a numerical model with field observations and estimation of unsaturated soil properties for clay fill is required to investigate the influence of soil permeability, vegetation cover and extreme climate on embankment hydrology.

Chapter 3

Water flow in soils

To analyse the influence of climate and weather on pore water pressure variation within embankments an understanding of water flow within soils and available flow models is required. This includes a combination of concepts from hydrology, hydrogeology and soil mechanics. Hydrology is the study of water, addressing the ‘occurrence, distribution, movement and chemistry of all waters of the earth’ (Fetter, 1980). Hydrogeology concerns the interactions of water with the soil and rocks of the earth’s crust, particularly groundwater flow.

3.1 The hydrological cycle

The hydrological cycle forms a fundamental concept of hydrology, describing the cycling of water between land, ocean and air and characterising the incidence, behaviour and transformations of water in the environment. The hydrological cycle is illustrated in Figure 3.1 and is driven by solar energy, changing water between solid, liquid and vapour states. The process of *evaporation* causes liquid water in the oceans and on land to change to water vapour in the air. On land, this atmospheric moisture returns to the surface, having first condensed to form clouds and eventually precipitation. On reaching the ground surface, water has many routes by which to return to the atmosphere or the oceans, completing the hydrological cycle. This forms the area of interest for hydrologists, hydrogeologists and others who are interested in water interactions with the ground.

Not all precipitation reaches the ground. *Interception* is the process

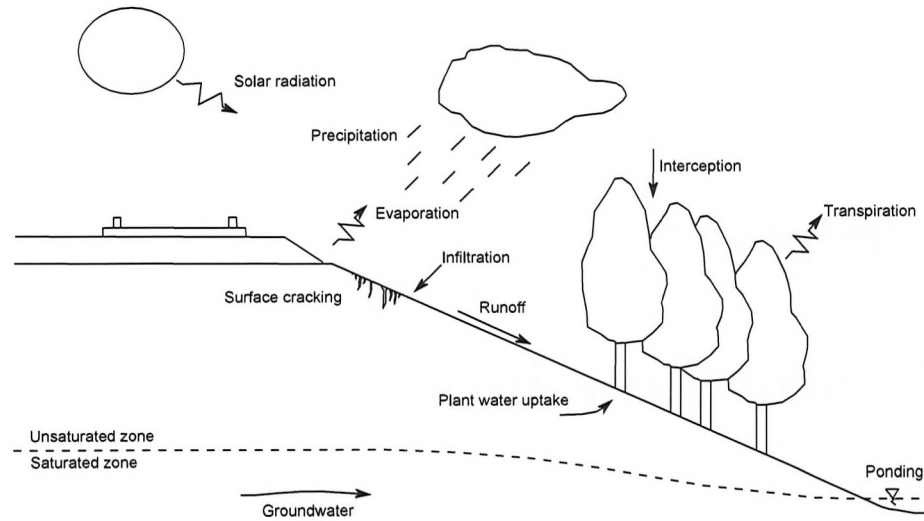


Figure 3.1: The hydrological cycle of a railway embankment

by which precipitation is temporarily stored on plant or other above ground surfaces, before being evaporated back into the atmosphere. If temperatures are cold enough some precipitation, falling as snow, may accumulate and store as snow pack before melting at a later date when temperatures increase.

When liquid water reaches the ground surface, some of the water moves into the soil by the process of *infiltration*. Once the infiltration capacity of the ground is exceeded excess water runs off the ground surface, flowing into nearby rivers and streams. Water that infiltrates the soil is stored as *soil water*, which is held in the unsaturated zone between the soil surface and the water table. Soil water returns to the atmosphere through evaporation from the soil surface or plant uptake within the root zone, as plants replenish water lost during *transpiration*.

Soil water also moves vertically and horizontally through the ground in response to pressure and gravity head gradients. Within the ground, downward movement of water is known as *percolation*, which can recharge the saturated region known as *groundwater*. The water table defines the upper boundary of groundwater, at atmospheric pressure, above which lies the *capillary fringe* or *tension-saturated zone*. This is a zone of soil in which the soil pores are completely filled with water, but the pressure head is less than atmospheric pressure. Lateral groundwater flow recharges streams, rivers and lakes, combining with overland flow to ultimately return water to

the ocean.

In hydrogeology the lateral flow of water within the ground is called *seepage*, consisting of flow through saturated and unsaturated soil. Within both the saturated and unsaturated zones, water movement (liquid and vapour) is driven by hydraulic head gradients. Total hydraulic head consists of pressure head, elevation head and velocity head. Since flow velocity within soils is very low, velocity head can be discounted. This makes pressure head (due to differences in soil water pressure) and elevation head (due to differences in elevation) the dominant forces of water seepage. Liquid water, vapour and heat flow in unsaturated soil must be quantified in order to understand water movement and its influence on soil pore water pressures within embankments.

3.2 Steady state and transient water flow

Pioneered by Casagrande (1937), the industry standard for slope stability focusses on flow within the saturated zone and assumes steady state flow. Steady state flow assumes that the hydraulic head and soil permeability are constant with time, throughout the soil mass. Within a flow field the magnitude and direction of the flow is constant with time.

Transient, unsteady flow allows for variation of hydraulic head and soil permeability in space and time. Water flow within a flow field will vary with time in direction and magnitude. As with steady state analysis, a particle of water entering the system at an inflow boundary will flow along a flow path towards the outflow boundary. However, unlike steady state analysis, the flow path is able to vary due to time dependent changes in hydraulic head and soil permeability.

To model soil water flow in response to a climate boundary condition, equations describing transient flow are required. In unsaturated soils both liquid and vapour water flow must be considered.

3.3 Liquid water flow within soils

The flow of water in saturated soil is commonly calculated using Darcy's law. Darcy's law states that the rate of water flow, or flux, through a soil mass is proportional to the hydraulic head gradient:

$$v_w = -k \frac{\delta h}{\delta y} \quad (3.1)$$

where

v_w = Flow rate of water in the y direction (ms^{-1}),

k = Coefficient of permeability (ms^{-1}),

$\delta h/\delta y$ = Total hydraulic head gradient in the y direction

The coefficient of permeability, k , is called the hydraulic conductivity (K) when referring to water flow. Hydraulic conductivity describes the ease with which a fluid can flow through the voids between soil particles and is relatively constant in saturated soil but not in unsaturated soil. Note that the Darcy seepage velocity, above, is derived by dividing the total volumetric flow rate by the cross sectional area of flow and is not the true fluid velocity through the pore spaces. This is found by dividing the flow rate by the cross-sectional area of the voids.

Equations for groundwater flow have been derived using Darcy's law, combined with the laws of mass conservation, the conservation of energy and the second law of thermodynamics. For two dimensional saturated flow, the rate of change in head with time is given by Freeze & Cherry (1979) (with the derivation attributed to Jacob (1950)) as:

$$K_x \frac{\delta^2 h}{\delta x^2} + K_y \frac{\delta^2 h}{\delta y^2} = S_s \frac{\delta h}{\delta t} \quad (3.2)$$

where

K_x, K_y = Coefficient of hydraulic conductivity in the x and y directions respectively (ms^{-1}),

h = Total hydraulic head,

S_s = Specific storage (m^{-1})

Specific Storage (S_s) describes the volume of water released owing to the expansion of water or compression of soil matrix due to change in head within a unit volume (Hantush, 1964):

$$S_s = \rho g(\alpha + n\beta) \quad (3.3)$$

where

ρ = Fluid density (kgm^{-3}),

α = Compressibility of porous medium (m^2N^{-1}),

n = Porosity (m^3m^{-3}),

β = Compressibility of the fluid (m^2N^{-1})

The flow equation is often used to calculate head and transient flow within aquifers, representing confined flow in a saturated, anisotropic porous medium. In steady state isotropic flow, where there is no change in head with time, this reduces to the Laplace Equation (shown for two dimensions):

$$\frac{\delta^2 h}{\delta x^2} + \frac{\delta^2 h}{\delta y^2} = 0 \quad (3.4)$$

In the field of soil mechanics, the flow of water in a compressible, saturated soil was presented as the ‘theory of consolidation’ by Terzaghi (1943). This consolidation theory provides a differential equation governing one dimensional consolidation due to changes in effective stress and the resulting excess pore water pressures (u_e):

$$\frac{\delta^2 u_e}{\delta z^2} C = \frac{\delta u_e}{\delta t} \quad (3.5)$$

Where C is the consolidation coefficient, KE'_0/γ_w and E'_0 is the one-dimensional stiffness modulus. The consolidation equation is a solution to the groundwater flow equation, for one dimension where the rate of water expulsion is able to remain equal to the rate of soil compression (Domenico, 1972). The consolidation coefficient, accounting for the stiffness and permeability of the soil, equates to the permeability and specific storage terms used in the groundwater flow equation. Specific storage describes compressibility of the soil skeleton and change in fluid density in response to pressure changes. This has been expanded by Biot (1940), creating a general theory of three dimensional consolidation. The Terzaghi (1943) and Jacob (1950) equations can be used to calculate one dimensional and two dimensional flow in saturated, compressible soils. However, to model water flow in embankments, above the water table, flow in the unsaturated zone must be described.

Darcy's law can be applied to water flow in unsaturated soil (Buckingham, 1907; Richards, 1931; Childs & Collins-George, 1950). However the coefficient of permeability (k) is replaced with the hydraulic conductivity, which varies with changes in soil water content and hence pore water pressure. Since water flow is partly saturated, the equation of continuity must contain terms for both the rate of change of moisture content and the rate of change of soil water storage. Richards' equation (1931) is a non-linear partial differential equation combining the equation for conservation of water mass and the Darcian flow law to create an equation governing transient water flow through a partly saturated porous medium. In two dimensions Richards' equation is as follows, in terms of pressure head h_ψ (Richards, 1931):

$$\frac{\delta}{\delta x} \left[K_{(\psi)} \frac{\delta h_\psi}{\delta x} \right] + \frac{\delta}{\delta y} \left[K_{(\psi)} \left(\frac{\delta h_\psi}{\delta y} + 1 \right) \right] = C_{(\psi)} \frac{\delta h_\psi}{\delta t} \quad (3.6)$$

The solution requires knowledge of characteristic curves relating hydraulic conductivity to pressure head, $K_{(\psi)}$ and *specific moisture capacity* to pressure head, $C_{(\psi)}$. Specific moisture capacity represents the unsaturated storage property of the soil and is derived from the slope of the Soil Water Retention Curve (SWRC), relating moisture content to pressure head. This equation can be converted to one in terms of total hydraulic head $h(x, y, t)$ through the relation $h = h_\psi + z$. Richards' equation, used in groundwater flow calculations, considers liquid-phase transport in the unsaturated zone but neglects vapour-phase transport (moisture movement). When considering interactions at the soil-atmosphere boundary such as infiltration and evaporation, it is correct to assume that water infiltrates in the liquid phase and evaporates in the vapour phase for a saturated soil. In an unsaturated soil however, both liquid and vapour phases are present within the soil voids, requiring formulations based on liquid and vapour flow.

3.4 Liquid-vapour flow within soils

Water movement in unsaturated soil consists of liquid and vapour phase flow. As water molecules move between the liquid and vapour phase, heat exchange occurs. Therefore analysis of moisture flow in unsaturated conditions, with atmospheric boundary conditions must provide for water vapour,

liquid water and heat flow.

Philip & de Vries (1957) presented two non-linear partial differential equations describing the simultaneous flow of liquid water, water vapour and heat transfer in porous materials:

$$\frac{\delta\theta}{\delta t} = \Delta(D_T\Delta T) + \Delta(D_\theta\Delta\theta) + \frac{\delta K}{\delta z} \quad (3.7)$$

and

$$c \frac{\delta T}{\delta t} = \Delta(\lambda\Delta T) - L_v\Delta(D_{\theta vap}\Delta\theta) \quad (3.8)$$

where

$\frac{\delta\theta}{\delta t}$ = Change in volumetric water content with time,

D_T = Thermal moisture diffusivity due to ΔT ($m^2s^{-1} \text{ } ^\circ C^{-1}$),

ΔT = Temperature gradient,

D_θ = Isothermal moisture diffusivity due to $\Delta\theta$ (m^2s^{-1}),

$\Delta\theta$ = Moisture content gradient,

$\frac{\delta K}{\delta z}$ = Change in hydraulic conductivity (unsaturated) with depth,

c = Volumetric heat capacity of the soil ($Jm^{-3} \text{ } ^\circ C^{-1}$),

$\frac{\delta T}{\delta t}$ = Change in temperature with time,

λ = Thermal conductivity ($Wm^{-1}s^{-1}$),

L_v = Latent heat of vapourisation (Jkg^{-1}),

$D_{\theta vap}$ = Isothermal vapour diffusivity due to $\Delta\theta$ (m^2s^{-1})

These equations apply for a homogeneous, isotropic porous medium with a rigid matrix structure within the limits of boiling and freezing (De Vries, 1987). In this formulation the flow of water vapour in the unsaturated soil is described using Fick's law ($D_{\theta vap}\Delta\theta$) (Fick, 1855). The Philip & de Vries (1957) formulation has been used in a number of soil atmosphere models giving good estimates of evaporative flux, water content and temperature profiles for short periods of evaporation ranging between two and seven days (Sophocleous, 1979; Camillo et al., 1983; Witono & Bruckler, 1989).

However, the accuracy of the models for extended periods of evaporation has not been demonstrated.

There are limitations which prevent the Philip and de Vries theory from being of use in geotechnical applications. First, the assumption of a rigid soil matrix does not allow for soil volume change, making it unsuitable for analysis of compressible soils. Secondly, the formulation assumes that liquid flow is due to gradients in volumetric water content, which is incorrect since flow of liquid water is due to gradients of total head (Buckingham, 1907; Richards, 1931; Childs & Collins-George, 1950). Finally, the formulation is only applicable to a homogeneous, isotropic porous medium, making it unsuitable for analysis of the multi layered, anisotropic soils encountered in geotechnical analysis. De Vries (1987) supports this by explaining that differences between theoretical fluxes and those measured in the laboratory and field may be due to the variability of natural soil. The issue of modelling hysteresis in the relationship between pore water pressure and soil moisture content was also identified. This continues to be an area that is difficult to quantify and is discussed in Chapter 5.

Dakshanamurthy & Fredlund (1981) formulated three differential equations governing the flow of water, air and heat in unsaturated soils. The flow model presented (Dakshanamurthy & Fredlund, 1981) is based on dimensional units commonly used by geotechnical engineers and accounts for volume change due to changes in total stress. Solutions to the equations were compared with field observations in a 2 m thick layer of Regina clay, replicating predicted volume change with time. Field measurements of moisture and heat flow rates were not compared with predicted values. A restriction of the Dakshanamurthy & Fredlund (1981) model is that only heat flow due to conduction is considered. This is acceptable for isothermal, low flow conditions. However, where there are likely to be large temperature gradients and flow rates, such as at the soil-atmosphere boundary, heat flow due to convection and phase change (latent heat of vapourisation) must be considered.

Wilson (1990b) and Wilson et al. (1994) presented a one dimensional flow model, combining heat and moisture flow equations. Heat energy consumption due to condensation and vapourisation was incorporated into the formulation, allowing soil-atmosphere modelling where significant liquid-vapour transformation occurs. Wilson (1990b) presented a derivation of the mois-

ture and heat flow equations, with simplifying assumptions to remove minor secondary terms and increase usability for calculating surface boundary flux:

For Moisture Flow

$$\frac{\delta h}{\delta t} = C_w^1 \frac{\delta}{\delta y} \left[k \frac{\delta h}{\delta y} \right] + C_w^2 \frac{\delta}{\delta y} \left[D_{vap} \frac{\delta P_{vap}}{\delta y} \right] \quad (3.9)$$

For Heat Flow

$$c \frac{\delta T}{\delta t} = \frac{\delta}{\delta t} \left[\lambda \frac{\delta T}{\delta t} \right] - L_v \left[\frac{P + P_{vap}}{P} \right] \frac{\delta}{\delta y} \left[D_{vap} \frac{\delta P_{vap}}{\delta y} \right] \quad (3.10)$$

where

h = Hydraulic head (m),

C_w^1 = Coefficient of consolidation with respect to liquid phase,

$$= \left(\frac{1}{\rho_w g m_w^2} \right),$$

m_w^2 = Slope of the moisture retention curve (1/kPa),

k = Coefficient of permeability (ms^{-1}),

C_w^2 = Coefficient of consolidation with respect to vapour phase,

$$= \left(\frac{1}{(\rho_w)^2 g m_w^2} \right),$$

D_{vap} = Coefficient of diffusion for water vapour through soil (kgm/kNs),

P = Total pressure in the bulk air phase (kPa),

P_{vap} = Partial pressure in the soil due to water vapour (kPa),

c = Volumetric heat capacity ($Jm^{-3} \text{ } ^\circ C^{-1}$),

T = Temperature ($^\circ C$),

λ = Thermal conductivity ($Wm^{-1} \text{ } ^\circ C^{-1}$),

L_v = Latent heat of vapourisation (Jkg^{-1})

The moisture and heat flow equations, which are non-linear with respect to head, position and time, were solved using a finite difference approach (Wilson, 1990b). Results were compared with laboratory data from a sand column drying test, recording the rate of evaporation and water content

change over a prolonged period of time, resulting in the development of high soil suctions. Close agreement was found between the measured and computed water contents and soil temperatures. Discrepancies occurred at low water contents as the drying front progressed. This was attributed to the choice of function describing the relationship between permeability and soil suction (Wilson, 1990b). The function used (Brooks & Corey, 1964) is thought to break down at residual degrees of saturation, resulting in a more abrupt change in calculated water contents at the drying front than was observed in the laboratory. Alternative methods for deriving this function are described in Chapter 5.

The heat and moisture flow equations derived by Wilson (1990b) have been incorporated into a number of finite element programs. A one dimensional finite element model was produced by Joshi (1993), reproducing the sand column drying test with reasonable agreement and taking 1% of the running time of the Wilson (1990b) program. A finite element model, based on the computer program SoilCover (SoilCover, 1993) was created, with an additional vegetation sink term (Tratch et al., 1995). This was used to replicate a laboratory drying experiment for a column of silt with vegetation cover, showing close agreement. SoilCover (SoilCover, 1997) was used to compare the performance of landfill cover materials (Wilson & Fredlund, 2000). This considered a fine silty loam, in addition to a fine sand, to facilitate choice of a landfill cover material but there was no validation against field data.

A number of assumptions have been made in the Wilson (1990b) mass transfer equations to reduce their complexity. Air and partial vapour pressure changes due to changes in soil volume have been ignored, therefore this model may not represent clay soils undergoing rapid volume change or sands exposed to intense infiltration. Wilson (1990b) considered this to be a reasonable assumption for soil wetting and drying under atmospheric conditions. This was a reasonable assumption for Wilson's experiment with uniform sand as this will experience little volume change during evaporation. However, for highly plastic clays this may not be valid since volume change is likely to occur, particularly near the ground surface where high moisture gradients may exist. Wilson (1990b) presented a more rigorous form of the transient flow equation for the liquid water phase, including the effects of air pressure changes due to volume change. This is far more complicated than

the simplified equation and has not been evaluated against a laboratory soil wetting or drying experiment.

3.5 Comment

A review of the literature has shown that the Wilson (1990b) equations provide simplified equations for heat and moisture flow in unsaturated soils. However, while the heat and moisture transfer equations quantify water and heat flow within a soil, they do not describe flow at the soil-atmosphere boundary or the relationship between hydraulic conductivity and soil suction. Further equations are required to model unsaturated flow in response to climate and vegetation using finite element analysis. A review of soil-atmosphere boundary equations and unsaturated soil water retention and hydraulic conductivity relationships are described in the following chapters.

Chapter 4

Soil-atmosphere boundary equations

The movement of water in soils is driven by hydraulic head differentials throughout the soil. In embankments and cuttings the zone of greatest pressure head variation is predominantly above the water table, driven by flow conditions at the soil-atmosphere boundary and influenced by atmospheric conditions. An understanding of the mathematical models representing water flow and changes in head at the soil-atmosphere boundary are required if soil water flow and changes in pore water pressure are to be modelled.

The soil water balance describes the inflow and outflow of water from the soil surface in response to atmospheric conditions. Water infiltrates the soil as rainfall and is lost via evaporation and transpiration, changing the volume of water stored in the soil. Blight (2003) describes the soil water balance equation as

$$\sum (R - I - RO) - \sum ET + S - RE \approx 0 \quad (4.1)$$

Where the sum of rainfall (R), interception (I) and runoff (RO), represent water input into the soil. Evapotranspiration (ET) is a function of the interaction between vegetation, soil and climate which, combined with recharge to the water table (RE), represents water output from the soil. (S) is the change in total water stored within the soil, allowing periods of net water input and net water output, which in the UK usually occurs over seasonal cycles. As described in Chapter 3.1, precipitation may also occur

as snow, sometimes infiltrating the soil at a later date as snow-melt. This is not a common occurrence in much of the UK.

The equations governing water input and output from the soil are described by first considering the equations for water input, and then the methods for describing water output via evaporation and transpiration.

4.1 Water input - infiltration and runoff

The process of water input into the soil via infiltration has been studied by both hydrologists and soil physicists. Water available for infiltration consists of rainfall not intercepted before reaching the soil surface. The Horton (1933) hydrological concept of infiltration is empirical, based on field observations showing that, during a rainfall event, water infiltration can be defined by a limiting curve of infiltration rate versus time. An initially high infiltration rate decreases with time until reaching a constant rate as the soil saturates (Figure 4.1). When the rainfall rate exceeds the infiltration rate capacity and the available surface storage capacity, water is assumed to run-off the soil surface creating overland flow.

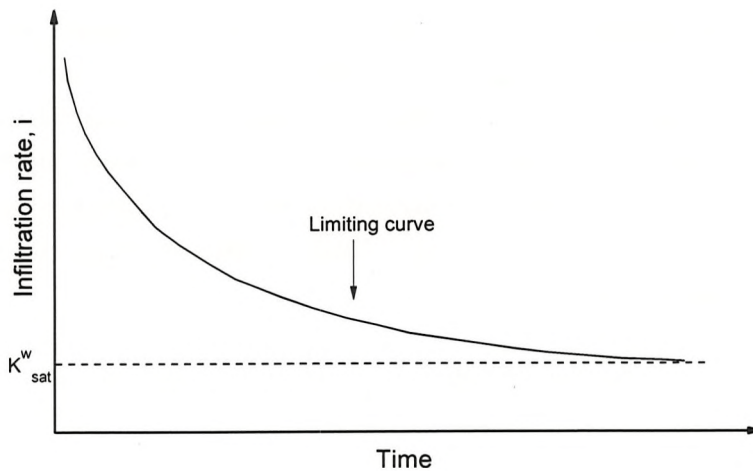


Figure 4.1: Infiltration rate versus time (Horton, 1933) (Redrawn from Giti-rana Jr. (2005))

This curve can be described by the expression (Horton, 1940)

$$i = i_L + (i_0 - i_L)e^{-kt} \quad (4.2)$$

where

i = Infiltration rate (ms^{-1}),

t = Time (s),

i_0 = Initial infiltration rate at $t = 0$ (ms^{-1}),

i_L = Limiting rate of infiltration (ms^{-1}),

k = Infiltration rate decrease parameter (s^{-1})

This empirical relationship requires experimental values for the constants i_0 , i_L and k , which describe the initial, final and rate of change of infiltration rate with time during a rainfall event. While not describing the physical processes controlling infiltration, this relationship has been widely used in hydrology (Wilson, 1990a).

Philip's expression (Philip, 1957):

$$i = i_L + \frac{1}{2}St^{-1/2} \quad (4.3)$$

reproduces the empirical curve given by Horton (1940), presenting an analytical solution based on the Darcy-Richards equations, assuming surface ponding. The limiting rate of infiltration i_L , corresponds to the saturated hydraulic conductivity of the soil. The sorptivity, S , is a single parameter embodying the influence of water content on transient flow ($ms^{-1/2}$) (Philip, 1957).

A simplified approach to calculating infiltration rate is attributed to the flow equation of Green & Ampt (1911). The solution has been shown to give good estimates of infiltration rate and cumulative infiltration in coarse grained soils producing a sharp wetting front. The Green & Ampt approach assumes a well defined wetting front, behind which the soil is uniformly wet and of constant hydraulic conductivity. At the wetting front the soil is assumed to change water content abruptly from its initial condition to that of the advancing saturated front, by an amount $\Delta\theta$. The Green & Ampt (1911) equation

$$i = \frac{\delta D}{\delta t} = \Delta\theta \frac{\delta z_f}{\delta t} = K_s \left(\frac{\psi_0}{z_f} + 1 \right) = K_s \left(\frac{\psi_0 \Delta\theta}{D} + 1 \right) \quad (4.4)$$

where

i = Infiltration rate (ms^{-1}),

D = Cumulative Infiltration (m) (where $D = \Delta\theta \times z_f$),

t = time (s),

$\Delta\theta$ = Change in volumetric water content at the wetting front (m^3/m^3),

z_f = Depth of wetting front (m),

K_s = Saturated hydraulic conductivity (ms^{-1}),

ψ_0 = Initial matric suction of the soil (m)

This assumes that the soil surface is maintained at a pressure head of zero, i.e. equivalent to shallow ponding. Difficulties may occur in the field when defining ψ_0 where the moisture profile is not uniform and for soils other than sand, where the wetting front may not be well defined (Hillel, 1980).

The Green & Ampt (1911) and Philip (1957) equations provide analytical solutions based on physical principles but are limited by the assumption of constant surface water ponding, which is not representative of a typical rainfall event. The Horton (1940) equation, while empirically based, qualitatively reproduces the infiltration curve and is not so restrictive in its mode of water infiltration.

In the soil physics literature, Hillel (1980) describes infiltration rate due to rainfall and ponding as being initially high and then falling to a lower rate, approximately equal to the saturated hydraulic conductivity of the soil. Infiltration into an unsaturated soil is influenced by both gravitational and suction gradients (Philip, 1957). Once the soil has saturated, suction gradients are negligible and infiltration continues at a rate equal to the saturated hydraulic conductivity, driven by the gravitational head gradient. The soil type influences infiltration rate, with the decline in initial infiltration rate being more rapid and the final constant rate lower for clay soils than sandy soils (Freeze & Cherry, 1979).

The effects of ponding depth and initial soil suction are significant during the early stages of infiltration but decrease with time, with the infiltration rate tending towards the saturated hydraulic conductivity of the soil.

Hillel (1980) describes the relationship between rainfall rate and infiltration, ignoring other near surface processes, in forming a number of phases.

When the rainfall rate exceeds the soil infiltration rate, the infiltration process can be described as that for surface ponding. If the rainfall rate is less than the initial infiltration rate of the soil but greater than the saturated infiltration rate, water will initially infiltrate at a rate equal to the rainfall rate. With time, as the soil infiltration rate reduces from its initial value to a value less than the rainfall rate, the soil surface will become saturated and ponding infiltration will occur. If rainfall rate is constantly less than the saturated infiltration rate, the soil will continue to absorb rainfall continuously without reaching saturation. These stages are described by Rubin (1966b) as

1. *Rainpond infiltration*, due to the presence of ponded water
2. *Preponding infiltration*, involving rainfall intense enough to produce ponding as the soil infiltration rate decreases
3. *Nonponding infiltration*, involving rainfall not intense enough to produce ponding

When rainfall ponding occurs at the soil surface (1) infiltration is controlled by the soil conditions and is described as *profile controlled*. Preponding (2) and nonponding (3) infiltration rates are controlled by the rainfall intensity and are described as being *flux controlled*. Under profile controlled conditions the surface boundary condition is assumed to be one of constant pressure at the surface, whereas for flux controlled conditions the water flux through the surface is assumed to be constant, or increasing (Rubin, 1966b). It is necessary to note that ponding is unlikely to occur on sloped surfaces as excess water is likely to run-off.

The stages of flux controlled and profile controlled infiltration are best illustrated by considering calculated infiltration rates into a sandy soil for different, constant rainfall rates (Figure 4.2). These curves were calculated using a finite difference technique, based on a pressure head based infiltration theory developed by Rubin (1966a). The horizontal parts of the curves correspond to preponding infiltration, followed by a reduction of infiltration rate during rainpond infiltration, when all rainfall intensities approach the same limiting infiltration rate.

Freeze (1974) produces infiltration rate curves similar to those given by Rubin (1966a) and measured empirically by Horton (1933) using an analyti-

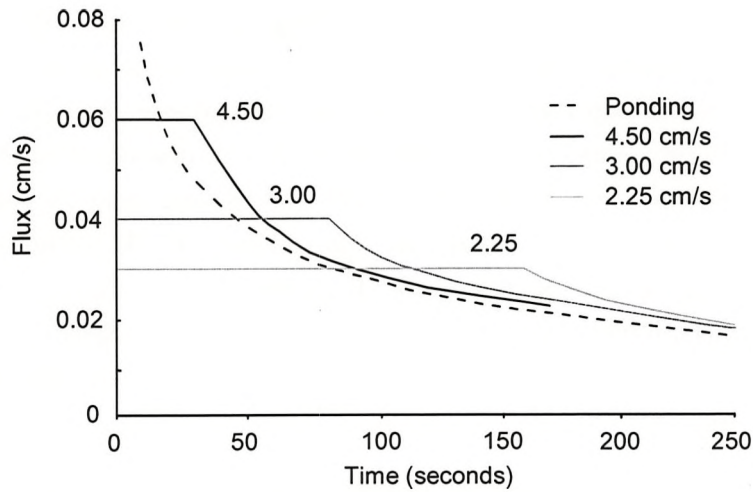


Figure 4.2: Surface flux with time for varying rainfall infiltration into Rehevet sand (Redrawn from Rubin (1966b))

cal approach. The curves were produced for a hypothetical, constant rainfall event using a numerical finite difference method solving Richards' equation for saturated and unsaturated flow in one dimension (Equation 3.6).

A precipitation boundary condition for numerically modelling infiltration into sloped surfaces has been developed by Smith (2003), using the Imperial College Finite Element Program. Smith (2003) modelled the profile controlled and flux controlled stages of rainfall infiltration by switching between pressure head and unit flux boundary conditions, preventing ponding and positive water pressures at the surface and using a predetermined pressure threshold value (THV). While this maintains realistic pore water pressures at the surface, unrealistic pore water pressure distributions can be created below the surface during periods of rapid infiltration. Therefore an iterative procedure for reducing modelling time steps to sub-increments during precipitation is required, details of which are summarised by Smith et al. (2008).

Gitirana Jr. (2005) does not switch between boundary conditions to prevent ponding at the slope surface. Instead a flux boundary, comprising two separate conditions is applied at the slope surface, reproducing the infiltration stages predicted by Rubin (1966a). When ponding occurs, and positive pore water pressures are created at the slope surface, a net flux (ms^{-1})

$$NF = EF \times (0 - u_{ws}) \text{ if } u_{ws} \geq 0 \quad (4.5)$$

is applied, where u_{ws} = positive pore water pressure at the surface and EF = ‘a large number’ (Gitirana Jr. et al., 2005). If EF tends to infinity then the net flux becomes a large negative value, removes ponded water from the surface and becomes equivalent to a boundary condition $u_{ws} = 0$. A regular flux boundary condition (e.g. Rainfall - Evapotranspiration) can then be applied. This has been implemented into the seepage analysis package SVFlux (SoilVision Systems Ltd, 2005) using FlexPDE (PDE, 2005) as a partial differential equation solver engine. Gitirana Jr. (2005) compared this method with the switching boundary condition technique by comparing infiltration calculated using FlexPDE with Vadose/w (Geo-Slope, 2005) for a range of rainfall rates. Close agreement between the methods was found for rainfall rates below $2 \times K_s$. Above this rate, Vadose/w (2005) was found to initially underestimate water infiltration when compared to the Horton (1933) infiltration curve as it was slow to respond to high pore water pressure gradients. SVFlux gave closer agreement to the Horton (1933) infiltration curve by using an adaptive meshing technique where high pore water pressure gradients existed. Smith et al. (2008) and Gitirana Jr. (2005) highlighted the importance of meshing and calculation time steps when modelling infiltration with high pore water pressure gradients. The latest version of Vadose/w (2007) includes an adaptive time-stepping function to facilitate this, however adaptive meshing is not available. Therefore a finer mesh should be used in areas of high pore water pressure gradient, such as near the soil surface.

When there are layers of more than one soil type in a column of soil, the infiltration wetting front may become hindered, producing a positive pressure front within the soil. Edgers & Nadim (2004) used Seep/w (Geo-Slope, 2007) to model a low conductivity layer within a soil column, mimicking the change in conductivity found within steep hillsides in Norway. They found that a low conductivity layer acted as a seepage barrier, allowing positive pore pressures to develop at the soil layer boundary. It was also found that for soils with a steep hydraulic conductivity function the progression of a positive pore water pressure through the soil causes a large conductivity contrast with the unsaturated soil below. This causes the unsaturated soil

to act as a seepage barrier creating a transient, perched water table.

The methods based on solution of the Richards equation (Freeze, 1974; Smith, 2003; Edgers & Nadim, 2004; Gitirana Jr., 2005) provide a more rigorous analysis of infiltration than the empirical equation proposed by Horton (1940) or the Green & Ampt (1911) and Philip (1957) equations, which are limited by the assumption of surface ponding. However, care must be taken when choosing time steps within the model if reliable results are to be obtained.

4.2 Water output - evaporation and transpiration

Water removal from the soil occurs due to evaporation from the soil surface and transpiration by plants removing water from within the soil. Often, due to difficulties in separating measurement of evaporation and transpiration, the term *evapotranspiration* is used to describe both interdependent processes (Hillel, 1980). Both evaporation and transpiration are driven by solar energy and limited by soil water availability. Conditions where evaporation and transpiration are at their maximum possible value, given the available solar energy, are termed ‘potential’. Where evaporation and transpiration rates fall below the potential, due to lack of available water, the rate is described as ‘actual’.

4.2.1 Potential evaporation

Three conditions are necessary for evaporation from a soil surface to occur (Penman, 1948; Hillel, 1980). First, there must be a continual supply of heat to provide energy for the vaporisation of water. This can come from the soil itself, or more commonly from an external heat source such as the sun. Second, the vapour pressure in the air above the soil must be lower than the vapour pressure at the soil surface, and vapour must be transported away by diffusion or convection. Both of these conditions – the supply of energy and removal of water vapour – are external to the soil body and are influenced by the atmosphere. The third condition is that a continual supply of water must be available for evaporation. This is controlled by subsurface conditions within the soil.

The Penman Equation (Penman, 1948) is a model for calculating potential evaporation (PE) from a free water surface, requiring the input of

routine weather parameters such as relative air humidity, air temperature, solar radiation and wind speed. This builds on the Dalton type evaporation equation calculated using differences in near surface and air vapour pressures, combined with an energy budget equation (Brutsaert, 1982):

$$PE = \frac{\Gamma Q_n + \eta E_a}{\eta + \Gamma} \quad (4.6)$$

where

PE = Potential vertical evaporative flux ($mm \ day^{-1}$),

Γ = Slope of the saturation vapour pressure versus temperature curve at the mean temperature of the air ($kPa \ ^\circ C^{-1}$),

Q_n = Net radiant energy available at the surface ($mm \ day^{-1}$),

η = Psychrometric constant,

E_a = A vapour removal parameter, $0.35(1+0.15W)(P_{vsat}^{air} - P_v^{air}) \ (ms^{-1})$,

W = Wind speed ($km \ hr^{-1}$),

P_v^{air} = Near surface air vapour pressure (kPa),

P_{vsat}^{air} = Surface saturation vapour pressure at the mean air temperature (kPa)

The Penman equation, derived for evaporation from a free water surface, can be applied to a bare soil surface, assuming that water is freely available. This makes it unsuitable for evaporation from dry soils, where the supply of water may be limited. Linsley et al. (1949) showed that temperature assumptions made when calculating Q_n in the Penman equation can result in overestimation and underestimation of potential evaporation under calm, humid conditions and windy, dry conditions respectively. However, it does provide a widely adopted method for calculating potential evaporation under most atmospheric conditions.

4.2.2 Actual evaporation

The Penman Equation (Penman, 1948) describes potential evaporation from a free water surface, and can be applied to a bare soil surface where water

is freely available. However, when water is not readily available for evaporation the actual rate of evaporation decreases below its potential rate (Hillel, 1980). Hillel (1980) describes the evaporation process as consisting of three stages.

1. *Stage I drying*, is the maximum or potential evaporation rate when the soil is near saturation. This is flux controlled.
2. *Stage II drying*, occurs when soil conductivity decreases and evaporation cannot be maintained at the potential evaporation rate as water availability reduces. This is profile controlled.
3. *Stage III drying*, occurs when the soil is sufficiently dry that the liquid-water phase becomes discontinuous and water vapour movement occurs at a residual rate. This is profile controlled.

The Penman equation describes flux controlled drying due to atmospheric conditions (Stage I). Wilson (1990b) provided a physical relationship, based on the Penman equation for calculating actual evaporation from an unsaturated soil, for flux and profile controlled evaporation. The Wilson equation is a modified Penman equation, replacing the water surface vapour pressure with the soil surface vapour pressure and considering hydraulic properties of the soil profile. Wilson (1990b) presented the modified Penman-Wilson equation:

$$E = \frac{\Gamma Q_n + \eta E_a}{\Gamma + \eta A} \quad (4.7)$$

where

E = Evaporative Flux ($mm \ day^{-1}$),

Γ = Slope of the saturation vapour pressure versus temperature curve at the mean air temperature ($mm \ Hg \ ^\circ C$),

Q_n = Net radiant energy available at the surface ($mm \ day^{-1}$),

η = Psychrometric constant,

$E_a = 0.35(1 + 0.146 W) P_v^{air}(B - A) \ (ms^{-1})$,

W = Wind speed (kmh^{-1}),

P_v^{air} = Near surface air vapour pressure (kPa),

A = Inverse of relative humidity of the soil surface,

B = Inverse of relative humidity of the air

This replaces the saturated vapour pressure at the soil surface p_{vsat}^{air} from equation 4.6 with the actual vapour pressure at the soil surface. If the soil surface is saturated (i.e. A = unity for a relative humidity of 100%) the equation reduces to the original Penman equation.

Wilson (1990b) conducted a laboratory sand drying experiment to verify a soil-atmosphere evaporation model. The model calculated evaporative flux at the soil surface based on Dalton type evaporation and calculated soil water heat and moisture flow below the soil surface using equations 3.9 and 3.10. Both the soil-atmosphere model and the laboratory experiment showed the three stages of evaporation as described by Hillel (1980) and show that actual evaporation can be determined for unsaturated soil conditions by calculating actual vapour pressure. Wilson et al. (1994) suggested that the Penman-Wilson equation describing actual evaporation, combined with the soil heat and moisture flow equations would be applicable to field conditions where evaporation is controlled by atmospheric and profile conditions.

4.2.3 Potential evapotranspiration

Water removal from soil by plants, in addition to surface evaporation (when water is freely available) is called potential evapotranspiration (PET). During a crop growing cycle, total evapotranspiration will vary between 100% evaporation at sowing and 10% evaporation, 90% transpiration when full crop cover is achieved (Allen et al., 1998). A number of evapotranspiration models exist (Penman, 1948; Thornwaite, 1948; Blaney & Criddle, 1950; Priestley & Taylor., 1972; Doorenbos & Pruitt, 1977). These methods have been evaluated for a grass reference crop and a single guideline has been developed (Allen et al., 1998). This is described below.

Transpiration is the evaporation of water from plants. Transpiration, like evaporation, is controlled by available energy, vapour gradients and air movement but can be limited by the plant resisting water flow by closing stomata on the plant leaves in response to a lack of available soil water. The Penman-Monteith equation (Allen et al., 1994) describes evapotranspiration

including factors for surface resistance (r_s) and aerodynamic resistance (r_a):

$$ET = \frac{\Delta(Q_n - G) + p_a c_p \left(\frac{e_s - e_a}{r_a} \right)}{\Delta + \eta \left(1 + \frac{r_s}{r_a} \right)} \quad (4.8)$$

where

ET = Evapotranspiration ($mm \ day^{-1}$),

Q_n = Net radiation at the crop surface ($MJm^{-2}day^{-1}$),

G = Soil heat flux density ($MJm^{-2}day^{-1}$),

p_a = Mean air density at constant pressure (kgm^{-3}),

c_p = Specific heat of air ($Jkg^{-1} \ ^\circ C^{-1}$),

e_s = Saturation vapour pressure (kPa),

e_a = Actual vapour pressure (kPa),

$e_s - e_a$ = Saturation vapour pressure deficit (kPa),

Δ = Slope of vapour pressure curve ($kPa^\circ C^{-1}$),

η = Psychrometric constant ($kPa^\circ C^{-1}$)

r_s = Surface resistance (sm^{-1}),

r_a = Aerodynamic resistance (sm^{-1})

The surface resistance describes the resistance of water vapour flowing through stomata openings, leaf area and root zones. Aerodynamic resistance describes the friction from air flowing over vegetated surfaces. Both resistance factors describe a complex process which is constantly changing, depending on environmental conditions and the development of plant growth. Therefore, a simplified approach is recommended by the World Meteorological Organisation (WMO) and the Food and Agriculture Organisation of the United Nations (FAO). The modified FAO Penman-Monteith equation estimates potential evapotranspiration (PET) for a standard crop known as a 'reference crop' using the Penman-Monteith equation. Reference evapotranspiration, PET_0 , describes a 15 cm tall, well watered grass crop, for which values of r_s and r_a have been defined. PET for different crop

types and crop growth stages is then calculated by factoring the reference crop PET_0 , by a crop factor K_c :

$$PET = PET_0 \times K_c \quad (4.9)$$

Resistance factors (crop factors) for a range of crop types and crop growth stages can be found in Allen et al. (1998).

4.2.4 Actual evapotranspiration

The modified Penman-Monteith method is recommended as the sole standard method by the Food and Agriculture Organization of the United Nations (FAO) and is commonly used for crop irrigation (Allen et al., 1998). In addition to the standard method, for a well watered crop, empirically measured coefficients are available for calculating actual evapotranspiration (ET). This may be less than PET where soil water is not freely available to the plants under soil water stress conditions.

Actual evapotranspiration is limited by the total available water (TAW) within the plant root zone. Some of this water is readily available water (RAW), contained in large voids and fissures, but once this water is removed soil water stress conditions occur and further evapotranspiration is reduced below the potential rate. It is assumed that there is no upward flow into the root zone from the soil below. Allen et al. (1998) provided empirically measured coefficients for calculating total and readily available water for a range of crop types. These can be used to derive a value for the water stress coefficient K_{st} (where $0 \leq K_{st} \leq 1$), which can be used to convert PET to actual ET for soil water limiting conditions. For soil water limiting conditions ($D_r \geq RAW$),

$$K_{st} = \frac{TAW - D_r}{TAW - RAW} = \frac{TAW - D_r}{(1 - p)TAW} \quad (4.10)$$

where

D_r = Root zone water depletion (mm),

p = Fraction of TAW that a crop can extract from the root zone without causing plant stress

This method, derived for crop irrigation, has been incorporated into geotechnical engineering analysis. A modification of the Penman-Monteith equation was used to calculate the water balance (Equation 4.1) for a cutting near Newbury (Smethurst et al., 2006), using the program CROPWAT (Clarke et al., 1998). Close correlation was found between measured and calculated soil moisture deficit over one year, replicating observed seasonal variation in soil water. The concept of Soil Moisture Deficit (SMD) provides a tool for understanding and comparing the wetness and the dryness of the soil for different years and seasonal cycles. This is of use to engineers and infrastructure owners when assessing seasonal risk to infrastructure and identifying SMD thresholds where seasonal problems may occur (Birch & Dewar, 2002).

The FAO Penman-Monteith equations form the basis of the Meteorological Office Rainfall and Evaporation System (MORECS), which provides weekly soil moisture deficit estimates for $40\text{km} \times 40\text{km}$ grid squares over the UK. These outputs are for use in assessment of catchment water balance, the leaching of nutrients and short-term irrigation requirements (Hough et al., 1997). MORECS has been used to compare seasonal embankment movement with the SMD for a site in London (Scott, 2006; Scott et al., 2007), showing qualitative agreement, but Smethurst et al. (2006) highlight the importance of using site specific data if close correlation is to be achieved.

4.2.5 Potential transpiration

Transpiration is difficult to measure and calculate because it can be difficult to determine the proportion of solar radiation received by the soil and that received by the plant (Blight, 2003). Hence evapotranspiration is often considered as one term. This is useful for large scale remote sensing applications, however, at the local scale this is not suitable because evaporation and transpiration remove water from different depths within the soil profile. Evaporation occurs at the soil surface, removing near surface water. Transpiration removes water from within the plant rooting zone, therefore removing water at depth. For large vegetation, such as trees, this can be considerably deeper than for smaller vegetation such as grass and shrubs.

Feddes et al. (1978) and Tratch et al. (1995) calculated potential transpiration as a fraction of evapotranspiration depending on the degree of vegetation cover, as proposed by Ritchie (1972). The level of vegetation

cover, the Leaf Area Index (LAI), is used to divide available solar energy between that available for direct evaporation from the soil surface and that available to the plant for transpiration. LAI (m^2m^{-2}) represents the total one-sided area of photosynthetic tissue per unit area of ground surface (Watson, 1947; Monteith, 1973). Many measurement methods are available, from direct, leaf collection methods to indirect non-contact methods, such as hemispherical photography (Jonckheere et al., 2004) and satellite measurement (Morissette et al., 2006). While a number of LAI measurement methods are available and a large number of estimation methods are described in the literature, each has varying strengths and weaknesses, with there being no standard procedure. The various measurement methods, combined with the dynamic nature of LAI, varying seasonally and annually, has resulted in a large variation in published LAI values.

The potential transpiration equation proposed by Ritchie (1972) is an empirical relationship requiring estimation of the LAI:

$$PT = PE(-0.21 + 0.70 LAI^{0.5}) \quad (4.11)$$

where

PT = Potential transpiration rate ($mm \ day^{-1}$),

PE = Potential evaporation rate for a bare soil surface ($mm \ day^{-1}$),

LAI = Leaf area index ($0.1 \leq LAI \leq 2.7$)

Ritchie (1972) describes three degrees of vegetation cover assuming either: surface evaporation only, combined evaporation and transpiration or solely transpirative conditions. These three phases are described as bare soil, partial cover and full cover conditions. Ritchie (1972) defines the LAI for full leaf cover as $2.7 \ m^2m^{-2}$ and as $0.1 \ m^2m^{-2}$ for a bare soil surface, where transpiration is negligible. Therefore, when there is full leaf cover all solar energy is assigned to transpiration, while for the bare soil condition all solar energy would be assigned to surface evaporation only. Between these limits partial vegetation cover exists, allowing both evaporation and transpiration.

Measurements of LAI greater than 2.7 have been measured for deciduous trees (Dantec et al., 2000). Ritchie (1972) would not consider LAI

greater than 2.7 as contributing to greater transpiration as full cover has already been achieved. This is a reasonable assumption conceptually, as leaves shaded by other leaves would receive less solar radiation, but the value of 2.7 LAI might not equate to full cover for all crop types.

Ritchie (1972) warned that the proposed empirical relationship requires validation in climates other than that in the study (Texas) but it was shown to compare well with results for barley in England (Monteith et al., 1965). The Ritchie (1972) relationship applies to transpiration from a row crop canopy. This could be used for calculating transpiration from a uniform vegetation cover, such as grass, but would not be applicable to trees, where plant distribution, leaf orientation and ground cover would not be uniform. Information regarding LAI has been determined at a large scale for grass cover using remote sensing methods (Scurlock et al., 2001), showing seasonal LAI variation. This could be applied to the Ritchie (1972) equation to demonstrate seasonal variation in transpiration due to grass crop cover. This would be indicative because it cannot be assumed that the Ritchie (1972) method is applicable to grass crops and compatible with the LAI measurements of Scurlock et al. (2001). However, this would be an improvement on the current method of transpiration modelling in geotechnical engineering, where a constant, average daily transpiration is applied (Indraratna et al., 2006), or vegetation leaf cover is varied seasonally but is not crop specific (Rouainia et al., 2009).

4.2.6 Actual transpiration and root water uptake

Plants transmit to the atmosphere more than 90% of water they extract from the soil, making water uptake a function of the evaporative demand of the atmosphere rather than a function of plant use (Hillel, 1980; Radcliffe et al., 1980). A plant has roots in a soil-water reservoir while above the surface the vapour pressure gradient between the leaves and the atmosphere cause transpiration, creating a potential gradient and flow through the plant. A plant must balance daily evaporative demand with an irregular supply of water from intermittent rainfall, relying on reserves of soil-water during dry periods (Hillel, 1980). During dry periods the plant's ability to draw water from the soil is dependent on the pore water pressures within the ground. Root water uptake describes the rate and spatial distribution of water removal from the soil by plant roots in response to transpiration.

Root water uptake in plants has been described using mesoscopic and macroscopic models. Mesoscopic models consider radial flow of water towards a single plant root (Gardner, 1960; Nimah & Hanks, 1973; Hillel et al., 1976). Difficulties occur when trying to incorporate this root water uptake term into water flow models due to the in difficulty measuring the total number of plant roots, which can vary with time. Macroscopic models are often used to describe the general behaviour of root water uptake.

Macroscopic models describing transpiration using mathematical equations represent root water uptake as a volumetric sink term applied to the flow continuity equation (e.g. Equation 3.9). Various forms of the volumetric sink term have been developed, using parameters to describe atmospheric, root growth and soil water conditions (Gardner, 1964; Feddes et al., 1974, 1976; Prasad, 1988; Tratch et al., 1995; Nyambayo & Potts, 2010). Root distribution at the macroscopic scale has been treated differently by various authors. Gardner (1964) assumed a root density function, considering the surface area of the roots per unit volume of soil and the distance that water moves through the soil towards the root. The pressure head at the soil root interface is assumed to be constant throughout the root zone. Feddes et al. (1974) reviewed literature for twenty three crops, showing that root water uptake is proportional to root mass, which varies exponentially with depth. This requires sampling of the root mass with depth to determine an empirical parameter for root water uptake, making this approach unsuitable for use outside the laboratory. Feddes et al. (1978) proposed an approach for root water uptake as a function of soil water content, applied uniformly over a given root depth:

$$S_{max} = \frac{PT}{z_r} \quad (4.12)$$

Where S_{max} ($mm^3 \ mm^{-3} \ day^{-1}$) is the maximum extraction rate for a well watered soil, PT ($mm \ day^{-1}$) is the potential transpiration rate and z_r (mm) is the total depth of the root zone. For conditions where available soil water limits root water uptake a plant limiting function was recommended by Radcliffe et al. (1980), Perrochet (1987) and Novak (1987), of which the most commonly adopted is (Feddes et al., 1978):

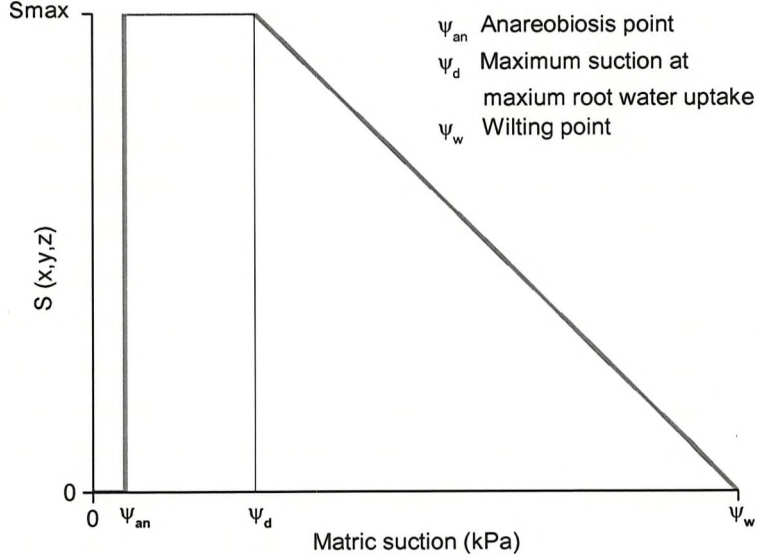


Figure 4.3: Water uptake - soil suction relationship (From Feddes et al. (1978) showing the anaerobiosis (ψ_{an}), maximum uptake (ψ_d) and wilting point (ψ_w)

$$S(h) = \alpha(h) S_{max} \quad (4.13)$$

Where $\alpha(h)$ is a prescribed function of the soil pressure head describing the plants limiting ability to withdraw water from the soil as soil suctions increase, assuming the root depth has achieved its maximum value. This is shown in Figure 4.3 where ψ_{an} is the anaerobiosis point, below which oxygen deficiency prevents transpiration, ψ_d is the maximum suction before water uptake reduces and ψ_w is the soil suction at wilting point, at which point the plant would cease to uptake water. The concept of a plant limiting function has been experimentally confirmed by Kutilek & Nielsen (1994) and adopted in subsequent root water uptake models (Prasad, 1988; Tratch et al., 1995; Indraratna et al., 2006; Nyambayo & Potts, 2010).

Prasad (1988) proposed a linearly decreasing water extraction rate with depth, as described by Hoogland et al. (1981), adjusted to ensure that zero water uptake occurs at the base of the root zone with maximum water uptake at the surface:

$$S_{max} = a - b.z \quad (4.14)$$

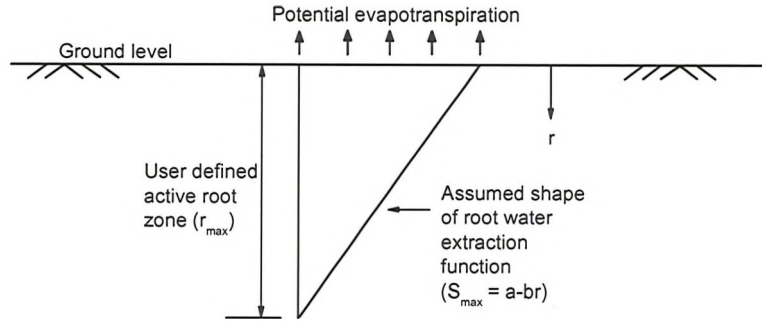


Figure 4.4: Shape of the root water uptake function using a linearly decreasing water extraction rate with depth (Prasad, 1988). (From Nyambayo & Potts (2010))

Where S_{max} is the maximum water extraction at depth z below the ground surface when soil water is readily available. Coefficients a and b are the intercept and the slope gradient of the water uptake-depth relationship respectively (Figure 4.4). The total transpiration rate is obtained by integrating Equation 4.4 over the whole root depth.

Root water uptake was simulated using the Feddes et al. (1978) and Prasad (1988) root water uptake models for five crops under well watered conditions, assuming transpiration only, and compared to laboratory measurements by Ernie et al. (1965). It was shown that the linearly varying root uptake term (Prasad, 1988) gave much closer agreement with the experimental results, replicating the variation in water removal with depth within the plant root zone (Figure 4.5). This is in agreement with Ernie et al. (1965), showing that the plant roots mainly remove water from the upper soil layers, with less removal at depth. This appears to be suitable for modelling water uptake by small plants such as grass, which give uniform ground and root cover, but may not be applicable to large trees.

Indraratna et al. (2006) used a volumetric sink term, applied to the flow equations, to model root water uptake by a tree. Tree root zones differ from those of smaller plants, spreading to a greater extent to remove a greater volume of water from the soil and provide structural support to the tree (Biddle, 1998). Indraratna et al. (2006) assumed the root length density distribution (m/m^3) reduces exponentially with depth and radial distance from a maximum, predetermined point away from the tree trunk, based on

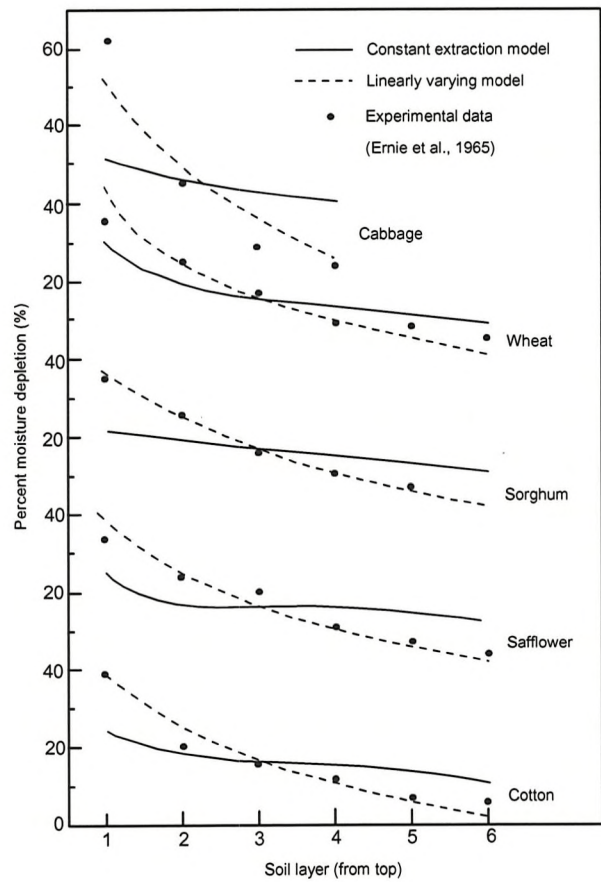


Figure 4.5: Comparison of experimental and theoretical soil water removal with depth for five crop types (From Prasad (1988))

the findings of Docker & Hubble (2001) and Landsberg (1999). Landsberg (1999) suggested that the relationship between relative water uptake rate and root length density is non-linear and produces an inverted cone shaped root zone.

The Indraratna et al. (2006) model showed good agreement with pore water pressures measured adjacent to a eucalyptus tree by Jaksa et al. (2002). However, comparison of calculated and field measured moisture content for a single lime tree in the UK (Biddle, 1998), showed less agreement. Indraratna et al. (2006) attributed this to uncertainties in the assumptions of soil, atmospheric and root distribution parameters. Using the Prasad (1988) linear root water uptake model, Nyambayo & Potts (2010) showed that the size and pattern of the dessication profile adjacent to a tree is dependent on the maximum root depth. However, the numerical results were not compared with field measurements.

Crow (2005) provided probable root depth for a variety of UK tree species in different soils, adapted from Mitchell & Jobling (1984) and Pyatt et al. (2001). Root depths for trees and soil types relevant to the railway embankment case studies presented in later chapters are shown in Table 4.1.

Table 4.1: Probable rooting depth ranges for selected tree species. (Adapted from Crow (2005))

| Species | | Soil groups (Crow (2005)) | | |
|--|--------------|-----------------------------|----|--------|
| Scientific name | Common name | 1 | 2 | 3 |
| Acer pseudoplatanus | Sycamore | * | ** | ≤ 1.5m |
| Fagus sylvatica | Beech | ** | ! | ≤2 m |
| Fraxinus excelsior | Ash | * | ** | ≤2 m |
| Malus sylvestris | Apple | ≤3 m | ! | ≤4 m |
| Populus alba | White poplar | ** | ** | ≤2 m |
| ** Conditions not recommended for growth | | 1 = Loose well drained soil | | |
| * Not ideal and growth may be impeded | | 2 = Shallow soil over rock | | |
| ! Values are conjectural (not from database) | | 3 = Loamy soil | | |

Green & Clothier (1999) measured the spatial and temporal patterns of water uptake for a well watered, mature apple tree using Time Domain Reflectometry (TDR) and root sap flow measurements. It was observed that 70% of tree water uptake occurred in the top 0.4 m of the root zone, where approximately 70% of the tree roots were located. Application of partial irrigation, to one side of the tree, showed that the roots responded

rapidly, shifting the pattern of water uptake within hours. Because of this ‘highly opportunistic’ (Biddle, 1998), transient nature of root distribution and root water uptake, modelling tree water uptake poses a considerable modelling challenge. Vrugt et al. (2001) found that model errors regarding the geometry of the rooting system and the inhomogeneity of unsaturated, variable soils made comparison between modelled and site measured root water uptake very difficult. Biddle (1998) also warned that any description of root systems must allow for local soil conditions, which can influence a root system. In an embankment constructed of uncompacted fill, the nature of the fill may alter the spatial root distribution beyond ‘typical’ extents.

4.3 Comment

A review of the literature described the range of soil-atmosphere boundary equations available for calculating the soil water balance. The equations show that the rate of actual evaporation and transpiration reduces below the potential rate when soil water is not freely available. This is likely to occur in railway embankments, which are typically unsaturated. The literature shows that evaporation and transpiration can be considered separately, or as a combined evapotranspiration term. A root water uptake term may be used to model water removal at depth by deep rooted vegetation such as trees, which are commonly found on embankment slopes. However there is limited ability to model the transient nature of root distribution and patterns of root water uptake due to trees, other than to consider transpiration rate and the depth of root water uptake.

Chapter 5

Soil water retention and hydraulic conductivity

The equations describing liquid water flow through porous materials require a hydraulic conductivity coefficient, K , to describe the ease with which water can flow through a material. In a saturated soil this is constant for a given material and fluid (described as the *intrinsic permeability*). However, negative pore water pressures within a soil can cause de-saturation, altering the soil's hydraulic and mechanical properties. In an unsaturated soil, the ease with which water can flow varies with the degree of soil saturation, soil water content and soil suction; all of which are interrelated. To model water flow through unsaturated soils using equation 3.9 the relationship between hydraulic conductivity, soil water storage and the interrelated soil saturation properties must be understood and quantified. This can be achieved by using a Soil Water Retention Curve (SWRC) which forms a 'conceptual, interpretive and predictive model' for understanding unsaturated soil behaviour (Barbour, 1998) and has been 'shown to be key to the implementation of unsaturated soil mechanics' (Fredlund, 2000).

5.1 The Soil Water Retention Curve

As a soil de-saturates, the soil water content reduces and the total suction between soil particles increases, restricting flow. During the first stage of the de-saturation process large pores in the soil drain and fill with air, reducing the flow path area and decreasing the hydraulic conductivity of the soil. As

de-saturation continues due to soil suction, the water in the soil is drawn increasingly closer to the soil particles, further reducing the flow area. The term soil suction can refer to matric suction (the pore air pressure minus the pore water pressure) or the total suction (matric plus osmotic suction). It is suggested that the term SWRC is used to describe the relationship between volumetric water content and matric (soil) suction (Fredlund & Xing, 1994).

The soil suction can be used to describe the change in soil hydraulic conductivity with reduction in water content (de-saturation). This is achieved by defining two curves. The first is known as a SWRC, describing the volume of water stored in the soil in relation to soil suction. The second is the hydraulic conductivity curve, defining the change in soil hydraulic conductivity with change in soil suction. This can be predicted with sufficient accuracy for many engineering problems using the saturated permeability and the SWRC (Fredlund, 2000).

The SWRC can be broken down into four components (Figure 5.1):

- The saturated water content describes the water content of the soil when all voids are filled with water (θ_s).
- The Air Entry Value (AEV) describes the soil suction at which air first enters the largest soil pores during de-saturation and they drain freely (Brooks & Corey, 1964). Beyond the AEV, increase in soil suction results in reduction of volumetric soil water content and hydraulic conductivity.
- The slope function defines the steepness of the curve beyond the AEV and is related to the uniformity of the pore sizes. A fairly uniform pore size in sand produces a steep slope function as all the pores drain over a small range of negative pore water pressures. A clay soil has a larger range of pore sizes and hence will produce a shallower slope function.
- The residual water content (θ_r) describes the point at which further increases in soil suction do not produce significant reductions in water content. This is described, for consistency, as the ordinate of the intersection of lines drawn at tangent to the inflection point and high suction curve (Fredlund & Xing, 1994). Removal of water to less than residual requires evaporative or osmotic forces.

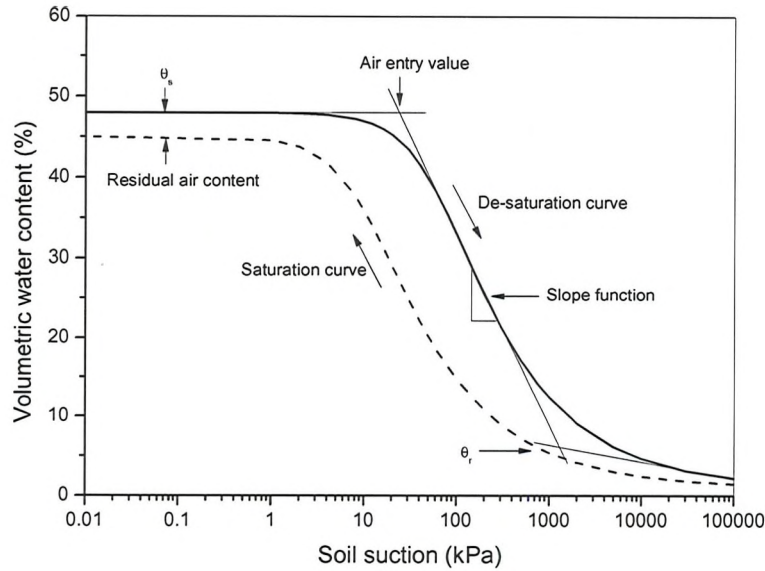


Figure 5.1: The soil water retention curve (Adapted from Fredlund & Xing (1994))

Comparison of a clay and sand soil demonstrates how the SWRC varies for different soil types. Figure 5.2 shows how for a coarse grained soil, such as sand, the uniform nature of the pore sizes allows water to be removed from the soil over a short suction range, producing a steep slope function. Yang et al. (2004) found that a clay soil with a larger range of pore sizes will release water over a large suction range and a coarse-grained soil has a lower air-entry value and less total hysteresis than a fine-grained soil. SWRCs of uniform soils have steeper slopes and less total hysteresis than those of less uniform soils. The maximum total suction in soils has been experimentally established as slightly less than 10^6 kPa (Croney & Coleman, 1961) and corresponds to zero relative humidity in a porous material (Richards, 1965). The residual air content shown in Figure 5.1 illustrates that the end of the saturation curve may differ from the starting point of the de-saturation curve if air is trapped in the soil (Fredlund & Xing, 1994).

The relationship between the SWRC and the hydraulic conductivity of a sand and a clayey silt, between 1 kPa and 1000 kPa suction is shown in Figure 5.3. The hydraulic conductivity of the soils remains constant until the air entry value is reached, beyond which volumetric water storage and hydraulic conductivity rapidly decreases. The unsaturated permeability of a soil can be predicted by integration of the SWRC with respect to water

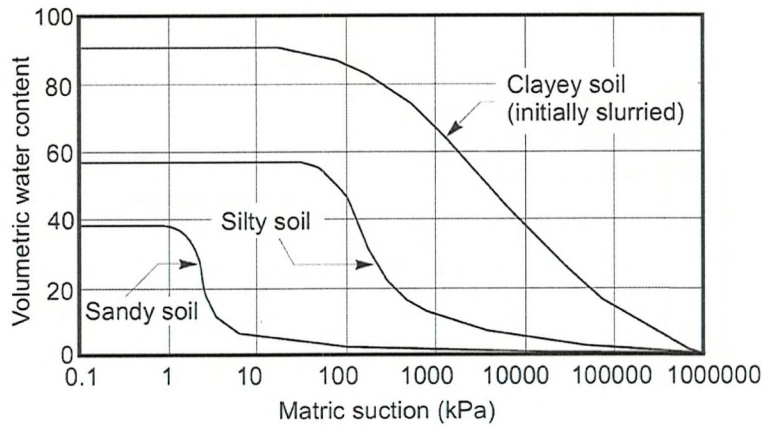


Figure 5.2: Typical Soil Water Retention Curves (After Fredlund & Xing (1994))

content (Marshall, 1958; Mualem, 1976) and therefore the rate of decrease in hydraulic conductivity is related to the SWRC. For example, Figure 5.3 shows the saturated permeability of the sand is two orders of magnitude greater than the clayey silt, however, reduction in hydraulic conductivity with increasing suction occurs more rapidly in the sand, and beyond 200 kPa suction the hydraulic conductivity of the sand is lower.

5.2 Hysteresis

The components of the Soil Water Retention Curve are shown in Figure 5.1. Figure 5.1 primarily shows the de-saturation or ‘drying’ SWRC. The saturation or ‘wetting’ curve is also shown. These two *main branches* describe changes from saturation to dryness and vice versa, between which intermediate stages of wetting and drying may occur as a soil moves from one main branch to another along scanning curves (Figure 5.4). The hysteresis effect means there is no single or unique SWRC for a particular soil, with an infinite number of wetting and drying scanning curves bounded by the main wetting and drying curves .

The main branches representing the de-saturation and saturation phases of soil often differ, with the amount of water held in a soil during de-saturation being greater than that during saturation, at a given suction. This effect means that more force is require to exude than absorb water from a soil at a given water content. The dependence of the soil water

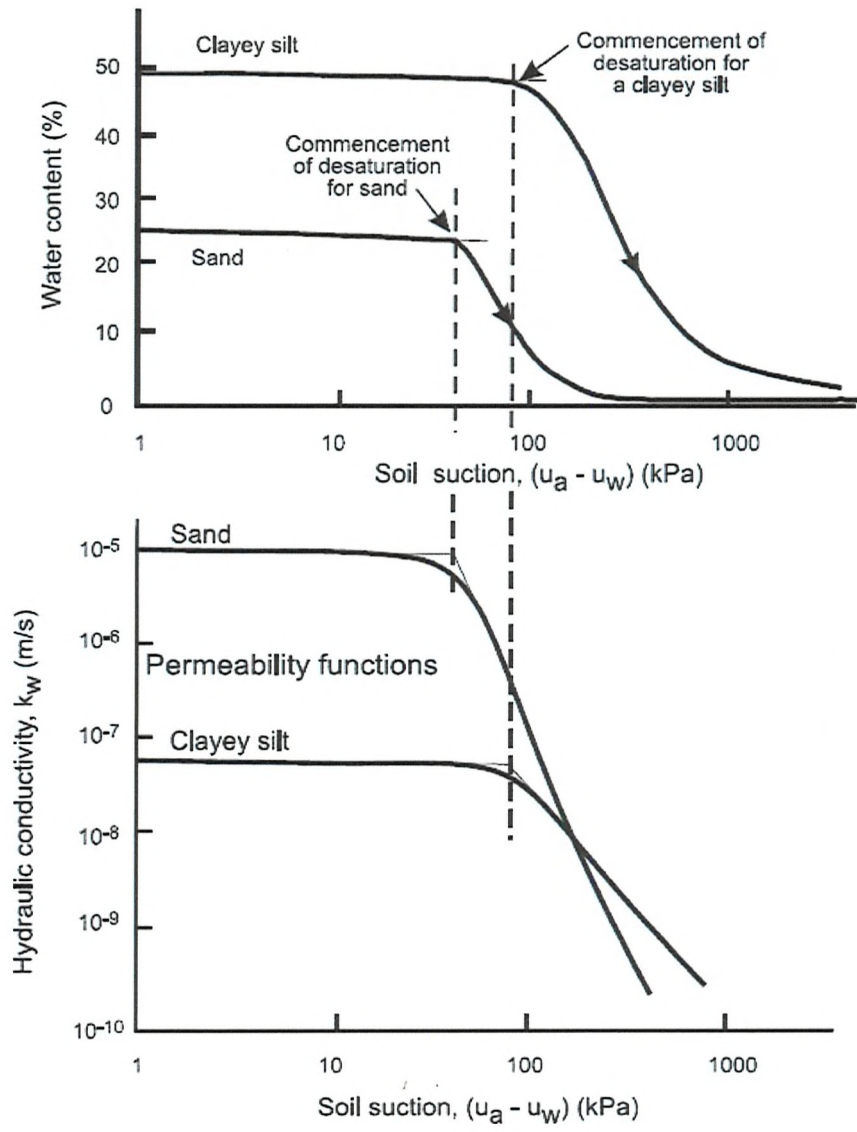


Figure 5.3: Typical soil water retention and hydraulic conductivity functions for a sand and a clayey silt (From Fredlund (2000))

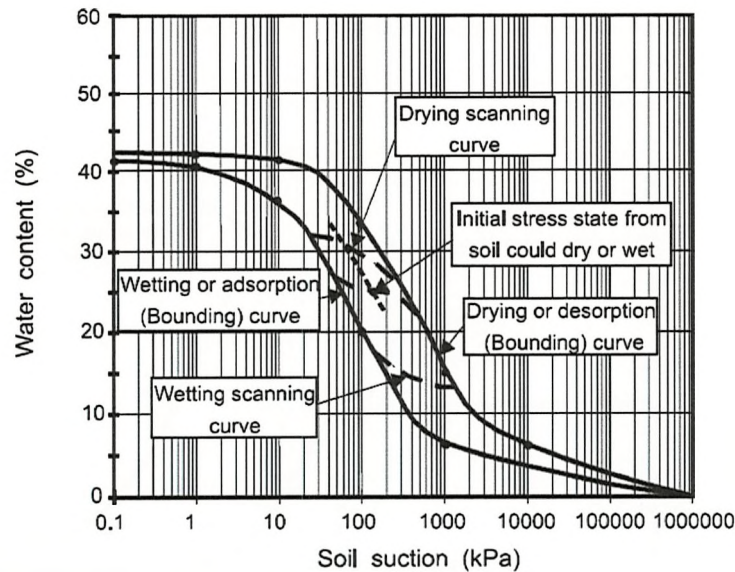


Figure 5.4: Wetting and drying Soil Water Retention Curves and scanning curves (From Fredlund (2000))

content on the process leading up to it is called *hysteresis* and has been attributed by Hillel (1980) to

1. The 'ink bottle' effect where the irregular voids in a soil, connected by smaller passages, require de-saturation through the narrow connecting channels while saturation is limited only by the size of the large pores.
2. The liquid-solid 'contact angle' of the water meniscus on the walls of soil pores tends to be greater in an advancing, wetting meniscus than a receding, drying one, resulting in greater suctions in drying than wetting.
3. Entrapped air within soil voids decreases the water content of a wetting soil and may increase the hysteresis effect.
4. Changes in soil structure due to shrinking, swelling and aging of the soil.

Croney (1952) demonstrates that hysteresis affects the equilibrium moisture content in a soil profile, producing a different equilibrium profile depending on whether the soil is wetting or drying towards equilibrium. How-

ever, the range of possible SWRCs and hysteresis is often ignored in geotechnical analysis due to the complexity of its use. The saturation or wetting curve is difficult to determine and its derivation is seldom attempted (Hillel, 1980). Therefore the term SWRC is often used to describe the de-saturation or drying curve only. The wetting curve is of importance when considering embankment instability because increases in pore water pressure result from wetting of the soil. Limitations in available data and methods for inclusion of both wetting and drying SWRCs in numerical models will therefore limit the accuracy of computed results.

5.3 Soil Water Retention Curve measurement

The principles of SWRC measurement are based on methods developed in the early 1900s which involve bringing the soil specimen to thermodynamic equilibrium with a reservoir of water at a known energy state (Barbour, 1998). The Richards pressure plate (Richards, 1928), the capillary potentiometer (later high suction tensiometer) and osmotic desiccator (Richards, 1928) are all used to measure changes in soil water content with soil suction. The soil water content corresponding to high suctions (greater than 1500kPa) requires an osmotic desiccator containing a salt solution, while the other methods are more suitable for measuring lower suctions (Fredlund, 2000). Fredlund & Rahardjo (1993) provide a detailed review of available measurement methods. Steady-state laboratory measurement of SWRCs over a large suction range (beyond 1500 kPa) is expensive and time consuming (Benson & Grib, 1997).

Experimentally obtained drying curves for a range of soils are available in the SWRC literature (Croney, 1977) and soil properties databases for the USA (USDA, 2009) and Europe (Wosten et al., 1999). The preparation of the soil samples should be considered when selecting a SWRC; Croney (1952) showed that slurring of a soil sample and destruction of the soil structure drastically alters the ability of the soil to absorb and release water, producing a different SWRC to an undisturbed sample. Examples of drying SWRCs for undisturbed samples of London clay and other clays found in the South East of England can be found in Croney (1977).

5.4 Theoretical methods for estimating the Soil Water Retention Curve

A number of methods have been developed to describe SWRCs and hydraulic conductivity relationships based on measurable soil properties and curve fitting parameters (Mualem, 1976; van Genuchten, 1980; Fredlund & Xing, 1994; Aubertin et al., 2003). The use of such curves has been adopted in the analysis of slope stability and other geotechnical problems involving unsaturated water flow and unsaturated soil strength (Childs, 1940; Fredlund & Rahardjo, 1993; Barbour, 1998; Smethurst et al., 2006; Davies et al., 2008; Mott MacDonald, 2009). Leong & Rahardjo (1997) evaluated the available SWRC estimation methods and found the van Genuchten (1980) and Fredlund & Xing (1994) equations, which are both of a similar form, to best describe SWRCs. The SWRC of a soil can also be estimated using a grain size distribution, as proposed by Aubertin et al. (2003), allowing preliminary prediction of SWRC for use in geotechnical practice. The derivation of the SWRC, describing soil water storage variation with suction, and curves describing hydraulic conductivity variation with suction will be described using the methods of Aubertin et al. (2003), van Genuchten (1980) and Fredlund & Xing (1994).

5.4.1 The Aubertin grain size distribution

Aubertin et al. (2003) presented a method to predict the relationship between volumetric water content and soil suction (SWRC) using a particle size distribution, based on a modification of the method proposed by Kovacs (1981). Particle size distribution can be measured in the laboratory using sieve analysis. Soil information such as the particle-size, the particle shape and the soil porosity are used to define the degree of saturation as forming two components. This is then converted to a volumetric water content function. The first component of the degree of saturation is the amount of water stored by capillary forces at relatively small suctions S_c . This is obtained from a cumulative pore-size distribution function. The second component, S_a , relates to the degree of saturation at large suctions, where water within the soil is held by adhesion. This is based on the approximations of Kovacs (1981) relating the adhesion saturation to suction. The degree of saturation is defined as follows:

$$S = \frac{\theta}{n} = S_c + S_a^*(1 - S_c) \quad (5.1)$$

where

S = Degree of saturation,

θ = Volumetric water content,

n = Porosity,

S_c = Degree of saturation due to capillary forces,

S_a^* = Degree of saturation due to adhesion (S_a)

S_a^* is used instead of S_a to ensure that the adhesion component does not exceed unity at low suctions. For S_a greater than or equal to 1, $S_a^* = 1$ but if S_a is less than 1, $S_a^* = S_a$. Derivation of the S_c and S_a components are described in Aubertin et al. (2003).

Aubertin et al. (2003) provided a tool for deriving the de-saturation curve of SWRCs but did not describe the relationship between hydraulic conductivity and soil suction, for which another equation must be used. Aubertin et al. (2003) warned that the proposed SWRC estimation does not consider factors such as hysteresis or the soil stress history. Importantly the method neglects soils with a heterogeneous or multimodal pore size distribution (Burger, 2001) or very coarse particles (Yazdani et al., 2000), as are likely to be encountered in an infrastructure embankment.

5.4.2 The van Genuchten equation

The van Genuchten (1980) equation is a four parameter curve fitting equation used to describe the SWRC. This enables derivation of closed form analytical expressions for the relationship between hydraulic conductivity and suction, using the models of Burdine (1953) and Mualem (1976). The van Genuchten equation is as follows:

$$\theta = \theta_r + \frac{(\theta_s - \theta_r)}{\left[1 + \left(\frac{h_{vp}}{a_v}\right)^{n_v}\right]^{m_v}} \quad (5.2)$$

where

θ = Volumetric water content,

θ_s = Saturated water content,

θ_r = Residual water content,

h_ψ = Pressure Head (cm),

a_v = Soil parameter related to the air entry value (AEV) (cm),

m_v, n_v = Constants defining the slope gradient (Where $m_v = 1 - 1/n_v$)

van Genuchten (1980) recommends that the residual water content should be measured where the SWRC gradient reduces to zero, or at a large suction such as -1500 kPa. This differs from the approach of Fredlund & Xing (1994) shown in Figure 5.1. With knowledge of an SWRC, defined using curve fitting parameters, van Genuchten (1980) proposed using the hydraulic conductivity equation of Mualem (1976) to calculate changes in hydraulic conductivity with soil suction. The Mualem (1976) hydraulic conductivity equation, in terms of pressure head is:

$$K_\psi(h_\psi) = \frac{(1 - (\frac{h_\psi}{a_v})^{n_v})^{m_v} \left[1 + (\frac{h_\psi}{a_v})^{n_v} \right]^{-m_v}}{\left[1 + (\frac{h_\psi}{a_v})^{n_v} \right]^{m_v/2}} \quad (5.3)$$

where

a_v, m_v, n_v = van Genuchten curve fitting parameters,

h_ψ = Pressure head (cm)

SWRCs experimentally derived by van Genuchten (1980) were used to predict hydraulic conductivity curves for five soils (1 No. Sandstone, 3 No. Loam and 1 No. Clay) and compared with experimental data produced by Mualem (1976). Excellent agreement was found when matching predicted and experimental SWRCs for the sandstone and loam samples. Difficulty matching the clay sample curves was experienced and doubt was expressed over the accuracy of the θ_r value for high suctions, for which there was little experimental data. The van Genuchten (1980) SWRC estimation method does not compare well with experimental data at high suctions due to assumptions made regarding the residual water content, for which van Genuchten had little data.

5.4.3 The Fredlund and Xing equations

Fredlund & Xing (1994) describe SWRC estimation using a closed form solution, fitting a curve to laboratory data over the entire suction range, to $10^6 kPa$. This requires four parameters, of a similar form to those proposed by van Genuchten (1980). The soil pore-size distribution is used as a basis for derivation of a SWRC curve to match experimental data, with a correction factor to ensure zero water content at $10^6 kPa$ suction and to produce a smooth curve. The equation describing the Fredlund & Xing (1994) SWRC is as follows:

$$\theta = C_\psi \theta_s \left[\frac{1}{\ln [e + (\psi/a_f)^{n_f}]} \right]^{m_f} \quad (5.4)$$

where

θ = Volumetric water content,

θ_s = Saturated volumetric water content,

C_ψ = Correction function,

$$C_\psi = \frac{\ln(1 + \psi/\psi_r)}{\ln[1 + (1000000/\psi_r)]}$$

ψ = Negative pore water pressure (kPa),

ψ_r = Negative pore water pressure at residual water content (kPa),

e = The natural number,

a_f, m_f, n_f = Curve fitting parameters

The curve fitting parameters (a_f, m_f, n_f) differ slightly to those proposed by van Genuchten (1980). a_f describes the inflection of the SWRC beyond the air entry value (ψ_i), which can represent a value slightly higher than that given by van Genuchten (1980) for steep slope functions (Figure 5.1). The parameters are defined as follows:

$$a_f = \psi_i$$

$$m_f = 3.67 \ln \left(\frac{\theta_s C_\psi}{\theta_i} \right)$$

$$n_f = \frac{1.31^{m_f+1}}{m_f \theta_s C_\psi} 3.72s$$

where

s = Slope function (Shown in Figure 5.1),

ψ_i = Negative pore water pressure at the curve inflection point (Figure 5.1)

The SWRC derived using the Fredlund & Xing (1994) method has been critically evaluated against experimental data by Leong & Rahardjo (1997), with ‘robust’ results, and can be used to derive the hydraulic conductivity variation with soil suction. The relative hydraulic conductivity, K_ψ , can be obtained by integrating with respect to volumetric water content along the entire curve of the SWRC. Fredlund (2000) suggests integrating the SWRC with an additional factor, q , to account for tortuosity (Mualem, 1986). Leong (1997) showed that the integration procedure demonstrated by Fredlund et al. (1994) can be reproduced indirectly using:

$$K_\psi = C_\psi K_s \left[\frac{1}{\ln [e + (\psi/a_f)^{n_f}]} \right]^{m_f q} \quad (5.5)$$

where

K_s = Saturated hydraulic conductivity (ms^{-1}),

q = A curve fitting parameter accounting for tortuosity and to match theory and experimental results

The parameter q can be assumed to be unity for silts and sands (Fredlund, 2000). Equation 5.5 has been shown to give a close fit to experimental data for the drying of seven soils, matching the results produced by integration, providing a simplified method for determination of K_ψ .

5.4.4 Soil Water Retention Curve summary

Experimental data is available for describing the SWRC of a number of soils. From this, the estimation methods of Aubertin et al. (2003), van Genuchten (1980) and Fredlund & Xing (1994) can be used to create additional SWRCs, for other soils. Of these methods, the one proposed by Aubertin et al. (2003)

requires parameters most likely to have been measured during site investigation, such as the particle size distribution (PSD), but care must be taken where the soil particle size is highly variable or heterogeneous as inappropriate assumptions may be made. The van Genuchten (1980) and Fredlund & Xing (1994) methods both require similar curve fitting parameters to produce SWRCs (θ_s, θ_r, a, m and n). The key difference between the choice of method occurs in the high suction range (greater than 1500kPa) where the curves differ because the Fredlund & Xing (1994) method uses a parameter to ensure the curve fits through zero water content at a 10^6 kPa soil suction. For general geotechnical application soil suctions are not likely to exceed 1500 kPa, making both methods appropriate, although, under evaporative conditions high suctions may develop in soils at shallow depth. Hydraulic conductivity functions can be developed for all three methods by integration of the SWRC (Mualem, 1976; Fredlund et al., 1994; Leong, 1997).

While the above methods can be used to derive the desaturation (drying) and saturation (wetting) curves of SWRCs, obstacles to true representation of the soil storage and hydraulic conductivity remain. First, there is little experimental data to confidently define the wetting curve. Secondly, although a drying and wetting SWRC are defined, they represent the upper and lower extremes, with scanning curves between these bounds actually representing the water storage, depending on the saturation history of the sample. Further understanding of soil water storage hysteresis and the influence of stress-strain history is required before the full potential of SWRCs is to be incorporated into the soil water flow equations. However, knowledge of the saturated permeability and the SWRC does allow prediction of the relationship between hydraulic conductivity and suction with sufficient accuracy for most engineering problems (Fredlund, 2000).

5.5 Soil water retention and hydraulic conductivity of a clay fill

A SWRC for clay fill and the saturated permeability is required to calculate hydraulic conductivity in an unsaturated railway embankment. Experimental data describing the relationship between soil suction and volumetric water content is not available for a clay fill. However, the SWRC can be estimated from comparison with SWRCs of similar soils and sensitivity analysis using van Genuchten (1980) curve fitting parameters. Using the saturated permeability of the clay fill measured in the field, the unsaturated hydraulic conductivity of the fill can be estimated.

5.5.1 Structure and composition of clay fill

The structure of the dumped clay fill used to construct railway embankments is described in Chapter 2. This differs from the intact structure of a natural clay. During embankment construction clods of natural clay were excavated and mixed with other soils during handling and transportation of the fill, creating a clod and matrix structure (O'Brien et al., 2004). Loose compaction during construction and slow consolidation of the material then occurred. Therefore in a clay fill some of the structure present in an intact clay will be lost, due to a process similar to slurring, and a new structure created by loose compaction and consolidation. Relative to the parent material, a clay fill would have larger pores filled with matrix material and a larger range of pore sizes. The clod and matrix structure would have greater permeability than an intact clay. van Genuchten (1980) curve fitting parameters can be used to investigate the influence of soil structure on the shape of the SWRC and, using the SWRC for London clay, propose a SWRC for clay fill.

5.5.2 Influence of wetting and drying Soil Water Retention Curve on hydraulic conductivity

Wetting and drying SWRCs for London clay (Croney, 1977), from which the clay fill is derived, are shown in Figure 5.6(a). Comparison of the calculated hydraulic conductivity, using equation 5.3 and assuming a saturated permeability of $5 \times 10^{-9} \text{ ms}^{-1}$ is shown in Figure 5.6(b). This shows that

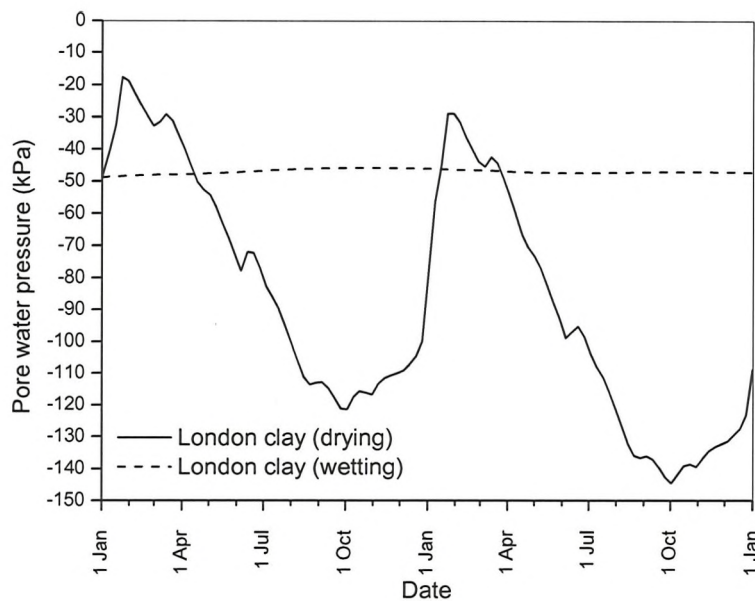
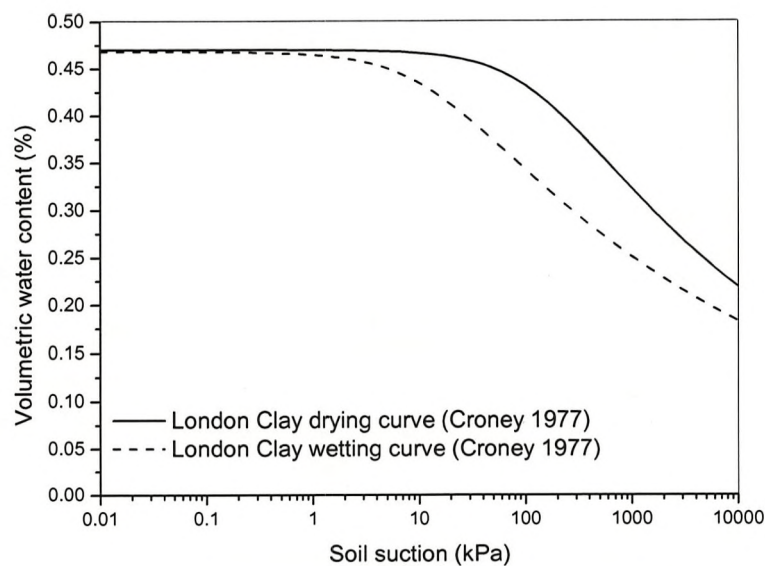


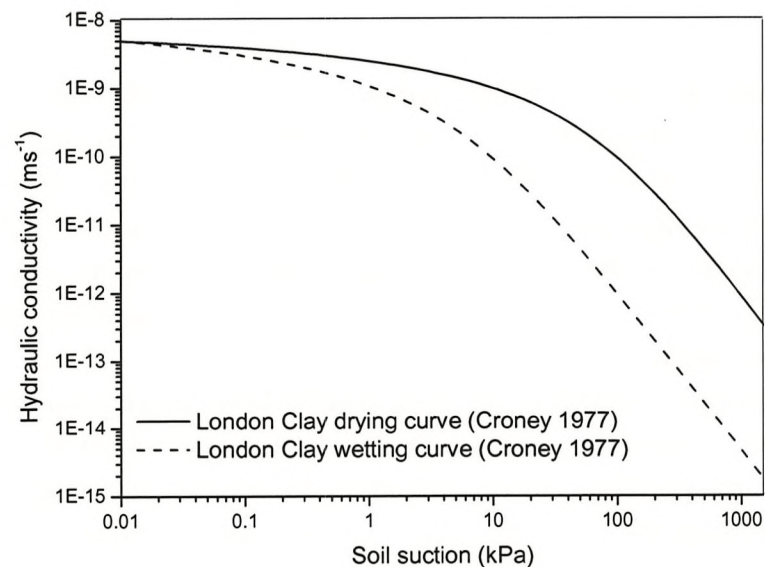
Figure 5.5: Comparison of calculated pore water pressure variation at 2 m depth using Croney (1977) wetting and drying SWRCs for London clay

the hydraulic conductivity of London clay can reduce by between four and six orders of magnitude over a suction range of 0 kPa to 1000 kPa. The wetting and drying SWRCs show a difference in hydraulic conductivity of an order of magnitude at 10 kPa suction, increasing to more than two orders of magnitude at 1000 kPa suction. Actual soil water content and hydraulic conductivity for a given soil suction will lie on a scanning curve bounded by the main wetting and drying curves.

Preliminary analysis of the finite element model presented in Appendix B compared pore water pressures calculated using a drying SWRC and a wetting SWRC (Published by Croney (1977)) for a slope constructed of London clay (permeability of $5 \times 10^{-8} ms^{-1}$ in this example). Figure 5.5 compares calculated pore water pressures at 2 m depth at the embankment midslope (10 m from the crest) over a two year period. A lower magnitude of pore water pressure variation was calculated using the London clay wetting SWRC than the London clay drying SWRC. This is because, for a given suction, the hydraulic conductivity derived using the wetting curve is lower than that for the drying curve (Figure 5.6). Sensitivity analysis showed calculated pore water pressures to be sensitive to the choice of SWRC.



(a) London clay wetting and drying SWRC (Croney, 1977)



(b) London clay wetting and drying hydraulic conductivity curve

Figure 5.6: Soil water retention and hydraulic conductivity curves for wetting and drying of London clay

5.5.3 Influence of van Genuchten (1980) curve fitting parameters on hydraulic conductivity

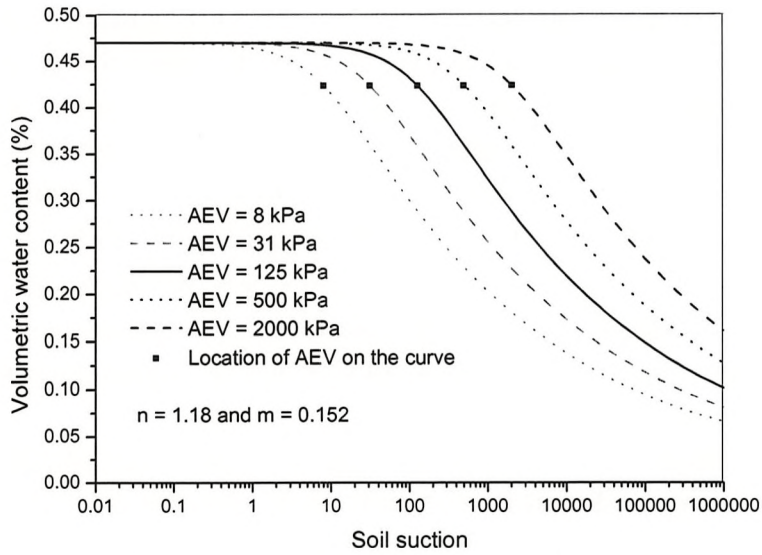
The influence of the van Genuchten (1980) curve fitting parameters on curve shape can be observed by varying each of the curve fitting parameters (a, n, m), relative to a curve fitted to the London clay drying curve measured by Croney (1977). Figure 5.7(a) demonstrates the lateral translation of the SWRC as a result of varying the a parameter (AEV) while keeping n fixed (and m since $m = 1 - 1/n$). The hydraulic conductivity for different values of AEV (calculated using equation 5.3) is shown in Figure 5.7(b). For the range of AEVs shown, a difference in hydraulic conductivity of nearly two orders of magnitude occurs at 10 kPa suction, increasing to five orders of magnitude at 1000 kPa suction.

The influence of the parameter n on the SWRC and hydraulic conductivity is shown in Figures 5.8(a) and 5.8(b) respectively. Comparison of the curves shows that once the soils begin to desaturate the reduction in volumetric water content differs greatly across the range of n values shown. Low values of n compare well with the SWRC for fine clay soils, where a range of pore sizes are present, while high values of n compare well with the SWRC for coarse sandy soils, with a more uniform pore size distribution. This is reflected in the hydraulic conductivity of the soils; a sharp decrease in permeability with reduction in water content is shown for the typically sandy soil, with a high value of n .

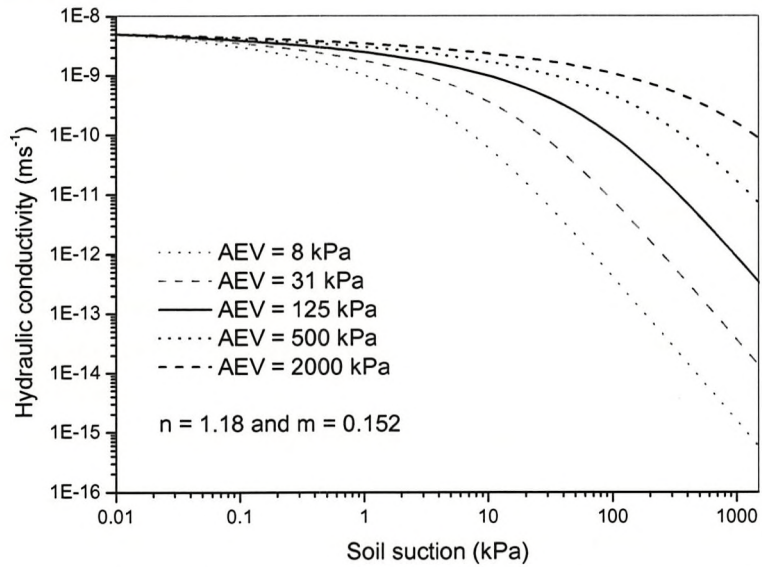
Sensitivity analysis of the impact of the van Genuchten (1980) parameters on hydraulic conductivity shows that the a parameter (AEV) controls the point at which the soil changes from saturated permeability to unsaturated hydraulic conductivity. The rate of reduction in hydraulic conductivity as the soil continues to desaturate is controlled by the n parameter.

5.5.4 Estimated soil water retention of a clay fill

A SWRC for clay fill can be defined by considering the properties of a clay fill relative to an *in situ* London clay. A clay fill, consisting of a clod and matrix structure of loosely compacted material is likely to have larger voids and a larger range of void sizes than an *in situ* London clay. The larger voids of the clay fill would start to drain at lower suctions than the *in situ* London clay, resulting in a lower AEV (defined by the a parameter). The

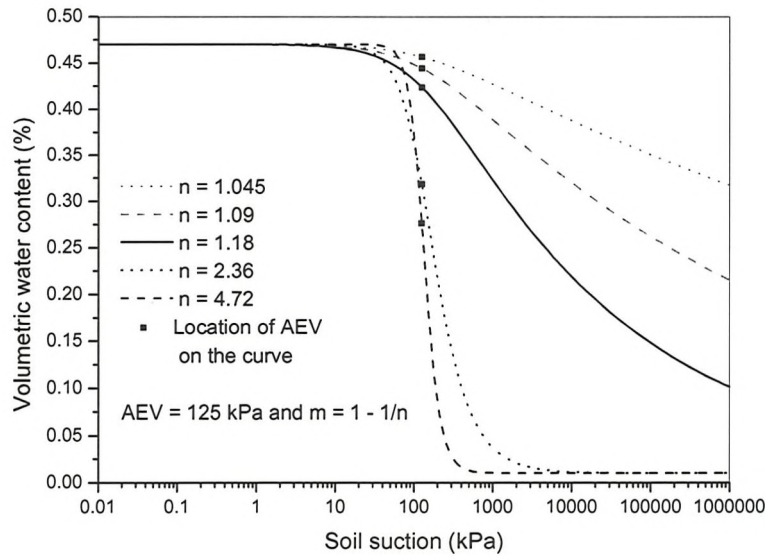


(a) Plot of the van Genuchten (1980) equation with n and m constant and AEV varying

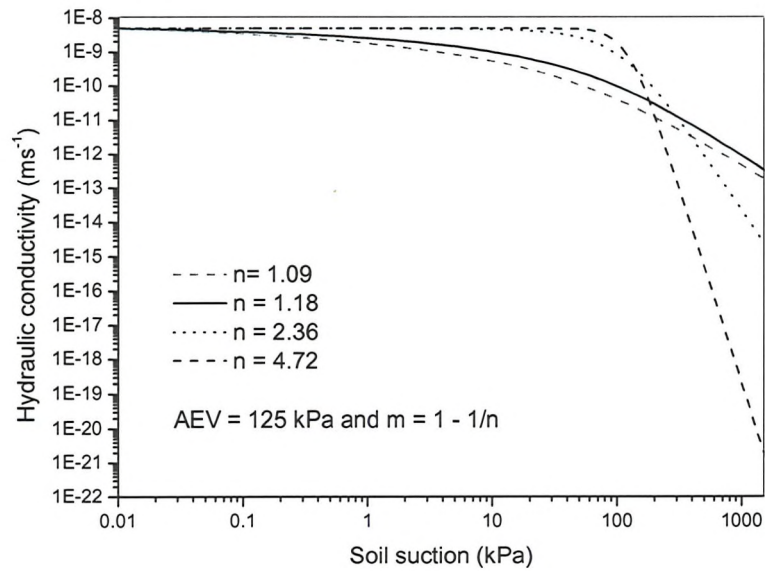


(b) Hydraulic conductivity curves derived from SWRCs of varying AEV

Figure 5.7: Soil water retention and hydraulic conductivity curves for varying AEV (based on Croney (1977) London clay)



(a) Plot of the van Genuchten (1980) equation with AEV constant and n and m varying



(b) Hydraulic conductivity curves derived from SWRCs of varying n and m

Figure 5.8: Soil water retention and hydraulic conductivity curves for varying n and m (based on Croney (1977) London clay)

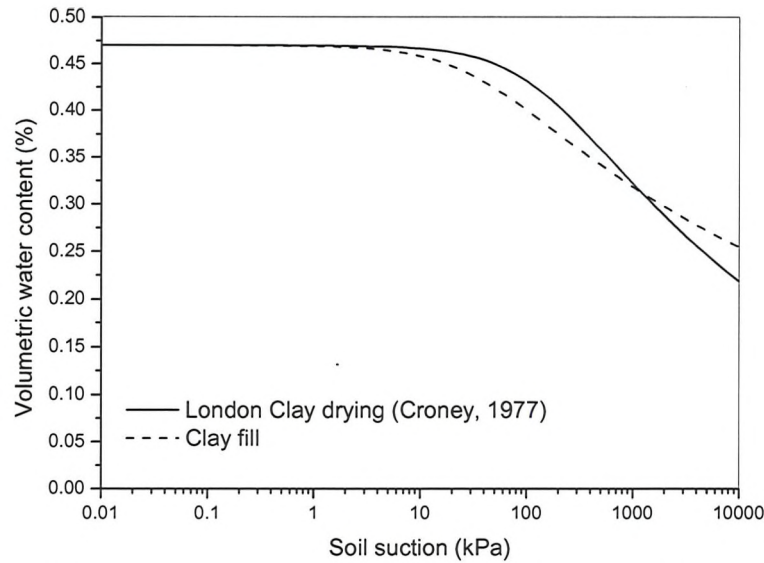
Table 5.1: Summary of soil properties

| Soil type | permeability (ms^{-1}) | van Genuchten constants | | | | |
|-------------------|--------------------------------------|-------------------------|------------|------------|------|------|
| | | AEV (kPa) | θ_s | θ_r | m | n |
| Clay fill | 5×10^{-8} | 30.3 | 0.47 | 0.1 | 0.13 | 1.15 |
| Surface clay fill | 5×10^{-7} | 30.3 | 0.47 | 0.1 | 0.13 | 1.15 |
| London clay | 5×10^{-9} | 125 | 0.47 | 0.1 | 0.15 | 1.18 |

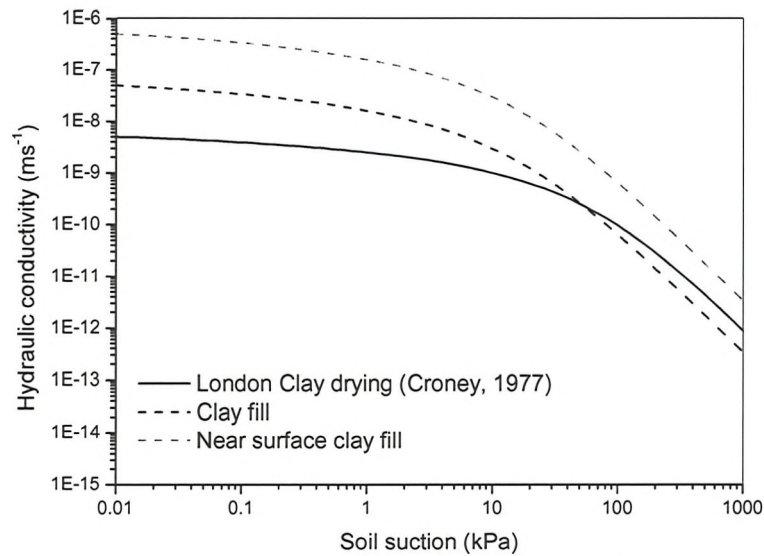
greater range of pore sizes in the clay fill would create a shallower curve gradient (defined by n and m) than the *in situ* clay. This is because the steepness of the curve is related to the distribution of pore sizes within the soil, with a larger pore size range being defined by a shallower curve gradient and a uniform pore size distribution being defined by a steep curve gradient. A comparison of SWRCs and unsaturated hydraulic conductivity of London clay and the estimated clay fill (assuming the saturated permeabilities shown in Table 5.1) is shown in Figure 5.9. The estimated clay fill SWRC was compared with field data at Hawkwell embankment, showing good agreement (Chapter 8).

5.6 Comment

A review of the literature showed that the SWRC can be used to describe unsaturated soil water storage and estimate unsaturated hydraulic conductivity. Methods for measuring and estimating the SWRC were reviewed and the limitations of the methods were discussed (Section 5.4.4). A measured SWRC for drying of London clay was obtained from Croney (1977) and curve fitted using van Genuchten (1980) constants. A SWRC for clay fill was estimated using the van Genuchten (1980) constants, informed by sensitivity analysis, by considering the structure and composition of clay fill relative to *in situ* London clay. Section 5.4.4 showed that the drying SWRC is a simplified model of unsaturated soil water retention. However, the drying SWRC for London clay and the estimated SWRC for clay fill provide a basis for calculating unsaturated flow. This can be used in a finite element model, from which parametric studies of soil permeability, weather extremes and vegetation influence on railway embankments can be conducted.



(a) Soil Water Retention Curves for London clay (Croney, 1977) and clay fill



(b) Hydraulic conductivity curves derived from SWRCs of London clay and clay fill

Figure 5.9: Soil water retention and hydraulic conductivity curves for London clay (Croney, 1977) and clay fill

Chapter 6

Climate influence on embankment hydrology: Charing embankment case study

Approximately 5,000 km of embankment has been supporting the UK's railway infrastructure for more than 100 years. Failure and deformation of these ageing embankments affects track alignment, causing delay and disruption to rail services. Network Rail estimates that train delays directly attributable to poor earthwork performance totalled 400,000 minutes over the period 2000-2003, at a cost of £26m (Scott et al., 2007).

Instrumentation was installed at Charing embankment as part of the Network Rail commission 'Seasonal Preparedness Earthworks' to investigate the causes of poor earthwork performance and improve understanding of embankment behaviour (Mott MacDonald, 2009). The project undertaken by Mott MacDonald comprised site investigation, installation of instrumentation, mechanical analysis and hydrological finite element modelling. Analysis of the monitoring data and a hydrological finite element model is presented.

A hydrological model using recorded daily weather data and site measured soil properties was used to model transient pore water pressures within Charing embankment. Calculated pore water pressures were compared with site monitoring data and projected distributions of pore water pressure dur-

ing an extremely wet winter and an extremely dry summer were considered. The hydrological model was used to investigate the relationship between climate, slope vegetation cover and soil permeability. O'Brien (2007) highlighted the need to improve this understanding to assess overall embankment behaviour.

6.1 Charing embankment

Charing Embankment is situated on the line between Charing and Ashford stations in Kent. It is believed to have been constructed in 1874 and is 590 m in length, with a maximum height of 8.5 m. The embankment was constructed by end-tipping, without compaction, of locally excavated Gault clay. This construction method, commonly used in the 19th Century (Skempton, 1996), has created a structure and macrofabric which is quite different to natural clay and modern compacted clay fills (O'Brien et al., 2004). A clod and matrix structure exists within railway embankments where clods of original clay are surrounded by a matrix of softened, more permeable material (Section 2.2).

The Embankment fill is described as being of intermediate to high plasticity, with the reworked Gault clay at Charing being slightly less plastic than the London clay fill encountered on the London Underground network (Mott MacDonald, 1999) due to its higher sand content (Mott MacDonald, 2009). Laboratory testing revealed soil moisture content to be highly variable and influenced by the presence of a significant number of high water demand trees on the embankment surface (Appendix C).

Instrumentation was installed and monitored at two cross sections within the embankment (54 m 39 ch) by Geotechnical Observations on behalf of Mott MacDonald. Two inclinometer tubes were positioned at the mid to lower slope and two were installed closer to the crest of the embankment. An additional four inclinometers were installed at other parts of the site. Slope displacement was measured at monthly intervals between January 2007 and October 2008. Geo-piezometers were installed in 11 boreholes, between 1.9 m and 4.6 m depth, to monitor pore water pressures for a period of 12 months between January 2007 and January 2008. A number of standpipe piezometers were also installed within the embankment but these were typically dry throughout the monitoring period. A Campbell Scien-

tific BWS200 Series weather station was installed at the site in March 2007, providing hourly measurements of air temperature ($^{\circ}\text{C}$), relative humidity (%), wind speed (ms^{-1}), wind direction ($^{\circ}$), rainfall (mm) and solar radiation (Wm^{-2}) (Campbell Scientific, 2006). A typical cross section at the instrumentation site is shown in Figure 6.1.

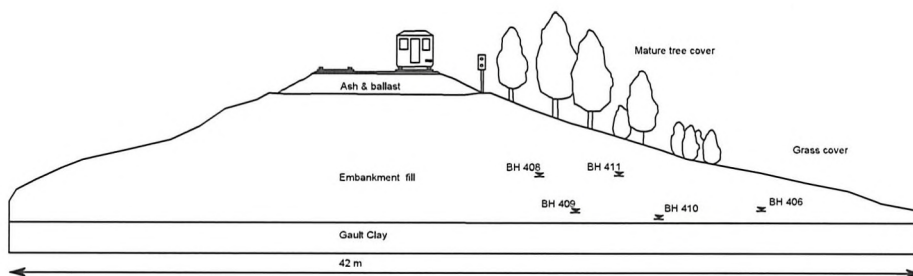


Figure 6.1: Charing embankment cross section at the instrumentation site

6.2 Monitoring results

Daily rainfall data was recorded by the Charing weather station between June 2007 and June 2008. During the summer of 2007 (June-August), 205.2 mm of rainfall was recorded at Charing, compared to a 158.4 mm 1972-2000 Long Term Average (LTA) in South East England (Met Office, 2009). This is an increase of 46 mm compared to the LTA (130 %). During the winter (December 2007-February 2008) 97.7 mm of rainfall was recorded, compared to a 220.7 mm 1972-2000 LTA. This is 123 mm less than the LTA, corresponding to 44 % of the LTA rainfall.

Soil Moisture Deficit (SMD) from the Meteorological Office MORECS data (Section 4.2.4), published for $40 \text{ km} \times 40 \text{ km}$ squares across the UK, can be used to illustrate the influence of weather conditions on soil wetting and drying. Charing embankment is located within MORECS square 174 (Figure 6.2). Figure 6.3 shows that SMD values were low during the summer of 2007, being less than half of the LTA until August 2007. The spring of 2008 is also wetter than the LTA, with negligible SMD developed by May 2008. Weather conditions measured during the monitoring period show a wetter than average summer followed by a drier than average winter. Therefore weather data for the year 2007-2008 is not representative of a typical year (compared to the LTA) or of an extremely wet or extremely dry

year.

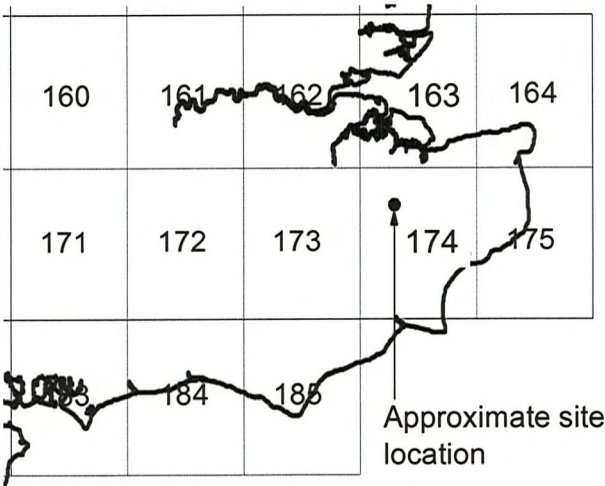


Figure 6.2: Location of MORECS square 174

The range of piezometer measured pore water pressure variation with depth is shown in Figure 6.4. There was limited pore water pressure variation over the monitoring period with relatively constant, negative pore water pressures measured. This is consistent with measurements adjacent to mature trees, where high negative pore water pressures would be expected (Biddle, 1998; Scott, 2006; Indraratna et al., 2006).

Trial pit inundation on excavation confirmed positive pore water pressures within the embankment at shallow depth (less than 2 m depth). Reference to similar field data (Biddle, 1998; Smethurst et al., 2006; Scott, 2006) shows that positive and negative pore water pressures occur within the top 1.0 m to 1.5 m of the soil. Inclinerometers installed on the embankment showed seasonal movement within this depth, indicating volume change in response to pore water pressure variation. Pore water pressure variation was not detected by the shallowest piezometers, installed at 1.9 m depth (Mott MacDonald, 2009). Therefore the piezometers at Charing do not show seasonal pore water pressure variation but may be more representative of localised effects, influenced by vegetation cover and local permeability.

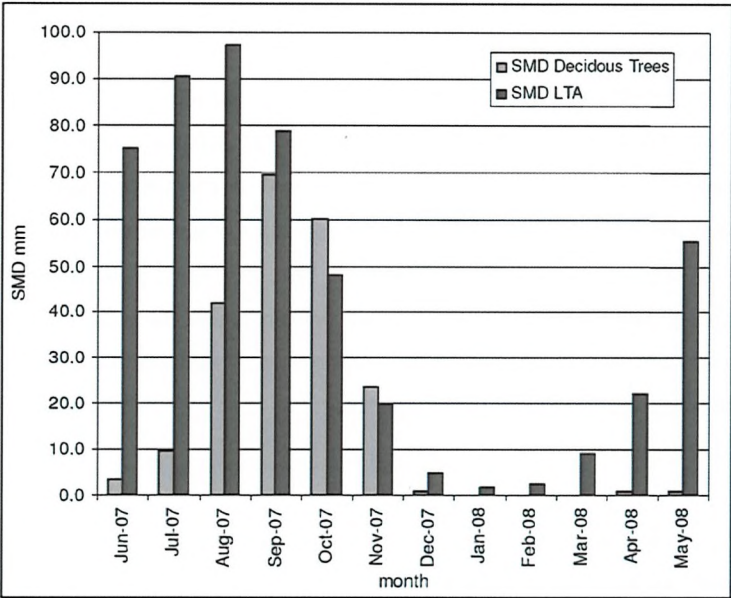


Figure 6.3: Soil moisture deficit data for MORECS square 174 in South East England. (Mott MacDonald, 2009)

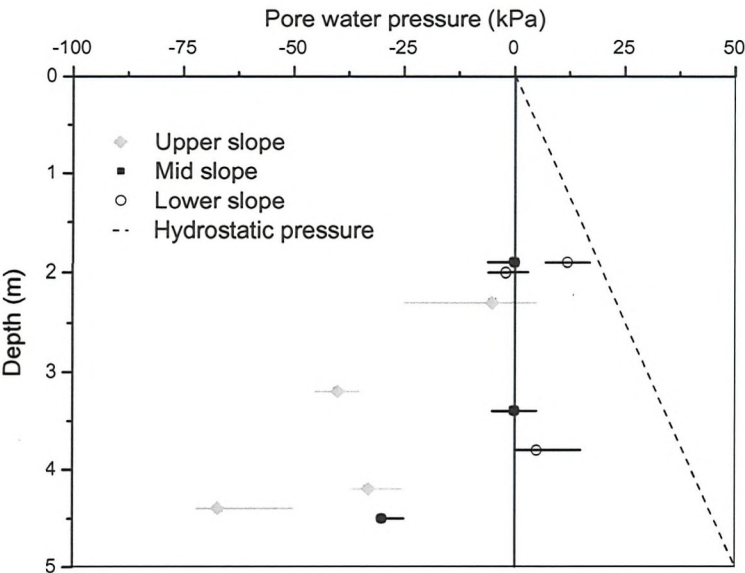


Figure 6.4: Typical value and range of measured pore water pressure variation with depth at Charing Embankment (Glendinning et al., 2009)

6.3 Finite element modelling

A finite element model of Charing embankment was created using Vadose/w (Geo-Slope, 2007) to calculate changes in pore water pressure in response to climate. Vadose/w calculates saturated and unsaturated water and heat flow in response to applied boundary conditions. A climate boundary condition can be applied; this uses daily climate data to calculate water infiltration and water removal from the surface of the soil and from a defined rooting zone. This enables variations in pore water pressure and volumetric water content with time, in response to changes in weather conditions or changes in vegetation cover, to be investigated.

The aims were:

1. To model seasonal pore water pressure variation at Charing embankment using site measured soil properties and recorded weather data and to compare with monitoring data.
2. To investigate the influence of clay fill saturated permeability on seasonal pore water pressure variation within the embankment.
3. To consider the impact of an extremely dry summer, such as 1995, and an extremely wet winter, such as the winter of 2000/2001, on embankment pore water pressures.

6.3.1 Mesh geometry

The hydrological model is shown in Figure 6.5. The model incorporates a Gault clay foundation, a clay fill embankment and an ash and ballast layer present at the crest. Model geometry is defined in Vadose/w using 'regions' of assigned mesh type and material properties. The climate boundary condition is applied to the 'surface region' where water inflow and water removal occurs. Root water uptake occurs within the surface region.

A fine mesh of 0.1 m rectangular elements (in the vertical direction) was used in the surface zone, to enable calculation of flow due to high pore water pressure gradients created by the boundary condition. A mesh of 0.5 m square elements was used for the embankment fill, the ash and ballast layer and in the foundation.

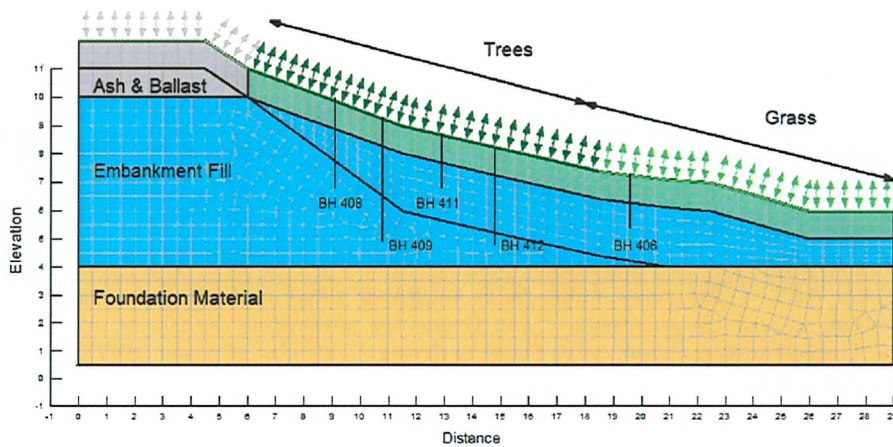


Figure 6.5: Charing Embankment model geometry

6.3.2 Material properties

Site investigation and laboratory testing of the clay fill at Charing found the *in situ* saturated soil permeability to be one order of magnitude greater than the laboratory measured permeability (Mott MacDonald, 2009). This demonstrates the importance of soil fabric (local silt and sand layers) in controlling permeability and is consistent with results from London clay embankment sites (O'Brien et al., 2004).

The Gault clay saturated permeability was measured using *in situ* falling head tests. Saturated permeability was measured between the range of $1.5 \times 10^{-6} \text{ms}^{-1}$ and $3 \times 10^{-9} \text{ms}^{-1}$. It was suggested that because the *in situ* falling head tests were conducted partially within the clay fill, the saturated permeability of *in situ* Gault clay would be lower than that measured (Mott MacDonald, 2009).

The saturated permeabilities assumed in the Vadose/w model, based on testing by Mott MacDonald (2009), are shown in (Table 6.1). The surface clay fill (to a depth of 1 m) was assigned a permeability 5 times greater than than the embankment core. This reflects the greater permeability of near surface soil, where the broken soil surface, cracking and voids created by roots increase the bulk permeability (Li et al., 2011).

Piezometer data showed the embankment to have high soil suctions and to be largely unsaturated. Therefore, in addition to the measured soil permeability, unsaturated soil hydraulic conductivity and soil water storage

Table 6.1: Summary of soil properties

| Soil Type | Permeability (ms^{-1}) | Van Genuchten Constants | | | | |
|------------------------------|--------------------------------------|-------------------------|------------|------------|-------|------|
| | | AEV (kPa) | θ_s | θ_r | m | n |
| Ash and ballast [‡] | 4×10^{-5} | 2 | 0.45 | 0.01 | 0.524 | 2.1 |
| Clay fill* | 5×10^{-8} | 30.3 | 0.47 | 0.1 | 0.13 | 1.15 |
| Surface clay fill* | 2×10^{-7} | 30.3 | 0.47 | 0.1 | 0.13 | 1.15 |
| Gault clay [†] | 5×10^{-8} | 33 | 0.59 | 0.1 | 0.15 | 1.18 |

Where AEV = Air entry value, θ_s = saturated water content, θ_r = residual water content, m and n = constants. * van Genuchten parameters derived in section 5.5.4, [†] van Genuchten parameters curve fitted to drying Gault clay (Croney, 1977), [‡] estimated van Genuchten parameters for a sandy gravel

was required to model unsaturated water flow. Unsaturated soil properties that describe the reduction in soil water storage and soil permeability with increasing suction were based on a modified version of the Croney (1977) SWRC for London clay. Using van Genuchten (1980) curve fitting parameters, the clay fill was assigned a lower air entry value and a shallower gradient to the curve than *in situ* London clay, consistent with its greater specific volume and wider range of pore sizes (Figure 6.6). Development of a SWRC for clay fill is described in Section 5.5.4. The Croney (1977) drying curve for Gault clay was used to model the Gault clay foundation at Charing embankment while the SWRC for a coarse granular material (Rouainia et al., 2009) was used to model the ash and ballast covering the slopes.

The SWRCs were used to define the variation of soil hydraulic conductivity with soil suction using the Mualem (1976) method with van Genuchten (1980) constants and the saturated permeability. The variation of hydraulic conductivity with soil suction is shown in Figure 6.7.

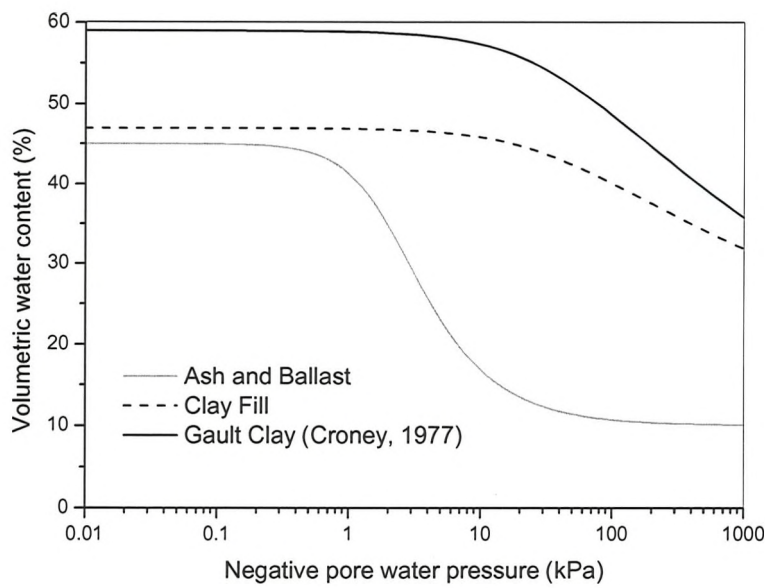


Figure 6.6: Soil water retention curves (SWRCs) describing variation of volumetric water content with pore water pressure

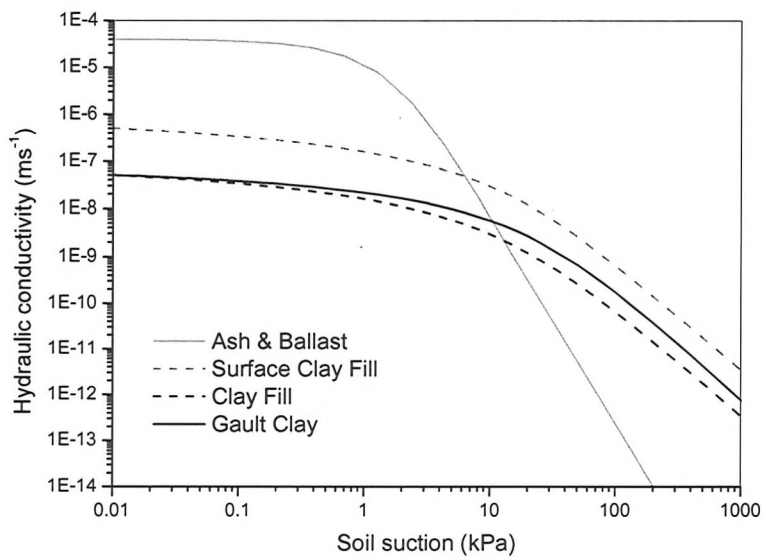


Figure 6.7: Hydraulic conductivity curves

6.3.3 Boundary and initial pore water pressure conditions

A climate boundary condition was used to calculate surface flux at the soil surface in response to weather. A series of measured climate data sets were available for application to the Vadose/w model. First, the weather station installed at Charing as part of the monitoring regime provided site specific weather data for the period 15 March 2007 to 10 June 2008. The measurement period corresponded with weather not typical of the Long Term Average (LTA South of England 1972-2000), consisting of a wetter than average summer followed by a drier than average winter (Section 6.2). Weather data for a year of seasonal weather variation, when a hot summer and wet winter occurred, was obtained from a weather station in Newbury (Smethurst et al., 2006) between 10 March 2005 and 9 March 2006.

Two ‘extreme’ climate scenarios were created by altering the Charing weather station data; a ‘wet winter’ and a ‘dry summer’. The climate scenarios represent scenarios of wetter and drier conditions than the Charing weather data, to demonstrate the sensitivity of the model to the climate boundary condition. They are not measured weather data.

The ‘wet winter’ scenario consists of the Charing weather station data applied through the summer, from 31 May 2007 to 29 September 2007. Following this, for 183 days from 30 September 2007 to 30 March 2008, the Charing weather station rainfall data was modified and 4.8 mm of ‘wet winter’ daily rainfall, as used by Scott et al. (2007), was applied. Constant, steady state rainfall will increase infiltration compared with discrete rainfall events, where surface soil drying occurs. This assumption therefore represents an upper limit of wet winter rainfall.

The ‘dry summer’ scenario consists of modified Charing weather station data from 31 May 2007, through the summer and autumn to 28 November 2007. To create a ‘dry summer’ the weather data was modified by increasing daily temperature by 20%, to increase potential evapotranspiration, and by reducing daily rainfall. Daily rainfall inputs in the ‘dry summer’ model were based on average monthly rainfall data for England and Wales during the dry summer months of 1995 (Met Office, 2009). This replicated a ‘dry summer’, benchmarked to recorded averages, rather than applying zero rainfall throughout the whole summer. A summary of the climate scenarios is provided in Table 6.2. Humidity and wind speed remain unchanged for all scenarios and are not included in the table.

Table 6.2: Charing climate scenarios

| Climate Scenario | Period | Input Parameters - Relative to Weather Station Data | | |
|------------------|-------------------|---|--------------|-----------------|
| | | Temperature | Rainfall | Solar Radiation |
| Charing Weather | 30/05/07-10/06/08 | As Charing | As Charing | As Charing |
| Wet Winter | 30/09/07-30/03/08 | As Charing | 4.8mm/day | As Charing |
| Dry Summer | 30/05/07-28/11/07 | 20% Higher | 1995 Average | As Charing |
| Newbury 2005 | 10/03/05-09/03/06 | Newbury 2005 | Newbury 2005 | Newbury 2005 |

The Vadose/w climate boundary condition calculates evaporation from an unsaturated soil using the Penman-Wilson equation (Wilson et al., 1994) and transpiration using a root water uptake model (Tratch et al., 1995). The Leaf Area Index (LAI), was used to define the proportion of solar energy intercepted by the vegetation for transpiration (Ritchie, 1972). Reduction in root water uptake due to soil drying, as the plant becomes stressed and reduces transpiration, was modelled using the Feddes et al. (1978) relationship, with transpiration reducing linearly between 100 kPa and 1500 kPa suction (Figure 6.9). The plant rooting depth from which transpired water can be removed from the soil by the plant roots was used to differentiate between vegetation type. The root water uptake function in Vadose/w models spatial variation of water removal at depth and infiltration from the surface. This differs from an evapotranspiration model, such as MORECS Soil Moisture Deficit (Section 4.2.4), which considers both evaporation and transpiration as one function applied at the soil surface (Figure 6.8).

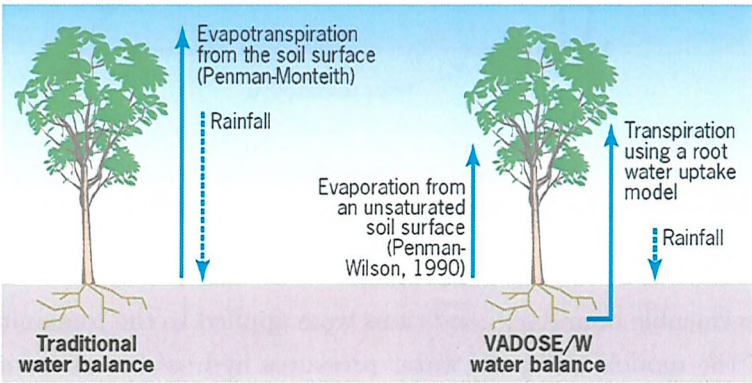


Figure 6.8: Surface water balance comparison

The instrumented section of Charing embankment is vegetated with High

Water Demand (HWD) trees, including two semi mature Oak trees with low level vegetation and grass covering the rest of the slope. ‘Tree Covered’ and ‘Grass Covered’ boundary conditions were therefore defined for ‘summer’ (April to September) and ‘winter’ (October to March). The Tree Covered boundary condition was applied during summer months only, characterised by a constant root depth function of 3 m. During the winter months, when tree water demand reduces, the Tree Covered boundary condition was considered to be equivalent to a Grass Covered boundary condition. The Grass Covered boundary condition is characterised by a rooting depth of 0.9 m, in agreement with existing grass root models (Smethurst et al., 2006; Greenwood et al., 2001; Allen et al., 1998). Both the Tree Covered and Grass Covered boundary conditions assume full leaf cover, allocating all solar energy to plant transpiration rather than bare ground evaporation. Both boundary conditions assume a linear root water uptake distribution, decreasing with depth.

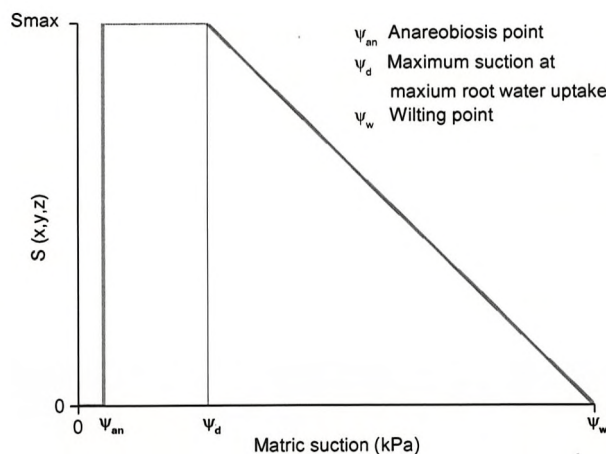


Figure 6.9: Water uptake - soil suction relationship (Feddes et al., 1978) showing the anareobiosis (ψ_{an}), maximum uptake (ψ_d) and wilting point (ψ_w). (From Section 4.2.6)

Impermeable boundary conditions were applied to the remaining boundaries of the models and pore water pressures hydrostatic above and below an initial water table, located 1 m below the surface at the embankment toe (Figure 6.5). Calculated gradients of total head at the embankment toe were orientated approximately perpendicular to the impermeable boundary, with flow occurring in the vertical direction only. However, the impermeable

boundary condition at the slope toe may need to be extended further if the simulation were to be coupled with a stability or deformation analysis.

Sensitivity analysis showed that after less than two years of applied climate data the pore water pressure distribution was independent of the initial condition (Chapter 7). Therefore the Newbury weather data (representative of a seasonally variable year) was cycled once, followed by one cycle of Charing weather data, to create an initial distribution of pore water pressures within the soil.

A summary of boundary conditions used in the model are shown in Table 6.5, at the end of the chapter.

6.4 Modelling results

A numerical analysis of pore water pressure variation at Charing embankment was conducted for the period May 2007 to June 2008 (376 days) using weather station data and site measured material properties. Results are presented in three formats; showing pore water pressure magnitude, spatial distribution and temporal variation.

1. *Spatial pore water pressure variation* is presented as two dimensional contour plots of pore water pressure for a specific day. This shows the distribution of pore water pressures within the whole embankment for a given point in time.
2. *Pore water pressure with depth* illustrates the pore water pressure distribution at a single location for a number of snapshots in time. This allows comparison of the magnitude and vertical distribution of pore water pressures over a number of seasons at a single point on the embankment, e.g. seasonal pore water pressure distribution at the toe.
3. *Single point pore water pressure variation* shows temporal pore water pressure variation at a single point within the embankment. This compares with piezometer data, providing a continuous record of pore water pressure variation.

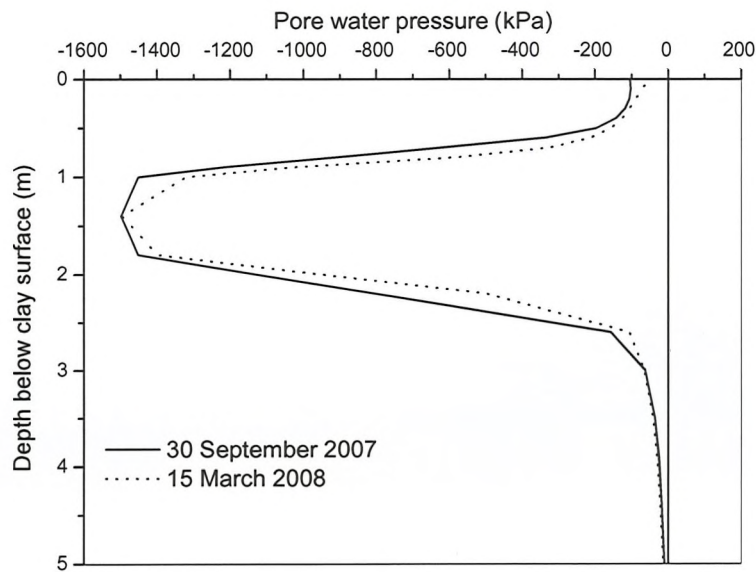
Results calculated using a finite element model are described as *calculated* while results obtained from field or laboratory measurements are described as *measured*.

Contour plots of pore water pressure for the end of summer (30 September 2007) and end of winter (15 March 2008) are shown in Figure 6.11. Plots of pore water pressure with depth for the same periods are shown in Figure 6.10. Pore water pressure profiles are closer to 0 kPa within the surface 1 m during the winter months, when evapotranspiration is reduced and a greater volume of water is able to infiltrate the soil. At the end of summer negative pore water pressures are present within the plant rooting zone, extending to 3 m depth at the tree covered mid slope and 1.3 m depth at the grass covered lower slope.

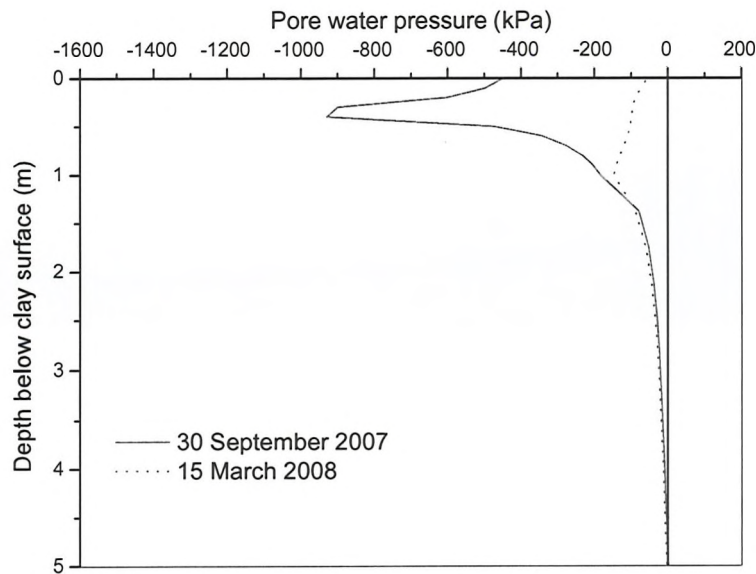
Within the rooting depth (to 3 m depth) at the tree covered mid slope there is little seasonal pore water pressure variation during the monitoring period (Figure 6.10(a)). This is in agreement with the piezometer measurements, which showed limited pore water pressure variation (Section 6.2). Therefore the negative pore water pressures calculated within the tree rooting zone fit the observed pattern of continuous seasonal drying at Charing due to the presence of mature trees.

General agreement was found between the monitoring and modelling data, however there were some limitations to the results. First, the monitoring period at Charing covered a period of unusual weather in the UK, with a wetter than average summer and a warmer, drier than average winter. It is therefore not possible to comment on the likely limits of seasonal wetting and drying that may occur in a railway embankment. Second, it was difficult to compare the magnitude and spatial distribution of pore water pressure variation with the monitoring data. A piezometer installed at 2 m depth measures pore water pressure variation at a single location and, because pore water pressures in the unsaturated zone are not hydrostatic, this is not influenced by wetting and drying fronts that may be occurring at shallower depth. Therefore it may be possible to have seasonal pore water pressure variation within the surface 2 m but very little variation in the piezometer data.

Sensitivity analysis of modelling parameters was used to evaluate the impact of soil permeability, seasonal weather extremes and slope vegetation cover. This provides a broader understanding of the main parameters influencing pore water pressure variation within clay fill embankments.



(a)



(b)

Figure 6.10: Calculated seasonal pore water pressure profiles: (a) tree covered mid slope, and (b) grass covered lower slope

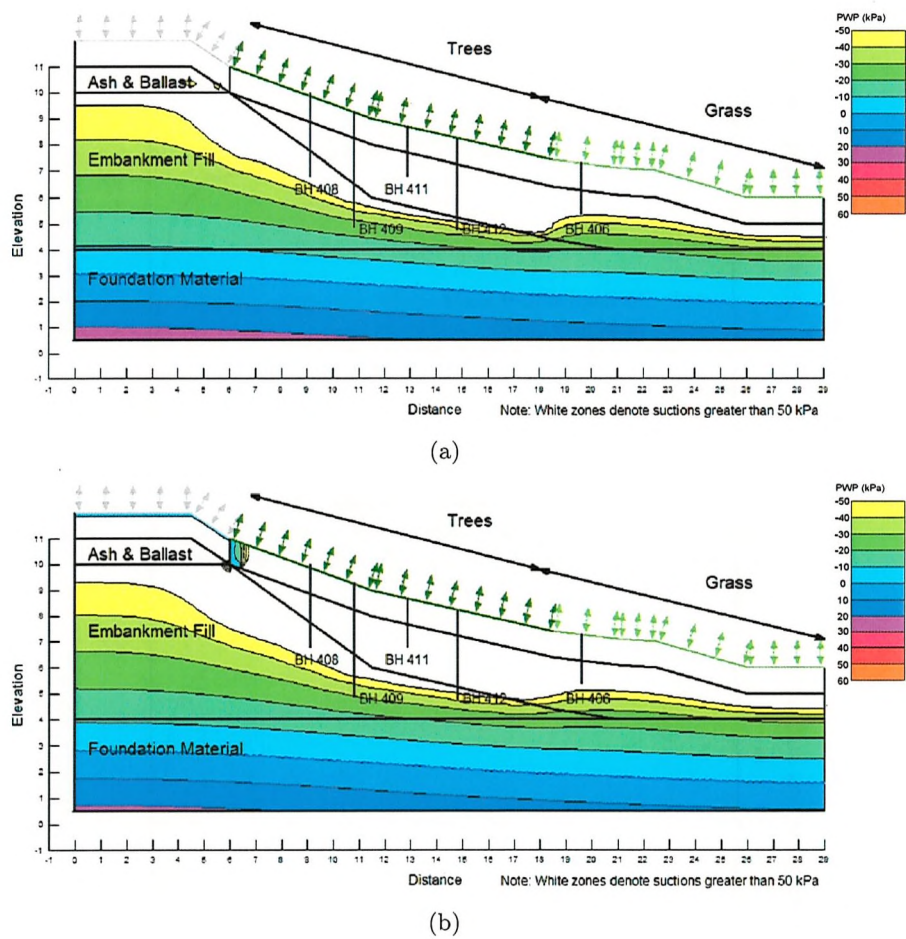


Figure 6.11: Calculated spatial pore water pressure (PWP) distribution: (a) End of summer (September 2007), and (b) End of winter (March 2008)

6.4.1 Clay fill permeability

Clay fill saturated permeability was varied within the model to examine its influence on seasonal pore water pressure variation within the embankment. This provides an indication of how earthworks of different saturated permeability may experience seasonal changes in pore water pressure. A climate boundary condition with large seasonal variation was applied, using weather data recorded at Newbury in 2005 (Section 6.3.3), and grass vegetation cover was assumed (Table 6.5).

The embankment fill saturated permeability of $5 \times 10^{-8} \text{ms}^{-1}$, as measured at Charing embankment (Mott MacDonald, 2009), was compared with a saturated fill permeability of $5 \times 10^{-6} \text{ms}^{-1}$, $5 \times 10^{-7} \text{ms}^{-1}$ and $5 \times 10^{-9} \text{ms}^{-1}$. The values were chosen to reflect the range of those measured at a variety of infrastructure sites (Table 6.4). The near surface clay fill was assumed to be equal to the clay fill while the permeability of the ash and ballast and the foundation material remained constant.

Calculated pore water pressures at 1.9 m depth near the embankment toe (BH 406 in Figure 6.5) are shown in Figure 6.12. For a saturated clay fill permeability greater than $5 \times 10^{-7} \text{ms}^{-1}$ a more rapid response to surface rainfall infiltration was calculated than for a saturated clay fill permeability of $5 \times 10^{-8} \text{ms}^{-1}$. Very limited seasonal pore water pressure variation was calculated for a fill permeability of $5 \times 10^{-9} \text{ms}^{-1}$.

The pore water pressure wetting response relates to the ability of water to infiltrate the soil. The maximum potential rainfall infiltration is limited by the saturated permeability of the clay fill, with excess rainfall running off the slope. Table 6.3 shows maximum potential rainfall infiltration (mm day^{-1}), assuming a saturated soil surface. For the more permeable clay fill (greater than $5 \times 10^{-7} \text{ms}^{-1}$) the potential maximum rainfall (43.2 mm day^{-1}) is greater than the rainfall on any given day (up to 25 mm day^{-1} at Newbury in 2005). For a saturated clay fill permeability of $5 \times 10^{-9} \text{ms}^{-1}$ or less, maximum potential rainfall infiltration is limited to 0.4 mm day^{-1} . As average rainfall events were greater than 5 mm day^{-1} this resulted in run off of excess rainfall and little change in calculated pore water pressure. This leads to a range of critical permeability, between $5 \times 10^{-8} \text{ms}^{-1}$ and $5 \times 10^{-7} \text{ms}^{-1}$ where saturated soil permeability is similar to typical rainfall rates and significant wetting will occur.

The drying response occurs in unsaturated soil (of variable hydraulic

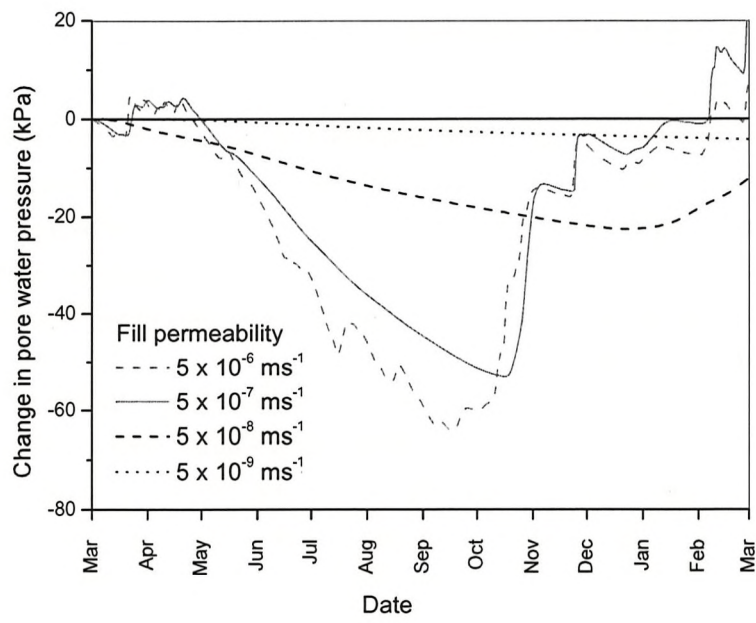


Figure 6.12: Comparison of clay fill permeability influence on calculated pore water pressure variation at 1.9 m depth (March 2005 to March 2006)

conductivity) so a less direct relationship exists between saturated permeability and daily evapotranspiration than the wetting response. However, Figure 6.12 shows that significant drying occurs close to the critical permeability of $5 \times 10^{-7} \text{ m.s}^{-1}$.

Table 6.3: Maximum potential daily rainfall infiltration

| Saturated permeability (ms^{-1}) | Maximum potential rainfall infiltration (mm day^{-1}) |
|---|--|
| 5×10^{-9} | 0.43 |
| 5×10^{-8} | 4.32 |
| 5×10^{-7} | 43.2 |
| 5×10^{-6} | 432 |

The range of critical permeability corresponds with that typically measured for clay fill railway embankments (Table 6.4). The damped pore water pressure variation of the $5 \times 10^{-9} \text{ ms}^{-1}$ clay fill corresponds with that measured in road embankments constructed of well compacted, lower permeability fill (below the 1 m surface layer).

Table 6.4: Permeability measured at infrastructure sites (From Loveridge *et al.* (2010))

| Earthwork type and geological formation | Earthwork material | Saturated permeability (ms^{-1}) |
|---|---------------------------------------|---|
| <i>Railway embankment</i> | | |
| Gault clay | Clay fill, near surface (≤ 1 m) | 1×10^{-6} to 1×10^{-5} |
| | Clay fill | 1×10^{-9} to 1×10^{-8} |
| | Clay fill, sandy pockets or layers | 1×10^{-6} to 5×10^{-6} |
| London clay, central London* | | 2×10^{-9} to 6×10^{-7} |
| London clay, west of London basin | | 1×10^{-7} to 5×10^{-6} |
| <i>Road embankment</i> † | | |
| Kimmeridge clay | Clay, near surface (≤ 1 m) | 1×10^{-7} to 5×10^{-4} |
| | Clay, 2 m depth | 1×10^{-10} |
| <i>Road cutting</i> ‡ | | |
| London clay | Weathered clay | 4×10^{-8} |
| | Grey clay | 4×10^{-9} |

* After O'Brien et al. (2004)

† After Anderson & Kneale (1980)

‡ After Smethurst et al. (2006)

6.4.2 Extreme climate

Extreme climate modelling examined a dry summer, such as 1995, and a wet winter, such as 2000/2001. The dry summer weather produced large suctions within the plant root zone, with drying to greater depth below the tree covered mid slope than the grass covered toe (Figure 6.13(a)). The depth and extent of negative pore water pressures developed during the dry summer of 1995 (Figure 6.13(a)) is similar to that calculated for the summer of 2007 (Figure 6.11(a)). As soil suction increases the hydraulic conductivity of the modelled soil continuum reduces (Figure 6.7), limiting the rate of drying from the surface. Root water uptake within the plant root zone also reduces with increasing suction (Figure 6.9), limiting soil drying during dry periods. Therefore the extent of extreme summer drying within the model is limited by the hydraulic conductivity of the soil and the ability of plants to remove water when large soil suctions are present.

A plot of spatial pore water pressures following a wet winter is shown in Figure 6.13(b). Pore water pressures close to hydrostatic occurred at the grass covered toe of the embankment, where rainwater infiltration recovered shallow soil suctions (to 1 m depth). Beneath the tree covered mid slope, water infiltrated to 1 m depth but soil suctions greater than 50 kPa were maintained within the root zone, between 2 m and 3 m depth.

Figure 6.14 shows pore water pressure variation with depth over the winter period at the tree covered mid slope and grass covered lower slope. Soil suctions within the tree root zone at the end of summer (30 September) were progressively recovered by water infiltration from the surface over the winter period. However, water was unable to infiltrate the full extent of the root zone by 15 March and residual suctions remained between 1.75 m and 3 m depth. In contrast, at the grass covered lower slope water was able to infiltrate the full extent of the root zone by 30 November and create a pressure profile close to hydrostatic by the end of winter (15 March). This shows that in a clay fill, negative pore water pressures can be maintained within the tree root zone during an extremely wet winter but the negative pore water pressures in the shallower, grass root zone are not maintained.

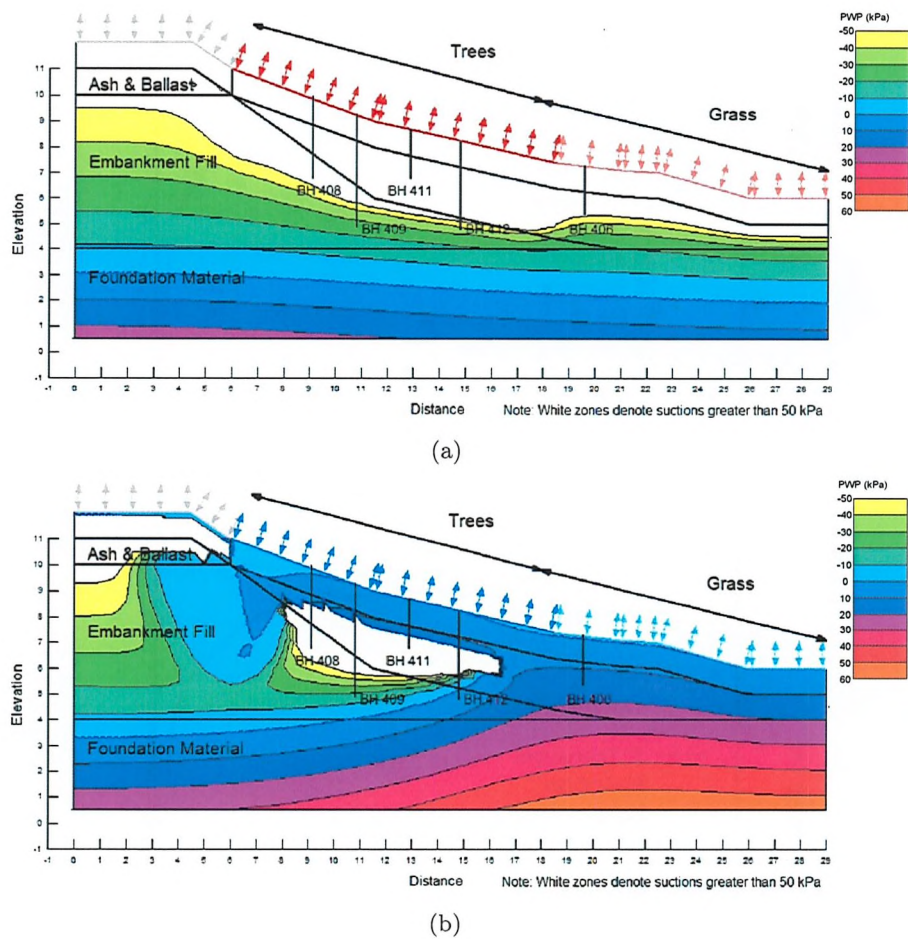
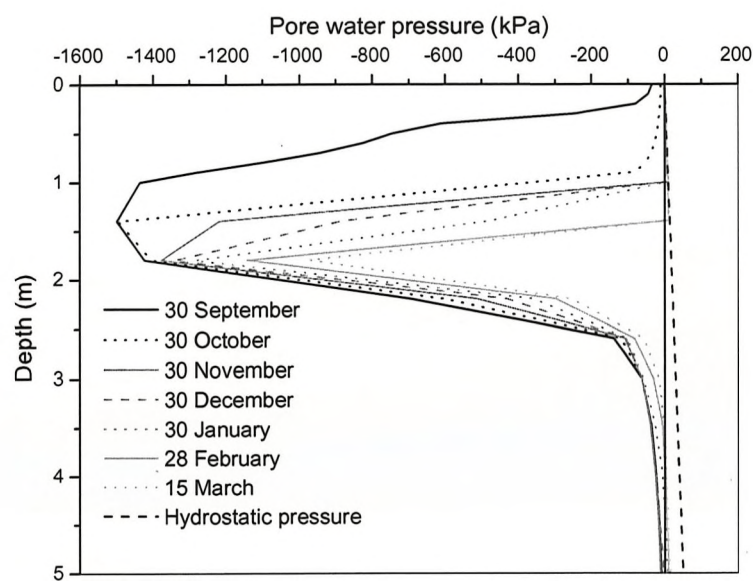
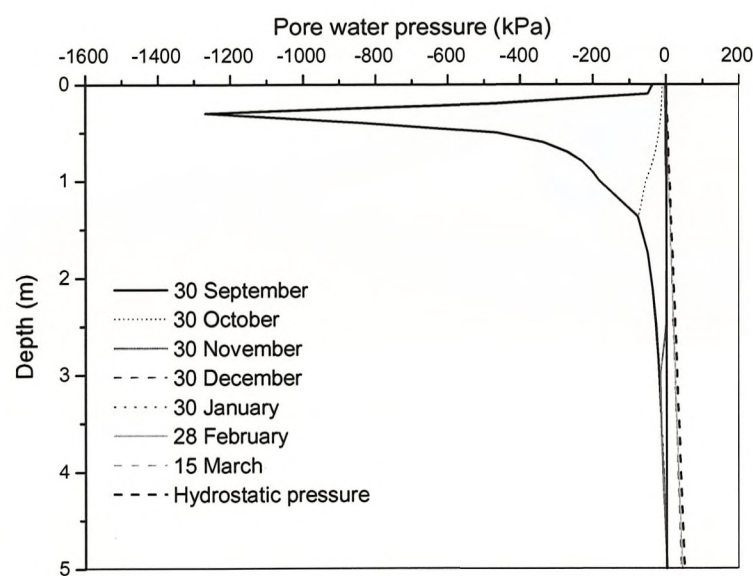


Figure 6.13: Calculated spatial pore water pressure (PWP) distribution during extreme weather: (a) End of dry summer, and (b) End of wet winter



(a)



(b)

Figure 6.14: Wet winter pore water pressure profiles: (a) tree covered mid slope, and (b) grass covered lower slope

6.5 Comment and conclusions

Hydrological modelling of Charing embankment and sensitivity analysis of soil permeability, climatic extremes and the influence of vegetation cover identified the key parameters governing calculated pore water pressure. Near surface seasonal pore water pressure variation to 1 m depth and drying at greater depth due to mature tree cover was observed at Charing embankment and recreated using the hydrological model.

Analysis showed that the saturated permeability typically measured at clay fill embankments lies within a critical range for seasonal weather influence on pore water pressure variation. Reducing the permeability of the clay fill to one order of magnitude lower than that measured at Charing created a damped pore water pressure response within the embankment. This demonstrates that railway embankments, constructed of clay fill, are more likely to experience large seasonal pore water pressure variation than modern, compacted embankments of lower saturated permeability.

Consideration of an extremely wet winter showed that pore water pressures close to hydrostatic can occur in grass covered areas, while in tree covered areas residual suctions are maintained at depth within the deeper tree root zone. This demonstrates that weather conditions and slope vegetation cover have a significant influence on embankment pore water pressures and must be considered when assessing the risk of slope failure and seasonal behaviour of railway embankments.

Table 6.5: Charing Model Summary

| Model Name | Permeability (ms^{-1}) | Climate Data | Vegetation Type | Tree LAI | Tree Depth | Rooting | Grass LAI | Grass Depth | Rooting | Plant Limit- ing Function |
|------------------------------------|-------------------------------|---|-----------------|-------------|---------------------------|---------|--------------|-----------------------------|---------|------------------------------|
| Initial Condition | 5×10^{-8} | Newbury Weather, Charing Weather | Grass & Trees | 2.7 | 3m-Summer, 0.9m-Winter | | 2.7 | 0.9m-Summer, 0.9-Winter | | As Feddes et al. (1978) |
| Charing 2007-2008 | 5×10^{-8} | Charing Weather | Grass & Trees | 2.7 | 3m-Summer, 0.9m-Winter | | 2.7 | 0.9m-Summer, 0.9-Winter | | As Feddes et al. (1978) |
| Charing Wet Winter | 5×10^{-8} | Wet Winter | Grass & Trees | 2.7 | 3m-Summer, 0.9m-Winter | | 2.7 | 0.9m-Summer, 0.9m-Winter | | As Feddes et al. (1978) |
| Charing Dry Summer | 5×10^{-8} | Dry Summer | Grass & Trees | 2.7 | 3m-Summer, 0.9m-Winter | | 2.7 | 0.9m-Summer, 0.9m-Winter | | As Feddes et al. (1978) |
| Charing (Fill 5×10^{-8}) | 5×10^{-8} | Newbury Weather | Grass & Trees | 2.7 | 3m-Summer, 0.9m-Winter | | 2.7 | 0.9m-Summer, 0.9m-Winter | | As Feddes et al. (1978) |
| Charing (Fill 5×10^{-7}) | 5×10^{-7} | Newbury Weather | Grass | N/A | N/A | | 2.7 | 0.9m-Summer, 0.9m-Winter | | As Feddes et al. (1978) |
| Charing (Fill 5×10^{-6}) | 5×10^{-6} | Newbury Weather | Grass | N/A | N/A | | 2.7 | 0.9m-Summer, 0.9m-Winter | | As Feddes et al. (1978) |
| Charing (Fill 5×10^{-9}) | 5×10^{-9} | Newbury Weather | Grass | N/A | N/A | | 2.7 | 0.9m-Summer, 0.9m-Winter | | As Feddes et al. (1978) |

Chapter 7

Permeability influence on embankment hydrology: London Underground Ltd study

Pore water pressures within railway embankments are influenced by seasonal weather patterns and the vegetation on the slope (O'Brien et al., 2004; Scott et al., 2007; Loveridge et al., 2010). Negative pore water pressures (suctions) typically occur following dry periods, particularly during the summer in temperate climates, when evaporation and transpiration remove soil water (Smethurst et al., 2006). Positive pore water pressures occur following wet periods as water infiltrates into the soil, and are typically highest at the end of spring (between March and May in the northern hemisphere) as there is little evaporation and transpiration during the winter months. In the UK, rainfall is generally of low intensity and high frequency, and distributed fairly evenly throughout the year. Therefore periods of prolonged, higher than average intensity rainfall are considered extreme events. Increases in pore water pressure during extreme wet periods can lead to slope instability and are of concern for infrastructure owners (Rail Safety & Standards Board, 2003).

During the winter of 2000/2001, the UK experienced the wettest weather since records began in 1766 (Birch & Dewar, 2002). Across England and Wales an average of 503 mm of precipitation was recorded from September

to November 2000, which is 196% of the 1972-2000 long term average (LTA). This wet autumn followed a wetter than average summer (Birch & Dewar, 2002) and preceding wet winters in 1998/1999 and 1999/2000 (Ridley et al., 2004), creating a wet initial condition at the start of winter. All these factors contributed to higher than average soil moisture contents and pore water pressures during the winter of 2000/2001. As a result, about 60 slope failures occurred on roads and more than 100 on railways across the UK (Turner, 2001).

Ridley et al. (2004) demonstrated a correlation between soil moisture content and slope stability by comparing the soil moisture deficit (SMD) for the London area with reported slope failures (Figure 7.1). The SMD is the volume of water per unit area that the soil can absorb before reaching 'field capacity', at which further precipitation cannot be stored and run off occurs. The SMD can be calculated by means of a soil water balance, taking into account rainfall infiltration and evapotranspiration of water from the soil (Smethurst et al., 2006) (Chapter 4). Figure 7.1 (reproduced from Ridley et al. (2004)) shows that in the South East of England between 1988 and 2001, periods of low SMD resulting from wet weather conditions correlate with earthworks failures. Figure 7.1 shows that the SMD for tree covered areas remained at zero for a period of 175 days during the winter of 2000/2001. This was an exceptionally long period of zero SMD (Ridley et al., 2004), resulting in embankment pore water pressures at or close to their maximum during the lifetime of the earthwork. Loveridge et al. (2010) suggest that the pore water pressures measured within embankments during this period could provide a design upper bound for embankment pore water pressures, corresponding to a rainfall return period of more than 1 in 100 years. Knowledge of this upper bound is useful for infrastructure owners when carrying out risk assessment of their geotechnical assets.

During the 1990s London Underground Ltd (LUL) identified the need to improve knowledge of pore water pressures within earthworks. A programme of pore water pressure monitoring was carried out on a number of embankments and cuttings around the LUL network. Following the wet winter of 2000/2001, spot measurements of pore water pressure were recorded at several of these sites, when pore water pressures would have been at their highest (Ridley et al., 2004). Open standpipes and flushable Geo-Piezometers (Ridley et al., 2003) were used. The Geo-Piezometers can measure suctions

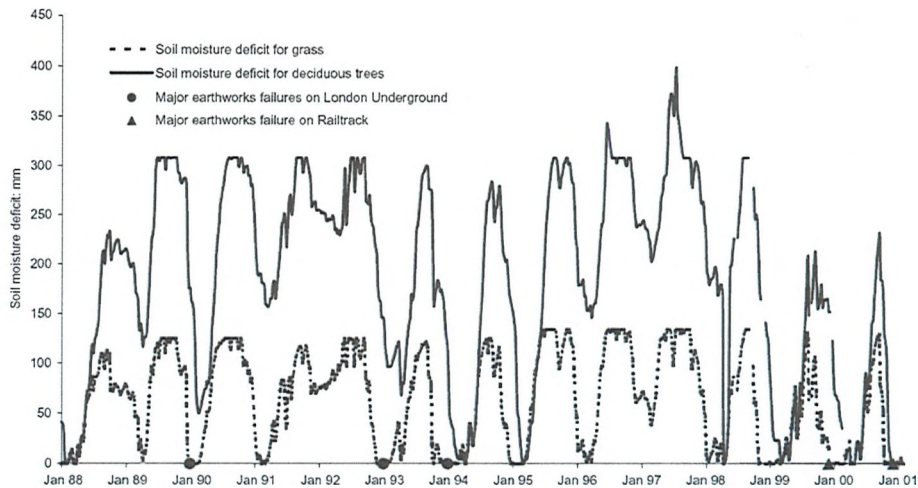


Figure 7.1: Variation of Soil Moisture Deficit (1988-2001) from the Meteorological Office Rainfall and Evaporation Calculation System, MORECS (Hough et al., 1997) with the timing of major earthworks failures indicated. (Reproduced from Ridley et al. (2004))

up to about 80 kPa.

Pressure heads within the embankments (Figure 7.2) demonstrate a wide variation in pore water pressure conditions. Many of the embankments were constructed from locally excavated clay material, with an ash capping at the embankment crest (Skempton, 1996). When analysing the data, Ridley et al. (2004) plotted pressure head against the depth below the top of the clay fill, assuming that the more permeable ash layer would be free draining in comparison with the clay fill material. The ash layer was between 0 m and 3.8 m thick for the embankments monitored.

Ridley et al. (2004) showed that some heads measured at shallow depths within the embankments reached hydrostatic below the top of the clay fill at the end of the wet winter. Hence for design and assessment purposes it could be argued that pore water pressure conditions may reach hydrostatic. However, this does not account for the factors contributing to increased pore water pressures, and as an upper bound is likely to be overly conservative for many embankments as the data indicate a significant number of measurements below hydrostatic, and some negative pore water pressures (Figure 7.2).

The aims are: (1) to re-examine the London Underground Ltd (LUL)

data set to understand the conditions contributing to the range of measured pore water pressures; and (2) to describe a range of factors which should be considered when assessing appropriate pore water pressures for design and assessment.

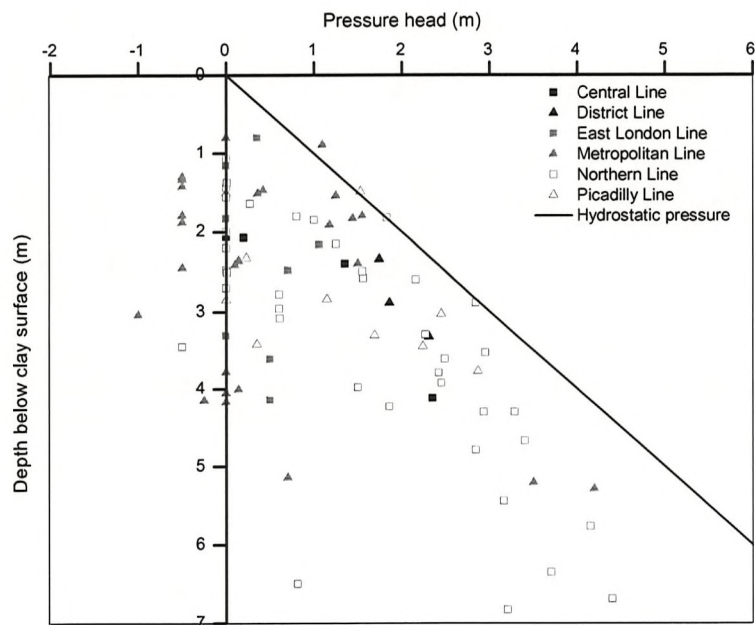


Figure 7.2: Pressure heads measured across the London Underground Ltd network during spring 2001, plotted as depth below the clay surface

7.1 Analysis of the LUL pore pressure data

Ridley et al. (2004) presented data from measurements made using a total of 75 no. flushable piezometers and 38 no. open standpipes during March and April 2001, for which the raw data were re-assessed. The depth of the ash layer at the piezometer locations allowed the measured pressure heads to be plotted against depth below the clay surface: Figure 7.2 shows that these data lie almost entirely below a hydrostatic condition extending from zero at the clay surface.

A few readings exceed the hydrostatic line, indicating water in the ash layer, whereas some measurements show very low, and even negative, pore water pressures. Records from London Underground Ltd including assessment, ground investigation, monitoring and interpretive reports were available, in varying degrees of detail, for 15 embankments; these provided supplementary information for 82 of the 113 piezometer locations, which was used to explore the factors influencing and responsible for the wide range of measured pore water pressures.

7.1.1 Method

The first stage of the data analysis was to identify each piezometer and confirm the reliability of its measurements. This enabled anomalous results to be identified (e.g. where there had been difficulties during measurement) and results relating to perched water tables, unrepresentative of the whole embankment, to be removed. Anomalous results, along with piezometers for which borehole location plans and geotechnical cross sections could not be obtained, were not considered further.

Information was obtained from London Underground Ltd records relating to:

- Embankment fill material
- Foundation material
- Remediation history (e.g. widening and early repairs)
- Embankment slope angle
- Borehole orientation and location

- Embankment vegetation type

Full details were obtained for 35 piezometers, and limited information for the remaining 78 (Table 7.1). All of the embankments were constructed predominantly from clay fill, with an average height of 5 m and slope gradient of 1 in 2.4.

Table 7.1: Summary of London Underground Ltd data

| Category | Number of sites (Total of 113) | | | |
|---------------------|--------------------------------|-----------------|-------------|--------------|
| Fill material | Clay (88) | | | Unknown (25) |
| Foundation material | London clay (54) | Chalk (20) | Gravel (14) | Unknown (25) |
| History of widening | Yes (11) | No (24) | | Unknown (78) |
| Slope angle | 10°- 20°(2) | 20°- 30°(32) | > 30°(8) | Unknown (71) |
| Slope orientation | North-East (13) | South-West (35) | | Unknown (65) |
| Slope position | Crest (33) | Midslope (7) | Toe (6) | Unknown (67) |
| Slope vegetation | Tree (71) | Grass (9) | | Unknown (33) |

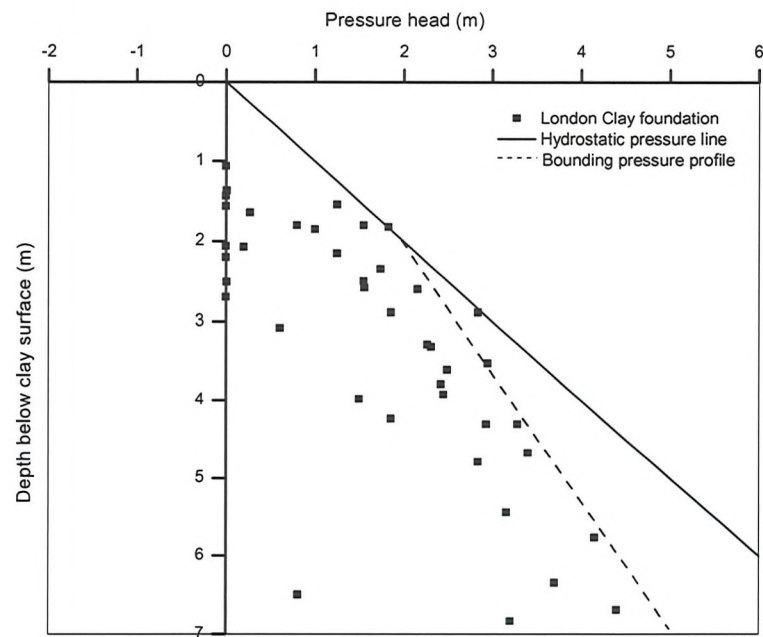
7.1.2 Foundation material

Figure 7.3 plots the piezometer measurements against depth below the clay surface, with the general type of foundation geology indicated. At sites with a London clay foundation (Figure 7.3(a)), the majority of pressure heads are bounded by the hydrostatic line to a depth of about 2 m below the clay surface. Beneath this, the bounding rate of increase in pore water pressure with depth reduces to about 60% of hydrostatic, creating a bilinear profile. Relatively low pore water pressures were recorded at many locations, with about 20% (8 out of 41) of the readings at zero pressure, and more than half (24 out of 41) at pressure heads of 2 m or less.

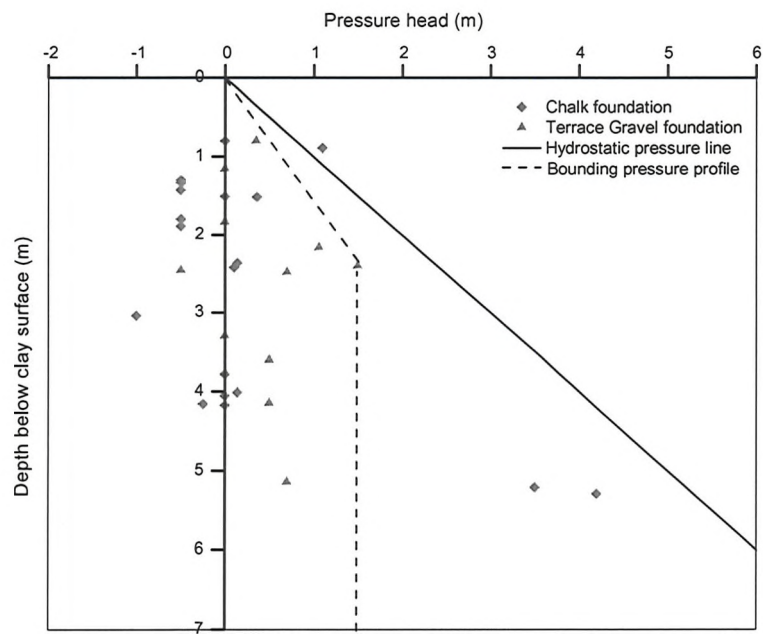
Embankments with a chalk or terrace gravel foundation (Figure 7.3(b)) were underdrained with pressure heads below 1 m at all depths for 29 of 34 piezometers (85% of cases). For >90% of the data points the pressure head profile can be described as sub-hydrostatic to 2.5 m below the clay surface before reducing to less than 1 m head throughout the soil profile below.

7.1.3 Embankment vegetation cover

Limited information describing site vegetation was available for 80 piezometers; 9 of which were on grass covered embankments and 71 on tree cov-



(a)



(b)

Figure 7.3: Comparison of March / April 2001 measured pressure head by embankment foundation material: (a) London clay foundation; (b) Chalk / terrace gravel foundation

ered slopes. Detailed information describing the tree water demand and the spatial distribution of the trees was not available. O'Brien (2007) states that tree water demand is an important factor in assessing the likelihood of maintaining low winter pore water pressures. High water demand trees (e.g. oaks, poplar, etc) are often able to generate a moisture deficit and suctions in lower permeability clays that can be sustained through winter periods (Biddle, 1998). In contrast, the generation of significant soil drying and suctions for grass and low water demand trees is typically limited to a shallow rooting zone of about 0.9 m depth (Biddle, 1998; Smethurst et al., 2006), and is rarely sustained through an average winter (Clarke & Smethurst, 2010; Smethurst et al., 2011).

Ridley et al. (2004) used data from two sites (N2 and N3) in which high (near hydrostatic) pressure heads occurred in tree covered embankments (Figure 7.4) to argue that that during periods of prolonged wet weather, the soil profile re-saturates and the soil desiccation created by trees is reversed. However, while some pressure heads close to hydrostatic were measured at shallow depth, the majority of the readings in Figure 7.4, including some of those for sites N2 and N3, lie well below the hydrostatic line. Thus a range of pressure heads were measured at tree covered, London clay founded embankments following the wet winter of 2000/2001. Detailed monitoring adjacent to trees in clay soils (Biddle, 1998; O'Brien, 2007; Scott et al., 2007) indicate that the pattern and extent of seasonal soil moisture content and pressure head variation depends on a number of factors such as the soil permeability, surface cracking of the clay fill, tree species, rooting depths and tree water demand. This information was not available for the sites considered in this study.

7.1.4 Slope angle, construction history and borehole position

Information relating to the slope angle, remediation history (i.e. widening or early repairs) and borehole position on the embankment slope was collected for boreholes from 7 embankments where data were available. No correlation with any of these factors was found; the effect of foundation material dominated in all cases. The influence of borehole position is shown in Figure 7.5, which plots the piezometer measurements against depth below the clay surface, with the borehole slope position indicated.

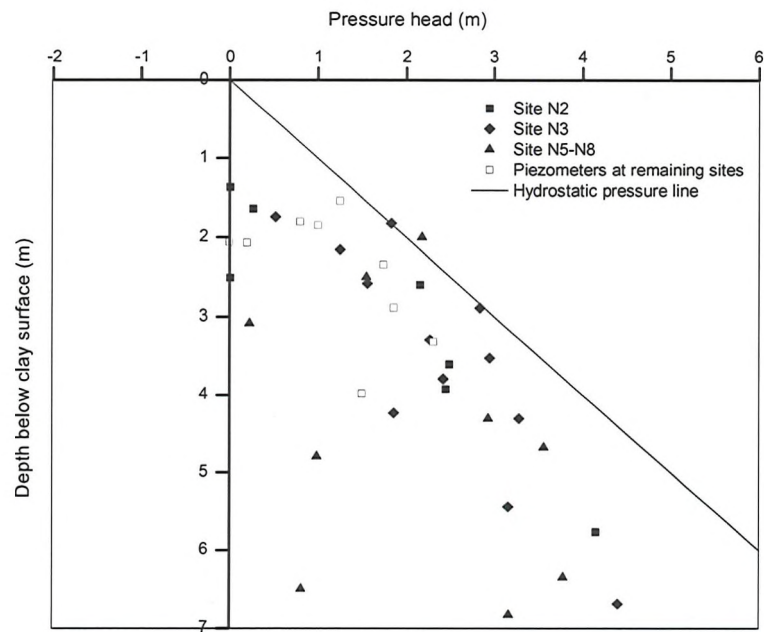


Figure 7.4: Open standpipe (N2, N3 and N5-N8) and flushable Geo-Piezometer measurements at tree covered, London clay founded embankments in March / April 2001 (tree species and water demand not known)

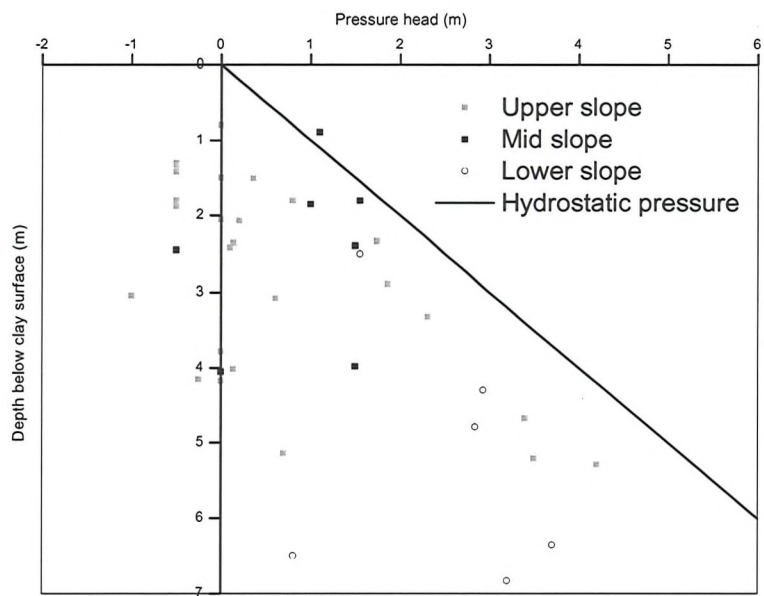


Figure 7.5: Comparison of March / April 2001 pressure head by borehole slope position

7.2 Finite element modelling

Finite element analysis was used to understand the observed patterns of pore water pressure found in the case study data. The influence of foundation permeability on embankment pore water pressures was examined using the software Vadose/w (Geo-Slope, 2007).

Vadose/w calculates saturated and unsaturated water and heat flow in response to applied boundary conditions. A climate boundary condition can be applied; this uses daily climate data (temperature, humidity, windspeed, rainfall and solar radiation), as described later, to calculate water infiltration and water removal from the surface of the soil and from a defined rooting zone. This enables variations in pore water pressures with time, in response to weather patterns of different duration and intensity, to be investigated.

7.2.1 Mesh geometry

Four soil columns (A to D) with one-dimensional vertical flow were used to calculate pressure head profiles for different foundation types in response to wet winter weather. One dimensional models were used to simulate infiltration into a monitored slope in Hong Kong (Li et al., 2005) and a 10 m high dry ash dump in South Africa (Fourie et al., 1999), while comparison with a laboratory experiment showed a one-dimensional model to give adequate results (Essig et al., 2009). Field measurements showed that soil water contents tend to be higher near the toe of a slope than at the crest, irrespective of rainfall events, due to subsurface flow in the downslope direction (Rahardjo et al., 2005). Comparison with a two dimensional embankment model showed the one dimensional soil column to approximate to the midslope of a uniform embankment (Appendix B).

The one dimensional model may differ from field conditions at individual sites or slope locations where downslope subsurface flow may affect pore water pressure distributions. However, the purpose of the model is to compare with monitoring data from 113 boreholes at different locations to demonstrate the influence of permeability variation with depth, rather than to replicate local conditions.

The 9 m deep soil column consisted of a surface clay layer (to 1 m depth), 4 m of clay fill and 4 m of foundation material, which was varied for models A to D (Figure 7.6). A fine mesh of 0.1 m square elements was used in the

surface zone to enable calculation of the response to high pressure gradients created by the boundary condition. In the remainder of the soil column, a mesh of 0.5 m square elements was used.

7.2.2 Material properties

The saturated permeability of the clay fill was based on test data reported by O'Brien et al. (2004). Unsaturated soil properties describing the reduction in soil water storage with increasing suction were based on a modified version of the Croney (1977) SWRC measured for London clay, using the van Genuchten (1980) curve fit. van Genuchten (1980) parameters for London clay shown in Table 7.2 were used to produce a curve fitted to the drying curve for *in situ* London clay measured by Croney (1977). The clay fill was assigned a lower air entry value and a shallower curve gradient than *in situ* London clay, consistent with its greater specific volume and wider range of pore sizes (Figure 7.7). These SWRCs were used to define the variation of soil hydraulic conductivity with soil suction, calculated using the Mualem (1976) method with van Genuchten (1980) constants (Figure 7.8). Unsaturated properties of the clay fill are described in Section 5.5.4.

Models A to C had a typical saturated clay fill permeability of $5 \times 10^{-8} \text{ ms}^{-1}$ while model D had a saturated clay fill permeability of $5 \times 10^{-9} \text{ ms}^{-1}$ representing a likely lower limit (O'Brien et al., 2004). Model B had a saturated foundation permeability of $5 \times 10^{-8} \text{ ms}^{-1}$ and models C and D had a saturated foundation permeability of $5 \times 10^{-9} \text{ ms}^{-1}$; a range consistent with *in situ* London clay (Chandler et al., 1990; O'Brien et al., 2004; Smethurst et al., 2006). Model A had a saturated foundation permeability one order of magnitude greater than the clay fill ($5 \times 10^{-7} \text{ ms}^{-1}$), representing underdrainage by a chalk or gravel. The van Genuchten (1980) parameters and saturated permeability, used to characterise the SWRC and hence unsaturated hydraulic conductivity, are shown in Table 7.2.

The surface metre of clay fill was assigned a saturated permeability 10 times greater in the vertical direction than the clay fill in the core of the embankment. This represents the increased permeability of the surface clay, where cracking increases the bulk vertical permeability, facilitating rainfall infiltration (Novak et al., 2000). Li et al. (2011) showed that the vertical field hydraulic conductivity of a compacted clay fill can vary by up to two orders of magnitude between 0.08 m and 1.08 m depth. Calculated pore

Table 7.2: Summary of soil properties

| Soil Type | Permeability (ms ⁻¹) | Van Genuchten Constants | | | | | |
|--|-------------------------------------|-------------------------|------------|------------|------|------|--|
| | | AEV (kPa) | θ_s | θ_r | m | n | |
| Typical clay fill* | 5×10^{-8} | 30.3 | 0.47 | 0.1 | 0.13 | 1.15 | |
| Lower permeability clay fill* | 5×10^{-9} | 30.3 | 0.47 | 0.1 | 0.13 | 1.15 | |
| Surface clay fill* | 5×10^{-7} | 30.3 | 0.47 | 0.1 | 0.13 | 1.15 | |
| Chalk / gravel foundation [‡] (A) | 5×10^{-7} | 2 | 0.45 | 0.1 | 0.5 | 2 | |
| London clay foundation [†] (B) | 5×10^{-8} | 125 | 0.47 | 0.1 | 0.15 | 1.18 | |
| London clay foundation [†] (C&D) | 5×10^{-9} | 125 | 0.47 | 0.1 | 0.15 | 1.18 | |

Where AEV = Air entry value, θ_s = saturated water content, θ_r = residual water content, m and n = constants. * van Genuchten parameters derived in section 5.5.4, [†] van Genuchten parameters curve fitted to drying London clay (Croney, 1977), [‡] estimated van Genuchten parameters for a sandy gravel

water pressures in two dimensions were insensitive to anisotropic saturated permeability in the surface clay fill (Appendix B).

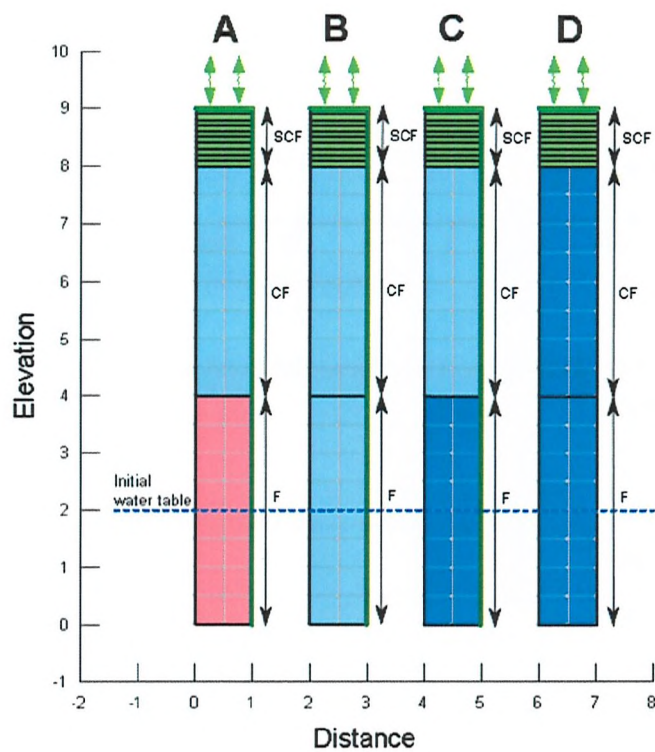


Figure 7.6: Model geometry - Soil columns A to D. (Material properties for surface clay fill (SCF), clay fill (CF) and foundation (F) are shown in Table 7.2)

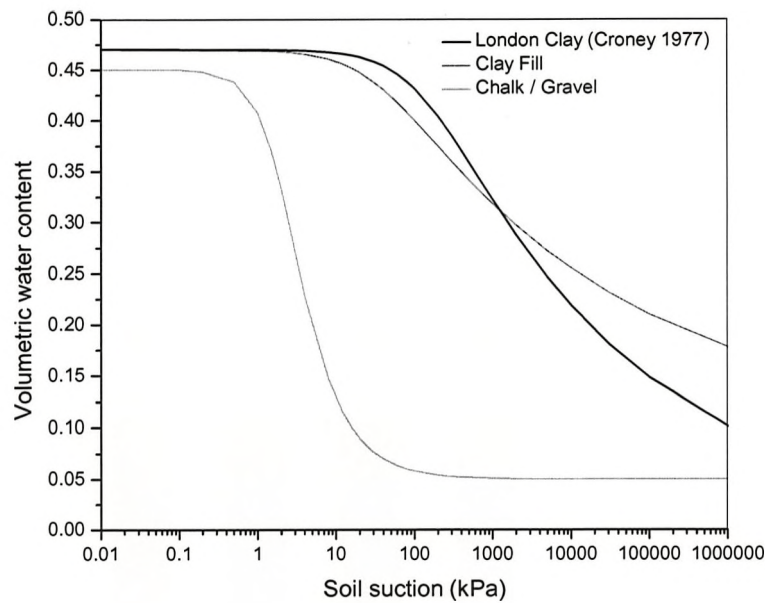


Figure 7.7: Soil Water Retention Curves for London clay (Croney, 1977), clay fill and chalk/gravel

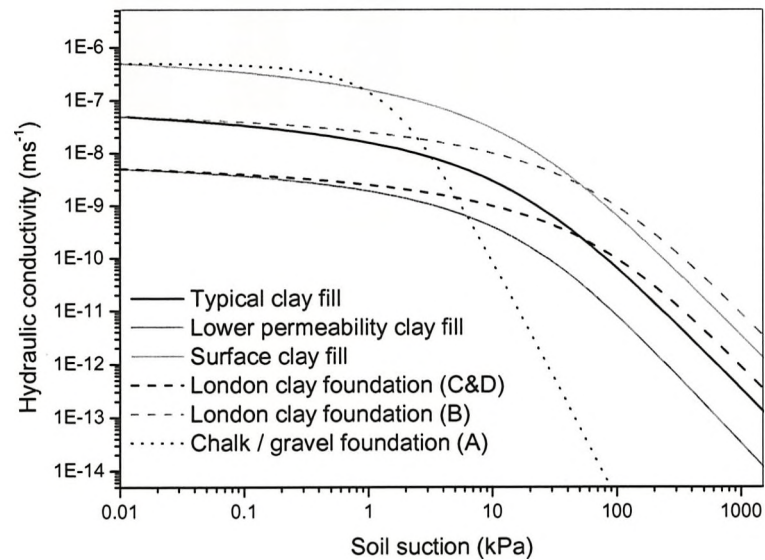


Figure 7.8: Hydraulic conductivity curves for London clay, clay fill and chalk/gravel

7.2.3 Boundary and initial pore water pressure conditions

The Vadose/w climate boundary condition calculates the surface water balance of water infiltration and water removal based on daily weather data (temperature, relative humidity, windspeed, rainfall and solar radiation). Water removal due to evaporation from an unsaturated soil is calculated using the Penman-Wilson equation (Wilson et al., 1994) and transpiration using a root water uptake model (Tratch et al., 1995). Grass and shrub vegetation with a rooting zone of 0.9 m, from which transpired water can be removed from the soil by the plant roots, was assumed in all of the models. Hence this model is intended to represent a slope with a cover of grass and low water demand trees, rather than the deeper desiccation effects of high water demand trees. The Leaf Area Index (LAI), defining the proportion of solar energy intercepted by the vegetation for transpiration (Ritchie, 1972), corresponded to full leaf cover during the summer period (1 April to 17 October) and zero during the winter, on the basis of plant leafing periods described by Biddle (1998). Reduction in root water uptake due to soil drying, as the plant becomes stressed and reduces transpiration, was modelled using the Feddes et al. (1978) relationship, with transpiration reducing linearly between 100 kPa and 1500 kPa suction. Effective rainfall (i.e. that not evaporated from the canopy or the soil surface) that is unable to infiltrate into the soil is considered to run off and is removed from the model.

A climate boundary condition was applied to determine pore water pressure changes at the soil surface in response to weather. A climate boundary condition was applied using daily weather data (temperature, relative humidity, windspeed and solar radiation) obtained from a weather station at Shoeburyness in Essex, to the East of London. Figure 7.9 shows that winter rainfall totals (1 October to 31 March) from this weather station are lower than rainfall at Heathrow Airport (Met Office, 2009) and from Newbury, approximately 60 km to the West of Heathrow. Figure 7.9 indicates that winter rainfall in the South East of England generally reduces from West to East and that rainfall measured at Shoeburyness is likely to be lower than the Greater London area, where most of the study sites are located. Therefore daily rainfall data measured near Heathrow Airport, which lies close to most of the study sites, was applied to the climate boundary data (Table 7.3).

The climate data for 2000/2001 represents an extreme event, correspond-

ing to a rainfall return period across much of England and Wales of at least 100 years (Loveridge et al., 2010). Weather data for 2002/2003 and 2004/2005 were used to create additional climate scenarios corresponding to less extreme rainfall periods, for comparison with the 2000/2001 calculated pressure head distribution (Table 7.3). 64 years of monthly rainfall data recorded at Heathrow Airport (Met Office, 2009) were used to calculate the winter rainfall return period for the climate scenarios, comparing winter rainfall between 1 October and 31 March for winters from 1948/1949 to 2010/2011 (a total of 63 winters). From this it was calculated that 2002/2003 and 2004/2005 correspond to winter rainfall return periods of approximately 1 in 10 years and 4 in 5 years respectively.

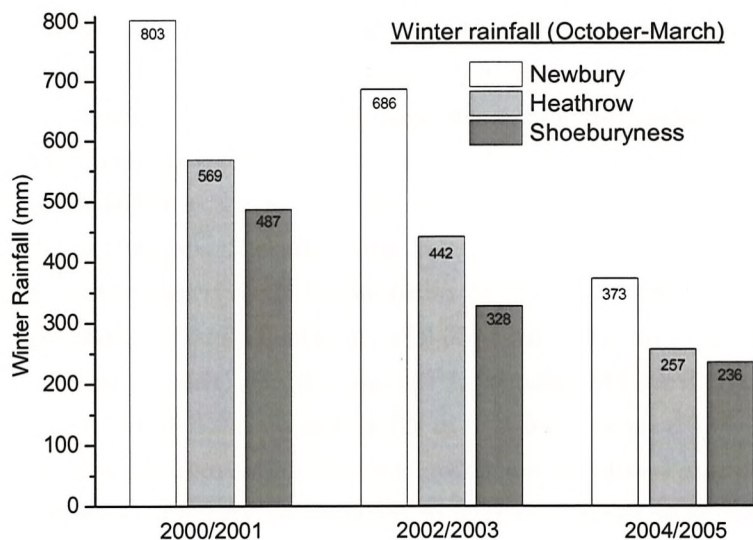


Figure 7.9: Comparison of winter rainfall (1 October to 31 March) at Newbury, Heathrow Airport and Shoeburyness

Sensitivity analysis showed that after two years of applied climate data the pore water pressure distribution was independent of the initial condition. Therefore an initial pore water pressure distribution was created within the soil by applying two years of climate data (Table 7.4) from an initial condition of pore water pressures hydrostatic above and below a water table 2 m below the foundation surface (Figure 7.6). Having established an initial pore water pressure distribution, a climate boundary condition for the winters of 2000/2001, 2002/2003 and 2004/2005 was applied to the surface boundary (Table 7.4).

Table 7.3: Summary of climate data

| Dates | Annual Potential Evapotranspiration (mm)* | Annual rainfall (mm) [†] |
|-------------------|--|-----------------------------------|
| Jan '98 - Jan '99 | Unavailable [‡] | 687 |
| Jan '99 - Jan '00 | 759 | 647 |
| Jan '00 - Jan '01 | 700 | 799 |
| Jan '01 - Jan '02 | 728 | 706 |
| Jan '02 - Jan '03 | 748 | 739 |
| Jan '03 - Jan '04 | 801 | 510 |
| Jan '04 - Jan '05 | 756 | 619 |
| Jan '05 - Jan '06 | 719 | 453 |

* calculated using weather data measured at Shoeburyness

[†] measured near Heathrow Airport

[‡] Potential Evapotranspiration for 1999 applied (759 mm)

Table 7.4: Summary of climate boundary conditions

| Climate boundary | Weather data | Applied timestep |
|-------------------|-------------------|------------------|
| Initial condition | Jan '98 - Jan '00 | Days 0 -730 |
| 2000/2001 | Jan '00 - Jan '02 | Days 731 - 1462 |
| 2002/2003 | Jan '02 - Jan '04 | Days 731 - 1462 |
| 2004/2005 | Jan '04 - Jan '06 | Days 731 - 1462 |

Remaining boundaries were assumed to be impermeable, allowing the water table to fluctuate vertically in response to pressure head changes within the initially unsaturated zone of the soil column, representing a transient situation in which groundwater recharge and discharge in the foundation are not in balance with surface infiltration and evapotranspiration (Freeze, 1969).

7.3 Modelling results

The surface water balance calculated using the Shoeburyness weather data for the winter of 2000/2001 is shown in Figure 7.10. This shows that a greater volume of water was able to enter the underdrained model during the wetting period (because run off was reduced), while water removal during dry periods occurred at a similar rate. Run off of excess rainfall occurred earliest in model D as the rainfall infiltration rate was limited by the saturated permeability of the clay fill.

Maximum envelopes of pressure head were determined, bounding daily

pressure head profiles calculated between the months of March and May. For example, Figure 7.11 shows pressure head profiles for model A during March 2001, together with the maximum envelope of pressure head (March-May 2001). Maximum pressure heads to 2.5 m depth are shown on the 17 March, while suctions remain at greater depth. The two later profiles show greater pressure heads below 2.5 m, as previously infiltrated water has continued to flow downwards, while drying from the surface boundary (as shown in Figure 7.10) has reduced pressure heads at shallow depth. The maximum pressure head envelope therefore reflects the maximum transient pressure head at any depth and the actual pressure heads on any specific day will lie below the maximum profile.

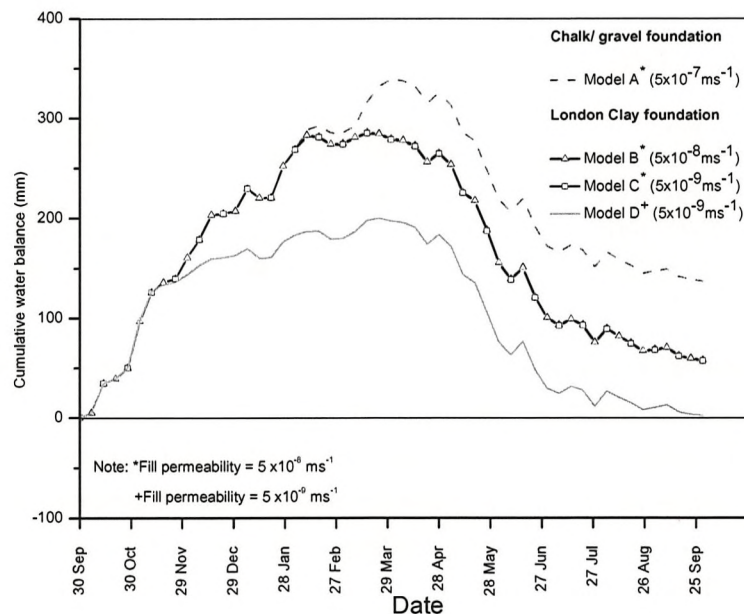


Figure 7.10: The cumulative surface water balance (Σ rainfall – run off – evapo-transpiration) calculated for soil columns A to D using Shoeburyness weather data, between October 2000 and October 2001

7.3.1 Foundation permeability

Figure 7.12 compares the maximum pressure head envelopes for models A to C. Positive pressure heads are indicated at shallow depths in response to direct infiltration into the higher permeability zone at the soil surface, while at greater depths the influence of clay fill and foundation permeability

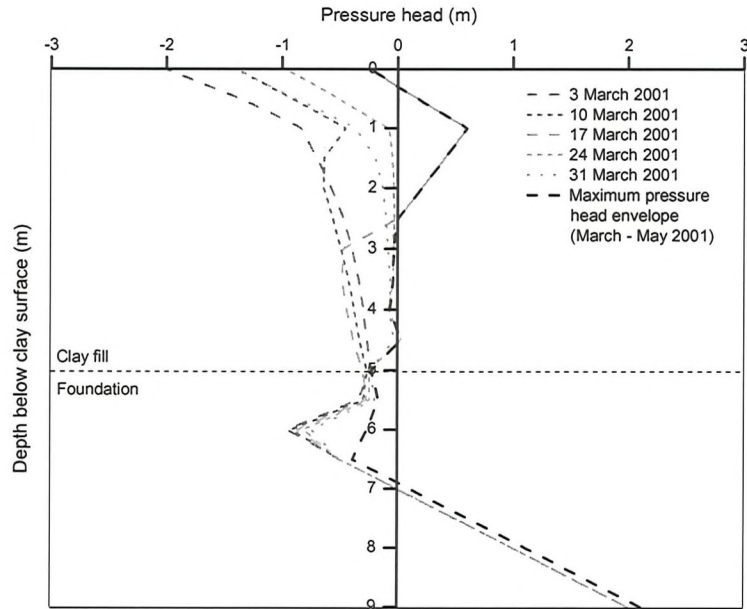


Figure 7.11: Pressure head profiles in March 2001 plotted with the maximum pressure head envelope (March to May 2001) for finite element model A

becomes apparent and significant differences between the profiles develop.

For a foundation saturated permeability of $5 \times 10^{-9} \text{ms}^{-1}$, one order of magnitude less than the clay fill, the maximum pressure head envelope was 99.8% of hydrostatic below 1 m depth. Increasing the foundation saturated permeability to $5 \times 10^{-8} \text{ms}^{-1}$, the same as the clay fill, made very little difference, resulting in a maximum pressure head envelope 99.5% of hydrostatic. For the underdrained soil column, with a foundation saturated permeability of $5 \times 10^{-7} \text{ms}^{-1}$, pressure heads close to zero were calculated within the clay fill and at the top of the foundation. Thus there is a distinct difference in the pressure head profile within the embankment between a clay foundation (of equal or lower saturated permeability than the fill) and a foundation of higher permeability material, in wet winter weather conditions.

Comparison of the surface water balance (Figure 7.10) with the pore water pressure profiles (Figure 7.12) shows that while the greatest volume of water entered model A, drainage from the foundation maintained low pore water pressures within the clay fill. The influence of transient flow is apparent because reference to the SWRC (Figure 7.7) shows that soil columns A, B and C are all saturated, but the reduction in saturated permeability at

depth in the clay founded soil columns (B and C) causes positive pore water pressures to develop during a high infiltration event such as the winter of 2000/2001.

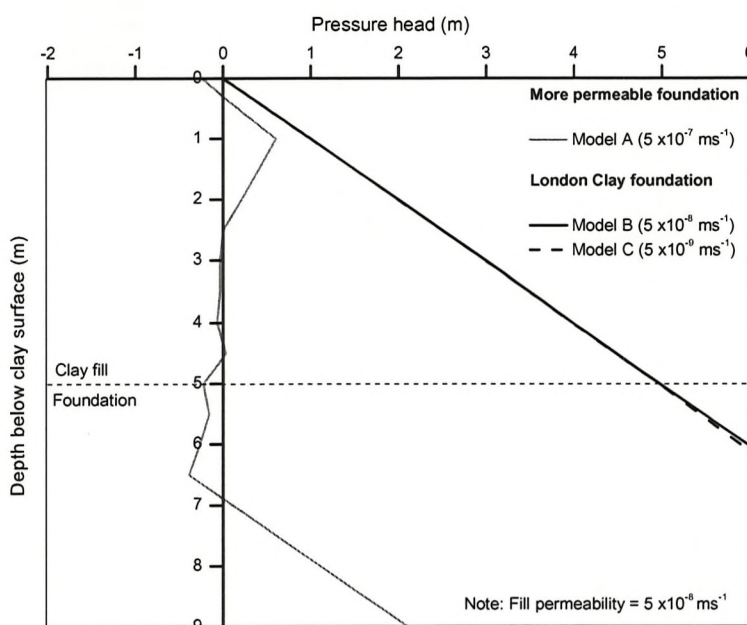


Figure 7.12: Maximum March - May 2001 pressure head envelopes calculated using finite element models A to C (foundation permeabilities shown), representative of a grass or Low Water Demand tree covered slope

7.3.2 Clay fill permeability

Comparison of pressure head variations at 2 m depth with time between 1st October and 31st May during the winters of 2000/2001, 2002/2003 and 2004/2005 for a clay fill of typical saturated permeability (Model C, saturated fill permeability of $5 \times 10^{-8} ms^{-1}$) and a lower saturated permeability clay fill (Model D, $5 \times 10^{-9} ms^{-1}$) are shown in Figure 7.13. The rate and magnitude of pressure head increase between 1 October, at the end of summer, and 31 March is greater in the typical clay fill than the lower permeability clay fill, in agreement with Loveridge et al. (2010). The lower permeability fill restricts surface infiltration into and drying from the soil, and the pressure heads are less affected by rainfall events than the higher permeability clay fill.

For both the typical clay fill and the lower permeability clay fill the maximum calculated pressure heads, at 2 m depth, occurred during late March 2001 (Figure 7.13). This is consistent with the measurements of Ridley et al. (2004), confirming that the measurements taken during this period should reflect the maximum or close to maximum pore water pressures.

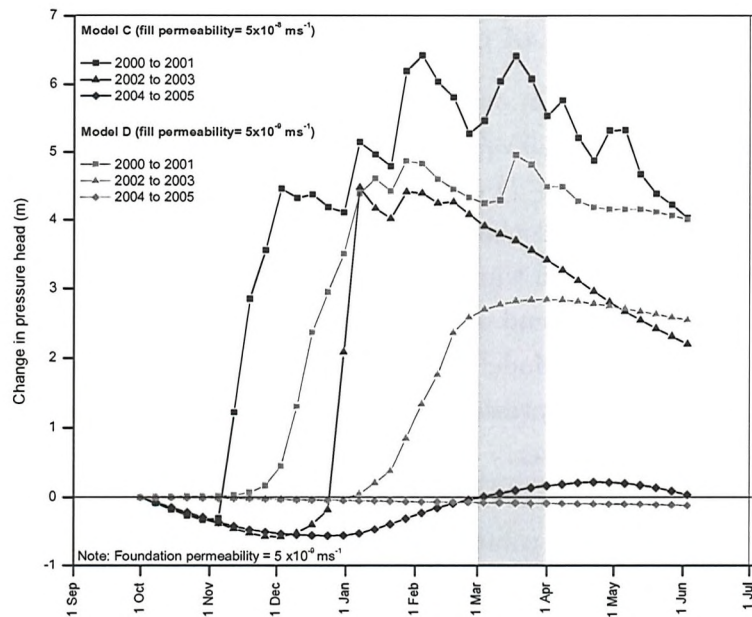


Figure 7.13: Change in pressure head at 2 m depth within a soil column of clay fill of typical permeability (model C) and lower permeability (model D) between 1 October and 31 May in 2000/2001, 2002/2003 and 2004/2005

7.3.3 Comparison of monitoring data and numerical model

The monitoring data obtained during the spring of 2001 following the wet winter of 2000/2001 showed the same distinct difference in pressure head profile between London clay founded and chalk/gravel founded embankments indicated by the numerical model. Figure 7.14(a) shows that the monitoring results from the London clay founded embankments are bounded by the pressure head profiles calculated using the finite element model with foundation saturated permeabilities of $5 \times 10^{-8} \text{ms}^{-1}$ and $5 \times 10^{-9} \text{ms}^{-1}$. This suggests that at some of the monitored sites the near hydrostatic profile of pressure head measured is caused by a foundation saturated permeability close to or less than that of the clay fill ($5 \times 10^{-8} \text{ms}^{-1}$).

Figure 7.14(b) compares the monitoring data from chalk and terrace gravel founded embankments with the finite element model pressure head profile for a more permeable foundation. The profile for a foundation saturated permeability of $5 \times 10^{-7} \text{ms}^{-1}$ shows a consistently low pressure head throughout the soil profile, in agreement with the monitoring data.

7.3.4 Comparison of climate scenarios

Climate boundary conditions for a less extreme winter (2002/2003) and a relatively drier winter (2004/2005) were applied to model A (more permeable foundation, $5 \times 10^{-7} \text{ms}^{-1}$) and model C (clay foundation, $5 \times 10^{-9} \text{ms}^{-1}$). Profiles of maximum calculated pressure head against depth between March and May, following each winter period, are compared in Figure 7.15.

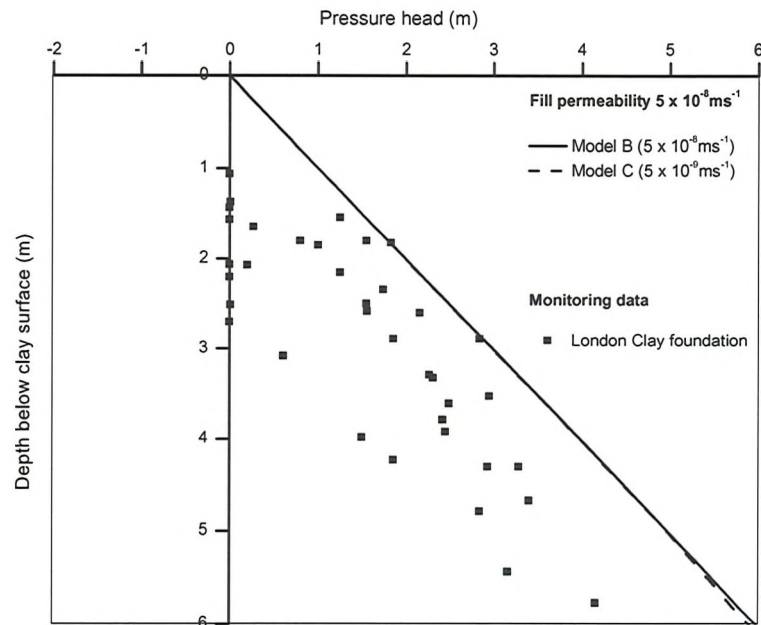
Comparison of the end of winter pressure head profiles for the soil column founded on clay (Model C, Figure 7.15(a)) demonstrates the significant difference between the pressure head profiles during an extreme wet winter and a less extreme winter.

Comparison of the end of winter pressure head profiles for a chalk/terrace gravel founded soil column (Model A, Figure 7.15(b)) shows lower pressure heads within the clay fill during less extreme winters. However, unlike model C the pressure head profiles for all winter scenarios in model A converge within the foundation layer and the water table within the foundation is unaffected.

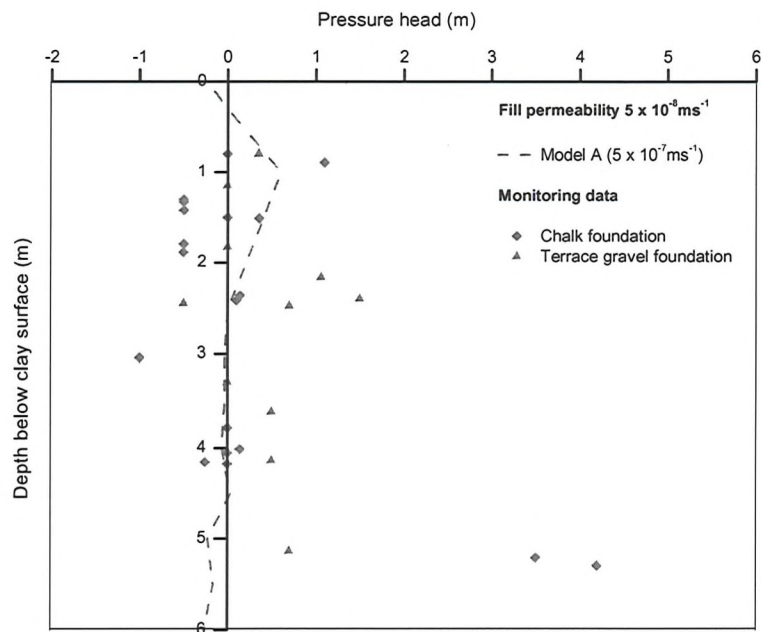
Both model A and model C show negative pressure heads near the soil surface (to 3.5 m depth) for less extreme winters (2002/2003 and 2004/2005) and the influence of foundation permeability on pressure head profile is less evident, in contrast to the 2000/2001 profiles.

7.4 Implications for earthworks assessment

Field monitoring data and numerical modelling has shown that the variation of permeability with depth has a major effect on the end of winter pore water pressures following a period of extreme autumn and winter rainfall. Clay fill embankments on chalk and terrace gravel foundations (of saturated permeability at least an order of magnitude greater than the clay fill itself) are underdrained, with pore pressures remaining low in comparison with those in an embankment on a clay foundation. This should be considered

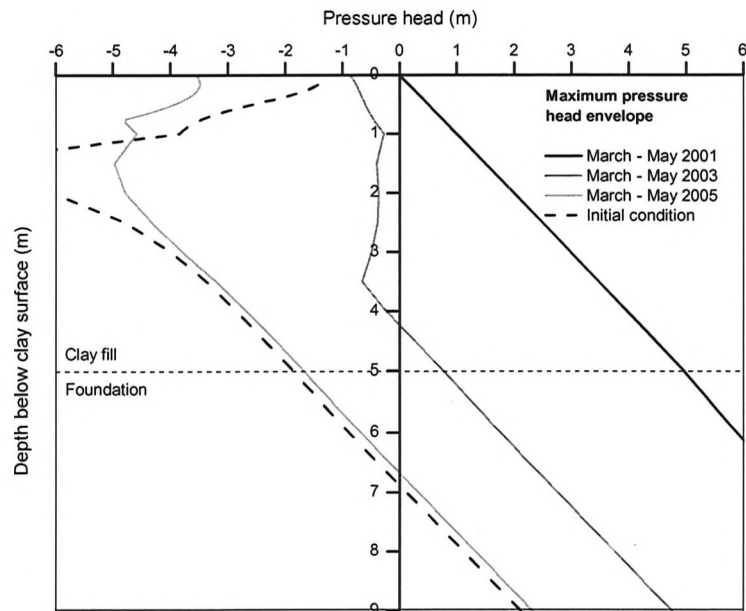


(a)

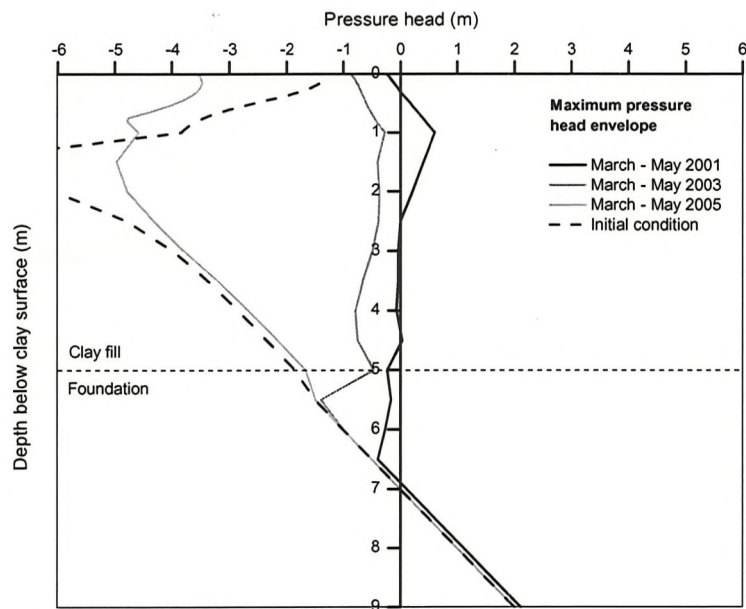


(b)

Figure 7.14: Comparison of maximum March - May 2001 pressure head envelopes from the finite element model with monitoring data: (a) London clay foundation; (b) Chalk / terrace gravel foundation



(a)



(b)

Figure 7.15: Maximum March - May pressure head envelopes calculated for 2001, 2003 and 2005: (a) London clay foundation (model C); (b) Chalk / terrace gravel foundation (model A)

in assessing the long-term stability of earthworks.

The field monitoring data showed that even during an extreme wet winter, relatively low (0 kPa up to 2.5 m depth) pore water pressures can be sustained throughout an embankment founded on London clay. This is probably due to the influence of high water demand (HWD) trees, as discussed elsewhere (Briggs, 2010; O'Brien, 2007; Scott et al., 2007) but not included in the numerical models discussed in this chapter.

The higher permeability of a near surface zone of cracked clay fill is clearly important and full hydrostatic pore water pressures can rapidly become established in this zone. The numerical model assumed this zone to be 1 m in depth, but it may be deeper in the field (Anderson et al., 1982). Mechanisms potentially leading to deeper zones of cracking, and higher mass permeability warrant further research.

7.5 Conclusions

Pore water pressure measurements in London Underground clay railway embankments at the end of the very wet winter of 2000/01 have been analysed to investigate the effect of foundation saturated permeability, which was shown to be a dominant influence on pore water pressures.

Embankments underdrained by a more permeable layer, such as chalk or terrace gravel, maintained pore water pressures of less than 15 kPa throughout the soil profile despite the wet winter providing a high rate of water infiltration into the soil surface. Embankments founded on London clay, and therefore not underdrained, showed higher pore water pressures. A bilinear profile forms a reasonable upper bound, with pore water pressures being close to hydrostatic near the surface (<2 m depth), and sub-hydrostatic at greater depth.

A finite element model was used to investigate the influence of foundation and clay fill saturated permeability on embankment pore water pressures during a wet winter. Comparison of soil columns founded on clay and on a more permeable material demonstrated that during an extreme wet winter, underdrainage reduces pressure head throughout the soil profile, in agreement with the monitoring data. Seasonal pressure head variation in the clay founded soil columns was shown to depend on the saturated clay fill permeability, with less pressure head variation calculated for the lower

permeability clay fill. Pressure heads during the winter of 2001 were shown to peak during March, indicating that the measurements of Ridley et al. (2004) are probably representative of maximum winter pressure heads, as argued by Loveridge et al. (2010).

The numerical model has shown that for London clay founded embankments an extreme wet winter can significantly increase pressure heads compared with a less extreme winter, while for underdrained embankments pressure heads are much less sensitive to seasonal weather extremes. During less extreme winters, the influence of foundation material on end of winter pore pressures is less significant and sub-hydrostatic pressures are maintained throughout the soil profile.

The data analysed in this paper were from London Underground embankments. However, the general conclusions from this study are also relevant to other infrastructure embankments (e.g. Network Rail earthworks). In similar climates the variation of permeability with depth across three key zones (near surface, cracked clay fill; underlying clay fill; foundation soils) will have a profound impact on the winter pore water pressures developed in the embankment.

Chapter 8

Tree influence on embankment hydrology: Hawkwell embankment

Until the 1950s vegetation covering railway earthworks was actively managed to reduce risk of fire from steam locomotives. Vegetation management later ceased as a cost saving measure, allowing a wide range of vegetation including mature trees to establish on embankment slopes (Gellatley et al., 1995). Many of these trees are deciduous, transpiring and removing water from the soil during the summer months while remaining dormant during the winter, during which time rainfall rehydrates the soil from the surface. This seasonal wetting and drying of the soil causes volume change in high plasticity clays. Shrinking of the embankment during the summer and swelling during the winter often affects the line and level of the railway track it supports, which then requires constant maintenance to avoid line speed restrictions.

Trees draw water from their root zone, which typically extends to about 2-3 m depth (Biddle, 1998). Trees have been shown to cause a larger magnitude of embankment deformation than grass (Scott et al., 2007) and localised railway track deformations have been correlated with their presence (Andrei, 2000; O'Brien et al., 2004). In addition to seasonal wetting and drying, mature trees have been shown to develop persistent suctions within their root zone that help to maintain slope stability (O'Brien, 2007; Glendinning et al., 2009). In low permeability clay embankments, even during an extremely wet winter, infiltration of water from the surface is unable to recover suctions

below 1-2 m depth, allowing zones of persistent suction to develop (Chapter 6). In over steep embankments, or embankments where material has a reduced strength due to strain softening of the clay, these persistent suctions may be crucial in preventing deep seated instability (Scott et al., 2007).

To improve the serviceability of embankments and reduce maintenance costs, asset owners such as Network Rail have been removing vegetation from the slopes of earth structures. Vegetation is often removed from the upper part of the slope, to reduce local shrink-swell movements, and maintained close to the toe, where persistent suctions help to maintain slope stability (Loveridge et al., 2010). However, the removal of deep rooting vegetation, such as trees, from the upper slopes of railway embankments may lead to a loss of suction within the core causing deformation and possible instability. Observations of changes in pore water pressure and soil water content are needed to assess the impact of vegetation removal on embankment hydrology, so that a managed system of vegetation clearance may be developed.

This chapter describes how instrumentation was installed at Hawkwell embankment, a historically problematic site experiencing seasonal rail movements and track degradation. Instrumentation was located at a section identified by the Track Recording Vehicle (TRV) as being of poor track quality, with a large number of mature trees growing on the embankment slope. Monitoring of the embankment began during March 2006 and continued until March 2011. After the first year of monitoring, in March 2007, dense vegetation was removed from the embankment crest, and changes in pore water pressures were measured. This chapter describes collection and analysis of the monitoring data and the use of Vadose/w to model the hydrological effects of tree removal.

8.1 Hawkwell embankment

Hawkwell embankment is situated on the Shenfield-Southend Victoria line between Hockley and Rochford stations in Essex (OS grid reference TQ 8562 9236). At the instrumented section the embankment is 5.5 m high, with typical slope angles of 23° on the north side and 20° on the south side. An open ditch and stream lies at the toe of the south side for approximately 400 m. The embankment is constructed mainly of Intermediate to Very High plasticity, locally excavated London clay. This is overlain by a layer

of granular ash, covering the upper slope of the south side and the entire slope of the north side of the embankment. The embankment is founded on London clay, with superficial deposits of head and brick-earth present. Both the embankment fill and the London clay foundation are weathered, as evidenced by their brown-yellow colouring. A cross section through the embankment is shown in Figure 8.1.

Prior to vegetation clearance the embankment was vegetated with mature and semi-mature trees on both sides. The north side of the embankment contained a number of oak trees within 5-7 m of the cess rail. The south side of the embankment had no mature trees at the crest of the embankment but small trees within 10 m of the cess rail and a dense pattern of oak and ash trees 20 m from the track, at the embankment toe. After the first year of monitoring, in March 2007, trees were removed from the upper two-thirds of both slopes. Vegetation clearance from the top two thirds of the slope is in line with the Network Rail policy of removing trees to reduce seasonal rail variation and minimise expensive track re-levelling works. Trees present at the embankment, before and after tree felling are shown in Figure 8.2.

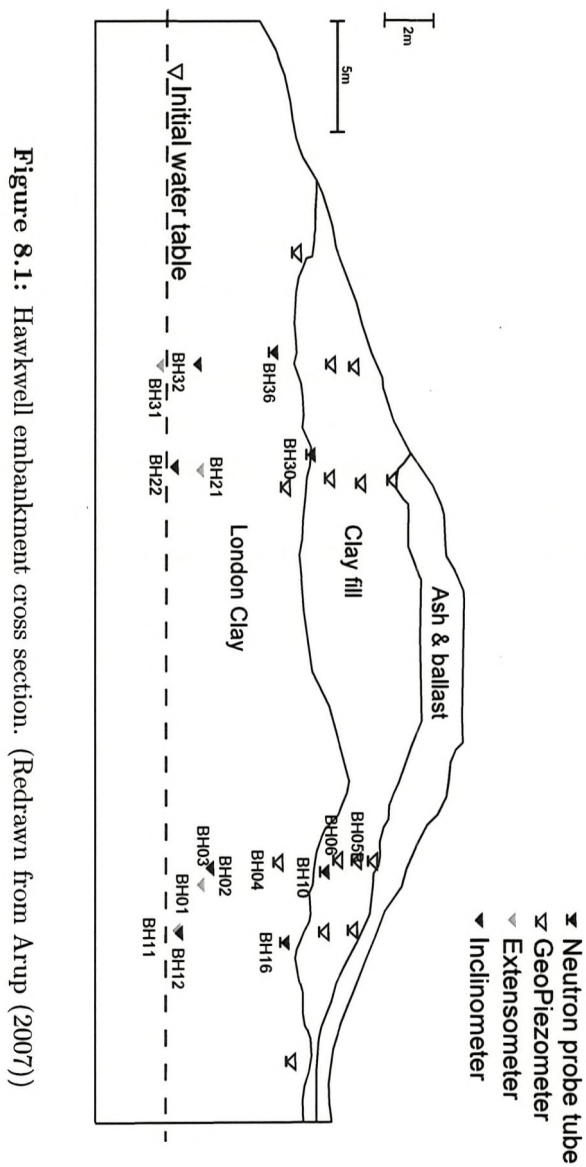


Figure 8.1: Hawkwell embankment cross section. (Redrawn from Arup (2007))

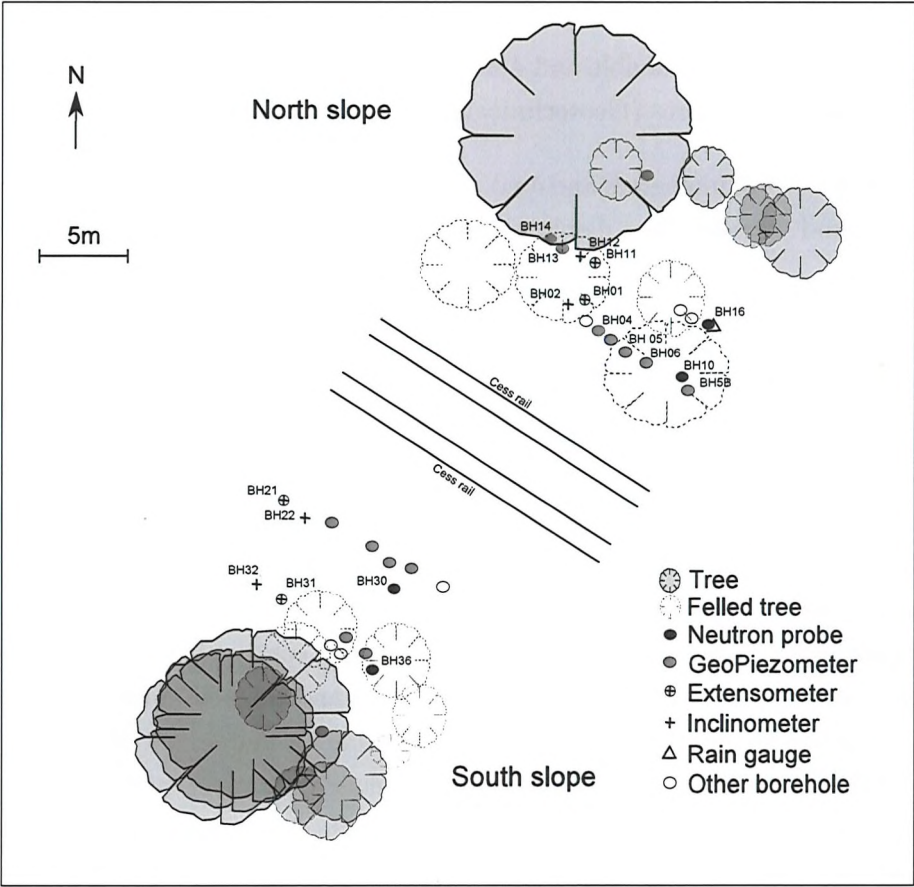


Figure 8.2: Hawkwell embankment tree plan. (Redrawn from Arup (2007))

8.1.1 Instrumentation

The following instrumentation was installed at the embankment on both the north and south sides, with instrument groups located at the crest, midslope and toe:

- 4 no. neutron probe access tubes and 4 no. TDR ThetaProbes to measure soil moisture content (University of Southampton)
- 14 no. Geo flushable and 4 no. standpipe piezometers to measure pore water pressures (Geotechnical Observations)
- 4 no. Inclinometers and 4 no. magnet extensometers to measure lateral and vertical slope displacements (Geotechnical Observations)
- A data logged tipping bucket rain gauge to measure rainfall (University of Southampton)

A summary of instrumentation is shown in Table 8.1.

Neutron probe measurements provide profiles of volumetric water content with depth at given points in time (e.g. weekly or monthly intervals), while piezometers and TDR probes measure pore water pressure and volumetric water content variation continuously at a specific depth. Flushable piezometers measure pore water pressure at the contact between the porous face of the filter (approximately 1 cm² area) and the soil. Intimate contact is required to produce an accurate and stable measurement (Ridley et al., 2003). The neutron probe measures volumetric water content for an approximately football sized volume of soil, potentially encompassing voids, matrix and clay clods in a clay fill.

Neutron probe access tubes were installed at the crest and the midslope of the embankment to a depth of 3.5 m. The access tubes were read at monthly intervals between June 2006 and November 2009. From June 2006 to January 2009 a Wallingford probe (Bell, 1987) was used, while from January 2009 to October 2009 a CPN 503DR Hydroprobe was used. The radiation count readings for both devices were calibrated against gravimetric water contents determined for samples from a London clay site at Newbury (Smethurst et al., 2006). Volumetric water content was calculated from gravimetric water content by means of the measured field bulk density. Due

to the sensitivity of the calibration method to soil type and the heterogeneous nature of the embankment the measurements of volumetric soil water content may not be exact. However, sufficiently detailed information can be obtained to observe patterns of soil water content changes.

Table 8.1: Summary of instrumentation

| Measurement | Type of instrument | Quantity and depths | Measuring range/accuracy | Source/reference |
|-----------------------|---------------------------|--|--|--|
| Soil water content | Neutron probe | 4 no. access tubes, to a depth of 3.5 m | Volumetric water content | Bell (1987) |
| Soil water content | TDR 'ThetaProbe' | 4 no., to depths of 0.75, 0.9, 1.5 and 1.6 m | Volumetric water content, 0-50% | Delta-T Devices Ltd, Cambridge, UK |
| Soil suction | Flushable piezometer | 14 no., to depths between 1.3 m and 5.8 m | Pore pressure between 300 and - 90 kPa | Ridley et al. (2003) |
| Pore water pressure | Standpipe piezometer | 4 no., to depths of 4.1, 5.7, 8.5 and 10.7 m | Pore pressure greater than 0 kPa | Geotechnical Observations Ltd, Weybridge, UK |
| Lateral displacement | Inclinometer | 4 no., to depths of 6.95, 8.15, 8.23, 9.5 m | Resolution of 0.1 mm per 0.5 m depth of tube | Geotechnical Observations Ltd, Weybridge, UK |
| Vertical displacement | Magnet extensometer | 4 no., to depths of 7.12, 8.82, 8.67, 8.67 m | Tape measurement at 1 mm resolution | |
| Rainfall | Tipping bucket rain gauge | North slope | Resolution of 0.2 mm | |

8.1.2 Climate

A rain gauge was installed on the north slope of the embankment in March 2006. Comparison of rainfall measured at Hawkwell with the 1971-2000 Long Term Average (LTA) for Greenwich, East London (49 km from the instrumented site), shows the summers of 2007 and 2008 to have above average monthly rainfall and the winters of 2007/08 and 2008/09 to have had below average rainfall (Figure 8.3).

Consideration of SMD data (Chapter 4) provides information about the ‘dryness’ and ‘wetness’ of seasons by considering changes in the surface water balance. SMD data for MORECS Square 174 (Kent, England) for the monitoring period shows the summer of 2006 to have been dry, and the summers of 2007 and 2008 wetter, compared with the 1971-2000 Long Term Average (LTA).

In addition to rainfall data collected at the site, daily weather data were obtained for a site at Shoeburyness, 11 km from the embankment, from an amateur weather station (Weather Underground, 2010) for use in the numerical model.

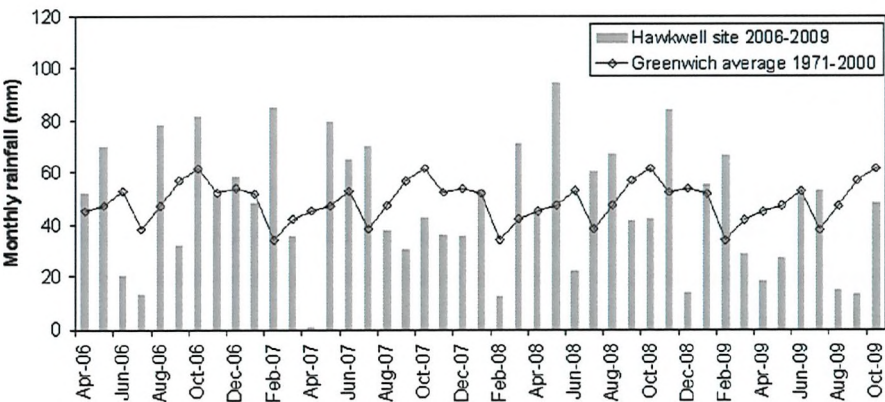


Figure 8.3: Monthly rainfall totals at Hawkwell embankment plotted with the 1971-2000 average rainfall for Greenwich

8.2 Neutron probe monitoring results

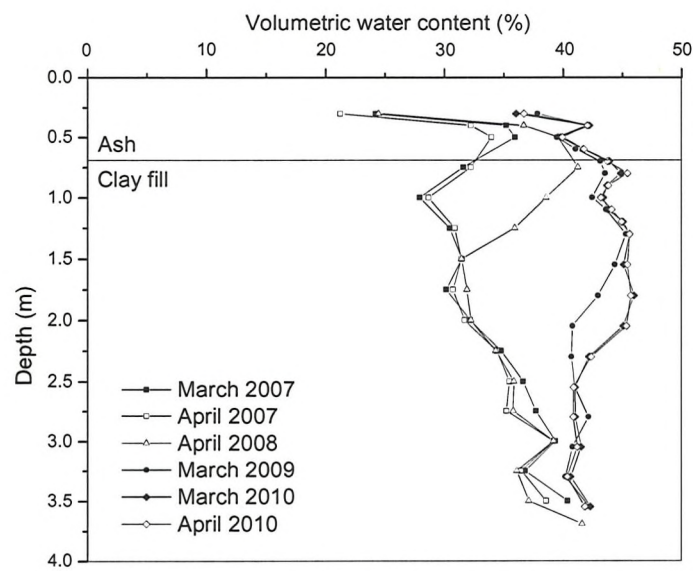
Neutron probe readings were taken at monthly intervals at 4 no. boreholes, to 3.5 m depth. Generally, readings were taken at 0.1 m intervals between

the surface and 1 m depth and at 0.25 m intervals between 1 m and 3.5 m depth.

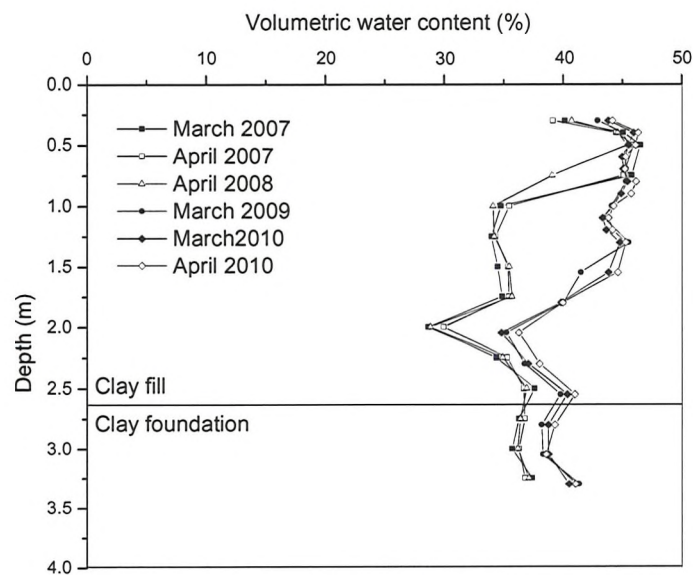
Figures 8.4 and 8.5 show end of winter profiles of volumetric water content, measured during March and April, for the 4 no. boreholes from March 2007 to April 2010. The difference in water contents between the soil layers is evident in each of the boreholes, with a lower volumetric water content in the ash layer. All cases show that re-wetting of the soil profile occurred within the clay fill following tree removal, in March 2007. On the north side of the embankment an approximately 10% increase in volumetric water content occurred within the clay fill between March 2007, at the time of tree removal, and one year later in April 2008. A similar increase of approximately 10% volumetric water content occurred on the south side of the embankment, and full re-wetting of the soil profile to 3.5 m depth by March 2009, two years after tree removal.

End of summer profiles of volumetric water content, measured during August or September, for the 4 no. boreholes are shown in Figures 8.6 and 8.7. The profiles show an increasing water content with successive years of monitoring, with the greatest wetting at the midslope boreholes between 1 m and 2 m depth of the surface. Figure 8.7(b) shows that, from an initial profile in September 2006, re-wetting of the soil had occurred to approximately 1.5 m depth by September 2007 and to 2.5 m depth by August 2008.

The profiles show that following tree removal in March 2007, end of summer volumetric water contents increased as water ceased to be removed within the tree rooting zone. Removal of trees from the slope altered the annual water balance, so that less water was removed from the soil within the tree rooting depth during the summer months and re-wetting of the profiles continued at this depth. This led to increased end of summer and end of winter volumetric water contents after tree removal.

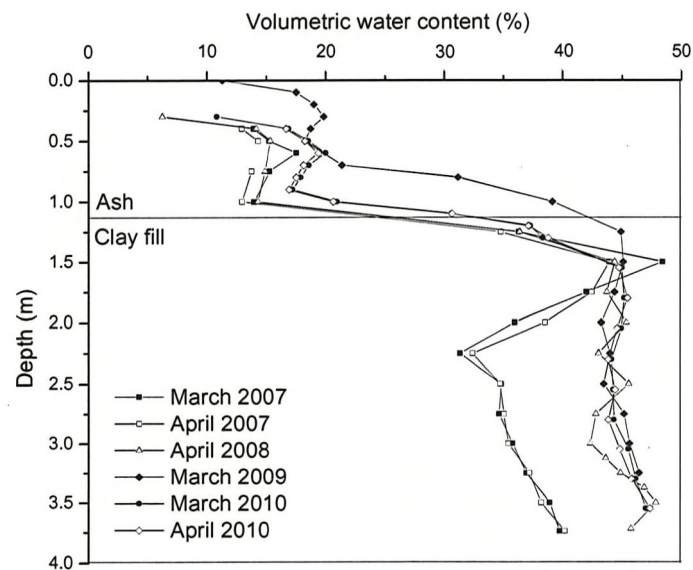


(a) South crest

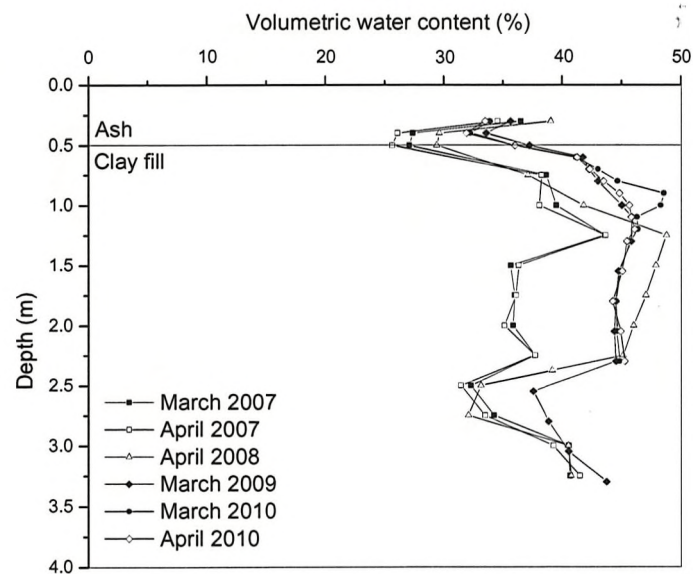


(b) South midslope

Figure 8.4: End of winter (March-April) volumetric water content, south embankment slope

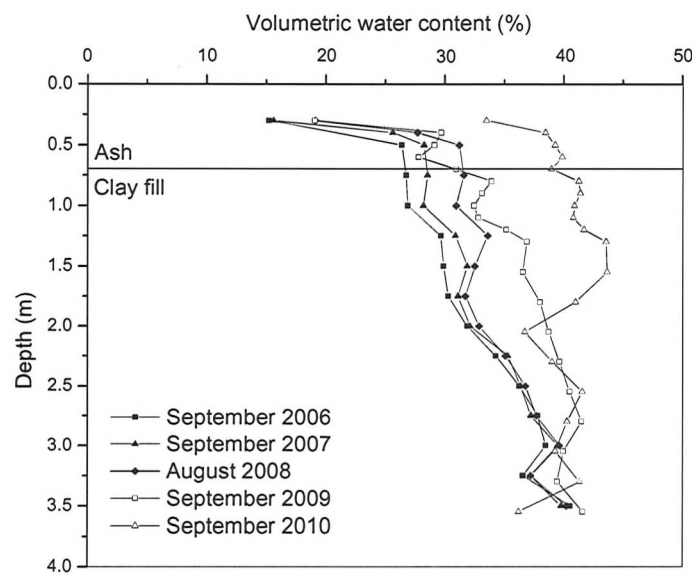


(a) North crest

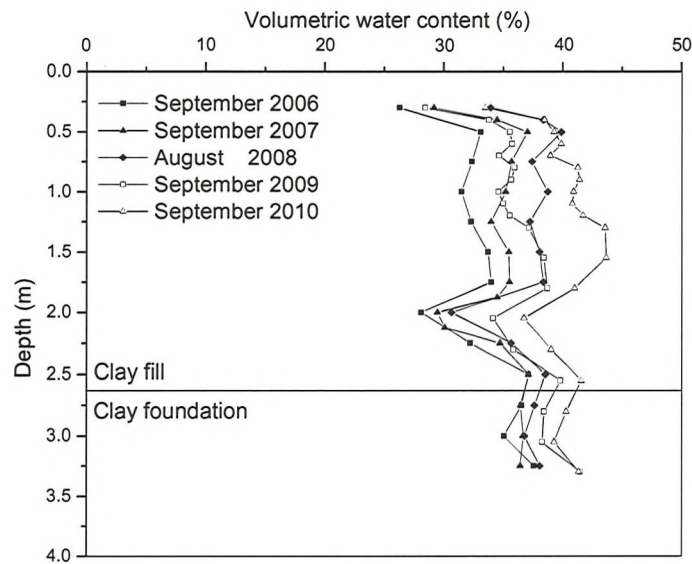


(b) North midslope

Figure 8.5: End of winter (March-April) volumetric water content, north embankment slope

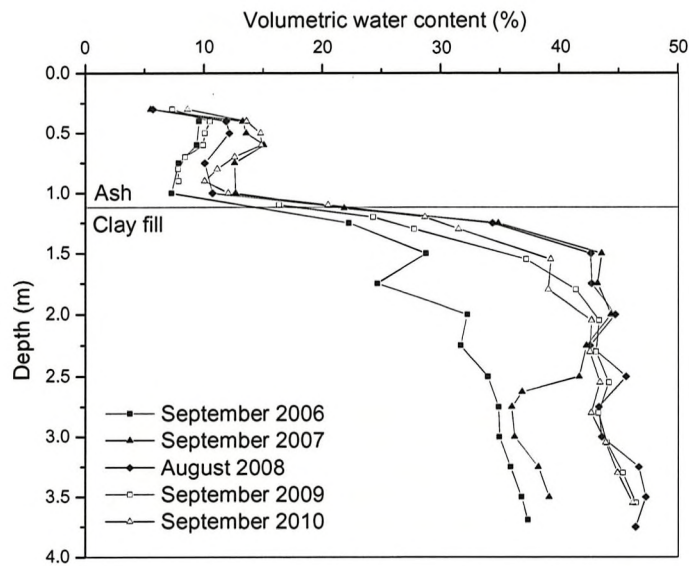


(a) South crest

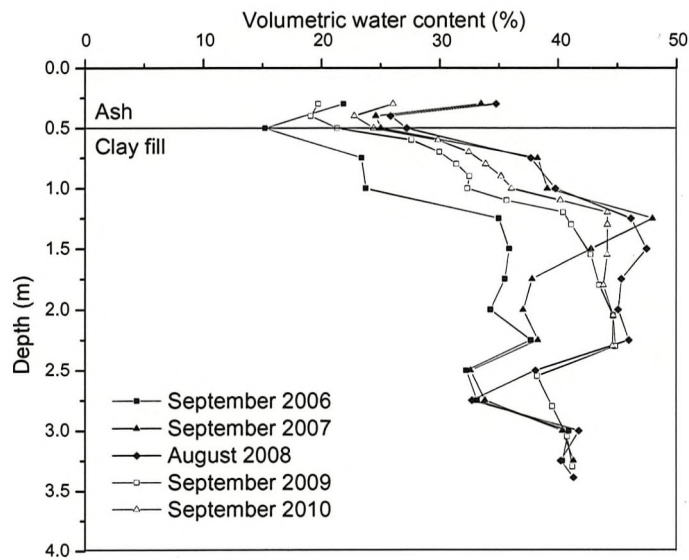


(b) South midslope

Figure 8.6: End of summer (August-September) volumetric water content, south embankment slope



(a) North crest



(b) North midslope

Figure 8.7: End of summer (August-September) volumetric water content, north embankment slope

8.2.1 Seasonal wetting and drying

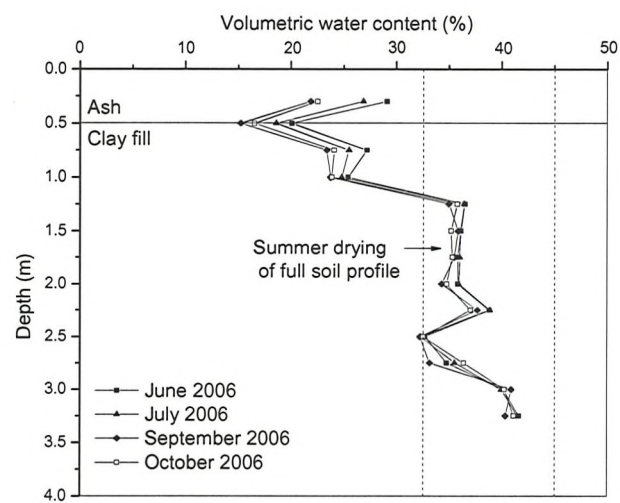
The neutron probe data showed re-wetting of the embankment over the years following tree removal. The profiles, measured at monthly intervals, may be used to demonstrate the nature of wetting and drying processes both before and after tree removal.

Figure 8.8 compares summer drying of the north midslope during 2006 and 2009 with summer wetting in 2007, when tree removal occurred. Figure 8.8(a) shows that during 2006 water was removed by tree roots throughout the soil profile. Following tree removal (March 2007) wetting, rather than drying, occurred to 1.75 m depth through the summer months and the following winter (Figure 8.8(b)). Two years after tree removal, in 2009, a soil profile of volumetric water content close to saturation was established below 2 m depth (Figure 8.8(c)), while a pattern of summer drying occurred at less than 2 m depth. Wetting during 2007 (Figure 8.8(b)) shows saturation of soil above an advancing wetting front while drying (Figure 8.8(c)) occurs more gradually as water is drawn upward by a suction gradient from the surface and shallow rooted vegetation.

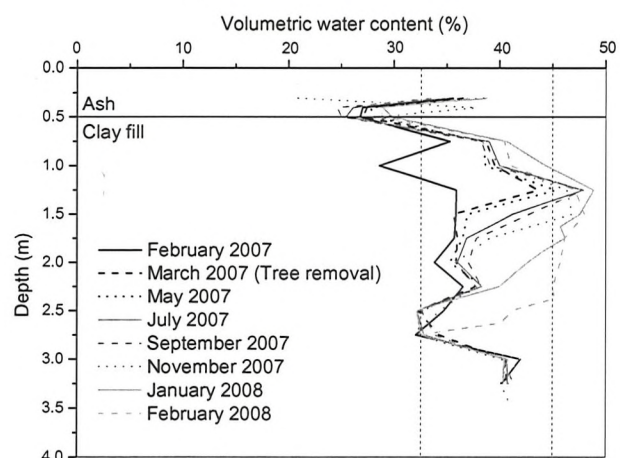
Figure 8.9 compares winter wetting (October to May) of the north crest during the winters of 2006/2007, 2007/2008 and 2009/2010. Figure 8.9(a) shows wetting of the soil profile towards saturation (45%) at 2.25 m depth via a wetting front during the winter of 2006/2007. Comparison with Figure 8.9(b), one year later, shows that following tree removal the profile was saturated to 2.5 m depth for the duration of the whole winter period and the wetting front extended to 3.7 m depth. During the winter of 2009/2010 (Figure 8.9(c)) soil wetting occurred above 2 m depth. However, in contrast to the 2006/2007 profile, the volumetric water content below 2.25 m depth was saturated, at approximately 45% volumetric water content. The low volumetric water content maintained at depth by the trees during the winter of 2006/2007 is not evident in the 2009/2010 profile, when the trees had been removed.

Seasonal displacement of the clay fill in response to wetting and drying is shown in the extensometer data. Figure 8.10 shows vertical displacements at the north crest and midslope between May 2006 and January 2010. Shrink and swell movement is shown in 2006, prior to tree removal. Following tree removal, swelling of the north embankment slope occurred. Swelling of the clay fill correlates with the increase in volumetric water content measured

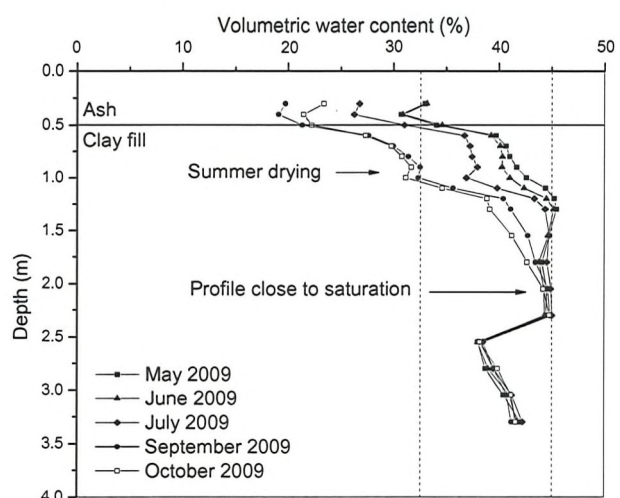
following tree removal (Figure 8.8(a) and 8.8(b)). In 2009 extensometer measurements at less than 1.6 m depth show shrinkage and swelling of the clay fill, but not at greater depth (Figure 8.10). This compares well with the pattern of seasonal wetting and drying measured in 2009 at less than 1.55 m depth (Figure 8.8(c)).



(a) June to October 2006

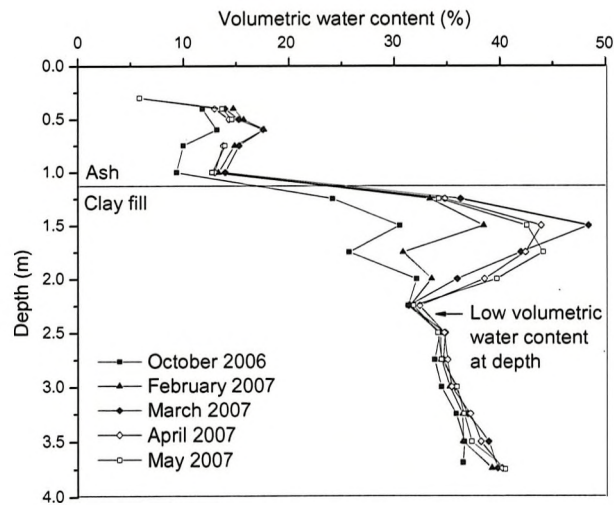


(b) February 2007 to February 2008

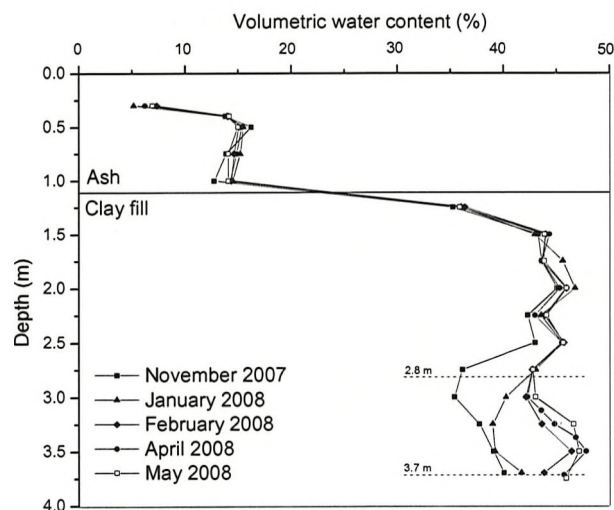


(c) May to October 2009

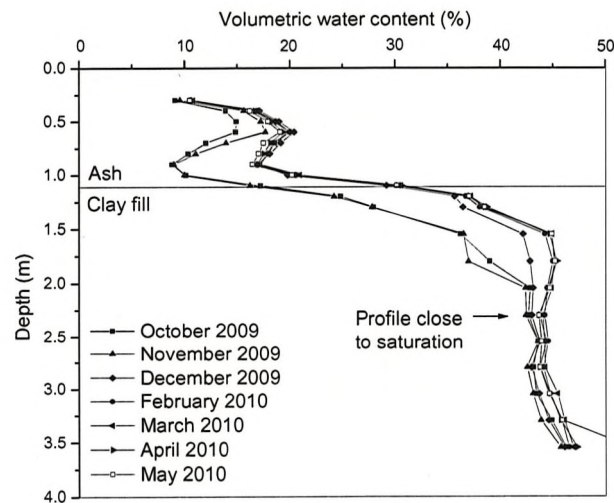
Figure 8.8: Comparison of summer volumetric water content variation, north midslope



(a) October 2006 to May 2007



(b) November 2007 to May 2008



(c) October 2009 to May 2010

Figure 8.9: Comparison of winter volumetric water content variation, north crest

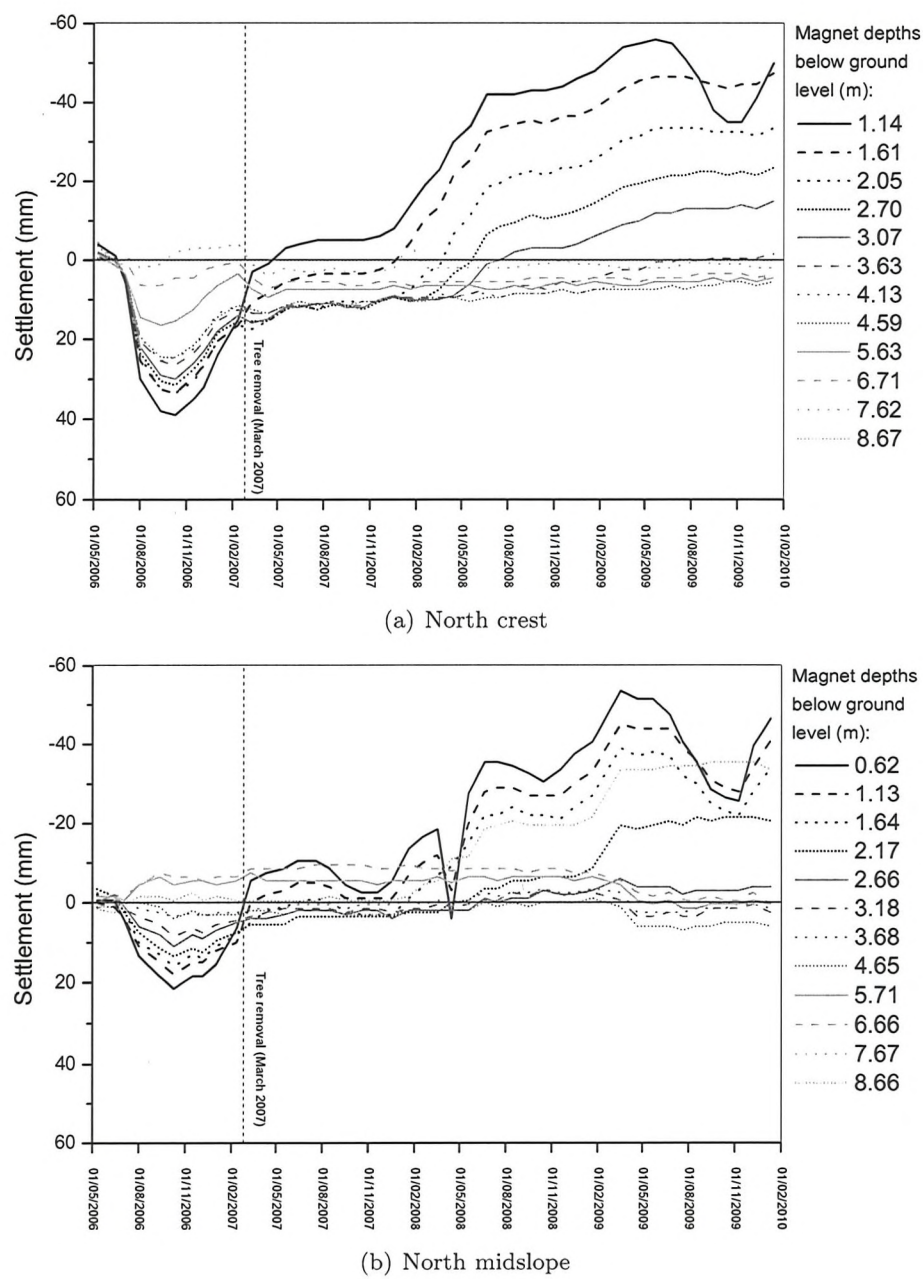


Figure 8.10: Vertical displacements plotted relative to initial magnet positions in April 2006

8.3 Piezometer monitoring results

Piezometers installed in the embankment measured pore water pressure continuously at specific depths. Figure 8.11 shows variations in pore water pressure measured at the crest of the north slope at depths of 2.8 m, 3.7 m and 5.8 m, between April 2006 and January 2010. Indicative lines plotted over the raw piezometer data illustrate the pore water pressure variation without daily fluctuations and piezometer flushing. Figure 8.11 shows a sharp increase in pore water pressure at 2.8 m depth on the 6th of December 2007 and at 3.7 m depth on the 1st of April 2008. This sharp increase was not measured at 5.8 m depth, but a gradual increase in pore water pressure is evident. Comparison with volumetric water content measured at the north crest between November 2007 and May 2008 shows that the sharp increases in pore water pressures coincide with the soil water content reaching saturation at the respective depth (Figure 8.9(b)). At 2.8 m depth the soil profile reaches saturation between November 2007 and January 2008, while the pore water pressure increases sharply from -54 kPa to 0 kPa during the same period. Similarly, at 3.7 m depth the soil profile reaches saturation between February 2008 and April 2008, while pore water pressure increases from -30 kPa to 0 kPa. The soil water content profiles measured after May 2008 show that the soil remained saturated at 2.8 m and 3.7 m depth (Figure 8.9(c)), in agreement with the piezometer data.

Figure 8.12 shows pore water pressure variation measured at the north midslope at depths of 1.3 m and 2.4 m, between April 2006 and January 2010. A sharp increase in pore water pressure of 52 kPa and 64 kPa was measured at 1.3 m and 2.4 m depth respectively on the 27th February 2007, after which pore water pressure remained relatively constant (between -1 kPa and -5 kPa). The rapid increase in pore water pressure simultaneously at 1.3 m and 2.4 m depth is not typical of a gradual wetting front, indicating the presence of a high permeability pathway for water infiltration or loss of contact between the porous face of the piezometer and the soil. In contrast the volumetric water content measurements show gradual rather than rapid wetting of the soil profile, reaching close to saturation at 1.3 m depth in May 2007 and at 2.4 m depth in April 2008. Therefore at the north midslope the piezometer data may be showing rapid water infiltration into a localised fissure or high permeability pathway while the neutron probe is measuring

fissures, matrix material and a gradual saturation of the low permeability clay clods within the measured soil volume.

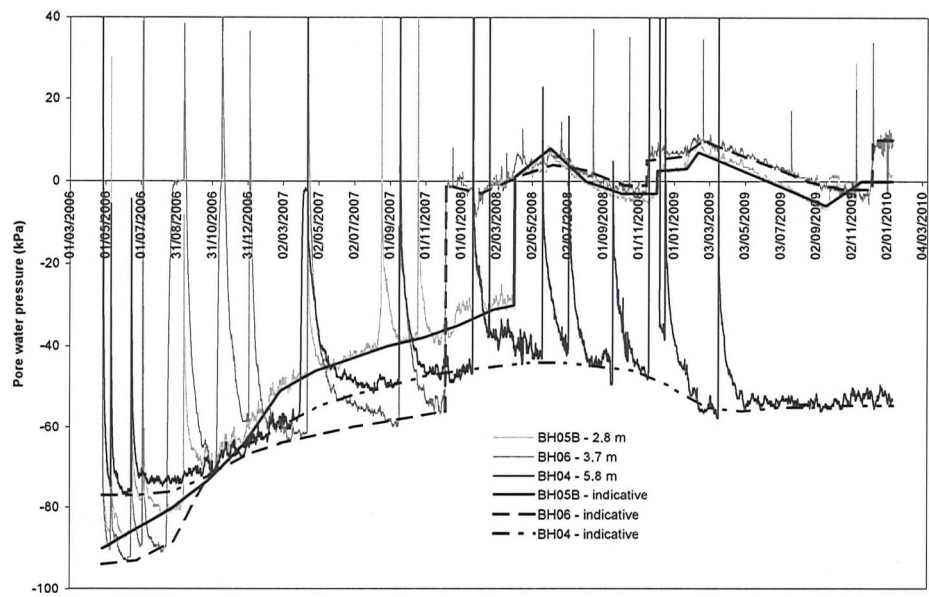


Figure 8.11: North crest piezometer measurements at 2.8 m, 3.7 m and 5.8 m depth

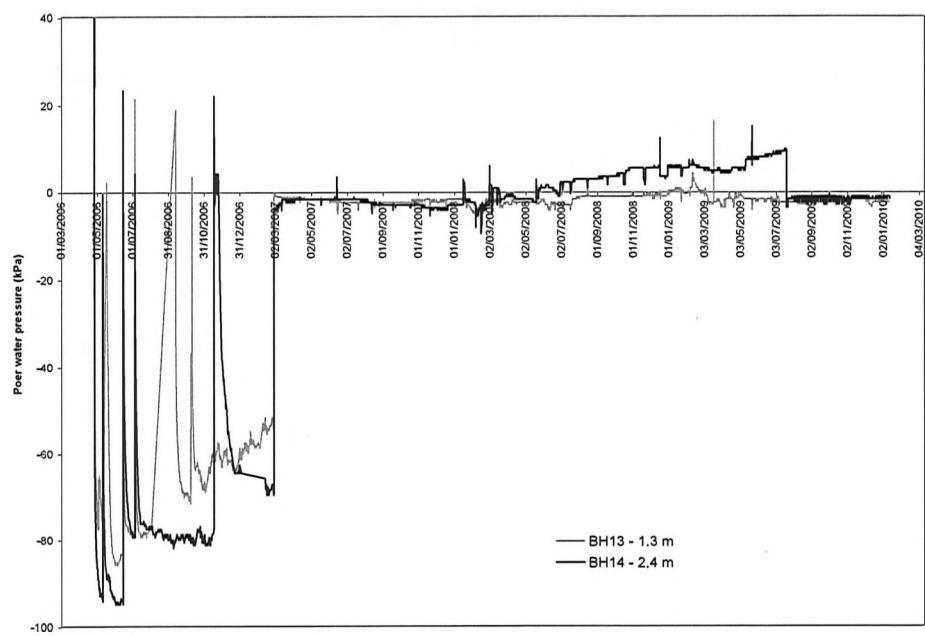


Figure 8.12: North midslope piezometer measurements at 1.3 m and 2.4 m depth

8.3.1 Comparison of measured data with Soil Water Retention Curves

Figure 8.13 shows the volumetric water content plotted against the pore water pressure measured at the north crest boreholes, where good agreement was found between piezometer and neutron probe data (Section 8.3). Plotted values correspond to neutron probe and piezometer measurements taken on the same date and depth from the surface at boreholes located ≈ 0.5 m apart.

The field data of volumetric water content plotted against pore water pressure was compared with laboratory measured SWRCs for wetting and drying of London clay (Croney, 1977) and the estimated SWRC for clay fill (Section 5.5.4). Measurements from the north crest boreholes at 2.8 m and 3.7 m depth lie close to the published SWRCs, with points plotted slightly below the laboratory measured wetting curve for London clay and the estimated clay fill SWRC (Figure 8.13). This would indicate lower volumetric water content for a given suction in the field than in the laboratory.

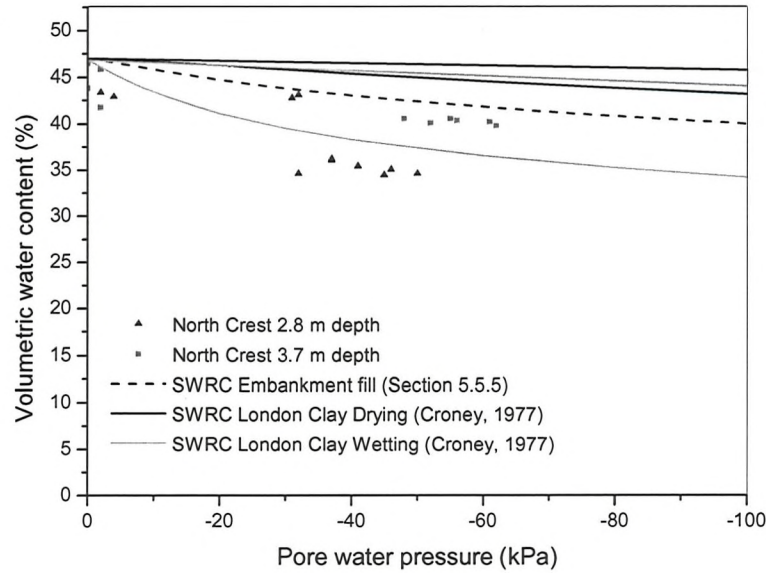


Figure 8.13: Comparison of SWRCs with field measured pore water pressure and volumetric water content at adjacent boreholes

8.4 Finite element modelling

Finite element analysis using the software Vadose/w (Geo-Slope, 2007) was used to examine the influence of tree removal at Hawkwell embankment and compare with monitoring data.

Vadose/w calculates saturated and unsaturated water and heat flow in response to applied boundary conditions. A climate boundary condition can be applied; this uses daily climate data to calculate water infiltration and water removal from the surface of the soil and from a defined rooting zone. This enables variations in pore water pressures and volumetric water content with time, in response to changes in weather conditions or changes in vegetation cover, to be investigated.

8.4.1 Mesh geometry

Models of soil columns with one-dimensional vertical flow were used to calculate volumetric water content profiles representing each of the four boreholes at Hawkwell embankment (Figure 8.14). The soil column model considers changes in pore water pressure and volumetric water content in response to transient pressure gradients applied at the upper surface boundary of the column only, in common with other infiltration-evapotranspiration modelling (Freeze, 1969; Philip, 1991; Essig et al., 2009). Each 17 m deep soil column consisted of clay fill on a London clay foundation. A near surface clay layer was assigned to 0.5 m depth from the surface for the south mid-slope column. The north midslope, north crest and south crest boreholes had an ash and ballast layer at the surface to 0.5 m, 1 m and 0.7 m depth respectively, as shown by the borehole information (Arup, 2007). A fine mesh of 0.1 m square elements was used in the surface zone (to 1 m depth) to enable calculation of the response to high pressure gradients created by the boundary condition. In the remainder of the soil column, a mesh of 0.5 m square elements was used.

8.4.2 Material properties

Borehole information collected during the site investigation was used to define the material layers in each soil column but saturated or unsaturated permeability testing was not conducted at the site. Therefore the saturated permeability of the clay fill was based on results of permeability testing by

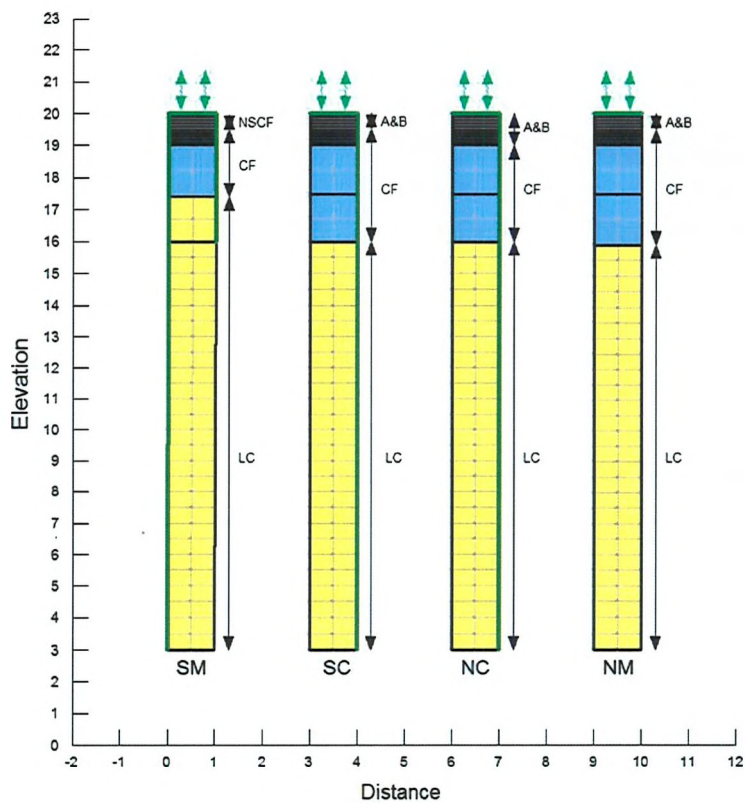


Figure 8.14: Model geometry - Soil columns representing the South midslope (SM), South crest (SC), North crest (NC) and North midslope (NM). (Material properties for Near surface clay fill (NSCF), Ash and ballast (A&B), Clay fill (CF) and London clay (LC) are shown in Table 8.2)

O’Brien et al. (2004) while the *in situ* London clay, forming the embankment foundation, was assigned a permeability consistent with the range measured by Chandler et al. (1990). Clay fill near the surface of the soil column was assigned a permeability 10 times greater than the clay fill below (Table 8.2). This represents the greater permeability of surface soil where cracking and fissures in the clay increase the bulk permeability (Li et al., 2011), facilitating rainfall infiltration.

Unsaturated soil properties that describe the reduction in soil water storage and soil permeability with increasing suction were based on a modified version of the Croney (1977) SWRC for London clay. Using the van Genuchten (1980) curve fitting parameters, the clay fill was assigned a lower air entry value and a shallower gradient to the curve than *in situ* London

Table 8.2: Summary of soil properties

| Soil Type | Permeability (ms^{-1}) | van Genuchten Constants | | | | |
|------------------------------|--------------------------------------|-------------------------|------------|------------|------|------|
| | | AEV | θ_s | θ_r | m | n |
| Ash and ballast [‡] | 4×10^{-5} | 2 | 0.45 | 0.1 | 0.5 | 2 |
| Clay fill* | 5×10^{-8} | 19 | 0.45 | 0.2 | 0.13 | 1.15 |
| Surface clay fill* | 5×10^{-7} | 19 | 0.45 | 0.2 | 0.13 | 1.15 |
| London clay [†] | 5×10^{-9} | 125 | 0.47 | 0.1 | 0.15 | 1.18 |

Where AEV = Air entry value, θ_s = saturated water content, θ_r = residual water content, m and n = constants. * van Genuchten parameters derived in section 5.5.4, [†] van Genuchten parameters curve fitted to drying London clay (Croney, 1977), [‡] estimated van Genuchten parameters for a sandy gravel

clay, consistent with its greater specific volume and wider range of pore sizes (Figure 8.15 and Section 5.5.4). Properties for the clay fill are consistent with those used by Loveridge et al. (2010) and Briggs (2010) to model a railway embankment and show reasonable agreement with field data measured at Hawkwell embankment (Figure 8.13). The Croney (1977) drying curve for London clay was used to model the London clay foundation at Hawkwell embankment while the SWRC for a coarse granular material (Rouainia et al., 2009) was used to model the ash and ballast covering the slopes.

The SWRCs were used to define the variation of soil hydraulic conductivity with soil suction using the Mualem (1976) method (Equation 5.3) with van Genuchten (1980) constants and the saturated permeability. The variation of hydraulic conductivity with soil suction is shown in Figure 8.16.

Derivation of the ash and ballast hydraulic conductivity using the Mualem (1976) method, which assumes inter-connected pores and a reduction of hydraulic conductivity with increasing suction, restricted rainfall infiltration into the ballast layer. This does not compare well with field observations of hysteresis behaviour, where ballast allows rapid water infiltration into large voids but restricts capillarity and evaporation. Therefore, the reduction of hydraulic conductivity of the ash and ballast was limited to $1.07 \times 10^{-8} \text{ms}^{-1}$ beyond 7 kPa suction.

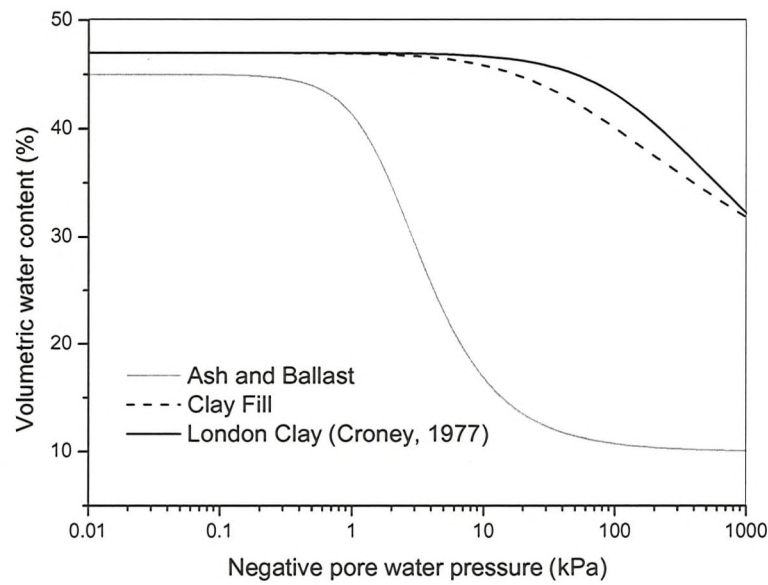


Figure 8.15: Soil water retention curves (SWRCs) describing variation of volumetric water content with pore water pressure

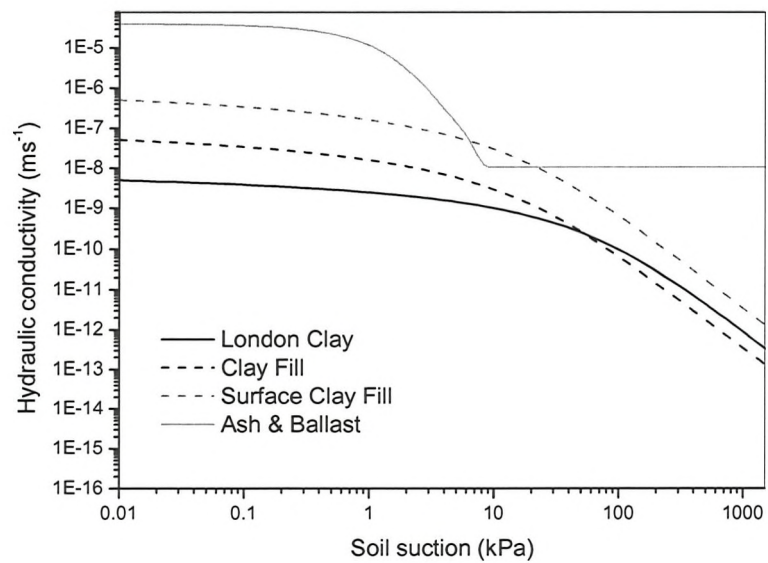


Figure 8.16: Hydraulic conductivity curves for London clay, clay fill, surface clay fill and ash and ballast

8.4.3 Boundary and initial pore water pressure conditions

A climate boundary condition was used to calculate the water flux at the soil surface in response to weather. Weather data recorded by a weather station at Shoeburyness, 11 km from the embankment, provided daily weather data consisting of solar radiation, temperature, relative humidity, windspeed and rainfall. Data from the period 1 January 2001 to the 1 March 2006 were used to define an initial climate condition and create an initial distribution of pore water pressures within the soil. Data from the same weather station was used to model the weather from March 2006 onwards.

The Vadose/w climate boundary condition calculates evaporation from an unsaturated soil using the Penman-Wilson equation (Wilson et al., 1994) and transpiration using a root water uptake model (Tratch et al., 1995). The Leaf Area Index (LAI), defining the proportion of solar energy intercepted by the vegetation for transpiration (Ritchie, 1972), corresponded to full leaf coverage throughout the year. Reduction in root water uptake due to soil drying, as the plant becomes stressed and transpiration reduces, was modelled using the Feddes et al. (1978) relationship, with transpiration reducing linearly between 100 kPa and 1500 kPa suction (Figure 8.17). The plant rooting depth within which transpired water can be removed from the soil by the plant roots was used to differentiate between tree and immature shrub vegetation cover, which were assigned rooting depths of 3 m and 0.2 m respectively. For one year following tree removal, from April 2007 to April 2008, the plant rooting depth was limited to 0.05 m depth, representing a sparse, immature vegetation cover with limited transpiration.

Impermeable boundary conditions were applied to the remaining boundaries of the models (vertical and base), and an initial water table was located 7 m below the surface of the south midslope and 8 m below the surface of the remaining boreholes, as described in the geotechnical interpretative report (Arup, 2007). The pore water pressure distribution at the beginning of 2006, following 5 years of applied weather data (2001-2006), was insensitive to the initial water table condition in 2001. Sensitivity analysis showed that after less than two years of applied climate data the pore water pressure distribution was independent of the initial condition.

A summary of the boundary conditions used in the model is given in Table 8.3.

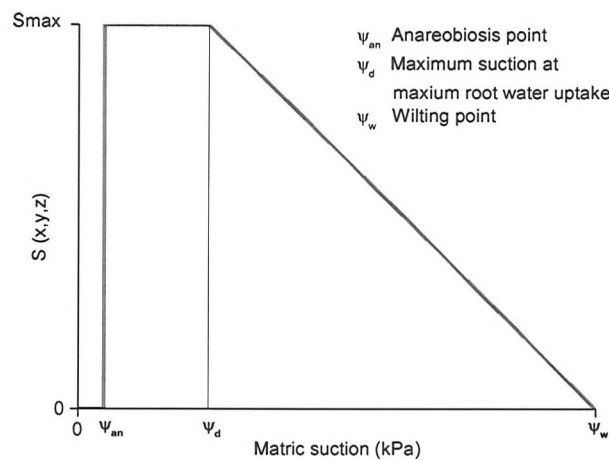


Figure 8.17: Water uptake - soil suction relationship (From Feddes et al. (1978) showing the anaerobiosis (ψ_{an}), maximum uptake (ψ_d) and wilting point (ψ_w). (See Section 4.2.6)

Table 8.3: Summary of climate boundary condition using Shoeburyness weather data

| Model stage | Date | Vegetation function |
|---------------------|--------------------------|---------------------------------------|
| Initial condition | 01/01/2001 to 31/12/2005 | Tree (3m root depth) |
| Before tree removal | 01/01/2006 to 31/03/2007 | Tree (3m root depth) |
| Tree removal | 01/04/2007 to 31/08/2007 | Immature plants (0.05m root depth) |
| After tree removal | 01/09/2007 to 01/09/2009 | Shrub (0.2m root depth) |

8.5 Modelling results

Figure 8.18 shows volumetric water content variation with depth calculated for 9 March 2003. The location of the sharp change in volumetric water content in the north crest, north midslope and south crest profiles is at the boundary between the ash and the clay fill soil layers.

Figure 8.19 shows the pore water pressures calculated at 2 m depth within each of the soil columns from 1 January 2001 to 30 March 2009. This shows that the magnitude of negative pore water pressure is greatest at the south midslope, while greater water infiltration occurs in the ash and ballast covered soil columns. Pore water pressures calculated for the initial condition period from 1 January 2001 to 1 January 2006 show seasonal pore water pressure variation between consecutive years. Calculated suctions reduce to a greater extent during the wet winter of 2002/2003 than the drier winter of 2004/2005 (Section 7.2.3 and Smethurst et al. (in press)). The maximum suction calculated by the model was limited to 1500 kPa by the input parameters (Figure 8.17), which was calculated in every summer. However, comparison of the duration of 1500 kPa suction between years shows the summer of 2006 at maximum suction for longer than the summer of 2004, in agreement with the climate data (Smethurst et al., in press).

Calculated patterns of wetting and drying at the north midslope are shown in Figure 8.20. Figure 8.20(a) shows infiltrated water progressively saturating soil above an advancing wetting front while Figure 8.20(b) shows gradual drying with depth via an upward gradient of suctions. This compares with the pattern of wetting and drying measured at the north midslope (Section 8.2.1 and Figure 8.8).

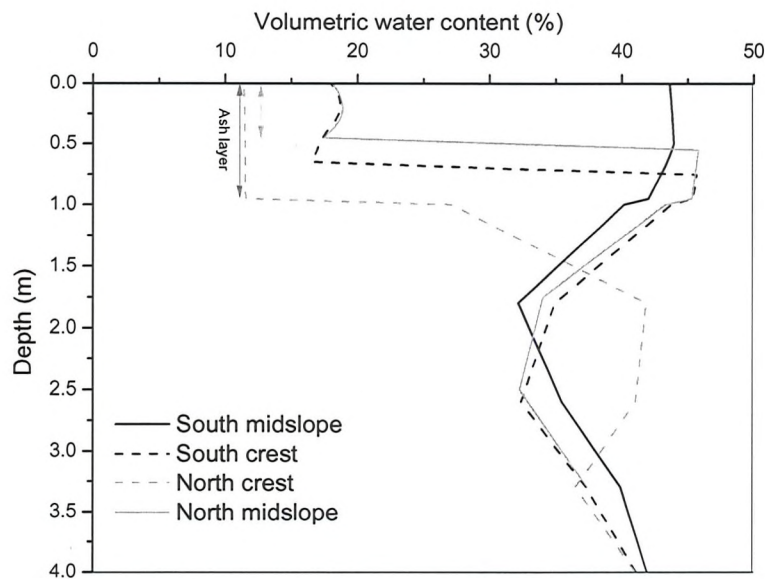


Figure 8.18: Comparison of calculated volumetric water content profiles calculated for 9 March 2003

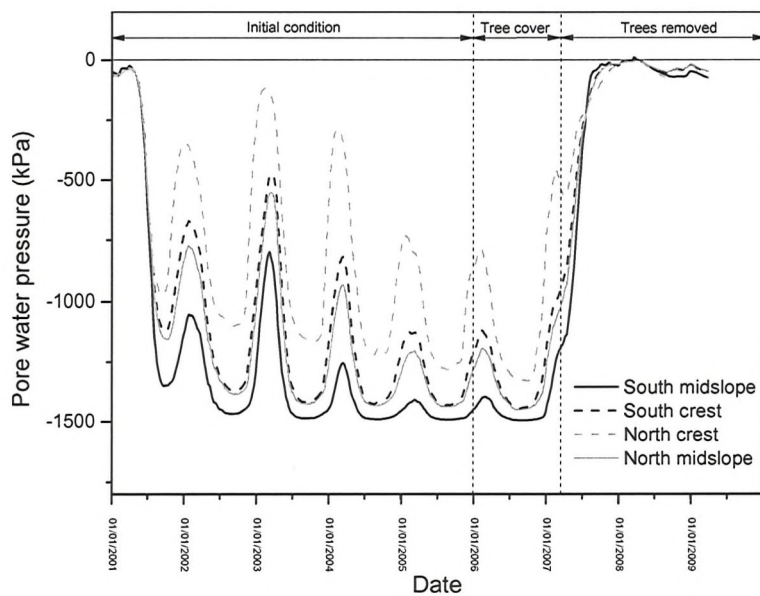
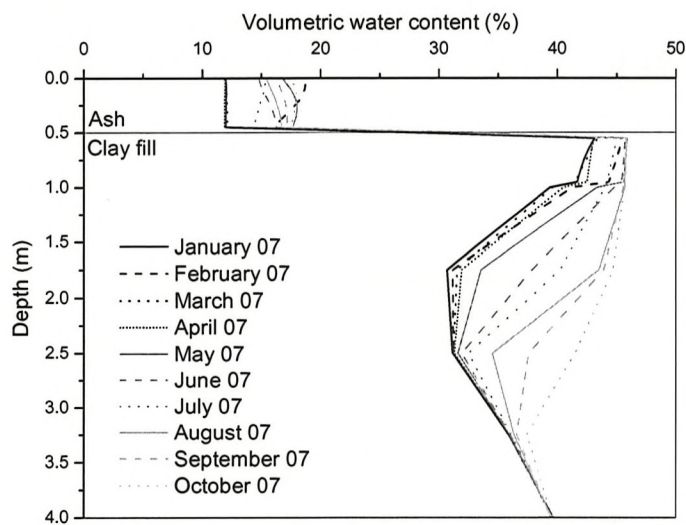
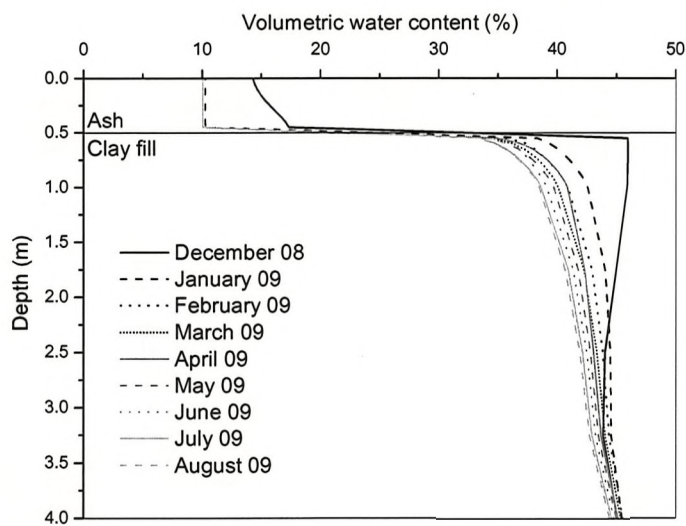


Figure 8.19: Calculated pore water pressure variation at 2 m depth from 1 January 2001 to 30 August 2009



(a) Wetting between January and October 2007



(b) Drying between December 2008 and August 2009

Figure 8.20: Calculated wetting and drying patterns at the north midslope

8.5.1 Tree removal

Figure 8.21 shows calculated pore water pressure variation at 2 m depth for the boreholes during the monitoring period (2006 to 2009). The pore water pressures increase by $\approx 500 - 1000$ kPa following tree removal in March 2007, shifting from a ‘tree’ condition of high suction (1500 kPa) to a ‘shrub’ condition giving lower suctions (0 to 50 kPa). This is in qualitative agreement with piezometer data at the north crest (2.8 m depth) (Figure 8.11).

Figures 8.22 and 8.23 compare the measured and calculated variations in volumetric water content with depth during March 2007 and March 2009 on the south and north slopes respectively. The profiles show a shift in volumetric water content with depth between March 2007 (prior to tree removal) and March 2009, in agreement with the monitoring data. Better correlation with the monitoring data was obtained for the north crest and midslope boreholes (Figures 8.22(a) and 8.22(b)) than for the south crest and midslope boreholes (Figures 8.23(a) and 8.23(b)).

Generally the analysis underestimated the increase in volumetric water content following tree removal within the tree rooting zone, between 1 m and 2 m depth. In the analysis water infiltration from the surface was restricted by the low hydraulic conductivity of the soil continuum, reduced by suctions present in the tree root zone. However in the field, high permeability pathways and the hysteresis nature of hydraulic conductivity during wetting, not replicated in the model, allowed rapid water infiltration from the surface (e.g. Figure 8.12). Therefore the hydraulic conductivity, calculated from the SWRC drying curve of clay fill using the Mualem (1976) method, underestimated the increased bulk permeability (which may include cracks and fissures) during wetting following tree removal. This is in agreement with Ng et al. (2011) which showed that hydraulic conductivity derived from SWRCs was underestimated during the wetting phase and overestimated during the drying phase when compared to field measurements.

8.6 Comment and conclusions

The model was used to investigate the influence of soil permeability, seasonal weather variation and vegetation on pore water pressures and volumetric water content with depth. Plots of pore water pressure against time demonstrate the variation of pore water pressure with seasonal weather changes

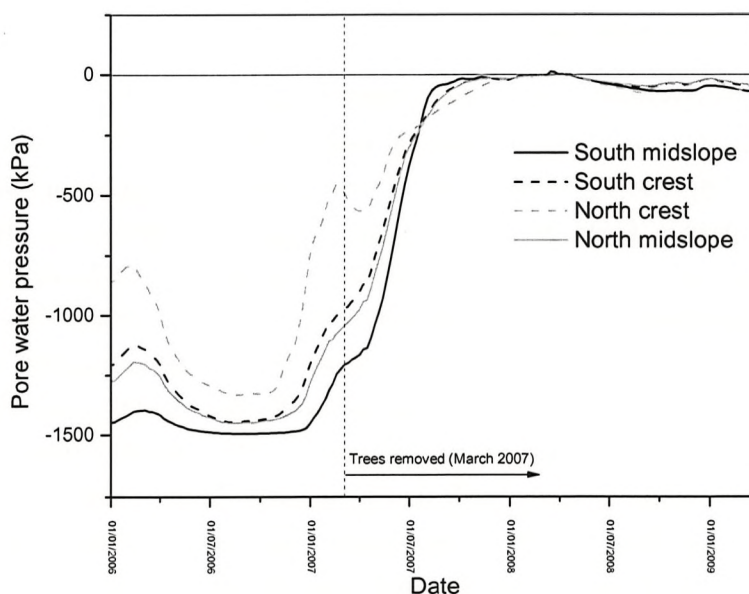


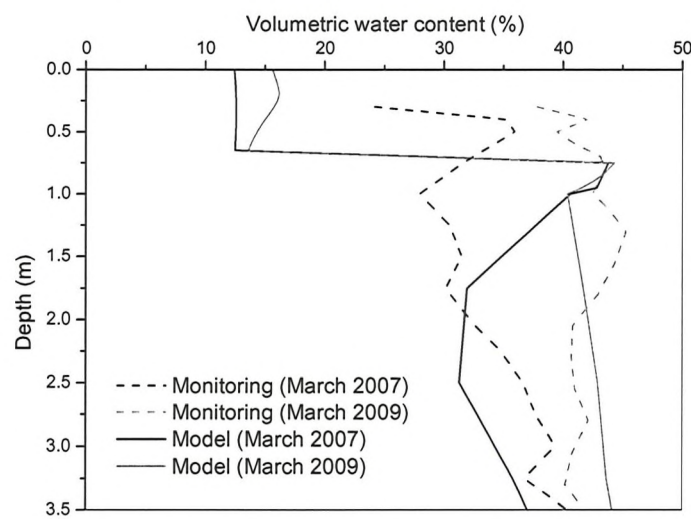
Figure 8.21: Calculated pore water pressure variation at 2 m depth from 1 January 2006 to 30 August 2009

at the soil surface, with increased suctions during dry periods than wetter periods. Comparison of the various soil columns formed of different soil layers demonstrates that changes in soil hydraulic conductivity influence the profile of volumetric water content with depth. Finally, varying the vegetation boundary condition between a tree cover (of 3 m rooting depth) and a shrub cover (of 0.2 m rooting depth) shows the influence of vegetation on the magnitude and extent of soil drying. During the tree covered period high suctions were calculated to a depth of 2 m. These were dissipated following tree removal, in agreement with the monitoring data, after a period of one year. This shows that the deeper rooting depth of the tree cover was maintaining low pore water pressures (and volumetric water content) at depth within the soil, and that this was lost when replaced by a shallow rooted shrub vegetation cover.

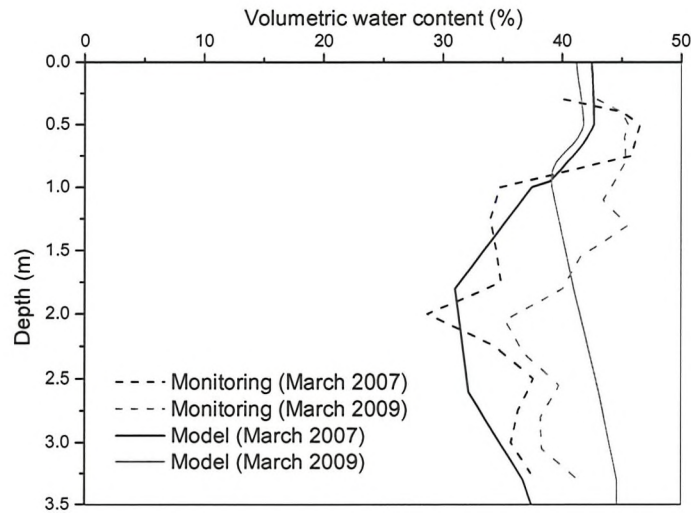
The following conclusions can be drawn:

1) Monitoring data for a tree covered embankment shows that a profile of low volumetric water content, corresponding with high soil suctions, can be maintained throughout the winter to 2.5 m - 3 m depth below the soil surface.

2) Removal of trees from an embankment slope causes volumetric water

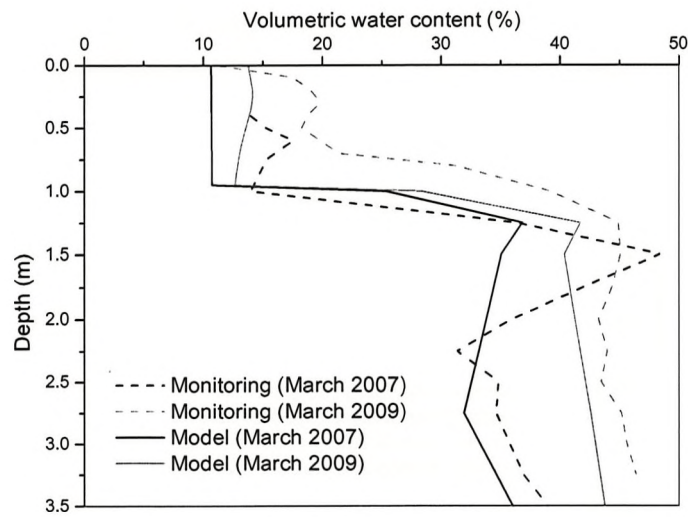


(a) South crest

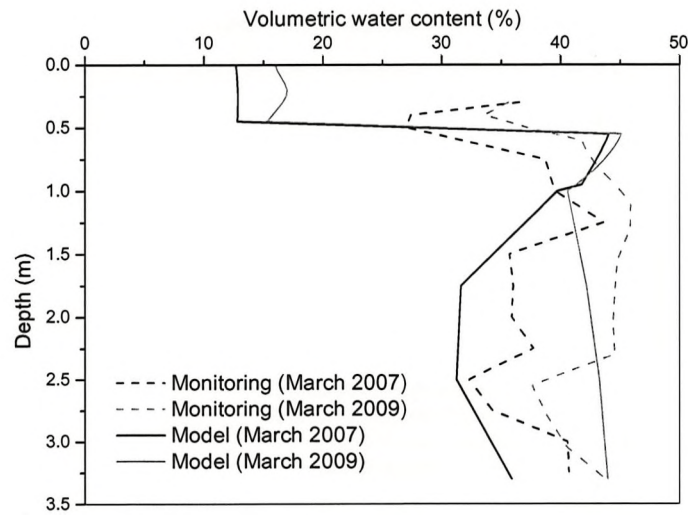


(b) South midslope

Figure 8.22: Comparison of calculated volumetric water content (before and after tree removal) with field measurements at the south embankment slope



(a) North crest



(b) North midslope

Figure 8.23: Comparison of calculated volumetric water content (before and after tree removal) with field measurements at the north embankment slope

content and pore water pressures to increase towards saturation throughout the tree rooting depth (2.5 m to 3 m depth) as a wetting front infiltrates the soil. Cyclic shrink-swell movements reduce and swelling occurs as the embankment re-wets. Two years after tree removal the drying created by trees below 1.5 m depth increases towards saturation while seasonal variation of volumetric water content and vertical shrink-swell to approximately 1.5 m depth occurs as shallow rooted vegetation is established.

3) A finite element model was used to investigate the influence of rooting depth on volumetric water content profiles. Reducing the vegetation rooting depth from 3 m (i.e. tree cover) to 0.2 m establishes a new hydrological condition of increased volumetric water content throughout the soil profile, in agreement with the monitoring data. During the same period the pore water pressures at 2 m depth increased from a condition of high suction (≈ -1500 kPa) to seasonal variation close to 0 kPa. Therefore while tree removal has reduced shrink-swell movements at Hawkwell embankment there is an increased risk of hydrostatic pore water pressures occurring during an extremely wet winter (Chapter 6).

4) The monitoring data and finite element model showed water infiltration occurred as a wetting front while drying occurred via an upward gradient of suctions. The clay fill hydraulic conductivity was derived from a drying SWRC using the Mualem (1976) method and the results showed agreement with monitoring data. However during wetting of the ash and ballast layer the SWRC derived hydraulic conductivity was underestimated and it was necessary to limit the minimum hydraulic conductivity. During rapid wetting of the soil following tree removal, when cracks and fissures were present, the calculated hydraulic conductivity derived using a SWRC was underestimated when compared to the monitoring data. This is in agreement with the comparison of predicted hydraulic conductivity and field data presented in Ng et al. (2011).

Chapter 9

Summary and conclusions

The literature review and case studies presented have investigated climate-atmosphere processes and examined their impact on seasonal pore water pressures within railway embankments in the UK. This will improve infrastructure owners' understanding of the transient influence of seasonal weather on the stability and performance of railway embankments.

Review of literature relating to water flow in soils and at the soil-atmosphere boundary identified relevant models for calculating pore water pressure variation in response to climate. Methods for calculating the SWRC, used to describe soil water retention and calculate hydraulic conductivity, were reviewed. Curve fitting parameters and measurements of similar soils in the literature were used to estimate a SWRC and hydraulic conductivity curve for clay fill.

Three case studies comparing monitoring data and numerical modelling were used to investigate the influence of climate, vegetation and soil permeability on embankment pore water pressures. The first study, at Charing, used a numerical model to investigate the influence of soil permeability, seasonal weather and vegetation cover on seasonal pore water pressure variation. The second study examined piezometer measurements recorded across the London Underground Ltd network. A numerical model was used to demonstrate the influence of extreme prolonged wet weather on pore water pressures within clay fill railway embankments. The third study, at Hawkwell, examined the influence of mature tree cover and tree removal on embankment pore water pressures using field monitoring and a numerical model.

9.1 Conclusions

The following conclusions can be drawn:

1) The typical saturated permeability of clay fill within railway embankments lies within a critical range ($5 \times 10^{-7} \text{ms}^{-1}$ to $5 \times 10^{-8} \text{ms}^{-1}$) corresponding to the rate of rainfall during a typical rainfall event in the UK. This makes clay fill railway embankments susceptible to seasonal pore water pressure variation. (See Chapter 6)

2) During an extremely wet winter, of prolonged winter rainfall, the saturated permeability of an embankment foundation influences the maximum pore water pressure in the clay fill. Hydrostatic pore water pressures occurred in embankments with a foundation permeability equal to or less than the saturated permeability of the clay fill (e.g. *in situ* clay). Embankments founded on a higher permeability material (e.g. chalk or terrace gravel) were underdrained and low pore water pressures ($< 15 \text{ kPa}$) were maintained. For clay founded embankments, an extreme wet winter (c. 1 in 100 year event) can increase pore water pressures significantly compared with a moderate winter (c. 1 in 10 year event), while for embankments underlain by a more permeable stratum pore water pressures are less sensitive to extreme winter rainfall. (See Chapters 6 & 7)

3) Trees can significantly influence pore water pressures within clay fill embankments by creating soil suctions up to 3 m depth below the soil surface. During extreme and moderate winters, soil suctions created by shallow rooting vegetation (e.g. grass and shrubs) are recovered by rainfall infiltration while soil suctions created by trees are maintained throughout the winter between 2.5 m and 3 m depth. Soil suctions created by trees in the root zone are lost within 2 years of tree removal and embankment swelling occurs. (See Chapters 6 & 8)

4) The SWRC derived hydraulic conductivity model, assumed in Vadose/w and the soil-atmosphere boundary models presented in the literature, do not account for the hysteresis behaviour of soils during the wetting and drying phases. Calculated hydraulic conductivity is underestimated for soil wetting and overestimated for soil drying, when compared to field measure-

ments. This can significantly influence infiltration into soils forming railway embankments, such as ballast and cracked clay, where increased hydraulic conductivity in the wetting phase can allow rapid water infiltration into a dessicated soil.

9.2 Implications for earthworks assessment

The following implications for earthworks assessment should be considered:

- 1) Pore water pressures within clay fill railway embankments are not static, varying in response to seasonal weather patterns and slope vegetation cover. During extreme events of prolonged wet winter weather hydrostatic pore water pressures can occur in railway embankments. This can cause slope instability, as occurred in the extremely wet winter of 2000/2001.
- 2) The saturated permeability of the clay fill and the foundation material have a significant impact on the rate of seasonal variation and maximum wet winter pore water pressures, affecting shrink-swell of embankments and slope stability respectively. Measurement of the clay fill, the near surface soil (to 1 m depth) and the foundation soil saturated permeability are required during site investigation if the influence of seasonal weather and extreme weather events on transient pore water pressures are to be assessed.
- 3) Slope vegetation cover influences the depth and extent of seasonal pore water pressure variation. Tree covered slopes are likely to maintain lower than hydrostatic pore water pressures at depth (2.5 - 3 m) during moderate (c. 1 in 10 year) and extreme (1 in 100 year) winters, below a hydrostatic pore water pressure profile at the near surface to 1 m depth. Slopes without trees (e.g. grass or shrubs) cannot rely on soil suctions created in the vegetation root zone during extreme winters. Therefore the presence of trees reduces the risk of slope instability during winter periods; this benefit would be lost if the trees are removed. Management of trees must be balanced with their contribution to seasonal rail deformation, which can be estimated using the method presented in Appendix A.
- 4) Extreme wet winter weather, such as the winter of 2000/2001, was shown to increase pore water pressures within clay fill embankments and for some

conditions (e.g. an *in situ* clay foundation and grass vegetation cover or recent tree removal) high pore water pressures, at or close to hydrostatic occurred. UKCIP climate change scenarios suggest that extremely wet winters, such as the winter of 2000/2001, may become more common in the future (Kilsby et al., 2009; Clarke & Smethurst, 2010), increasing the frequency of high pore water pressures and potential for slope instability. This has implications for vegetation management and risk assessment if infrastructure owners are to prioritise embankment maintenance in the future and minimise disruption to the rail network.

9.3 Further work

The research presented has examined the influence of climate, vegetation and soil permeability on railway embankment hydrology. On the basis of the research presented in this thesis the following suggestions for further work might be made.

- While field monitoring showed railway embankments to be unsaturated, information describing the unsaturated hydraulic conductivity and soil water storage of clay fill was not available. Further studies and finite element models would benefit from column testing of clay fill, to determine a typical bulk hydraulic conductivity in unsaturated conditions.
- Hysteresis of soil water retention in near surface soils such as ballast and cracked clay was shown to have a significant influence on the surface water balance. To model unsaturated flow in a predictive capacity, testing to characterise the unsaturated hysteresic behaviour of cracked clay and ballast in both the wetting and drying phases is required.
- While measurements of the saturated vertical permeability of cracked clay were available in the literature, measurements of the lateral extent and orientation of cracks in earthworks slopes and their behaviour during wetting and drying periods were not available. An improved understanding of dessication cracking and its influence on the surface water balance is required.

- Field measurements showed soil suctions and low water contents within railway embankments. Comparison with Neutron Probe measurements showed that the full extent of soil suction was not measured and was limited by the piezometer measurement range (approximately -80 kPa). A method for measuring the full range of soil suction in the field would benefit studies of the high soil suctions created adjacent to trees.
- The extent of the tree zone of influence was empirically shown in the study presented in Appendix A. Field monitoring showed the influence of trees on soil water content with depth but not the lateral extent. Monitoring and development of a model incorporating the lateral extents of tree root water uptake would be of benefit to infrastructure owners during embankment risk assessment and when managing line-side vegetation.
- The research presented aimed to improve assumptions of pore water pressure used in assessment of mechanical embankment behaviour. The results presented should be applied to mechanical models (e.g. limit equilibrium or finite element) of embankment stability and deformation presented in the literature review. This would provide improved predictive capacity of climate and vegetation influence on embankment stability and identify potential failure mechanisms.
- The work presented considered historic climate data measured by weather stations and likely rainfall return periods. The models presented could form the basis for further studies investigating the influence of climate change on embankment hydrology.

Appendix A

London Underground tree study

Trees covering many of the UK's railway embankments and cuttings provide a natural habitat for wildlife and biodiversity while creating a visual and acoustic screen from human activity. From an engineering perspective, trees maintain slope stability through mechanical root reinforcement and, by the establishment of soil suctions within embankments, naturally stabilising otherwise unstable slopes (Chapter 2). However, while trees provide benefits to slope stability, they are known to cause serviceability problems, disrupting rail journeys and causing delays for passengers. A tree's ability to transpire and remove water from the root zone causes soil volume change and can lead to movement and deformation of the railway track itself. A dichotomy therefore exists for earthworks managers between keeping trees and removing trees, with little guidance available. A study was therefore undertaken by Mott MacDonald, on behalf of London Underground Limited (LUL), to investigate the influence of vegetation on the serviceability of LUL's geotechnical assets and provide 'LUL Vegetation Management Guidelines' (Mott MacDonald, 2008). This provides empirical evidence demonstrating the impact of vegetation species on seasonal rail movement when considering serviceability failure of geotechnical assets.

A study of 16 sites on the London Underground (LUL) network relating railway adjacent trees to seasonal track movements was conducted using methods employed by the National House Building Council (NHBC). This method describes a tree's zone of influence; taking into account soil type,

tree dimensions and tree species. The study evaluated the relevance of the NHBC guidelines (NHBC, 2007) to railway embankments and cuttings, comparing data stored in a GIS database of trees with site measured rail movements.

Historically it has been observed that bare slopes are vulnerable to ultimate slope failure (McGinnity et al., 1998), while embankments with mature tree cover experience seasonal embankment movements. Following stabilisation works of a London Clay fill embankment, up to 30 mm of seasonal vertical track movement was observed by Andrei (2000), in the vicinity of mature oak trees. Similarly, monitoring of a LUL embankment with mature tree cover showed a seasonal shrink swell cycle of 48 mm vertical movement, with only 5- 7 mm of movement observed at a nearby grass covered slope over the same period (Scott, 2006). Vertical shrink swell movements were also linked to lateral outward ground movements, which did not recover. This ratcheting mechanism has been identified as being linked to progressive slope failure over a large number of cycles (O'Brien et al., 2004; Take & Bolton, 2011; Scott, 2006), linking seasonal deformations to long term ultimate failure mechanisms.

The issue of tree induced ground movements is not confined to railway embankments and cuttings. The influence of vegetation on the shrinking and swelling of clay soils received interest following the severe drought of 1975-76 where building damage was observed close to trees. During this period annual insurance claims relating to damage of low rise buildings reached £60m, prompting further investigation of the foundation risk associated with trees (Driscoll et al., 1996). Subsequent research at a London Clay site in Chattenden in Kent showed that seasonal ground movements of 18 mm were measured adjacent to Lombardy poplar trees and insurance data was used to compile a damage ranking of tree species (Driscoll et al., 1996; Cutler & Richardson, 1989). Of equal importance was research relating to soil heave following tree removal. Over a period of 4 years, 160 mm of heave was observed at the ground surface following Lombardy poplar tree felling as long term moisture deficits were recovered (Driscoll, 2000). This research, along with the work of Biddle (1998), formed the basis for the National House Building Council guidelines 'Building near trees' (NHBC, 2007).

The National House Building Council (NHBC) Standards, Chapter 4.2 'Building near trees' provides technical guidance on the design of founda-

tions in shrinkable soils close to trees (NHBC, 2007). A minimum required foundation depth is calculated, taking into account the depth, extent and intensity of soil drying due to nearby trees. Although patterns of soil drying near trees are highly variable and unpredictable, a zone of influence is defined within the guidelines using simple, measurable parameters. The zone of influence is calculated by considering soil volume change potential, tree species and tree dimensions. Volume change potential is classified by soil plasticity while tree species are grouped into low, medium and high water demand species (Table A.1). High water demand trees have the greatest zone of influence while low water demand trees have a limited zone of influence. Using the water demand classification the NHBC calculation prescribes a minimum D/H ratio, where D is the distance of the tree from the building and H is the mature tree height. Climate is accounted for by dividing the UK into climatic zones, allowing reduction in foundation depth with increasing distance from London, which is considered the driest and most vulnerable part of the country. As all of the study sites were within the London area, regional climate variation was not accounted for.

Table A.1: Classification of water demand for various tree species (adapted from NHBC (2007))

| Broad Leafed Trees | | Coniferous Trees | |
|--------------------|----------|------------------|-------------|
| Water Demand | Species | Water Demand | Species |
| High | Elm | High | Cypress |
| | Oak | | |
| | Poplar | | |
| | Willow | | |
| Moderate | Ash | Moderate | Cedar |
| | Beech | | Douglas Fir |
| | Cherry | | Spruce |
| | Sycamore | | Yew |
| Low | Birch | | |
| | Holly | | |

The vegetation management study investigated 16 sites spread across the LUL rail network, with varying degrees of tree cover (Mott MacDonald, 2008). The study sites included thirteen railway embankments, one cutting and two ‘at grade’ sections, all of which have historically poor track per-

formance or risk of instability. Of these, ten were identified as having high volume change potential, being constructed of high plasticity London Clay fill. For each study site asset performance was evaluated by creating a pro-forma referencing available assessment reports, track maintenance reports and ground investigations. At eight of the sixteen sites railway monitoring data were available, having been previously undertaken for assessment of earthwork stability or to confirm the performance of remedial works. The most valuable rail monitoring data were obtained for earthworks beyond the extents of these remediated sections, providing detailed rail monitoring of tree adjacent areas unaffected by slope stabilisation measures. Tree data was obtained from the Norton Tree Database, detailing the location, height and species of trees on the LUL network, illustrated as a tree location plan for each site. From this it was possible to compare measured rail movements with the parameters described in the NHBC guidelines.

For each study site it was possible to plot the D/H ratio for each tree, grouped by water demand type and compare them to the NHBC minimum recommended D/H ratio. The minimum recommended D/H ratio describes the minimum tree planting distance from a building, relative to the tree height. This is presented in the form $D = R \times H$, where R is the ratio. The results for two of the study sites, A and B, are shown in Figures A.1 and A.2. It can be seen that for site A there are many high water demand trees lying within the minimum recommended planting distance (D). For the second site, B, there are many more trees but most of them lie outside the minimum D, being outside the zone of influence. It is therefore not surprising that site A (Figure A.1) has experienced seasonal track deformation, has required remediation and is the monitored site described in Scott et al. (2007). In contrast site B, although identified as being at risk of instability, does not show any signs of seasonal movement. A further site of interest (C) is shown in Figure A.3. At this location, ground heave has been measured in response to felling of adjacent high water demand trees. Figure A.3 shows that the felled trees previously lay within the minimum planting distance (D) and therefore soil moisture recovery in their zone of influence is causing ground heave and rail movements.

Figure A.4 compares rail deformation to D/H ratio by tree species at the eight study sites where rail monitoring data was available. Seasonal track movements greater than approximately 10 mm (where movements may be

unacceptable) are attributed to HWD trees, all within the $1.25H$ minimum planting distance. The data suggests that the minimum planting distance could be reduced to $1.0H$ for tree influence on rail movement, although a larger sample of data would be required to validate this conclusion. The greatest track movements are adjacent to Poplars and felled Willow trees, whereas no rail movements greater than 10 mm are adjacent to MWD or LWD trees.

When comparing rail deformations with tree D/H ratios it is important to consider the many factors affecting rail movement other than the presence of trees, such as over steepening of the crest, poor track bed or other observed seasonal deformation, not fully associated with shrink swell. However, it is evident that seasonal rail deformation of greater than 10 mm occurs where high water demand trees, particularly Oaks and Poplars, are within the minimum planting distance (D). Moderate and low water demand trees are associated with only one rail movement above 10 mm, regardless of D/H ratio, indicating that high water demand trees are the primary cause of track deformation and serviceability failure. The one moderate water demand tree associated with high rail movements is a cherry tree, although under one classification method this is considered to be high water demand (McCombie, 1993). It should be noted that in this study, when the absolute distance of the tree from the track was compared to measured rail movements without consideration of tree height, there was limited correlation.

Heave caused by the felling of Willows at study site C induced large rail movements of up to 30 mm in one year, although this would be a continual upward movement, rather than seasonal variation. In soils of high volume change potential the NHBC guidelines suggest that up to 150 mm of total heave may occur, agreeing with the results of Driscoll (2000) who observed 160 mm of ground swelling over four years. It is therefore likely that study site C, containing the felled Willows, will continue to experience upward rail movements over a number of years.

From this study, considering sixteen sites across the LUL network, a number of broad conclusions and empirical observations can be made to inform future research. High water demand trees such as Oaks, Poplars and Willows were observed at locations of seasonal rail deformation greater than 10 mm where the distance of the trees from the track (D), relative to the tree height (H), fell within the NHBC recommended planting distance.

Sites with a history of track serviceability problems were shown to contain trees that do not comply with the minimum planting distance. In contrast, sites containing trees satisfying the minimum D/H ratio did not experienced noticeable seasonal movements. Over the eight sites where rail monitoring was available, moderate and low water demand trees were not located adjacent to seasonal rail movements, suggesting that high water demand trees are the main cause of earthwork serviceability failure. As described in the NHBC guidelines, it has been shown that removal of high water demand trees results in ground heave. As a result up to 30 mm of rail movement was observed adjacent to tree felling, which is likely to continue over a number of years.

This case study provides an insight into the general trends of tree influences on the railway and shows that a similar pattern of behaviour to that observed in building construction is occurring. This may be used as an earthwork assessment tool to identify where tree interference may be a primary cause of poor track performance. Particularly, it highlights the important influence of high water demand tree species growing adjacent to the railway and the continued influence following tree removal. Modelling and analysis of trees on railway infrastructure can be compared to this observed behaviour. However, first the process of water removal from the soil by vegetation and other soil-atmosphere processes must be understood.

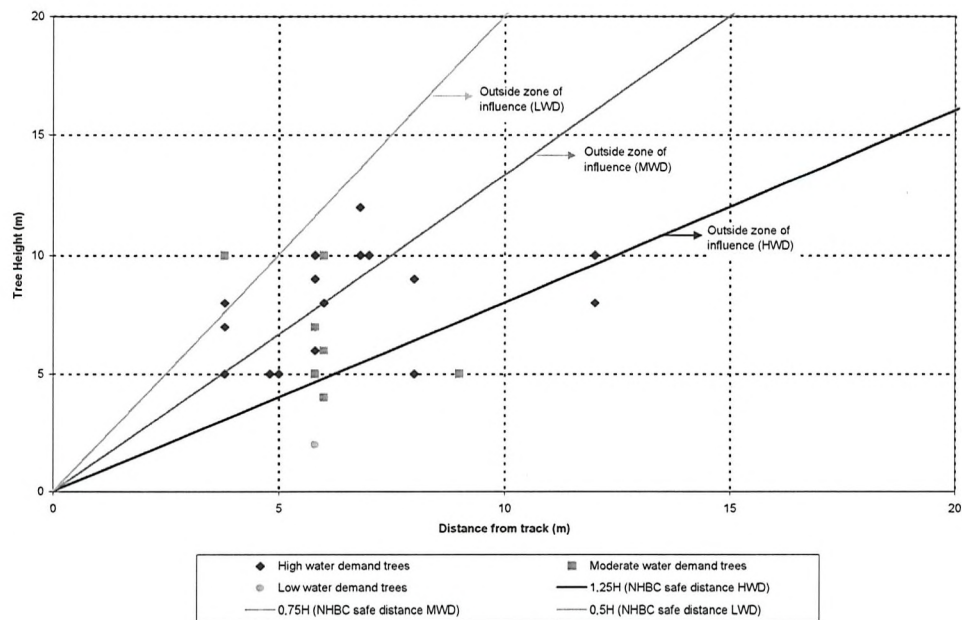


Figure A.1: Minimum tree planting distance at Site A (seasonal rail movement)

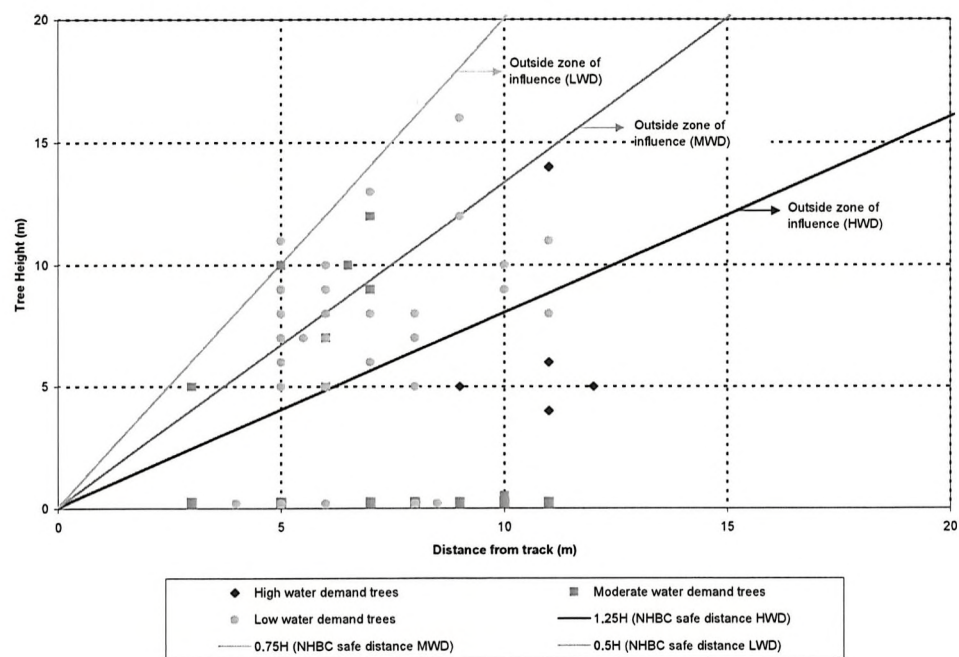


Figure A.2: Minimum tree planting distance at Site B (no seasonal rail movement)

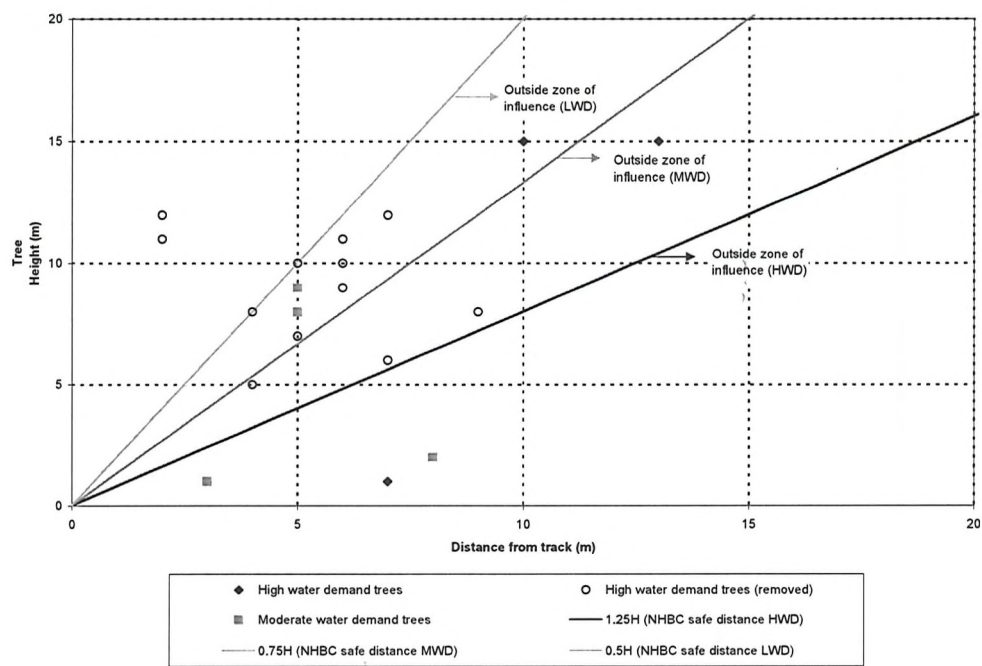


Figure A.3: Minimum tree planting distance at Site C (following tree felling)

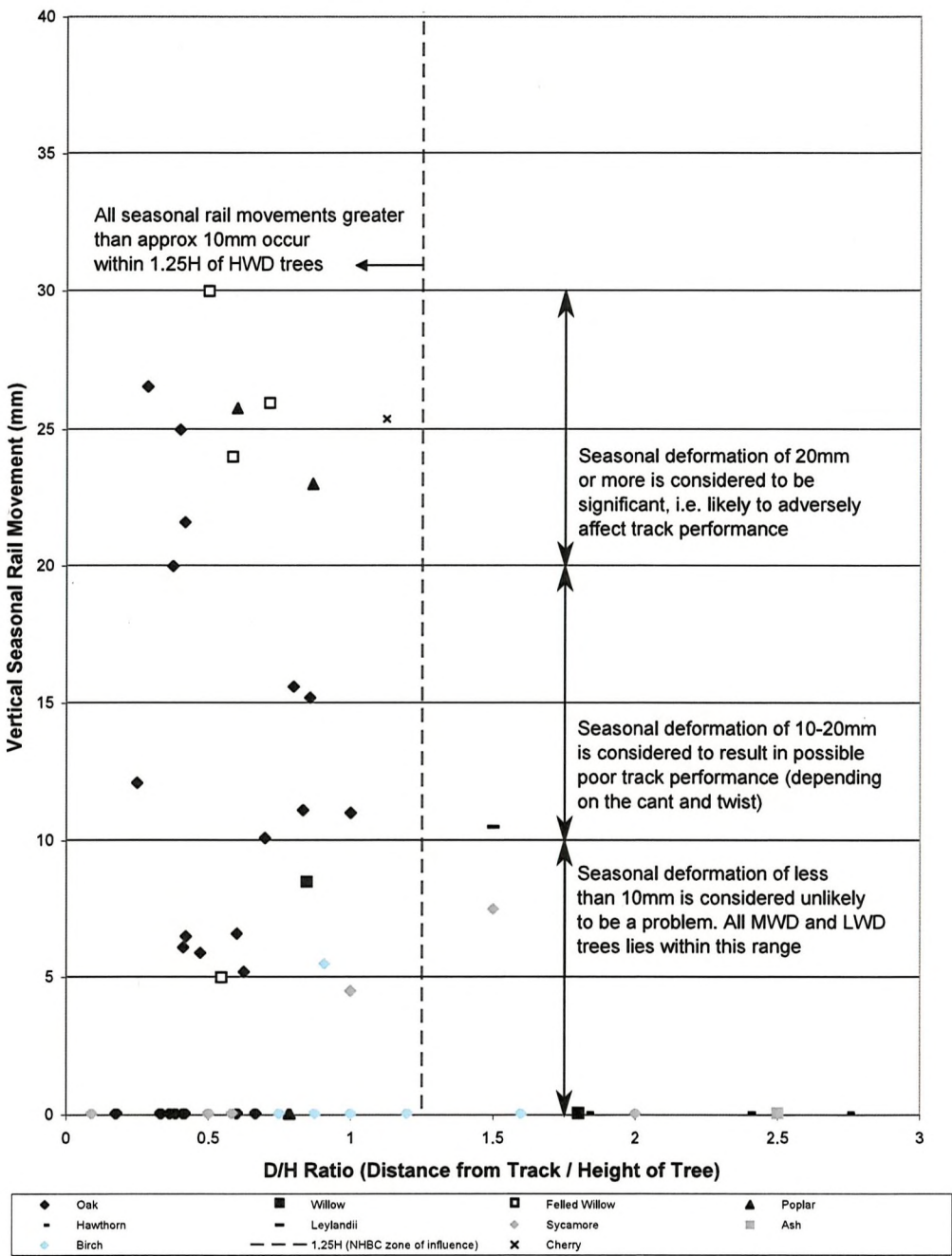


Figure A.4: Measured seasonal movement by tree species

Appendix B

Infiltration and flow in an embankment slope

One dimensional finite element soil columns have been presented in Chapters 7 and 8. One dimensional models were used to simulate infiltration into a monitored slope in Hong Kong (Li et al., 2005) and a 10 m high dry ash dump in South Africa (Fourie et al., 1999). Field measurements show that soil water contents tend to be higher near the toe of a slope than at the crest, irrespective of rainfall events, due to subsurface flow in the downslope direction (Rahardjo et al., 2005). The influence of the surface clay fill on calculated pore water pressures in two dimensions is unclear.

A two dimensional model of a London Underground Ltd embankment was used to investigate the influence of subsurface downslope flow on calculated pore water pressure. Two models were considered and compared with soil column C, presented in Chapter 7 :

- Increased saturated permeability of the surface clay fill relative to the clay fill in the vertical direction only (Model A)
- Isotropic saturated permeability of the surface clay fill (Model B)

B.1 Finite element modelling

A finite element model of embankment EM7 was created using Vadose/w. EM7 is 6.5 m high, with a slope angle of approximately 15°. It is located on the Central line between Perivale and Greenford stations. The embankment

Table B.1: Summary of soil properties

| Soil Type | Permeability (ms^{-1}) | van Genuchten Constants | | | | |
|--------------------|--------------------------------------|-------------------------|------------|------------|------|------|
| | | AEV | θ_s | θ_r | m | n |
| Ash and ballast | 4×10^{-5} | 2 | 0.45 | 0.1 | 0.5 | 2 |
| Clay fill | 5×10^{-8} | 19 | 0.45 | 0.2 | 0.13 | 1.15 |
| Surface clay fill* | 5×10^{-7} | 19 | 0.45 | 0.2 | 0.13 | 1.15 |
| London clay | 5×10^{-9} | 125 | 0.47 | 0.1 | 0.15 | 1.18 |

Where AEV = Air entry value (kPa), θ_s = saturated water content, θ_r = residual water content, m and n = constants

* Vertical direction only (A), vertical and horizontal direction (B)

is constructed of clay fill, derived from the London clay foundation material. A granular layer of ash and ballast is located at the crest of the embankment.

B.1.1 Mesh geometry

The Vadose/w model geometry is shown in Figure B.1. This is a simplified version of the actual geometry. At section X-X the soil profile comprises 1 m of surface clay fill overlying 4 m of clay fill and 4 m of London clay foundation. This is equivalent to the profile of soil column C, presented in Chapter 7.

A fine mesh of 0.1 m elements (in the vertical direction) was used near the surface zone (to 3 m depth) to enable calculation of the response to high pressure gradients created by the boundary condition. In the remainder of the model a mesh of 0.5 m square elements was used.

B.1.2 Material properties

Material properties described in Chapters 7 and 8 were applied to the embankment models. A summary of soil properties is shown in Table B.1. In model A increased permeability of the surface clay fill relative to the clay fill (to 1 m depth) was assumed in the vertical direction only (Novak et al., 2000), with cracking and fissures assumed to be discontinuous in the lateral, downslope direction. As a comparison, the increased permeability of the surface clay fill due to cracking and fissures (to 1 m depth) was assumed to be isotropic in model B.

B.1.3 Boundary and initial pore water pressure conditions

The climate boundary condition applied to the soil columns presented in Chapter 7 was applied to the embankment model using daily weather data measured at Shoeburyness, Essex. A summary of climate data and boundary conditions are shown in Tables 7.3 and 7.4. Uniform, grass vegetation cover was assumed throughout the model (Chapter 7).

An initial condition of pore water pressures hydrostatic above and below a water table at 7 m depth was applied, consistent with the soil columns in Chapter 7. Remaining boundaries were assumed to be impermeable.

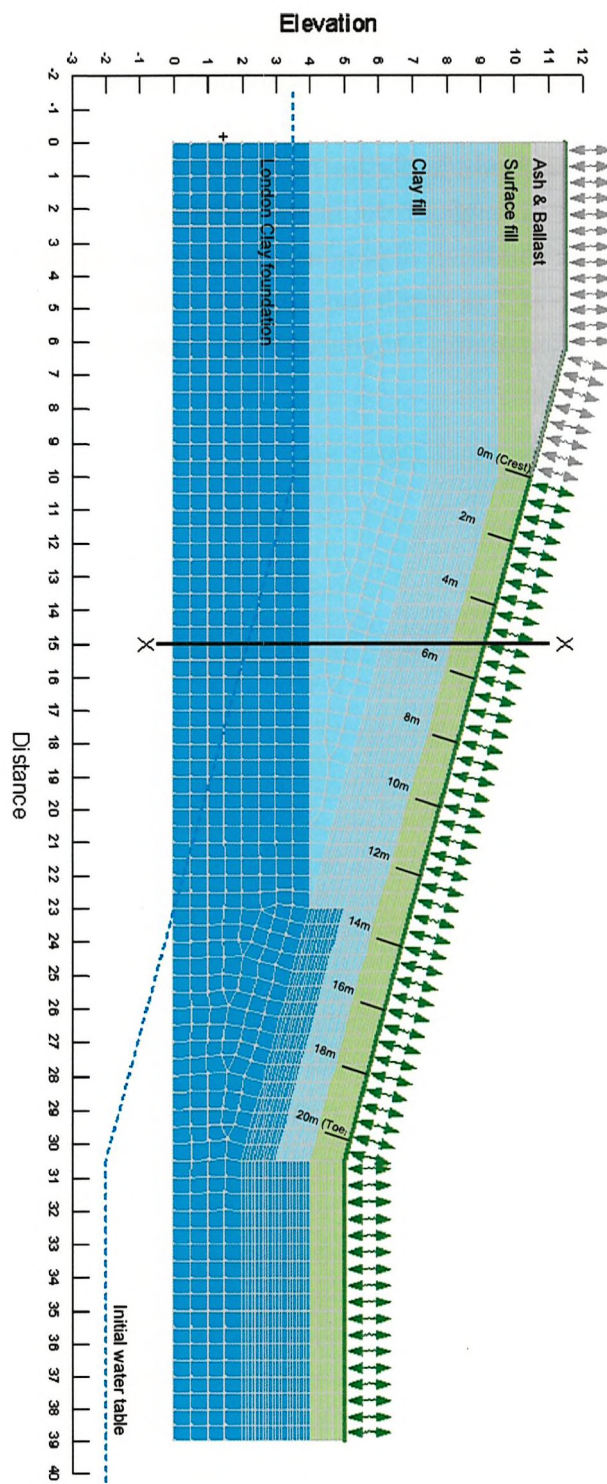


Figure B.1: Embankment model geometry

B.2 Results

Pore water pressures calculated for model A at 2 m depth at the embankment crest and then at the same depth below the ground surface at 2 m intervals downslope towards the toe are shown in Figure B.2. During wet periods calculated pore water pressures were generally higher near the toe than the crest, in agreement with field observations (Rahardjo et al., 2005). Pore water pressure variation at the crest of the slope (0 m in Figure B.1) provides an exception, due to increased water infiltration from the adjacent higher permeability ash and ballast layer.

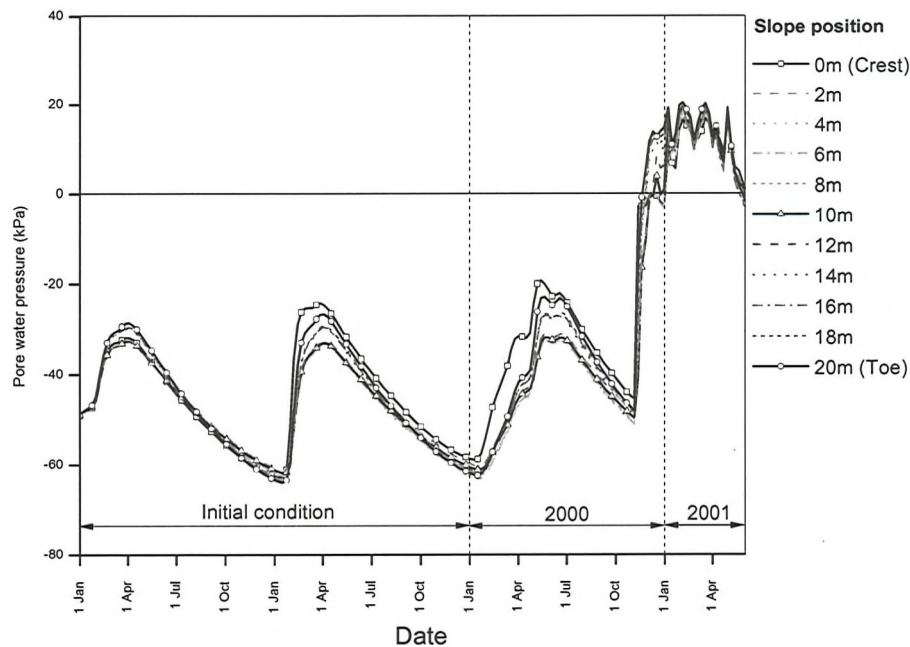


Figure B.2: Comparison of calculated pore water pressure at 2 m depth for slope positions at 2 m intervals (model A)

A similar pore water pressure variation was calculated for the midslope of model A, between 4 m and 16 m from the crest, for the period January 1998 to January 2001 (within approximately 2-3 kPa). Transient pore water pressure gradients were orientated parallel to the sloped surface at the midslope, causing transient flow perpendicular to the slope while downslope subsurface flow, due to elevation gradient (Philip, 1991), remained consistent throughout the central part of the slope at any instant (e.g. Figure B.6).

Comparison with model B, of isotropic surface clay fill saturated perme-

ability (5×10^{-7}) is shown in Figure B.3. Pore water pressure variation at the crest, midslope and toe of model B compares well with model A. The two dimensional model is not sensitive to anisotropy assumed in the surface clay fill. This is because the elevation pressure gradient (Figure B.6(a)), driving downslope subsurface flow, is negligible compared to pore water pressure gradients orientated parallel to the slope surface (Figure B.6(b)).

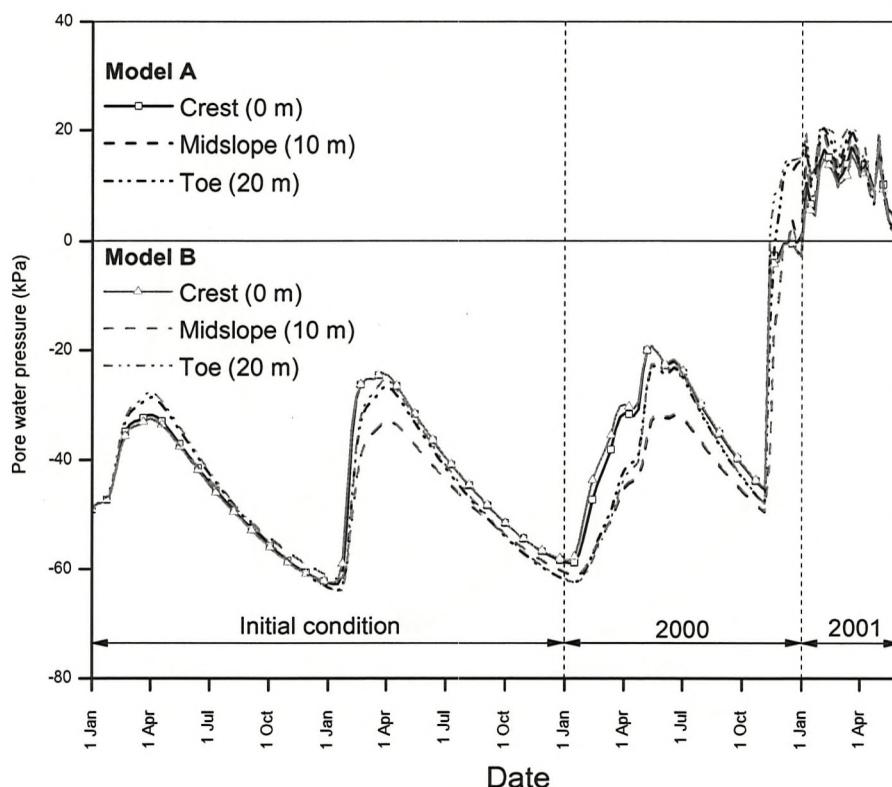


Figure B.3: Comparison of calculated pore water pressure at 2 m depth between model A and model B at the slope crest, midslope and toe

Comparison of model A with soil column C (Chapter 7) shows that pore water pressure calculated in the soil column lies very close to the range of pore water pressures calculated in the two dimensional embankment model (Figure B.4).

Figure B.5 compares pore water pressure at depth calculated for soil column C with the equivalent soil profile for embankment model A, located at section X-X (Figure B.1). Profiles for March, April, May and the maximum March-May 2001 pore water pressure envelope are shown. At each

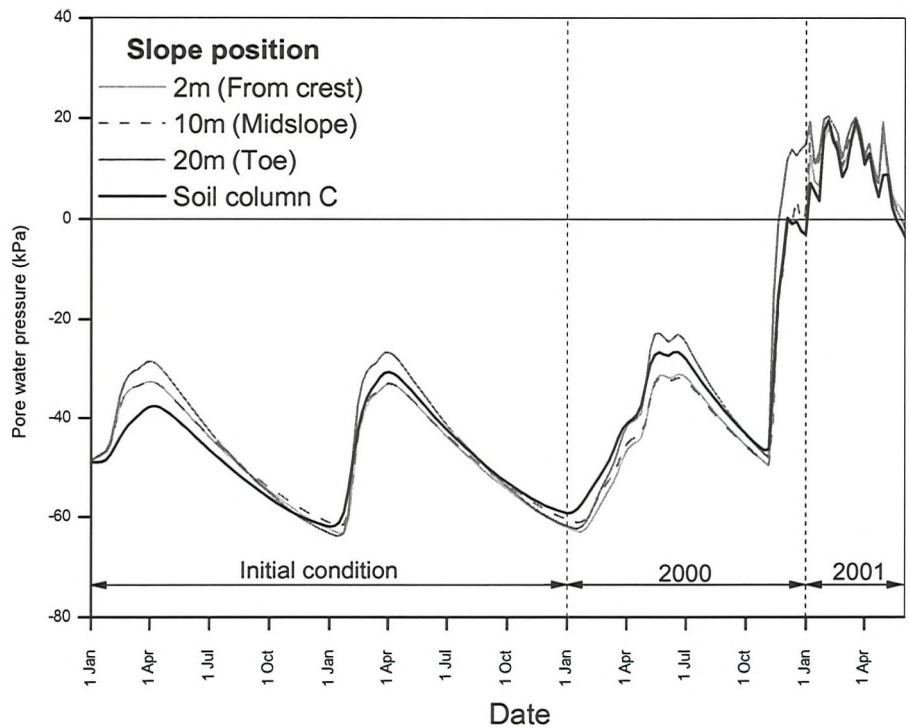


Figure B.4: Comparison of calculated pore water pressure at 2 m depth between soil column C and embankment model A

date similar profiles were calculated (within 5 kPa).

B.3 Comment and conclusions

A two dimensional model of a London Underground Ltd embankment showed that calculated pore water pressures were generally higher (by 5 kPa) at the toe of the embankment than the midslope and crest. Pore water pressures calculated at intervals between the crest and midslope were similar, showing that downslope subsurface flow was uniform through the central part of the slope. The influence of anisotropic saturated permeability in the surface clay fill was shown to be negligible.

Comparison of the two dimensional embankment model with a one dimensional soil column showed that pore water pressures calculated within the soil column lie between the range of values calculated for the embankment slope. Comparison of pore water pressure with depth between the

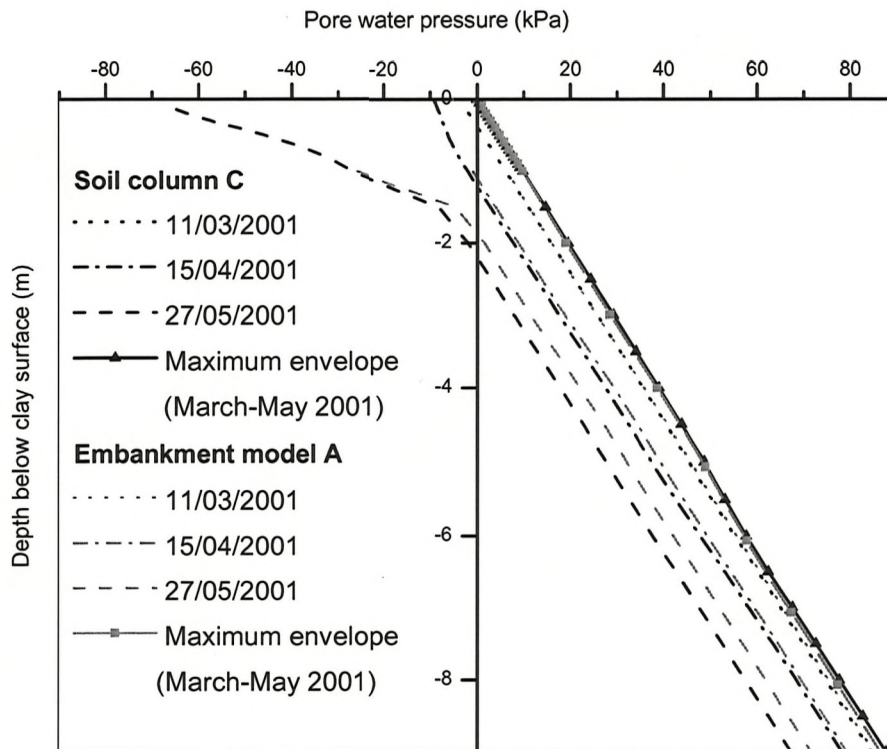
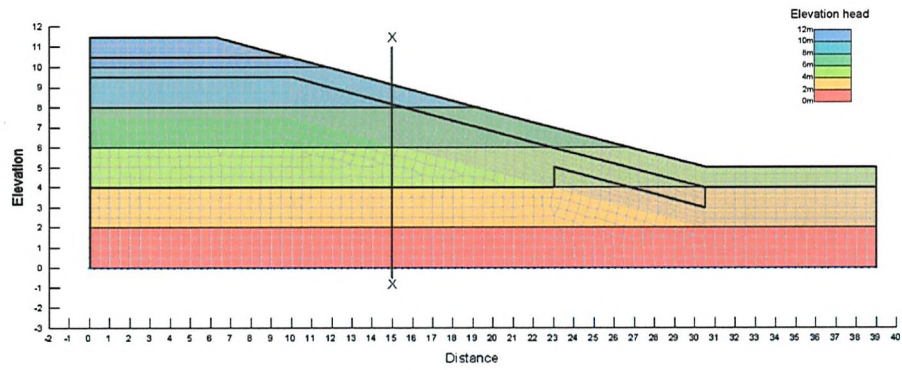


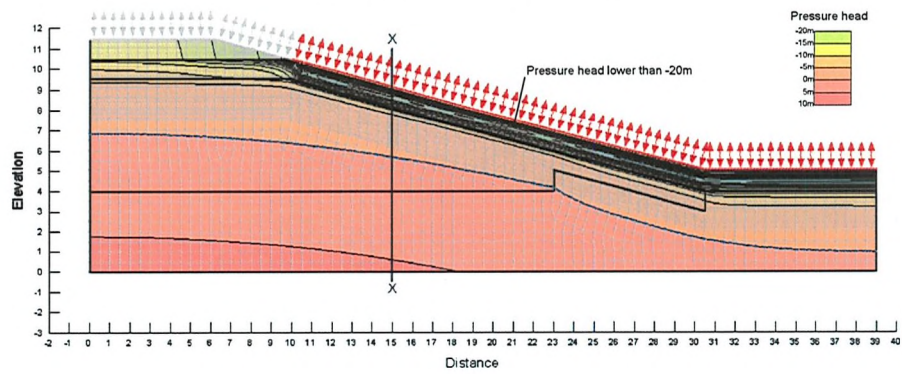
Figure B.5: Comparison of calculated pore water pressure profiles for March, April and May between soil column C and embankment model A

one dimensional soil column and a soil profile within the two dimensional embankment showed close agreement.

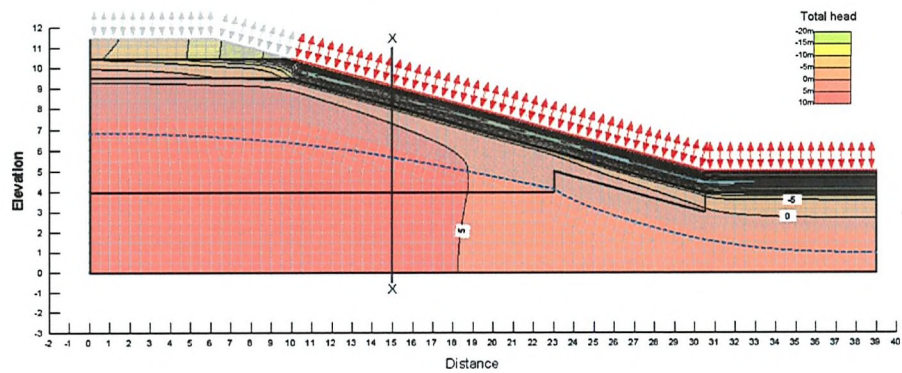
Comparison of the two dimensional embankment model with a one dimensional model shows that for a uniformly graded, uniformly vegetated slope a one dimensional model can adequately calculate pore water pressures for the midslope, where downslope subsurface flow is uniform. However, this may not be applicable where downslope subsurface flow is not uniform due to changes such as slope gradient at the toe and the crest, soil saturated permeability or slope vegetation cover.



(a) Elevation head (Constant)



(b) Pressure head (Transient)



(c) Total head (Transient)

Figure B.6: Calculated components of total head (model A, 30 September 2001)

Appendix C

Charing embankment: Ground investigation

Chapter 6 describes modelling of an instrumented Network Rail embankment at Charing. A ground investigation was conducted at Charing in three phases during 2006 and 2007:

1. Cone penetration testing (CPT) along the centre line of the upside tracks, undertaken by Lankelma on 15 October 2006.
2. Investigation of the southern slope was undertaken by Ritchies between 27 November 2006 and 26 January 2007. This comprised 25 no. boreholes, 6 no. trial pits and associated sampling, testing and monitoring across the lateral extent of the site. This stage of the investigation included installation of instrumentation and the excavation of high quality undisturbed soil samples, including block samples, for testing.
3. Investigation of the northern slope was undertaken by WA Developments between 21 May 2007 and 30 May 2007. The investigation comprised 15 no. boreholes and 5 no. trial pits.

Detailed interpretation of the ground investigation is provided in Mott MacDonald (2009). A summary of results contained within Mott MacDonald (2009) relating to the saturated permeability testing are presented for reference.

C.1 *In situ* and laboratory testing

In situ testing to determine the permeability of the clay fill was undertaken using falling head tests at 5 no. boreholes. Unsaturated permeability at the embankment surface was measured using a Guelph permeameter. The permeameter is a constant head device using a vacuum created above a water reservoir to balance atmospheric pressure and provide constant head (Reynolds et al., 1985).

Laboratory testing of permeability was conducted using the triaxial cell on a sub sample cut from an undisturbed block sample. Constant head saturated permeability was measured in the vertical direction, with a cell pressure of 320 kPa.

Moisture content was measured using index testing of routine samples and the high quality, undisturbed block samples. The mean effective stress of the samples was measured using the triaxial cell.

C.2 Results

Results of *in situ* saturated permeability measured using falling head tests and the Guelph permeameter are presented in Tables C.1 and C.2 respectively. The water table was not encountered in any of the falling head borehole tests and the results should not be treated as absolute, but as an indication of the permeability range within the embankment (Mott MacDonald, 2009). It was suggested that some smearing of the holes and clogging may have occurred during testing. The Guleph permeameter results represent a small volume of soil at the near surface and are unlikely to include the influence of surface cracking. However, higher saturated permeability relative to the clay fill at depth was measured.

Table C.1: Results of *in situ* permeability testing at Charing

| Borehole | Location | Depth range of test | Soil description | Permeability (ms ⁻¹) | Comments |
|------------|-----------|------------------------|--|--|--------------------|
| BH 405 | Shoulder | 2 m - 4 m | slightly gravelly CLAY [Fill] | 4×10^{-8} | |
| BH 307 (1) | Shoulder | 4 m - 6 m | gravelly CLAY [Fill] | 1×10^{-8} | |
| BH 307 (2) | Shoulder | 6 m - 8 m | | 2.5×10^{-8} | |
| BH 409 (1) | Shoulder | 3 m - 8 m | slightly to very gravelly CLAY | 1×10^{-8} to 3×10^{-8} | Hole collapsed |
| BH 409 (2) | Shoulder | 3 m - 7 m | over sandy gravelly CLAY [Fill over Gault clay] | 3×10^{-9} | clogging suspected |
| BH 410 | Mid slope | 1 m - 3 m | slightly sandy slightly gravelly CLAY [Fill] | 4×10^{-6} to 1×10^{-5} | |

Table C.2: Results of Guelph permeameter testing at Charing

| Soil type | Unsaturated permeability (ms^{-1}) |
|------------------------------|---|
| Ash | 4.2×10^{-5} |
| Sand pocket within clay fill | 2.2×10^{-6} |
| Clay fill | 1.7×10^{-6} |
| Clay fill | 1.2×10^{-6} |

A saturated permeability of $2.6 \times 10^{-9} \text{ms}^{-1}$ was measured in the triaxial cell. This is lower than the results measured *in situ*. This indicates the importance of soil fabric (local silt and sand layers etc) in controlling *in situ* saturated permeability, which are not represented in the small sample size (100 mm) of the triaxial test.

Based on permeability testing at Charing embankment and comparison with *in situ* testing from London Underground Ltd embankments the following values of permeability were suggested in Mott MacDonald (2009):

Surface clay fill: $1 \times 10^{-6} \text{ms}^{-1}$ to $1 \times 10^{-5} \text{ms}^{-1}$

Clay fill: $5 \times 10^{-8} \text{ms}^{-1}$ to $5 \times 10^{-9} \text{ms}^{-1}$

Sandy layers in fill: $1 \times 10^{-6} \text{ms}^{-1}$ to $5 \times 10^{-6} \text{ms}^{-1}$

A scatter of moisture content was measured within the samples (Table C.3). Local variation of moisture content was attributed to dessication of the soil caused by high water demand trees. Comparison of mean effective stress with vegetation in the vicinity of each sample (Figure C.1) showed large suctions measured close to high water demand trees (e.g. Oak).

Table C.3: Moisture content of clay fill at Charing

| Sample type | No. tests | Max % | Min % | Mean % |
|--------------|-----------|-------|-------|--------|
| Routine | 74 | 50 | 11 | 27 |
| High quality | 47 | 32 | 18 | 25 |

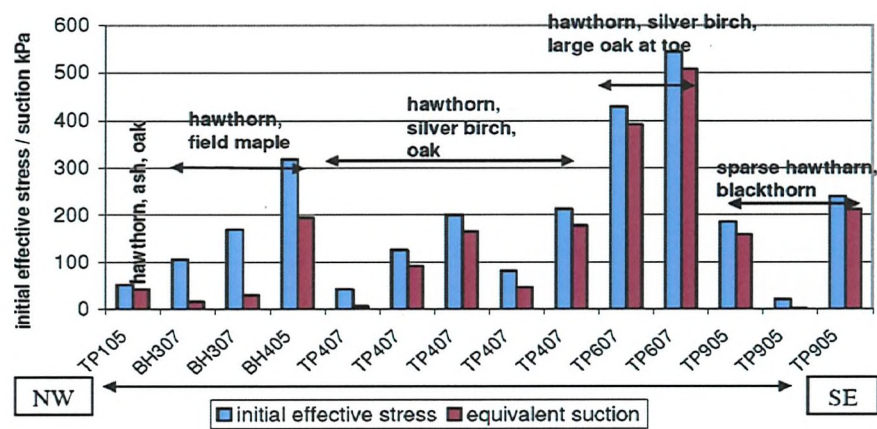


Figure C.1: Comparison of mean effective stress with local vegetation

Appendix D

Publications

Journal articles

Briggs, K. M. (2010). 'Charing embankment: Climate change impacts on embankment hydrology', *Ground Engineering*, June, pp. 28-31.

Loveridge, F. A., Spink, T. W., O'Brien, A. S., Briggs, K. M. and Butcher, D. (2010). 'The impact of climate and climate change on UK infrastructure slopes, with particular reference to southern England'. *Quarterly Journal of Engineering Geology and Hydrogeology* **43**, pp. 461-472.

Conference proceedings

Briggs, K. M. (2010), 'Charing embankment: Climate change impacts on embankment hydrology', in 'Geotechnical Engineering 20: View of Young European Geotechnical Engineers', Brno, Czech Republic, pp. 274-279.

Technical reports

Mott MacDonald. (2008) *Preliminary Guidelines for Vegetation Management Adjacent to London Underground Track and Structures*. Mott MacDonald, Croydon, 236048/FNG/REP/02/A. (Incorporated into London Underground Ltd Technical Advice Note G-058, January 2010)

Mott MacDonald. (2009) *Charing Embankment Monitoring and Modelling Report*. Mott MacDonald, Croydon, 244568/01/B.

Mott MacDonald. (2009) *Pound Green Embankment Monitoring and Modelling Report*. Mott MacDonald, Croydon, 244568/02/A.

Oral presentations

‘Tree influence on seasonal rail movements - an LUL case study’. Presented at Leeds Metropolitan University, June 2010.

‘Charing embankment: Climate change impacts on embankment hydrology’. Presented at the University of Dundee (March 2010), Mott MacDonald (June 2010) and the British Geotechnical Association (BGA) Conference (June 2010).

‘Railway embankment performance in response to seasonal climate variation in the UK’. (2009) Landslide Risk Assessment and Mitigation (LARAM) International School, Salerno, Italy.

Poster presentations

‘Climate change influence on infrastructure earthworks’. Presented at: SET for Britain, Engineering Exhibition, House of Commons, London. March 2011.

‘The influence of extreme wet weather on railway embankment hydrology’. Presented at: European Geosciences Union General Assembly 2011, Vienna, Austria. April 2011.

‘Climate change influence on infrastructure earthworks’. Presented at: ERA-Net Road Conference, Road owners getting to grips with climate change. Cologne, December 2010.

‘Modelling of pore water pressure variation within a railway embankment in response to climate’. Presented at: What’s new in hydrogeology?. University College London, February 2009

References

- Allen, R. K., Pereira, L. S., Raes, D., & Smith, M. (1998). *Crop Evapotranspiration: Guidelines for computing crop water requirements*. Technical report, Food and Agricultural Organisation's Irrigation and Drainage Paper, No. 56.
- Allen, R. K., Smith, M., Perrier, A., & Pereira, L. S. (1994). An update for the calculation of Reference Evapotranspiration. *ICID Bulletin*, 43(2), 35–92.
- Anderson, M. G., Hubbard, M. G., & Kneale, P. E. (1982). The influence of shrinkage cracks on pore-water pressures within a clay embankment. *Quarterly Journal of Engineering Geology and Hydrogeology*, 15, 9–14.
- Andrei, A. (2000). Embankment stabilisation works between Rayners Lane and South Harrow stations. *Ground Engineering*, 33, 24–26.
- Arup (2007). *Geotechnical Interpretative Report - Magnolia Road Embankment*. Technical report, Ove Arup and Partners, London.
- Aubertin, M., Mbonimpa, M., Bussiere, B., & Chapuis, R. P. (2003). A model to predict the water retention curve from basic geotechnical properties. *Canadian Geotechnical Journal*, 40, 1104–1122.
- Barbour, L. (1998). Nineteenth canadian geotechnical colloquium: The soil-water characteristic curve: a historical perspective. *Canadian Geotechnical Journal*, 35, 873–894.
- Bell, J. P. (1987). *Neutron probe practice*. Technical report, Institute of Hyrdology report 19, 3rd edition.
- Benson, C. & Grib, M. M. (1997). Measuring unsaturated hydraulic conductivity in the laboratory and field. In S. Houston & D. Fredlund (Eds.),

REFERENCES

- Unsaturated Soil Engineering Practice, Geotechnical Special Publication No. 68*: American Society of Civil Engineers, New York.
- Biddle, P. G. (1998). *Tree Root Damage to Buildings*. Wantage, England: Willowmead Publishing.
- Biot, M. A. (1940). General theory of three-dimensional consolidation. *Journal of Applied Physics*, 12, 155–164.
- Birch, G. P. & Dewar, A. L. (2002). Earthwork failures in response to extreme weather. In M. C. Forde (Ed.), *Proceedings of the International Conference Railway Engineering, London, UK*: Engineering Technics Press, Edinburgh.
- Blaney, H. F. & Criddle, W. D. (1950). *Determining water requirements in irrigated areas from climatological and irrigation data*. Technical report, Soil Conservation Service Technical Paper 96, Soil Conservation Service, U.S. Dept. of Agriculture: Washington, D.C.
- Blight, G. E. (2003). The vadose zone soil water balance and transpiration rates of vegetation. *Geotechnique*, 53(1), 55–64.
- Briggs, K. M. (2010). Charing embankment: Climate change impacts on embankment hydrology. *Ground Engineering*, June, 28–31.
- Brooks, R. H. & Corey, A. T. (1964). Hydraulic properties of porous media. *Colorado State University, Hydrology Paper*, 27(3), .
- Brutsaert, W. (1982). *Evaporation into the atmosphere : theory, history, and applications*. D. Reidel Publishing Company, Dordrecht, Netherlands.
- Buckingham, E. (1907). *Studies of the movement of soil moisture*. Bulletin 38, USDA, Bureau of Soils, Washington DC.
- Burdine, N. T. (1953). Relative permeability calculations from pore-size distribution data. *Petr. Trans., Am. Inst. Mining Metall. Eng.*, 198, 71–77.
- Burger, C. A. and Shackelford, C. D. (2001). Evaluating dual porosity of pelletized diatomaceous earth using bimodal soil water characteristic curve functions. *Canadian Geotechnical Journal*, 38, 53–66.

REFERENCES

- Camillo, P. J., Gurney, R. J., & Schmugge, T. J. (1983). A soil and atmospheric boundary layer model for evapotranspiration and soil moisture studies. *Water Resources Research*, 19, 371–380.
- Campbell Scientific (2006). Basic weather station BWS200 series. www.campbellsci.co.uk.
- Casagrande, A. (1937). Seepage through dams. *Journal of New England Water Works*, 51, 295–336.
- Chandler, R. J., Leroueil, S., & Trenter, N. A. (1990). Measurements of the permeability of london clay using a self-boring permeameter. *Geotechnique*, 40 (1), 113–124.
- Childs, E. (1940). The use of soil moisture characteristics in soil studies. *Journal of Soil Science*, 50, 239–405.
- Childs, E. C. & Collins-George, N. (1950). The permeability of porous materials. In *Proceedings of the Royal Society of London, Series A*, volume 201 (pp. 392–405).
- Clarke, D. & Smethurst, J. A. (2010). Effects of climate change on cycles of wetting and drying in engineered clay slopes in england. *Quarterly Journal of Engineering Geology and Hydrogeology*, 43(4), 472–486.
- Clarke, D., Smith, M., & El-Askari, K. (1998). New software for crop water requirements and irrigation scheduling. *ICID Bulletin*, 47(2), .
- Croney, D. (1952). The movement and distribution of water in soils. *Geotechnique*, 1, 1–16.
- Croney, D. (1977). *The design and performance of road pavements*. Technical report, Her Majesty's Stationary Office, London.
- Croney, D. & Coleman, J. (1961). Pore pressure and suctions in soils. In *Proceedings of the Conference on Pore Pressure and Suction in Soils* (pp. 31–37). Butterworths, London.
- Crow, P. (2005). *The influences of soils and species on tree root depth*, Information Note 78. Technical report, Forestry Commission, Surrey, UK.

REFERENCES

- Cutler, D. F. & Richardson, I. B. K. (1989). *Tree Roots and Buildings*. Harlow, England: Longman Scientific and Technical.
- Dakshanamurthy, V. & Fredlund, D. (1981). A mathematical model for predicting moisture flow in an unsaturated soil under hydraulic and temperature gradients. *Water Resources Research*, 17, 714–22.
- Dantec, V., Dufrene, E., & Saugier, B. (2000). Interannual and spatial variation in maximum leaf area index of temperate deciduous stands. *Forest Ecology and Management*, 134, 71–81.
- Davies, O., Rouainia, M., Glendinning, S., & Birkinshaw, S. J. (2008). Assessing the influence of climate change on the progressive failure of a railway embankment. In *The 12th International Conference of IACMAG, Goa, India* (pp. 4478 – 4486).
- De Vries, D. A. (1987). The theory of heat and moisture transfer in porous media revisited. *International Journal of Heat and Mass Transfer*, 30, 1343–1350.
- Docker, B. B. & Hubble, T. C. T. (2001). Strength and distribution of casuarinas glauca roots in relation to slope stability. In K. K. S. Ho & K. S. Li (Eds.), *Geotechnical Engineering*. Swets & Zeitlinger.
- Domenico, P. A. (1972). *Concepts and Models in Groundwater Hydrology*. New York: McGraw-Hill.
- Doorenbos, J. & Pruitt, W. O. (1977). *Crop water requirements*. Technical report, Food and Agricultural Organisation's Irrigation and Drainage Paper, No. 24, Rome, Italy.
- Driscoll, R. M. C. (2000). The behaviour of lightly loaded piles in swelling ground and implications for their design. *Proceedings of the Institution of Civil Engineers, Geotechnical engineering*, 143, 3–16.
- Driscoll, R. M. C., Crilly, M. S., & Butcher, A. P. (1996). Foundations for low-rise buildings. *The Structural Engineer*, 74(11), 179–185.
- Edgers, L. & Nadim, F. (2004). Rainfall-induced slides of unsaturated slopes. In *Landslides: Evaluation and Stabilization* (pp. 1091–1096). Rio de Janeiro, Brazil.

REFERENCES

- Ellis, E. A. & O'Brien, A. (2007). Effect of height on delayed collapse of cuttings in stiff clay. *Proceeding of the Institute of Civil Enigneers, Geotechnical Engineering*, 160, 73–84.
- Ernie, L. J., French, O. F., & Harris, K. (1965). *Consumptive use of water by crops in Arizona*. Technical bulletin 169, University of Arizona.
- Essig, E., Corradini, C., Morbidelli, R., & Govindaraju, R. (2009). Infiltration and deep flow over sloping surface: Comparison of numerical and experimental results. *Journal of Hydrology*, 374, 30–42.
- Ewen, J., Parkin, G., & O'Connell, P. E. (2000). Shetran: Distributed river basin flow and transport modelling system. *Journal of Hydrologic Engineering*, 5, 250–258.
- Feddes, R. A., Bresler, E., & Neuman, S. P. (1974). Field test of a modified numerical model for water uptake by root systems. *Water Resources Research*, 10, 1199–1206.
- Feddes, R. A., Kowaklik, P. J., & Zaradny, H. (1978). *Simulation of Field Water Use and Crop Yield*. John Wiley and Sons.
- Feddes, R. A., Kowalik, P., Kolinska-Malinka, K., & Zaradny, H. (1976). Simulation of field water uptake by plants using a soil water dependent root extraction function. *Journal of Hydrology*, 31, 13–26.
- Fetter, C. (1980). *Applied Hydrogeology*. Columbus, Ohio: Merrill Publishing Co.
- Fick, A. (1855). On liquid diffusion. *Philos. Mag. J. Sci.*, 10, 31–39.
- Fourie, A. B., Rowe, D., & Blight, G. E. (1999). The effect of infiltration on the stability of the slopes of a dry ash dump. *Geotechnique*, 49, 1–13.
- Fredlund, D. & Xing, A. (1994). Equations for the soil-water characteristic curve. *Canadian Geotechnical Journal*, 31, 521–532.
- Fredlund, D. G. (2000). The 1999 R.M. Hardy lecture: The implementation of unsaturated soil mechanics into geotechnical engineering. *Canadian Geotechnical Journal*, 37, 963–986.

REFERENCES

- Fredlund, D. G. & Rahardjo, H. (1993). *Soil mechanics for unsaturated soils*. John Wiley and Sons.
- Fredlund, D. G., Xing, A., & Huang, S. (1994). Predicting the permeability functions for unsaturated soils using the soil-water characteristic curve. *Canadian Geotechnical Journal*, 31, 533–546.
- Freeze, R. (1974). Streamflow generation. *Reviews of geophysics and space physics*, 12(4), .
- Freeze, R. A. (1969). The mechanism of natural ground-water recharge and discharge 1. one-dimensional, vertical, unsteady, unsaturated flow above a recharging or discharging ground-water flow system. *Water Resources Research*, 5, 153 – 171.
- Freeze, R. A. & Cherry, J. A. (1979). *Groundwater*. New Jersey, USA: Prentice Hall inc.
- Gardner, W. R. (1960). Dynamic aspects of water availability to plants. *Soil Science*, 89, 63–73.
- Gardner, W. R. (1964). Relation of root distribution to water uptake and availability. *Agronomy Journal*, 56, 35–41.
- Gellatley, M. J., McGinnity, B. T., Barker, D. H., & Rankin, W. J. (1995). Interaction of vegetation with the LUL surface railway system. In *Vegetation and Slopes* (pp. 60–71). Oxford, England.
- Geo-Slope (2005). *Vadose/W User's manual, Version 1.1*. GeoSlope International Ltd, Alberta, Canada.
- Geo-Slope (2007). *Vadose Zone Modeling with VADOSE/W 2007*. GEO-SLOPE International Ltd.
- Gitirana Jr., G. (2005). *Weather Related Geo-Hazard Assessment Model for Railway Embankment Stability*. PhD thesis, University of Saskatchewan, Saskatoon, Canada.
- Gitirana Jr., G., Fredlund, M., & Fredlund, D. (2005). Infiltration-runoff boundary conditions in seepage analysis. In *Canadian Geotechnical Conference* Saskatoon, Canada.

REFERENCES

- Glendinning, S., Loveridge, F. A., Starr-Keddle, R. A., Bransby, F. M., & Hughes, P. N. (2009). Role of vegetation in sustainability of infrastructure slopes. *Proceedings of the Institution of Civil Engineers, Engineering Sustainability*, ES2, 101–110.
- Gray, D. H. (1994). Influence of vegetation on the stability of slopes. In *Proceedings of the international conference on vegetation and slopes* (pp. 2–25). London: Thomas Telford.
- Green, S. & Clothier, B. (1999). The root zone dynamics of water uptake by a mature apple tree. *Plant and Soil*, 206, 61–77.
- Green, W. H. & Ampt, G. A. (1911). Studies on soil physics: I. flow of air and water through soils. *Journal of Agricultural Science*, 4, 1–24.
- Greenwood, J., Norris, J., & Wint, J. (2004). Assessing the contribution of vegetation to slope stability. *Proceedings of the Institution of Civil Engineers*, 157, 199–207.
- Greenwood, J. R., Vickers, A. W., Morgan, R. P. C., Coppin, N. J., & Norris, J. E. (2001). *Bioengineering: the Longham Wood Cutting field trial, CIRIA Project Report 81*. Technical report, CIRIA.
- Ground Engineering (1996). In the Limelight. *Ground Engineering*, (pp. 26–27).
- Hantush, M. S. (1964). Hydraulics of wells. In V. T. Chow (Ed.), *Advances in Hydrosience* (pp. 281 – 432). Academic Press, Inc.
- Hillel, D. (1980). *Introduction to Soil Physics*. Academic Press, Inc.
- Hillel, D., Talpaz, H., & van Keulen, H. (1976). A macrosopic-scale model of water uptake by a nonuniform root system and of water and salt movement in the soil profile. *Soil Science*, 121, 242–255.
- Hoogland, J. C., Feddes, R. A., & Belmans, C. (1981). Root water uptake model depending on soil water pressure head and maximum extraction rate. *Acta Horticulturae*, 119, 123–131.
- Horton, R. (1940). An approach toward a physical interpretation of infiltration capacity. *Soil Science Society of America*, 5, 399–417.

REFERENCES

- Horton, R. E. (1933). The role of infiltration in the hydrological cycle. *Trans. American Geophys. Union*, 14, 446–460.
- Hough, M., Palmer, S., Weir, A., & Barrie, I. (1997). *The meteorological office rainfall and evaporation calculation system: MORECS version 2.0*. Technical report, The Met Office.
- ICON (1997). Pore pressures and vegetation. Unpublished report for London Underground.
- Indraratna, B., Fatahi, B., & Khabbaz, H. (2006). Numerical analysis of matric suction effects of tree roots. *Proceedings of the Institution of Civil Engineers, Geotechnical Engineering*, 159, 77–90.
- ITASCA (1999). *FLAC Users Guide*. Minneapolis.
- Jacob, C. E. (1950). Flow of groundwater. In H. Rouse (Ed.), *Engineering Hydraulics* (pp. 321–386). New York: Wiley & Sons.
- Jaksa, M. B., Kaggwa, W. S., & Woodburn, J. A. (2002). Influence of large gum trees on the soil suction profile in expansive soils. *Australian Geomechanics Journal*, 37, 23–33.
- Jonckheere, I., Fleck, S., Nackaerts, K., Muys, B., Coppin, P., Weiss, M., & Baret, F. (2004). Review of methods for in situ leaf area index determination - part i. theories, sensors and hemispherical photography. *Agricultural and Forest Meteorology*, 17, 19–35.
- Joshi, B. (1993). A finite element model for the coupled flow of moisture and heat in soils under atmospheric forcing. Master's thesis, University of Saskatchewan, Saskatoon, Saskatchewan, Canada.
- Kilsby, C., Glendinning, S., Hughes, P., Parkin, G., & Bransby, F. M. (2009). Climate change impacts on long-term performance of slopes. *Proceeding of the Institute of Civil Engineers. Engineering Sustainability*, 162, 55–66.
- Kovacevic, N., Potts, D. M., & Vaughan, P. R. (2001). Progressive failure in embankments due to seasonal climate changes. In *Proc. of the 15th International Conference in Soil Mechanics & Geotechnical Engineering* (pp. 2127–2130). Istanbul, Turkey.
- Kovacs, G. (1981). *Seepage Hydraulics*. Elsevier Science Publishers.

REFERENCES

- Kutilek, M. & Nielsen, D. R. (1994). *Soil Hydrology*. Germany: Catena Verlag. ISBN 3-923381-26-3.
- Landsberg, J. J. (1999). *Tree water use and its implications in relation to agroforestry systems*. Technical Report RIRDC Publication No. 99/37, Rural Industries Research and Development Corporation (RIRDC), Kingston, Australia.
- Leong, E. (1997). Permeability functions for unsaturated soils. *Journal of Geotechnical and Geoenvironmental Engineering*, 123, 1118–1126.
- Leong, E. & Rahardjo, H. (1997). Review of soil-water characteristic curve functions. *Journal of Geotechnical and Geoenvironmental Engineering*, 123, 1106–1117.
- Leroueil, S. (2001). Natural slopes and cuts: movement and failure mechanisms. *Geotechnique*, 51, 197–243.
- Li, A. G., Yue, L. G., Tham, C., & Law, K. T. (2005). Field-monitored variations of soil moisture and matric suction in a saprolite slope. *Canadian Geotechnical Journal*, 42, 13–26.
- Li, L. J. H., Zhang, L., & Kwong, B. C. P. (2011). Field permeability at shallow depth in a compacted fill. *Proceedings of the Institution of Civil Engineers, Geotechnical Engineering*, 164, 211–221.
- Linsley, R. K., Kohler, M. A., & Paulhus, J. L. (1949). *Applied Hydrology*. New York: McGraw-Hill.
- London Underground Ltd, . (2000). *Engineering Standard E3321 A4. Earth Structures – Assessment*. Technical report, London Underground Limited.
- Loveridge, F. A., Spink, T. W., O'Brien, A. S., Briggs, K. M., & Butcher, D. (2010). The impact of climate and climate change on uk infrastructure slopes, with particular reference to southern england. *Quarterly Journal of Engineering Geology and Hydrogeology*, 43, 461–472.
- Marshall, T. J. (1958). A relation between permeability and size distribution of pores. *Journal of Soil Science*, 9, 1–8.

REFERENCES

- McCombie, P. F. (1993). The relative water demand of broad-leaved trees – a new analysis of the kew tree root survey. *Arboricultural Journal*, 17(4), 359–374.
- McGinnity, B. T., Fitch, T., & Rankin, W. J. (1998). A Systematic and Cost Effective approach to inspecting, prioritising and upgrading London Underground Earth Structures. In *ICE Proc. of Seminar, Value of Geotechnics in Construction* (pp. 302–332).
- Met Office, . (2009). UK climate and weather statistics. World Wide Web Address: www.metoffice.gov.uk/climate/uk/.
- Mitchell, A. & Jobling, J. (1984). *Decorative trees for country, town and garden*. HMSO. London.
- Monteith, J. L. (1973). *Principles of Environmental Physics*. Edward Arnold (Publishers) Ltd.
- Monteith, J. L., Szeicz, G., & Waggoner, P. E. (1965). Measurement and control of stomatal resistance. *Journal of Applied Ecology*, 2, 345–355.
- Morisette, J. T., Baret, F., Privette, J. L., Myneni, R. B., Nickeson, J. E., Garrigues, S., Shabanov, N. V., Weiss, M., Fernandes, R. A., Leblanc, S. G., Kalacska, M., Sanchez-Azofeifa, G. A., Chubey, M., Rivard, B., Stenberg, P., Rautiainen, M., Voipio, P., Manninen, T., Pilant, A. N., Lewis, T. E., Iiams, J. S., Colombo, R., Meroni, M., Busetto, L., Cohen, W. B., Turner, D. P., Warner, E. D., Petersen, G. W., Seufert, G., & Cook, R. (2006). Validation of global moderate-resolution lai products: A framework proposed within the ceos land product validation subgroup. *IEEE Transactions on Geoscience and Remote Sensing*, 44, 1804–1817.
- Mott MacDonald, . (1999). *LUL Research Stage II, Assessment of Clay Fill*. Reference: 5168/F&G/REP/360/A. Technical report, Mott MacDonald, Croydon.
- Mott MacDonald, . (2004). *LUL Earth Structures - The Practical Application of LUL Applied Research - Modified Soil Properties and Pore Water Pressures*. Technical report, Mott MacDonald, Croydon.
- Mott MacDonald, . (2005). *Seasonal Preparedness, Package 4: Statistics*. Technical report, Mott MacDonald, Croydon.

REFERENCES

- Mott MacDonald, . (2008). *LUL Vegetation Management Guidelines*. Technical report, Mott MacDonald, Croydon.
- Mott MacDonald, . (2009). *Seasonal Preparedness Earthworks (TSERV): Charing Embankment Monitoring and Modelling Report*. Technical report, Mott MacDonald, Croydon.
- Mualem, Y. (1976). A new model for predicting the hydraulic conductivity of unsaturated porous media. *Water Resources Research*, 12, 513–522.
- Mualem, Y. (1986). Hydraulic conductivity of unsaturated soils: prediction and formulas. In A. Klute (Ed.), *Methods of Soil Analysis. No. 9* (pp. 799–823).: American Society of Agronomy.
- Network Rail (2007). Network Rail Limited Annual Report and Accounts 2007. Retrieved on 20.04.07.
- Ng, C. W. W., Wong, H. N., Tse, Y. M., Pappin, J. W., Sun, H. W., Mills, S. W., & Leung, A. (2011). A field study of stress-dependent soil- water characteristic curves and permeability of a saprolitic slope in Hong Kong. *Geotechnique*, 61, 511–521.
- NHBC (2007). *National House Building Council Standards, Chapter 4.2, Building near trees*. Technical report, NHBC.
- Nimah, M. N. & Hanks, R. J. (1973). Model for estimating soil water, plant, and atmospheric interrelations: I. description and sensitivity. *Soil Science Society of America*, 37, 522–527.
- Novak, V. (1987). Estimation of soil water extraction patterns by roots. *Agricultural Water Management*, 12, 271–278.
- Novak, V., Simunek, J., & van Genuchten, M. T. (2000). Infiltration of water into soil with cracks. *Journal of Irrigation and Drainage Engineering*, 126, 41–47.
- Nyambayo, V. P. & Potts, D. M. (2010). Numerical simulation of evapotranspiration using a root water uptake model. *Computers and Geotechnics*, 37, 175– 186.

REFERENCES

- Nyambayo, V. P., Potts, D. M., & Addenbrooke, T. I. (2004). The influence of permeability on the stability of embankments experiencing shrink swell cyclic pore pressure changes. In *Proc. Advances in Geotechnical Engineering. The Skempton Conf.*, volume 2 (pp. 898–910). London: Thomas Telford.
- O'Brien, A. (2007). Rehabilitation of Urban Railway Embankments - Investigation, Analysis and Stabilisation. In *Proc. of the 14th International Conf. SMGE Madrid*.
- O'Brien, A., Ellis, E. A., & Russell, D. (2004). Old railway embankment fill - laboratory experiments, numerical modelling and field behaviour. In *Proc. Advances in Geotechnical Engineering. The Skempton Conf.*, volume 2 (pp. 911–921). London: Thomas Telford.
- PDE (2005). *FlexPDE 5.0 - Reference Manual*. PDE Solutions, Antioch, CA, USA.
- Penman, H. L. (1948). Natural evaporation from open water, bare soil and grass. In *Proc. R. Soc. London, Ser. A*, volume 193 (pp. 120–146).
- Perrochet, P. (1987). Water uptake by plant roots: a simulation model. i: Conceptual model. *Journal of Hydrology*, 95, 55–61.
- Perry, J. (1989). *A survey of slope condition on motorway embankments in England and Wales*. Technical report, TRL Limited.
- Philip, J. (1957). The theory of infiltration: 1 the infiltration equation and its solution. *Soil Science*, 83, 345–357.
- Philip, J. R. (1991). Hillslope infiltration: Planar slopes. *Water Resources Research*, 27, 109–117.
- Philip, J. R. & de Vries, D. A. (1957). Moisture movement in porous materials under temperature gradient. *Transactions, American Geophysical Union*, 38, 222–232.
- Phipps, P. J. & McGinnity, B. T. (2001). Classification and stability assessment for chalk cuttings: the metropolitan line case study. *Quarterly Journal of Engineering Geology and Hydrogeology*, 34, 353–370.

REFERENCES

- Potts, D. M., Kovacevic, N., & Vaughan, P. R. (1997). Delayed collapse of cut slopes in stiff clay. *Geotechnique*, 47(5), 953–982.
- Prasad, R. (1988). A linear root water uptake model. *Journal of Hydrology*, 99, 297–306.
- Priestley, C. H. B. & Taylor, R. J. (1972). On the assessment of surface heat flux and evaporation using large-scale parameters. *Monthly Weather Review*, 100, 81–82.
- Pyatt, G., Ray, D., & Fletcher, J. (2001). *An ecological classification for forestry in Great Britain*. Technical report, Forestry Commission Bulletin No. 124. Forestry Commission, Edinburgh.
- Radcliffe, D., Hayden, T., Watson, K., & Crowley, P. (1980). Simulation of soil water within the root zone of a corn crop. *Agronomy Journal*, 72, 19–24.
- Rahardjo, T. T., Lee, E., Leong, E., & Rezaei, R. B. (2005). Response of a residual soil slope to rainfall. *Canadian Geotechnical Journal*, 42, 340–351.
- RAIB (2008). *Network Rails Management of Existing Earthworks*. Technical report, Rail Accident Investigation Branch (RAIB), Department for Transport.
- Rail Safety & Standards Board, . (2003). *Railway Safety Implications of Weather, Climate and Climate Change: Final Report*. Technical Report AEAT/RAIR/76148/R03/005 Issue 2, AEA Technology.
- Reynolds, W. D., Elrick, D. E., & Clothier, B. E. (1985). The constant head well permeameter: Effect of unsaturated flow. *Soil Science*, 139(2), 172 – 180.
- Richards, B. G. (1965). *Moisture equilibria and moisture changes in soils beneath covered areas*, chapter Measurement of the free energy of soil moisture by the psychrometric technique using thermistors, (pp. 39–46). Butterworth & Co. Ltd.
- Richards, L. A. (1928). The usefulness of capillary potential to soil moisture and plant investigators. *Journal of Agricultural Research*, 37, 719–742.

REFERENCES

- Thornwaite, C. (1948). An approach towards a rational classification of climate. *Geographical Review*, 38, 55–94.
- Trans4m (2005). *Earth Structures Assessment Report, Northwick Park to Preston Road*. Technical report, Trans4m.
- Tratch, D. J., Wilson, G. W., & Fredlund, D. G. (1995). An introduction to analytical modelling of plant transpiration for geotechnical engineers. In *Canadian Geotechnical Conference (48th)* (pp. 771–780). Vancouver, Canada.
- Turner, S. (2001). Climate change blamed as landslip incidents treble. *New Civil Engineer*, 10 May, 8.
- USDA (Accessed 2009). Usda agricultural research service [online] available at: <http://hydrolab.arsusda.gov/soilwater/index.htm>. Accessed July 2009.
- van Genuchten, M. T. (1980). A closed-form equation for predicting the hydraulic conductivity of unsaturated soils. *Soil Society of America*, 44, 892–898.
- Vaughan, P. R., Kovacevic, N., & Potts, D. M. (2004). Then and now: Some comments on the design and analysis of slopes and embankments. In *Proc. Advances in Geotechnical Engineering. The Skempton Conf.* (pp. 241–290). London: Thomas Telford.
- Vrugt, J. A., vanWijk, M. T., Hopmans, J. W., & Simunek, J. (2001). One-, two- and three-dimensional root water uptake functions for transient modelling. *Water Resources Research*, 37, 2457–2470.
- Watson, D. J. (1947). Comparative physiological studies in the growth of field crops. i. variation in net assimilation rate and leaf area between species and varieties, and within and between years. *Annals of Botany*, 11, 41–76.
- Weather Underground (2010). Weather station isouthen6. Accessed June 2010.
- Wilson, E. M. (1990a). *Engineering Hydrology*. Macmillan, Basingstoke, 4th edition.

REFERENCES

- Wilson, G., Fredlund, D., & Barbour, S. (1994). Coupled soil-atmosphere modelling for soil evaporation. *Canadian Geotechnical Journal*, 31, 151–161.
- Wilson, G. W. (1990b). *Soil Evaporative Fluxes for Geotechnical Engineering Problems*. PhD thesis, University of Saskatchewan, Saskatoon, Canada.
- Wilson, G. W. & Fredlund, M. D. (2000). The application of knowledge-based surface flux boundary modelling. In D. Rahardjo, Toll & Leong (Eds.), *Unsaturated Soils for Asia* Balkema, Rotterdam.
- Witono, H. & Bruckler, L. (1989). Use of remotely sensed soil moisture content as boundary conditions in soil-atmosphere water transport modeling 1. field validation of a water flow model. *Water Resources Research*, 25(12), 2423 – 2435.
- Wosten, J. H. M., Lilly, A., Nemes, A., & Le Bas, C. (1999). Development and use of a database of hydraulic properties of european soils. *Geoderma*, 90, 169–185.
- Yang, H., Rahardjo, H., Leong, E., & Fredlund, D. (2004). Factors affecting the drying and wetting soil-water characteristic curves of sandy soils. *Canadian Geotechnical Journal*, 41, 908–920.
- Yazdani, J., Barbour, L., & Wilson, W. (2000). Soil water characteristic curve for mine waste rock containing coarse material. In *In proceedings of the 6th Environmental Speciality CSCE and 2nd Spring Conference of the Geoenvironmental Division of the CGS Ontario*.
- Zawadski, J. (1995). Report on the BGS meeting ‘Building on old railway embankments’ held at the ICE 10th May 1995. *Ground Engineering*, (pp. 27–32).